JET TO JET IMPINGEMENT IN A CONFINED SPACE

BY

ASHOK K. TYAGI, M.E.Sc., P.ENG.

A Thesis

Submitted to the School of Graduate Studies

in Partial Fulfillment of the Requirements

for the Degree

Doctor of Philosophy

McMaster University

DOCTOR OF PHILOSOPHY (1996)
(Chemical Engineering)

McMaster University
Hamilton, Ontario

TITLE: Jet to Jet Impingement in a Confined Space

AUTHOR: Ashok K. Tyagi
B.Sc. (Meerut University, Meerut, U.P)
B.E. (University of Roorkee, Roorkee, U.P)
M.E.Sc. (University of Western Ontario, London, Ontario)

SUPERVISORS: Dr. P. E. Wood
Dr. A. N. Hrymak

NUMBER OF PAGES: xvi, 305

Abstract

Reaction injection moulding (RIM) is commercially used in industry for making polymer parts. In this process, two or more jets produce impingement mixing of low viscosity monomers or oligomers in a mixhead. In order to better understand an impingement mixer, it is essential to understand the flow field created by the opposed laminar jets in a similar configuration. In this thesis, an experimental investigation and analysis of the flow field created by the two equal and opposed cylindrical laminar jets impinging near the closed end of a confined space (mixhead) has been conducted. Three important flow and geometrical parameters which influence the flow field are considered. These are (i) jet Reynolds numbers (Re), (ii) H/D, a ratio of the position (H) (the distance in - Z direction from the impingement point to the closed end) to mixhead diameter (D), and (iii) viscosity of the fluid used. Both qualitative and quantitative studies have been performed using an experimental model of the mixhead which simulates a RIM type configuration. For qualitative analysis, two flow visualization methods, namely, dye injection and particle tracing methods have been used. For quantitative analysis, the laser Doppler anemometer (LDA) technique has been used to quantify the velocity fields (only U and V components).

It has been found that Re shows a significant effect on the flow field. For Re < 50, flow remains in a statically stable mode and rotating vortices are formed near the impingement plane. At slightly higher Re (≥ 50), the flow pattern changes to dynamically stable mode and the impingement plane oscillates. At Re ≥ 90, the flow attains an unstable mode. In fact, the vortices gradually grow with increasing Re and at a critical value of Re they dynamically interact with each other causing oscillations

about the impingement plane. For both static and dynamic stable zones, the length of circulating region increases as a function of Re ($l/D = a - be^{-cRe}$) between 50 to 90. For Re > 90, the recirculating region shrinks before breaking into an unstable zone at a Re of approximately 125.

The piston position (H/D) plays an important role in the stability of the flow pattern. An unstable flow pattern transforms to a steady flow pattern when the piston is moved down from H/D = -0.5 to -0.75 at Re = 150. Furthermore, it appears that the flow patterns are always unstable at very high Re values since no stable patterns could be obtained up to H/D = -1.0 at Re = 200. In stable modes, flow fields of both side of impingement plane are like a mirror image of each other. It appears that viscosity of the fluid has no significant influence on the flow patterns at constant Re. The vector and streamline plots obtained by LDA for Re = 50, and 150 agree with the flow pattern obtained with flow visualization methods. Also, the experimental measurements confirm that the flow in the vortex regions is 3-dimensional.

Vigorous fluctuations are evident up to one-half mixhead diameter above the impingement point. The axial velocity (V) along the mixhead axis reaches a velocity profile of a developed one dimensional steady flow within 1 to 1.5 mixhead diameters. However, the radial velocity (U) along the mixhead axis reduces to an insignificant value at a distance equal to approximately two jet-diameters above the impingement point. The frequency analysis of the time series of velocity components showed higher harmonics as the Re increases from Re = 50 to 150. The periodic structure completely vanishes at Re = 200. The periodic nature of time series which vanishes at Re = 200 for H/D = 0, vanishes at Re = 150 when H/D = -0.5. This shows that H/D ratio also influences the breakdown of any periodic nature in the flow field.

Acknowledgement

I wish to express my sincere appreciation to my supervisors, Drs. P. E. Wood and A. N. Hrymak, for their guidance, enthusiasm, and encouragement throughout this work. For providing financial support Department of Chemical Engineering and the School of Graduate Studies of McMaster University are highly appreciated.

I would also like to thank Drs. M. L. Tikku and D. A. Goodings of McMaster University for providing guidance in various aspects of data analysis.

Unabated help of Mr. G. M. Slater (Technical services coordinator), Mr. W. Warriner (Machinist), and Ms. J. Derkach (Laboratory assistant) throughout the experimental work is highly appreciated. A warm and heartfelt thanks are due to my friend Dr. A. K. Srivastava whose timely encouragement and discussions helped me a lot.

Last but not least, I would like to thank my wife Seema, and my daughters Angele and Alka for their boundless support and encouragement for my endeavor during thick and thin times.

Table of Contents

List of Figures

List of figures (cont'd)

List of figures (cont'd)

List of figures (cont'd)

List of figures (cont'd)

List of figures (cont'd)

List of Tables

Nomenclature

Notations are locally defined. Only following variables are globally used.

d	= Jet diameter
D	= Mixhead diameter
H	= "Clean out" Piston position from jet axis
U	= Average velocity component in Y-direction
U_{avg_jet}	= Average jet velocity in Y-direction
u	$= \frac{U}{U_{avg\_jet}}$ Dimensionless average velocity in Y-direction
V	= Average velocity component in Z-direction
V_{avg_MH}	= Average mixhead velocity in Z-direction
v	$= \frac{V}{V_{avg\_MH}}$ Dimensionless average velocity in Z-direction

Greek symbols

μ	= Fluid viscosity
ρ	= Fluid density

Dimensionless group

Re	$= \frac{d\rho U_{avg\_jet}}{\mu}$ Jet Reynolds number
JNRE	= Jet Reynolds number (same as Re)
H/D	= Ratio of piston position and mixhead diameter

Note: At center line (0, 0, Z) U (also u) and V (also v) are radial and axial velocity, respectively.

1 Introduction

The main objective in evaluating any process in chemical engineering is to determine its performance at the maximum possible rate and efficiency. These are the principle components of the initial and operating costs. The performance of many processes are highly dependent on the transport phenomena (e.g. heat, mass, momentum etc.), and a method or technique which enhances these operations, also increases the overall efficiency of the process. Jet impingement flows of various configurations are widely used in industry due to their excellent heat and mass transfer characteristics. For example, drying of textiles, cooling of turbine blades, vertical-take-off aircraft, paint sprays, inertial impactors, impinging-streams emulsifier, side-dump combustors and reaction injection molding (RIM) machines use the jet impingement phenomenon in one form or an other.

The implementation of jet impingement yields good mixing in the impingement zone, and the fragmentation of the fluid clumps (or solid particles in the case of gas-solid systems) due to high collision rates. All of these effects result in a considerable increase in the contact area between various components of the system. These components may be different phases or may be the same fluid at different temperatures. This increased area, created by the hydrodynamics of jet impingement, results in the enhancement of heat transfer and mass transfer in the system. The phenomenon of jet impingement (especially two opposed jets) is also observed frequently in nature in the atmosphere and ocean, One type of hurricane wind, called the bora is created by the interaction of two opposing air jets at different temperatures over a mountain range (Bogdanov et al. (1983)).

Reaction injection molding (RIM) is a polymer processing method to produce large polymer parts. It is based on the injection of monomers or reactive oligomers into a mold, followed by a fast polymerization reaction. The details of RIM processing are described by Macosko (1989). The attractiveness of this process is in savings of energy and capital investment compared to thermoplastic injection molding. Originally, RIM used urethane chemistry almost exclusively but now new non-urethane polymer RIM systems have emerged such as nylons, polyureas, polyesters etc. The strong interest of the automotive industry in the RIM process is the main thrust behind the development of new RIM systems. The replacement of steel body parts with reinforced RIM parts reduces the body weight of the cars and thus improves their fuel economy.

Impingement mixing is an important step in the RIM process, because of the fast reaction rate and slow molecular diffusion. Poor mixing will leave unreacted monomers in the product and/or unbalanced stoichiometric portions. Thus the finished product will not meet the required specifications. Mixing defects will be superimposed on the defects created during mold filling.

Vertical-take-off aircraft, inertial impactors and paint spray are examples of impingement of a jet on a plate. RIM and side-dump combustors use jet to jet impingement in a confined space. These jet impingements may be in the laminar and/or turbulent regimes. The flow field and the associated transport characteristics of jet impingement on a fixed plate in a confined space or free space of laminar and turbulent jets have been theoretically and experimentally examined by many investigators. However, studies of flow fields during jet to jet impingement in a

confined space (the RIM environment) are sparse, especially, for highly viscous liquid jets. This thesis deals with a detailed experimental study of the flow field generated by two opposed laminar jets impinging in a confined space.

Literature review for the jet impingement and various flow visualization methods is summarized in Chapter 2. The objectives of the thesis are listed in Chapter 3. In Chapter 4, experimental setup for flow visualization with dye injection and suspended particles techniques to obtain 3-D and 2-D flow patterns and quantitative method of laser Doppler anemometry to measure the velocity field are discussed. Selection of the sample space, trigger mode, and the sampling frequency are given in Chapter 5.

Results of the flow visualization experiments presented in Chapter 6, indicate that jet to jet impingement in a confined space generates three types of flow modes, (i) static stable, (ii) dynamic stable, and (iii) unstable depending on the value of jet Reynolds number. It is also found that vortex grows as the jet Reynolds number is increased. There is a decrease in vortex length before the flow mode changes from dynamic stable to unstable mode. Flow patterns developed using the velocity measurements from laser Doppler anemometry agree with the flow patterns obtained with flow visualization.

Analysis of the center line velocities obtained with laser Doppler anemometry is given in the Chapter 7. Oscillating regions and the frequency analysis using time and frequency domains are described in the Chapter 8. The quantitative effects of jet Reynolds number, piston height, and viscosity on the flow field are discussed in both Chapter 7 and 8. Conclusions are described in Chapter 9.

2 Literature Review

2.1 Jet Impingement and Mixing

The impingement of plane and round jets on a smooth plate constitutes the simplest case of jet impingement. It has been reported by Beltaos and Rajaratnam (1973) as well as Deshpande and Vaishnav (1982) that three distinct regions of flow characteristics occur in both laminar and turbulent cases. In region I, known as the free jet region, the flow characteristics are identical to those of a free jet (in the case of round jet impingement on a fixed plate). The dominant velocity component is axial and the flow is not influenced significantly by the surface of impingement. In region II, referred to as the impingement region, the flow undergoes considerable deflection and is characterized by significant changes in flow direction. In region III, at the end of impingement region and known as the wall jet region, the flow becomes parallel to the wall assuming a pattern similar to a wall jet. The dominant velocity component is radial and the boundary layer is subject to nearly zero pressure gradient and thickens as one moves radially outward. There are transition zones between these regions. For this type of configuration, the extent of region I, the velocity vector field in region II and velocity field, jet thickness and the distribution of wall shear stresses are identified as the important parameters.

This type of flow has been analyzed theoretically and experimentally by many investigators. Wolfshtein (1970), Beltaos and Rajaratnam (1973), Gutmark et al. (1978) are examples of the references for turbulent jets and Deshpande and Vaishnav (1982) investigated impingement of laminar jets. The heat transfer and mass transfer

due to laminar slot and axisymmetric jet flows have also been investigated. These studies were conducted in a confined space (Law and Masliyah (1984 (a) & (b)), Saad et al. (1977), Van Heiningen et al. (1976)). Law indicated that the local Sherwood number along the impingement plate for a confined axisymmetric jet behaves similarly to that of an unconfined jet except in the region far away from the stagnation point. The maximum value of the Sherwood number is found close to the stagnation point. Marple et al. (1974) also found that the presence or absence of an upper confining boundary in the inertial jet impactor does not greatly affect the flow field in the impaction region directly below the impactor exit.

Jet to jet impingement has been investigated in a free space for turbulent flows. Makarov and Khudenko (1965) studied the mixing of intersecting turbulent air jets. They gave the experimental results for the flow parameters (velocity, static pressure and temperature fields) of the stream formed by the intersection of the two plane parallel turbulent air jets. The two angles of inclination of the jet nozzle reported are 30° and 60°. It was found that the temperature field in the resultant flow began to resemble the velocity field (the position of the temperature and velocity maxima begin to coincide) only at a considerable distance from the section where the velocity field becomes smooth. Kirillov and Khudenko (1965) calculated the direction of the axis of a stream that resulted from mixing two inclined turbulent jets and proposed that the resultant turbulent stream, at a certain distance from the point of intersection, may be regarded as one turbulent jet. Becker and Booth (1975) measured the concentration field in the interaction zone of two turbulent inclined air jets (jet Reynolds number = 70,000) intersecting at half-angles of 15°, 30°, and 45° by a light scattering method. They reported that the key length scale for the

system is the distance L from the virtual origin of either jet to the point of intersection of the nozzle axes. At the end of this zone, the material from the two jets is fully mixed and the process occurring thereafter is further mixing of this mixture with the ambient fluid. They found a relatively stagnant back mixing zone between the jets at the point where they meet. Ogawa et al. (1992) experimentally investigated turbulent jet to jet impingement in a free space using hot wire anemometry. They reported the existence of a stable impact position near the nozzle exit whenever large differences existed between the velocities of the opposite jets. In the case of nearly equal mass flow rate from jets, the impact position is not always unique but varies irregularly within a certain range. These experiments were carried at Reynolds number of 56100.

Denshchikov et al. (1978 & 1983) and Bogdanov et al. (1983) experimentally investigated the impingement of two unconfined opposed planer turbulent water jets. They reported that a single jet remains stable in the plane of its flow. However, the addition of an opposing jet developed oscillations of jets in a direction perpendicular to this plane. The amplitude and period of the oscillation is determined by the system itself. The mechanism of the oscillation is described in the following terms by Denshchikov et al. The collision of two jets is associated with the retardation in the jet velocities and thus increasing pressure in some regions. This causes jets to move to the side away from the plane of jet flow. After new jets have been formed away from the initial position, ordered motion develops in the retardation region. Essentially, two new jets are formed; these jets, displacing one another, are oriented at some angle to the initial direction in which the jets issued from the nozzles. This mode of flow is unstable. The pressure in the region between the jets

is depressed, and as a result, after diverging a certain amount, the jets begin to approach one another. This motion of jets towards one another ends with another collision, and a new increase in pressure in the region of the opposing jets, which again displaces the jets from their symmetry plane but this time in the opposite direction. They found that the dimensionless frequency of the oscillation could be well correlated with jet Reynolds number and the dimensionless distance the jets were apart.

Nosseir and Behar (1986) analyzed the characteristics of jet to jet impingement in a side-dump combustor (2-D model) simulator that was built on a water table (jet Reynolds number = 3000). Their initial approach to jet to jet impingement was guided by the Powell's (1960) mirror image concept. Powell indicated that the impingement of two jets separated by a distance H is theoretically equivalent to a single jet impinging on a flat surface at a distance H/2 downstream. The concept is plausible, although not proved yet. The previously described auto-oscillations of the impinging jets is strong evidence to disprove the image concept, but it has still to be proved that these oscillations are only due to the impingement and/or due to some flow disturbance. Nosseir and Behar proposed that the flow field of the jet to jet impingement can be viewed as the synthesis of a number of flow regimes that include free turbulent jets, jet to jet impingement and the jet-wall impingement. They also observed counter-rotating vortex pairs in the impinging region, and the strength of these vortices changes periodically due to stretching in the downstream direction of the combustor. Miau and Sun (1989) used a particle tracer technique for visualizing the flow pattern in a side inlet square duct. They reported an irregular distribution of the streamwise vortices developed in the stagnation region of the

impinging flows at a Reynolds number of 20000. Liou et al. (1990) made experimental and theoretical investigations of jet to jet impingement in a side inlet rectangular combustor. The Reynolds numbers based on air density, combustor hydraulic diameter and bulk velocity were in the range of 1000 to 200000. They also observed large scale oscillations as reported by Nosseir and Behar, and Miau and Sun. The existence of oscillations was confirmed using the time averaged analysis of the measured velocity probability density function.

Most of the work in the jet to jet impingement similar to the RIM mix-head was done to analyze the effects of various parameters in terms of the mixing quality. Malguarnera and Suh (1977) in their experimental work evaluated the performance of impingement by evaluating the quality of mixing by using a titration method. Samples taken from the mixer output were analyzed for acid concentration, and the standard deviation of these local samples was used to define the quality of mixing and thus the effect of impingement. Based on dimensional analysis they highlighted various parameters (density ratio, viscosity ratio, momentum ratio and chamber size) which may or may not influence the impingement performance. In this method of analysis, mix quality is treated as a dimensionless quantity (Tucker and Suh, 1980). The experiments were performed for the Reynolds number range between 250 to 3000. An increase in Reynolds number from 250 to 500 improved the mixing quality but further increases in Reynolds number brought no improvements in mixing. At Reynolds numbers greater than 500, the standard deviation of mixing quality among the samples was around 2% of the mean. But the accuracy of the titration method is also around 2%. It is possible that their method may not detect the improvement. Their main conclusion was that Reynolds number is the important

parameter and the mixing chamber volume (it was changed by an order of magnitude) has a little effect. A Reynolds number of 50 was selected as the lower limit for good mixing as a qualitative guide. Since they were collecting samples at the end of mixing chamber at high Reynolds number they could not notice the effect of the mixing chamber volume. It is possible that at the end of mixing chamber mixing induced due to the impingement of jets is superimposed over the chamber volume influence which may be of secondary nature.

Lee et al. (1980) used high speed photography to visualize the impingement mixing of a glycerine/water mixture and found the mixing at low Reynolds number (less than 90) was poor while at Reynolds number 150 the quality was improved due to the chaotic behavior of the impingement region. Tucker and Suh (1980) used a point light source to identify the local dye concentration in a glycerine/water model of RIM mixtures, and thus define the mixing quality. They found that mixing improved up to Reynolds number of 550; after this limit their method was not sensitive enough to identify any increase in mixing quality. The visualization techniques used by Lee et al. (density difference) and Tucker and Suh (color dye) are not useful beyond Reynolds number of 150. Kolodziej et al. (1982) used carbon black in the polyol side of a RIM experiment and measured the thickness of carbon black striations in the resulting part and related this distribution with mixing quality. They found that quality improved from a Reynolds number of 80 to 250 but no change occurred from 250 to 450. Sandell et al. (1985) concluded that impingement mixing quality increases as the Reynolds number increases. There is a decreasing rate of mixing improvement over the Reynolds number range of 250-700. They also observed the oscillation of the impingement region and formation and shedding

of vortices similar to other studies (Denshchikov et al. (1978 & 1983), Lee et al. (1980), and Tucker and Suh (1980)). They also observed that the flow field is made unstable by increasing the jet Reynolds number and that moving the mixhead piston further behind the nozzle improves the mixing. Jie et al. (1991) experimentally investigated the jet to jet impingement in RIM type mixhead. The range of the jet Reynolds number in the study was from 140 to 5400. They used LDA for studying the effects of jet Reynolds numbers, jet diameter to mixhead diameter ratio, piston distance from the jet axis. They concluded that the turbulence intensity increases with the increase of jet diameter to mixhead diameter ratio or the decrease of piston position from the jet axis.

2.1.1 Summary

The following conclusions are drawn from the previous works described in section 2.1.

1. Impinging jet flow consists of three regions: free jet, impingement and wall jet.
2. Auto-oscillation is observed in jet to jet impingement at Re = 50 while a single jet impinging on a plate is stable at the same Reynolds number.
3. Pairs of counter-rotating vortices are observed in the impingement region.
4. The mirror image concept of jet to jet impingement similar to jet to plate impingement had been proposed but still needs more analysis to either disprove or prove this concept.

5. Movement of confinement plate (jet to plate impingement) towards the impingement plate does not greatly affect the flow field in the impaction zone. If same is found in the jet to jet impingement in a RIM mixhead then the mixhead pipe diameter may become a less significant parameter.

6. The flow field of a jet created by the impingement of inclined jets, is similar to a jet generated from the virtual origin (intersection of the bisector of the inclined jets and the line joining the jets, Kirillov and Khudenko 1965).

7. The key length scale for the inclined jet impingement system is the distance between the jet origin to the impingement plane.

8. Mixing is achieved by a combination of three process namely molecular diffusion due to concentration gradients, eddy diffusion due to turbulence and the bulk diffusion due to convective transport (Tadmor and Gogos 1979).

9. The jet Reynolds number has been identified as an important parameter for mixing quality. Other parameters (like viscosity ratio, density ratio, momentum ratio between impinging jets and the geometry of the impinging zone) may be important for a RIM mixing head. Some workers found that mixing improved up to Re = 250 and then there was no improvement. Some researchers have observed the improvement up to Re = 550 and some have reported the improvement even up to Re = 700 though the rate of improvement decreased. These conclusions are

based on some mixing quality indices rather on the flow structure of the impingement zone. These indices measured over all mixing (measured at the end of the mixhead zone) which in fact, is the superimposed effect of different parameters and modes of mixing.

2.2 Flow Visualization Methods

The understanding of a physical process is vastly improved if a pattern produced by or related to this process can be visualized. By observing the flow pattern of a fluid process, one can get an idea of the whole flow development. The visualization of some fluid flows has an inherent difficulty due to the transparent nature of fluids. According to Quraishi and Fahidy (1985) flow visualization techniques can be divided into two main groups:

(a) Direct flow visualization

(b) Indirect flow Visualization

All of the techniques in which the flow field can be visualized by the naked eye without interpretation of a visual image (e.g. suspended-particles), are direct flow visualization methods. While in the indirect flow visualization method an interpretation of the flow field is required or the visual image is created at a plane outside the test area. The direct techniques are usually simple but are qualitative, while indirect techniques are usually complicated, but they provide quantitative information about the flow field.

All flow visualization techniques use light in one form or other. Most use the visible frequency spectrum (e.g. when using food dye). While some methods use

the ultraviolet and infrared spectrum (e.g. fluorescent-dye method). Before choosing one particular technique for flow visualization, it is essential to know the contents of the fluid motion picture and experimental techniques for flow pattern explanation. The visualization methods can trace a streamline, streakline or path-line. Some of the methods suitable for the flow pattern studies of the flow field created by impinging jets are reviewed in following sections.

2.2.1 Dye

The injection of the dye into a flowing fluid to visualize it is simple enough, though care must be taken to fulfill at least two requirements. (1) The density of the marked liquid (concentrated dye in the main liquid) and the main fluid should be matched. (2) The injection of the marked fluid should not affect the flow field. This type of injection is called isokinetic injection. Food-coloring agents may be used as the dyes. Ink, color pigments and certain chemicals (potassium perma-ganate) are also used. The addition of milk in the food dye enhances the reflectivity of the dye and reduces the rapid diffusion of dye in the main flow. This increases the observation time. But flow equipment requires good cleaning to avoid the decaying of milk in the model. Merzkirch (1974) suggested dyes suitable for water or water based working fluid.

McNaughton and Sinclair (1966) analyzed submerged water jets ($100<Re<28000$) in short cylindrical flow vessels by visualizing the jets with the use of chemical indicator (a jet containing 22ppm of methylene blue was injected

into a clear water flow). Their equipment was illuminated with 500 watt flood lamps and an opaque white Perspex sheet was installed between the test section and the light.

Quraishi and Fahidy (1985) reported the use of fluorescing-dyes for flow pattern studies. Fluorescing-dyes absorb ultraviolet light. The emission of the absorbed energy is in the visible region of the spectrum. Use of these dyes avoids the disturbances created by the injection of food dyes in the flow field since in these dyes excitation of the dye is achieved by laser light from out side the model. This advantage of these dyes are only acheivable if the dyes dissolve in the main fluid. The most commonly used fluorescence dyes are 4-methyl-umbelliferone, rhodamine-B, rhodamine-6G and fluorescence sodium (uramine). For example, sheet light from argon lasers with fluorescence dye produced a greenish-yellow color and Rhodamine dye produces a distinctive purple- red color.

Though the acid/base method is quite good for visualization, it is limited by poor color contrast. The appearance of color is plainly visible but the color contrast was not adequate for photography using phenolphthalein as an indicator.

2.2.2 Suspended particles

Flow visualization by observing the reflected light from suspended particles in the fluid is extensively used. The equivalence of the movement of the particles and the motion of the surrounding working fluid rests upon particle size and density. If the particles are small enough and neutrally buoyant in the fluid, the flow pattern captured on the recording media represents the flow pattern of the

working fluid. The particles should be good reflectors of light. Spherical polystyrene particles which fulfil these conditions are used for flow visualization. If the flow model is illuminated by flood light, the captured flow pattern represents the bulk flow. On the other hand, if only a slice through the model is illuminated, the flow pattern will indicate 2-D flow structure which may exist. Thus, this technique is used to get an overall picture and/or the 2-D structure of the flow field. Also, this method does not create flow disturbances associated with the dye injection method.

When a laser beam is passed through a cylindrical lens (or a simple glass rod), this beam diverges into a sheet or plane of light. The width of this plane of light is controlled by two variables: the diameter of the glass rod, and the distance between the rod and the flow section. This sheet of light illuminates the plane of the flow field (the flow may contain tracer particles or fluorescent dyes) which is made visible if viewed from perpendicular direction to the plane of light. This section of the flow field is easily photographed using a dark background and a 35mm camera.

Savas (1985) used reflective flakes (40 micron aluminum flakes) to visualize the flow in the cylindrical cavity during spinup from rest. A thin sheet of light from 2W argon ion laser illuminates the cylinder diametrically through the axis. The camera is at a right angle to the plane of light. Richards and Scheele (1985) made measurements of the laminar jet velocity distribution in liquid-liquid systems. A pulse ruby laser was used to activate the tracer dye (1,3,3-trimethylindolino-6'-nitrobenzopyrylospiran (TMINBPS)). The blue tracer line produced was photographed with high speed movie camera. Saripalli (1983)

used fluroescein-sodium dye and air bubbles as tracer particles for the visualization of single and multiple jet impingement on the fixed plate. The illumination of the flow field is achieved by a 3W argon laser. Woo et al. (1986) used this method to visualize the complex flow field caused by the prosthetic valves during various periods in the heart cycle. They employed a 7mW He-Ne laser as the light source and Amberlite particles of 100 microns as tracer in the blood analog fluid flow. Prenel et al. (1986) used 2-D periodic laser sweeps to produce 3-D laser sheet which illuminated the 3-D flow field in complex flow. The qualitative analysis of the flow field using a laser sheet is extensively used. However, the use of this method for quantitative purposes is generating interest these days and is usually referred as the particle image velocimetry. Buchhave (1992) had reviewed the particle image velocimetry method and compared the technique with conventional quantitative methods like LDA and hot-wire anemometry.

3 Objectives of the present work

The study of the flow field generated by jet to jet impingement in a confined space will enhance the understanding of the impingement mixers (like those used for RIM) or the side dump combustor. This will help in a better design of the present day mixers. The main objective of this study is to investigate experimentally the flow field generated by jet to jet impingement of two opposed laminar jets near the closed end of a cylindrical chamber. In particular, the effects of jet Reynolds numbers, viscosities and positions of closed end (piston positions) from jet axis on the flow field have been investigated. Flow visualization and laser Doppler anemometry are used for this investigation.

Initially, the acid/base (indicator) method was used to observe the mixing region. The method was not useful because of the poor color contrast of the flow field generated within the mixhead. Also, this method requires water as the working fluid. Thus, the effects of higher viscosities can not be easily investigated. The hydrogen bubble method was also rejected due to similar requirement of water as working fluid and insertion of electrodes in the flow field of interest. The insertion of electrodes may generate some permanent disturbance in the flow field. In the present study, the analysis of the flow patterns has been successfully carried out by dye injection and suspended particles flow visualization methods. Flow patterns were obtained on 35 mm slides and 8 mm video films by illuminating complete or partial flow field using flood white light or light sheets (laser and white). Qualitative and some quantitative information are extracted from flow visualizations methods.

Equipped with the information obtained with flow visualization, the quantitative information of the velocity field in the mixhead is obtained by laser Doppler anemometry (LDA). The LDA method is selected due to its following inherent advantages over methods involving probes:

1. It is nonintrusive and thus the flow is not disturbed. It can be used in flows that are hostile to material probes.
2. LDA is independent of the thermophysical properties of the fluid in contrast to thermal probes (hot-wire anemometer) or chemical probes.
3. LDA allows the measurement of one or more components of the velocity vector, independent of the fluctuation intensity (e.g. reversals could be sensed).
4. The ability to follow rapidly changing velocities in the fluid provided that sufficiently fast electronics is used.
5. The response is linear and needs no calibration.
6. Operation is not seriously affected by temperature.

LDA can only be applied for transparent models and fluids. To use LDA for flow studies, particle seeding is necessary to scatter the laser light. In this study, the mixhead has been made using plexiglass and the working fluid is mineral oil. Thus, both the model and the fluid used are transparent. To scatter the laser light, polystyrene particles are used for necessary seeding.

4 Experimental setup and procedures

4.1 Model and flow system

A mixhead has been designed to study the influence of geometric and flow parameters on the flow field developed due to the jet to jet impingement in a confined space.

The model mixhead has been fabricated from a solid block (101.6 mm x 50.8 mm x 222.25 mm) of plexiglass (acrylic) then finished and polished as shown in Fig. 4.1.1. A hole of diameter 25.4 mm was drilled through the center of the block to create the mix chamber. This chamber was polished to make the model optically transparent for laser beams and ordinary light. This chamber diameter will be further referred as the mixhead diameter (D). As shown in the Figure 4.1.1, two holes of 2.38 mm diameter (d) were also drilled and were used as two opposing jets impinging fluid in the mixhead with a jet impingement angle of 180°. Thus, the ratio of mixhead diameter to jet diameter (D/d) is 10.67 to 1. Two taps of 6.35 mm (1/4 inches) NPT were also made to facilitate the piping connections. A counterbore of diameter 38.1 mm and 6.35 mm deep was drilled at the top of the mixhead. A 152.4 mm long tube of 38.1 mm outer diameter and 25.4 mm internal diameter was glued at the counterbore. The other end of the tube was connected to a plug with 12.7 mm NPT female threads. A T connection was fitted to this plug. On one of the outlets of this T connection, a pressure gauge was attached to indicate the fluid pressure in the mixhead. On the other outlet, a gate valve was attached to obtain a specified back pressure in the mixhead.

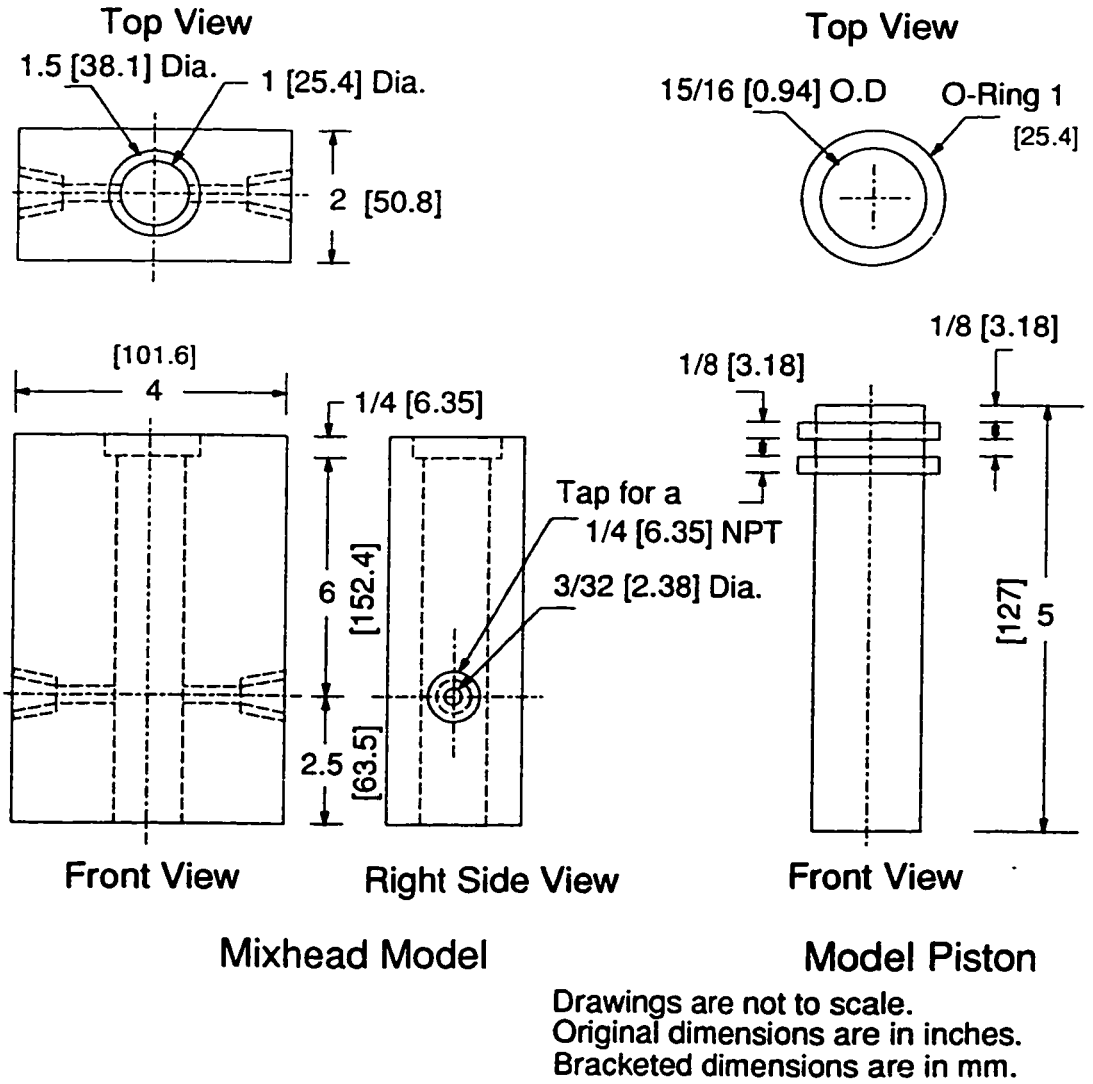

Fig. 4.1.1: Schematic diagram of the mixhead model

The piston was a 127 mm long solid plexiglass rod of diameter 23.81 mm. Two O-rings of 25.4 mm outer diameter were fitted on this piston as shown in Fig. 4.1.1. A 12.7 mm screw (24 thread per 25.4 mm) was used at the bottom of the piston to precisely control the vertical movement of the piston in the mixhead. This whole model was fixed within a frame of 12.7 mm thick aluminium plate as shown in Fig. 4.1.2. This frame was designed in such a way that the optical access to the model is available from all the sides (front, back and also from sides) except top and the bottom. A 3-D sketch of the model with the coordinate conventions used in this thesis is shown in Fig. 4.1.3.

The model with the flow system is shown in Fig. 4.1.4. Two positive displacement pumps (Robbins & Myers Canada Ltd., SP 33104 MOYNO Pumps) are used to supply working fluid from a tank to the mixhead. Each pump is run by a TEFC D.C. motor (1/2 HP, 1800 RPM) whose speed is regulated by a controller (Bronco model 110 SCR). This controller provided the setting for motor speed from 0 to 100% of its rated RPM of 1800 with 2% increment. During all the experiments, a fixed setting of 50% was used to avoid the influence of the speed of the motor on the system. Various recycling valves are used to control the fluid flow in the mixhead and the amount of fluid entering the jets is measured using two rotameters (Brooks model 1110-08H2G1A with float 8-LJ-48). The liquid from the mixhead outlet is either returned to the supply tank or discharged into the drain. Two spring loaded safety valves are used in the system which automatically open at 620 kpa (90 psig). The pressure drop in the system is observed to be negligible. Thus, depending on the fluid viscosity and flow rate a pressure of 10 to 30 psi is maintained within the mixhead by adjusting a gate valve located at the outlet of the mixhead.

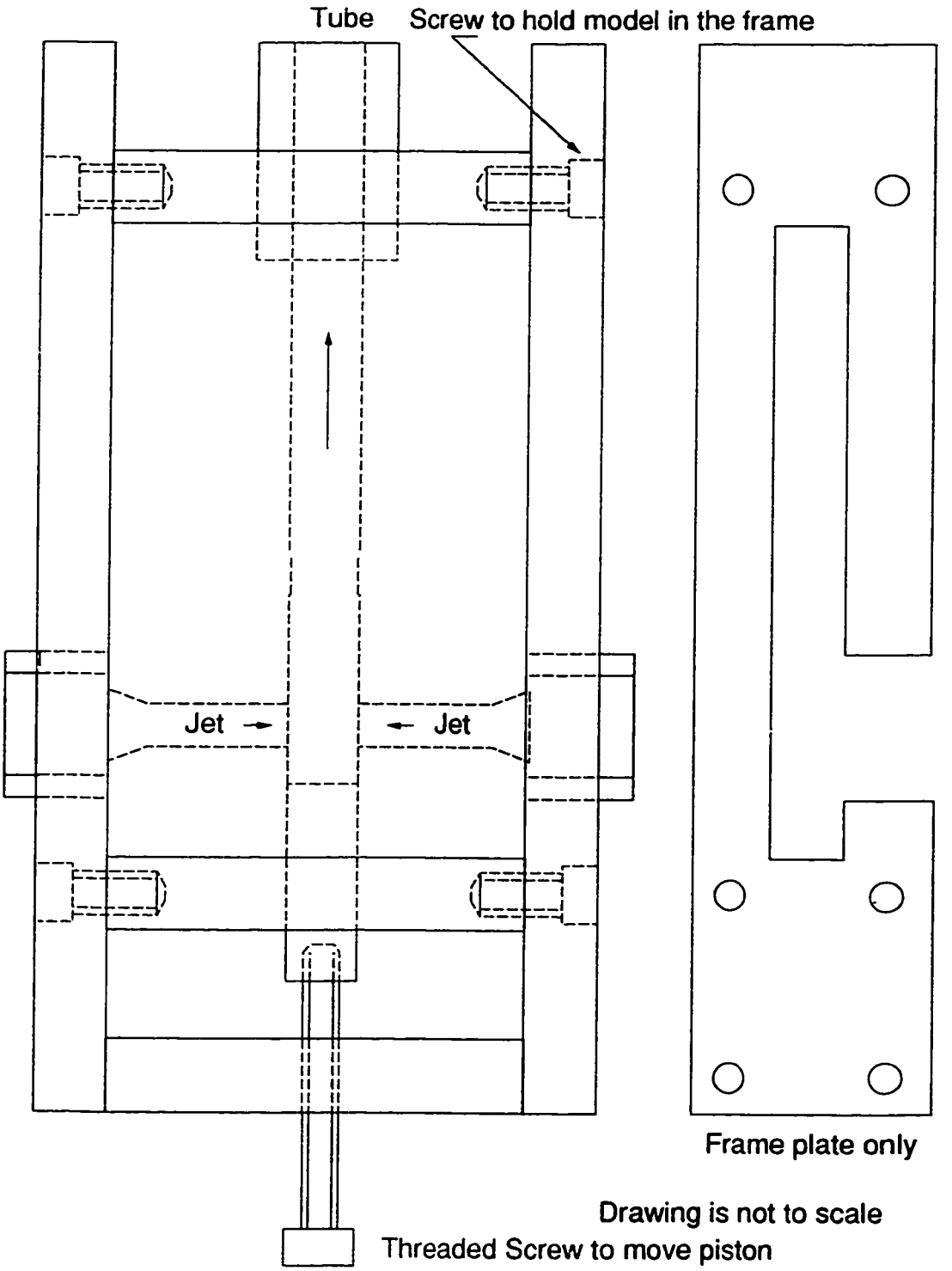

Fig. 4.1.2: Diagram of the model with frame

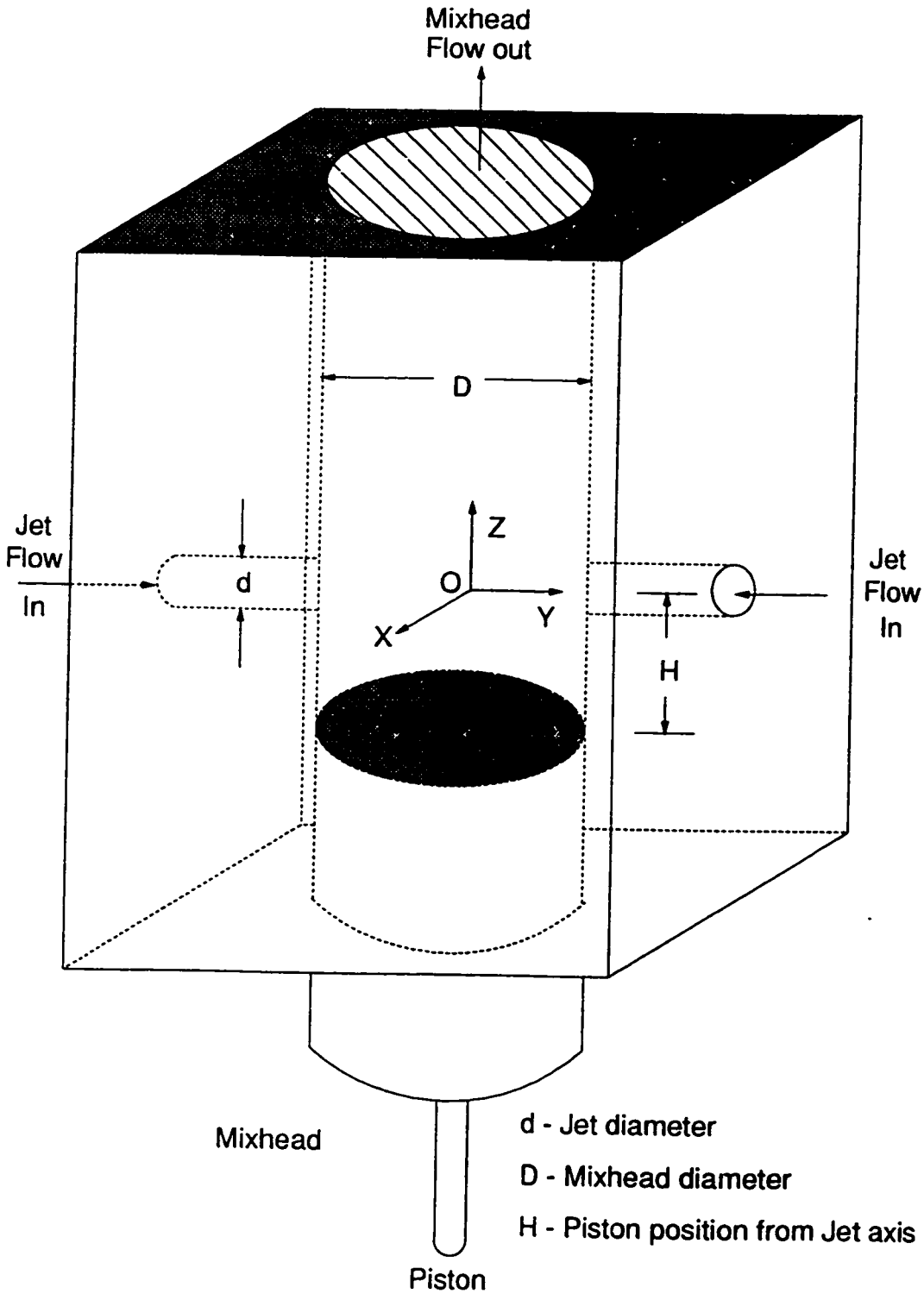

Fig. 4.1.3: 3-D diagram of the model and coordinate configuration

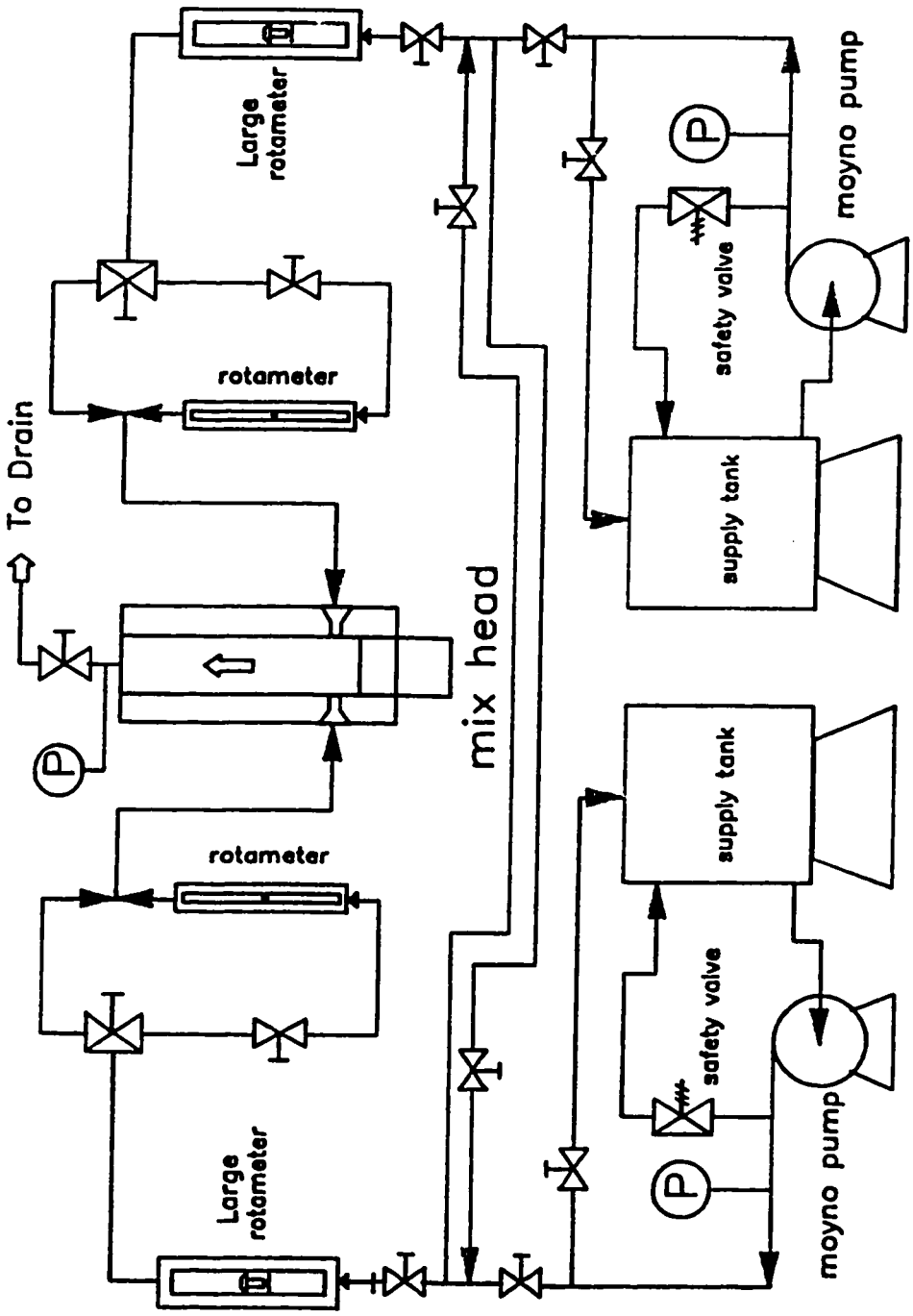

Fig. 4.1.4: Flow diagram of experimental setup

Two pumps were installed in the system (one for each jet); however, the piping network was so designed that one pump was sufficient to operate the system within the range of flow parameters of the present study. The use of a single pump eliminates the effects of variation in the speed of the two motors on the flow pattern which was unavoidable if two separate pumps are used to control the flow.

Prolonged pumping generates heat which increases the temperature of the working fluid especially at higher viscosities. The temperature increase reduces the viscosity and thus, increases the jet Reynolds number. The working fluid is maintained at a constant (room) temperature of 24°C during the experiments by using a cooling water coil immersed in the working fluid of the supply tank. The fluid in the supply tank was continuously stirred and the flow of water was regulated by adjusting a valve at the inlet of the cooling coil. This cooling network is not shown in the Figure 4.1.4 to maintain the clarity of the figure.

Copper tubes have been used for the piping network to the rotameter outlets. These outlets were further connected to the model using flexible Tygon tubing. Tubing provided the flexibility for the movement of the model and installation of dye injection port or syringe pump in the system as required during flow visualization experiments.

4.2 Flow visualization methods

The flow patterns created in the mixhead are observed by (i) dye injection, and (ii) suspended particle illumination methods. Permanent records of flow visualization are obtained using 35mm slides and 8mm video films.

4.2.1 Dye Injection

The dye injection method was used with water or a mixture of water and glycerine as the working fluid. The mixhead setup is shown in Fig. 4.2.1.

The dyes used are food coloring (Lowes Food Products Ltd.). These dyes in concentrated form have densities (red dye 1.127 g/cc and blue dye 1.088 g/cc) that are slightly higher than the working fluid density (1.00 g/cc). It is essential to match the dye solution density to that of the working fluid. A dye solution was prepared by mixing concentrated dye (1 or 2 cc) in 25 cc of working fluid and the density was measured. A few drops of ethanol were added to this dye solution, if necessary, to match the dye solution density to the density of the working fluid.

During the experiments, the total volumetric flow rate is measured by collecting the working fluid in a graduated cylinder within a specified amount of time measured with a stop watch. The jet Reynolds number is obtained using this volumetric flow rate through the mixhead (see Appendix A). If the calculated jet Reynolds number is not equal to the required Re, necessary changes in flow rates are made with rotameter settings. The jet Reynolds number is maintained within ±2% of the desired jet Reynolds number. In figures where comparisons are reported between various flow regions, the desired Re are used for captioning of figures (Chapter 6).

The back of the model is illuminated using a 300 watt tungsten light. A sheet of white paper is introduced between the light source and the model to reduce the intensity of the light. During the experiments, a 35 mm (Nikon F3) camera with 50mm lens and 7x magnification close up lens loaded with a Kodak color film of

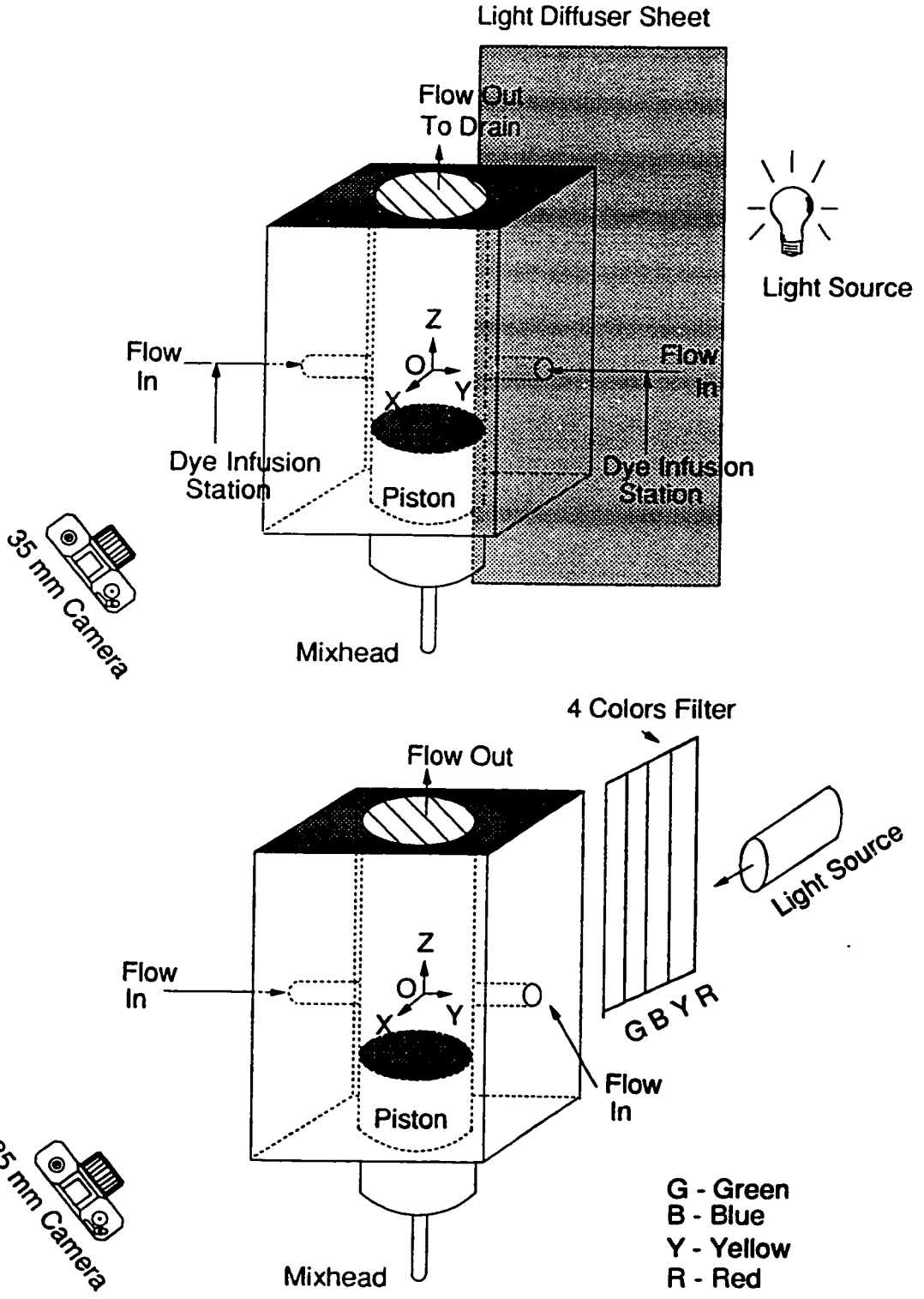

Fig. 4.2.1: Mixhead setup for dye injection and color filters

100 or 200 ASA is used for making slides. The camera faces the front of the model, and the light source and camera are on the same axis of the model (X-axis). The dye is injected into the fluid of either one or both jets using either a 10cc medical syringe or a syringe pump (Sage Instruments model 355). Once the flow disturbances due to dye injection subside (less than one second), photographs of the flow field are taken. Time varying features are captured using an 8mm video camera in place of the 35mm camera. The 35mm slides are taken at various aperture openings and shutter speeds. This information is given with the individual figures (Chapter 6).

4.2.2 Suspended solid particles illuminated by tungsten light (3-D)

Spherical polystyrene particles of roughly 40 μm diameter are mixed in the supply tank of the continuously stirred working fluid (mineral oil of 39 cp and 75 cp). The mineral oil batches of these viscosities are prepared by mixing mineral oil of viscosity 256 cp (Paraflex from Petro Canada Ltd.) and mineral oil of 4 cp (IsoparM from Esso Canada Ltd.) at 23°C. These polymer particles are good reflectors of light, small and have a similar density as the working fluid. The flow patterns generated in the mixhead are obtained by capturing the reflected light from these suspended particles on 35mm slides and 8mm video tapes. Laser (He-Ne) and white light are employed as light sources for the illumination of these particles. The fluid from the mixhead is returned to the supply tank. Thus, the flow system becomes a closed loop system. Depending upon the light source and the flow field under study, three variations of this method are used.

Fig. 4.2.1 shows the experimental setup (for these experiments, color filters are not used). During an experiment, the light source (Reticon Co. model IS703 with 300 watt Tungsten light) is activated after the steady state of the flow system is reached. This light source emits parallel straight beams of white light. Ideally, the light source should be parallel to the Y-axis and XY plane. This configuration was not possible, so the light source was inclined 60° to 70° to the XY plane due to the tubing and jet inlet connections which partially hide the area of interest inside the mixhead. The slides capture a 2-D flow field (in the YZ plane). Hence, the particle motion in the X direction (depth of the field) can not be obtained from the slides.

Van Meel and Vermij (1961) used a modified illumination system to get both qualitative and quantitative information of the 3-D flow field from a 35mm slide. They used several parallel sheets of light with different colors as illumination sources. The movement of a particle in the third dimension with respect to the plane observed by the camera (X-axis in our case) is indicated by a change of its apparent color while traversing the various colored light ribbons. A color filter was built by sandwiching four different color strips (63.5 mm x 6.35 mm) between two transparent plexiglass sheets (63.5 mm x 25.4 mm). This color filter was positioned between the light source and the model as shown in Fig. 4.2.1. The color filter generates four adjacent colored light beams from the white light. Now the 35mm slides will show particles path lines in different colors. A change of color of a particle path line indicates the movement of the particle in X direction. The direction of particle movement (positive or negative) is can be obtained due to prior knowledge of the known order of different incident beam colors. It is

possible to visualize the flow field using many color filters to get many slices of the flow field. However, the colors will overlap each other due to diffusion even though the white light source is parallel and straight. Thus, information quality will be lost. During the present study, four color filters were found adequate since this method has been used only for qualitative comparisons.

4.2.3 Suspended solid particles illuminated by a laser light sheet (2-D section)

To precisely study the flow behavior in 2 dimensions, it is essential to illuminate only a very thin planar slice of the flow field. This is achieved by illuminating the flow field using a thin light sheet which is generated by passing a 7 mW He-Ne laser beam of diameter 1 to 2 mm through a cylindrical lens (6.35 mm glass rod). The axis of the camera is kept parallel to the direction of maximum light scattering which is perpendicular to the illuminating plane. The particles outside of this illuminated plane will generate some disturbing background light reflectance. However, Berslin and Emrich (1967) showed that the disturbances are minimized if there is no strong velocity component in the third direction. The flow patterns were obtained with exposure time of few seconds (1 to 2 seconds average mixhead velocity is 17 mm/s at Re = 50 with 39 cp mineral oil). An exposure time smaller than this resulted in underexposed slides. This was due to low intensity of the laser light sheet. With the tungsten light as a light source an exposure time of only 1/250 second was found to be sufficient to obtain the flow

patterns. Thus, the flow patterns obtained with this method represent the integrated behavior of the flow field as compared to instantaneous flow patterns obtained with previous methods.

Three different sections of the model are illuminated with the laser light sheet. The experimental set up with illuminated sections are shown in figs. 4.2.3.1 and 4.2.3.2. These Figures show an idealized experimental set up. In practice, there is a problem in taking slides for all the planes (XY, YZ, and ZX planes). At constant X (YZ plane) slides, the flow field is illuminated by an inclined laser sheet as described earlier to overcome the optical obstructions in the neighborhood of the jet axis. At constant Y (ZX plane) slides, a small portion of the jet impingement region can not be pictured due to piping obstructions. At constant Z (XY plane) slides, the camera can not be kept parallel to the Z-axis at all due to obstructions at the outlet of the mixhead. For XY plane images, the camera was kept at a 60° to 70° to Z-axis looking from the front face of the model. Thus, the slides show an elliptical cross-section instead of actual circular cross section.

4.3 Laser Doppler Anemometry

In wave propagation, frequency changes can occur due to the movement of the source, receiver, propagating medium, or intervening reflector or scattering medium. These shifts are generally called Doppler shifts. In the velocity measurement, there is no relative movement between the source and receiver. The shift is produced by the movement of a particle that reflects or scatters light from the source to receiver.

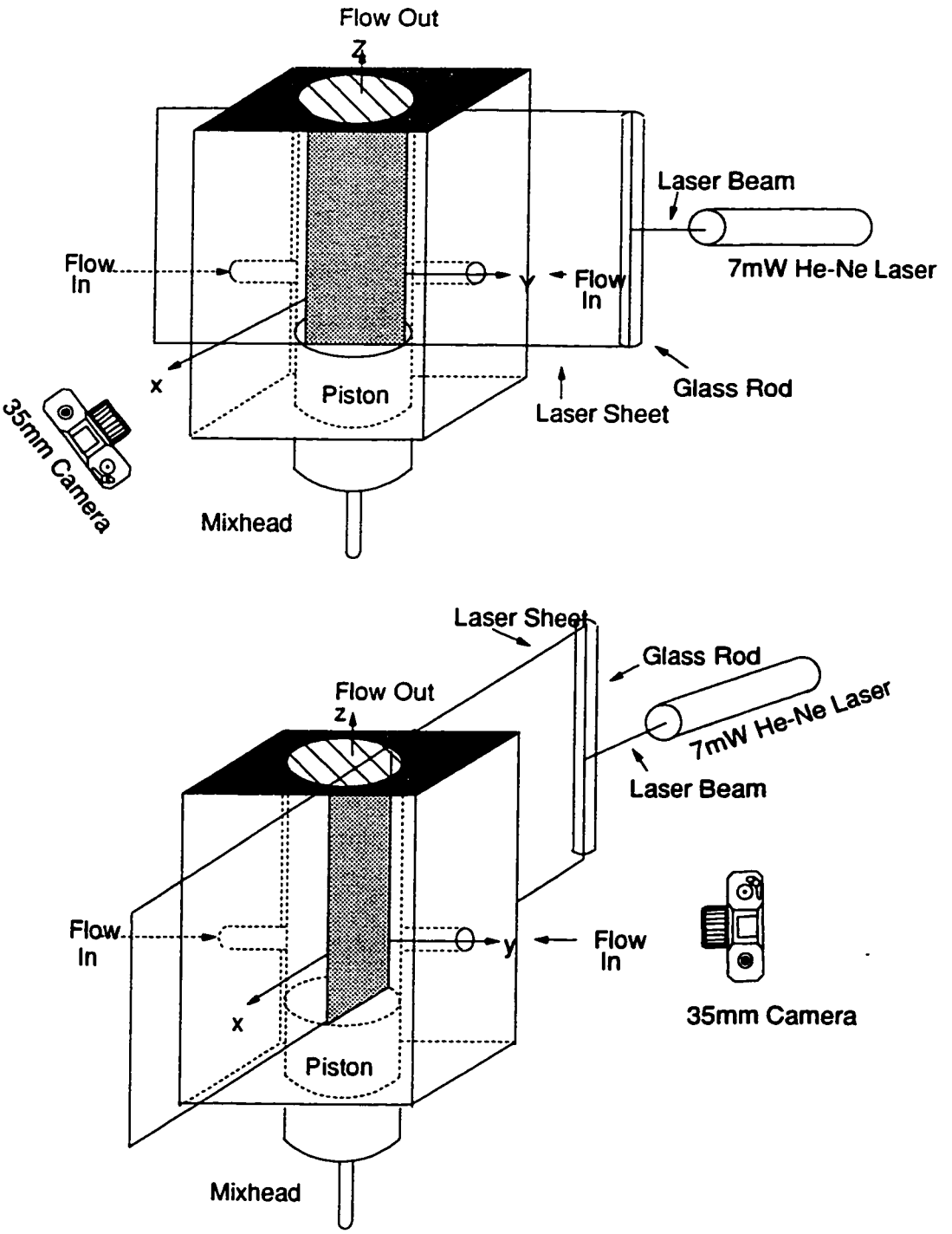

Fig. 4.2.3.1: Setup for flow visualization of X and Y - planes (2-D)

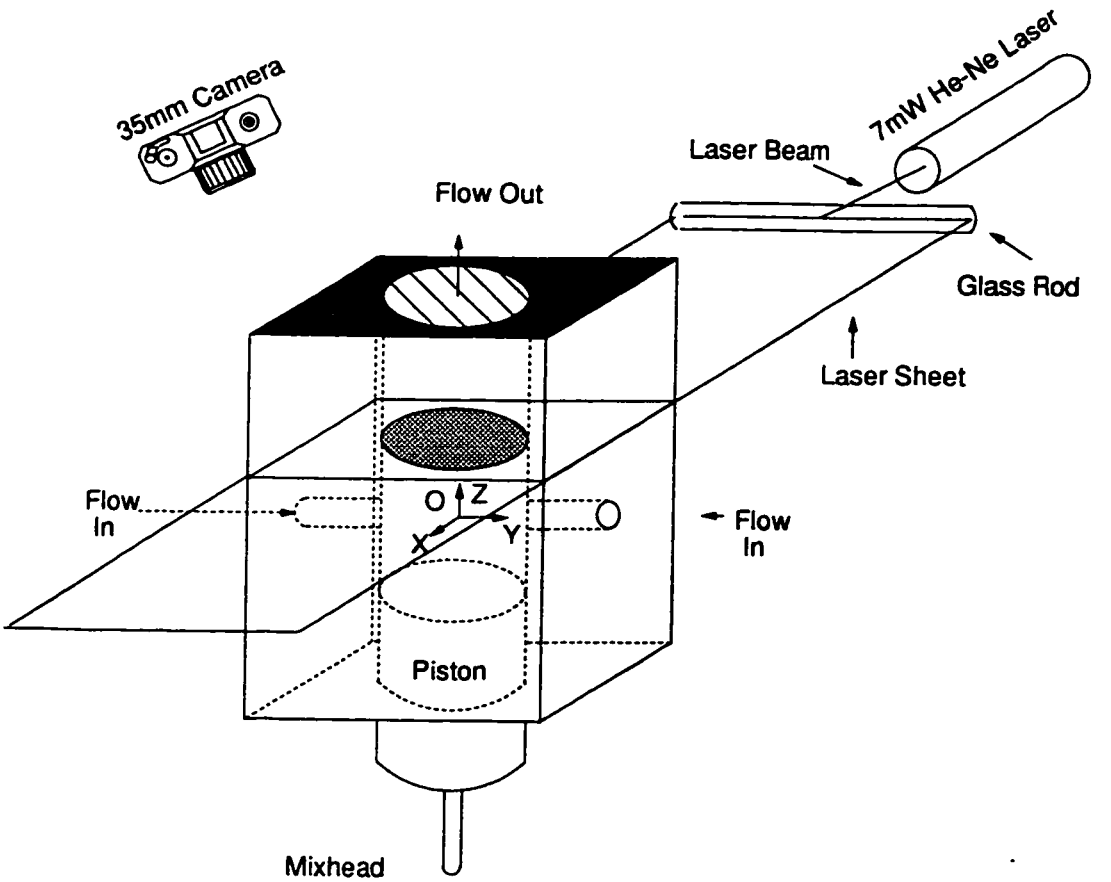

Fig. 4.2.3.2: Setup for flow visualization of Z - planes (2-D)

4.3.1 Heterodyning

The velocities in flow measurements are very small compared with the velocity of light, thus the corresponding Doppler shifts are also very small. For example, the Doppler frequency shift produced by a gas flow of 500 m/s is approximately 200×10^6 Hz, while the shift observed in 1 mm/s convection flow will be approximately 400 Hz (Adrian 1983). While these frequencies can be measured readily and accurately by modern electronics, they are miniscule compared to the basic frequency of laser light, which is on the order of 10^{14} Hz.

The technique suitable to measure the very small Doppler shifts uses the principle of heterodyning (or beating of two frequencies) in a device having a non-linear response. In LDA, the Doppler shifted scattered light is heterodyned either with unshifted light obtained directly from the original source or with further scattered light having a different shift because it is scattered through a different angle or from a different point. As shown in the Fig. 4.3.1.1 the laser light is split into two beams. Most of the light is focused by a lens to a point in the flow where the velocity measurement is required. Light scattered from the particles is received by the photomultiplier tube. The reference beam is directed to the detector by mirror. It is desirable that it is incident at the detector along the same path as the scattered light. The output from the photomultiplier contains a signal of the difference frequency between two beams which is the Doppler frequency.

There are three distinct modes of LDA optical systems, based on the three methods of combining the Doppler shift phenomenon with the optical heterodyne technique to develop a flow velocity measuring instrument. These modes are called

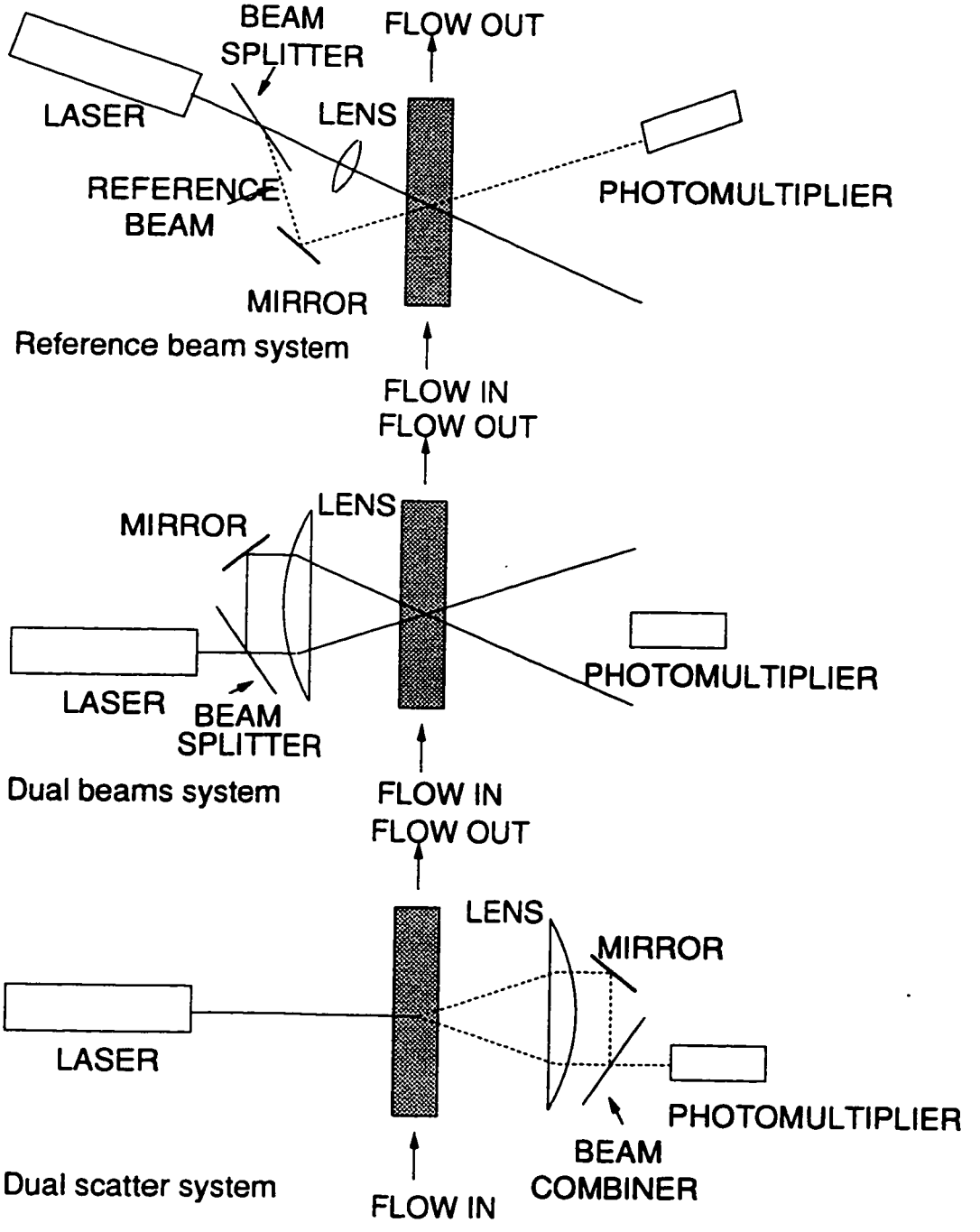

Fig. 4.3.1.1: 3-modes of heterodyning for LDA (from Drain 1980)

reference beam system, dual beam system and dual scatter system. These three modes are shown Fig. 4.3.1.1. In the reference beam mode the scattered light is mixed with a reference beam to detect the frequency difference. Only one light source is required at the measuring volume. In the dual beam mode, two plane light waves propagating in two different directions illuminate a scattering particle. This particle scatters two waves which are optically mixed to observe the Doppler shifts. The dual scatter mode uses a single illuminating beam as does the reference beam mode, but the hetrodyne detection is accomplished by mixing the two light waves scattered in the two different directions. The dual-beam mode is used in this study.

4.3.2 Dual-beam mode of LDA

The dual beam LDA can be easily described in two ways; either by Doppler shifts or by fringe model. The description by the fringe model is much easier to visualize than the Doppler shift model.

The light waves of the two illuminating beams interfere at their crossing and thus fringes (regions of high and low intensity due to positive and negative interference) are formed at the intersection of these beams. The laser beam generally has a Gaussian intensity distribution (George 1988). This intensity distribution of the laser beam reaches a minimum diameter at the beam waist where phase fronts are planar. This beam waist of the laser beams must be located at the point of their intersection. This generates approximately parallel and equally spaced interference planes (Hanson 1975). A particle moving through the crossing point in the plane of the two beams goes through patterns of very low intensity

and of high intensity (Fig. 4.3.2.1). The frequency of the signal (ν_D) is proportional to the velocity with which the particle is moving across the fringes. The fringe distance (d_f) depends on the wave length (λ) and angle (θ) through the relation:

$$d_f = \frac{\lambda}{2\sin\left(\frac{\theta}{2}\right)} \qquad (4.3.2.1)$$

Then the velocity u:

$$u = \nu_D d_f \qquad (4.3.2.2)$$

Only the intersection angle (θ) and laser wavelength (λ) are required for interpreting the frequency in terms of the velocity. These are usually fixed by the optics and laser used. There is ambiguity in the system; however, in that it can not distinguish between reverse flow or forward flow. This is corrected by zero offsetting using the frequency shift.

4.3.3 Frequency Shifting

The standard LDA system has a 180° direction ambiguity i.e. it can not tell whether the flow is forward or backward. In many flow systems, such as highly fluctuating flows or recirculating flows, the lack of a direction criterion becomes a major limitation of LDA. This limitation has been dealt with by introducing the frequency shift.

In the dual beam mode crossing of two beams of the same frequency causes a 'stationary' fringe pattern. If one of the beams is shifted relative to the other

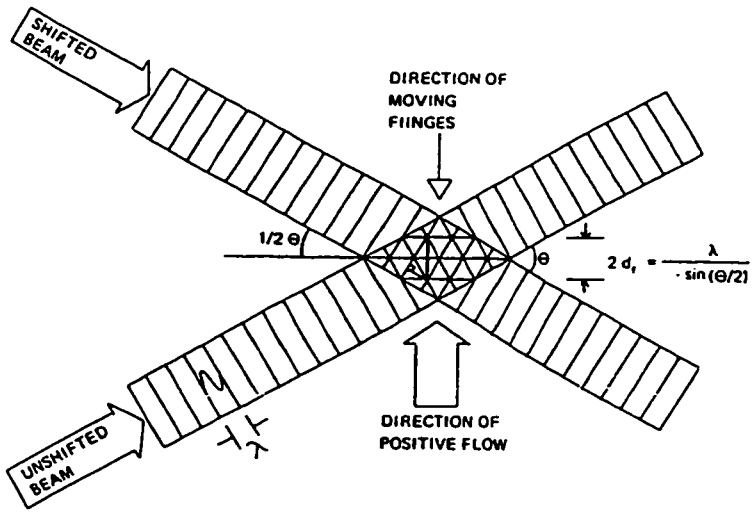

Fig. 4.3.2.1: Fringe model for dual beam mode (from DANTEC 1986)

beam (40MHz), the fringes can be thought of as 'moving' at zero flow condition. Movement of the particles in same direction as the 'moving fringes' will decrease the frequency shift while movement in the opposite direction will increase the frequency shift. Techniques used for frequency shifting are the Bragg cell and rotating diffraction gratings. In this system, the Bragg cell is used which shifts one of the beams by 40MHz. This is called optical shifting.

The photomultiplier converts the total flux of light energy into a voltage signal. This voltage is the inputted into the signal processor. The total light flux is the sum of the background light flux (e.g. room light, radiation from fluid, reflection and flare), the pedestal light flux, and the Doppler light flux. The pedestal light flux is the light received when a particle crosses each beam or the light scattered by a particle if one of the beams is absent. As far as the signal from one scattering particle is concerned, the pedestal signal can be completely separated from the sinusoidal one. However, in fluid flows with large variations of velocity with time the section of the frequency spectrum belonging to the pedestal of Doppler signals of a high velocity particle interferes with the frequency spectrum of the signal containing a low-velocity particle. This problem is solved by mixing the photomultiplier signal with a variable frequency shift generator signal f_{LO}. The mixer output signal f_d is fed to the counter processor for (see Fig. 4.3.3.1) electronic frequency shifting. Fig. 4.3.3.2 shows the measurement of motion of a flow with and without frequency shifting. In this LDA we use the combination of optical and electronic frequency shifting.

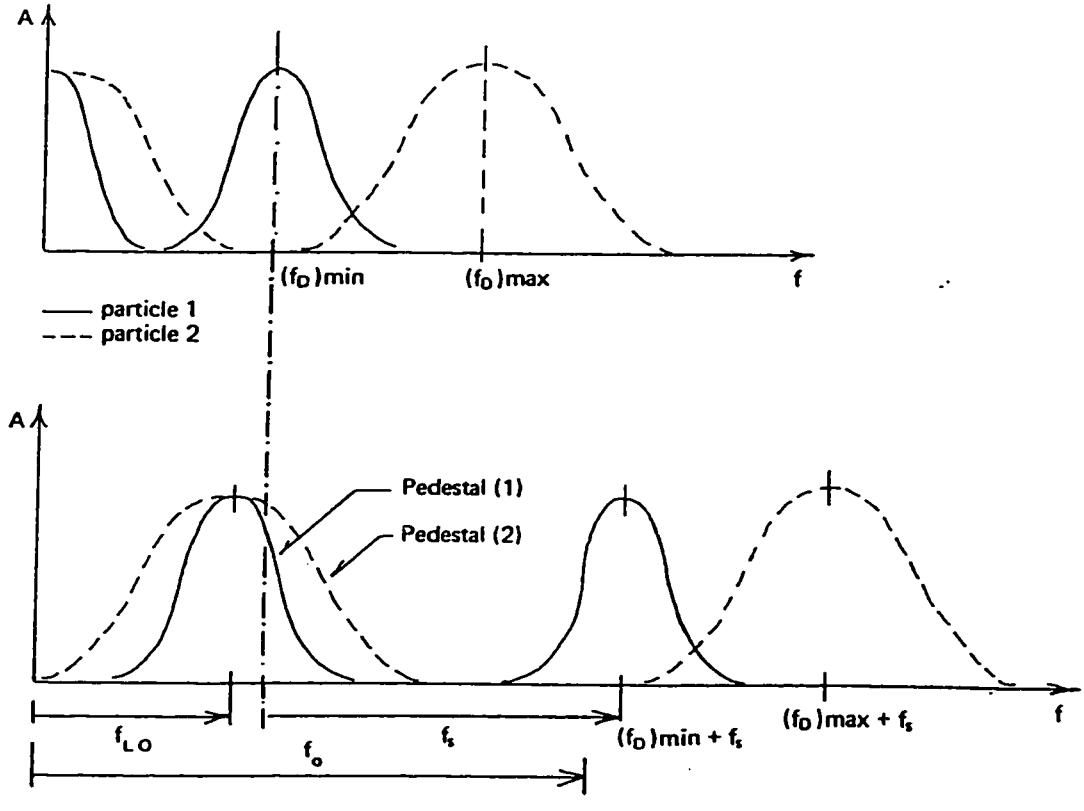

Fig. 4.3.3.1: Optical and electronic frequency shifting (from DANTEC 1986)

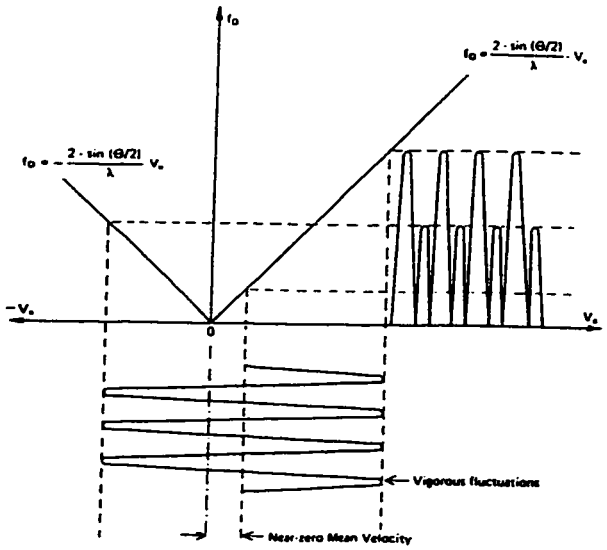

With out frequency shifting

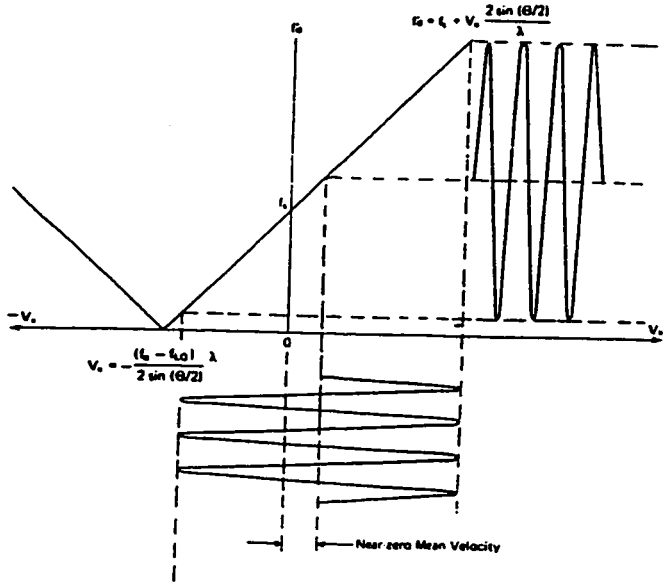

With frequency shifting

Fig. 4.3.3.2: Advantage of electronic frequency shifting

4.4 Laser Doppler Anemometry (Experimental Setup)

Instantaneous velocity measurements of the flow field, generated by jet-to-jet impingement in the mixhead, were obtained by the laser Doppler anemometer (LDA). Single component forward scattering differential mode LDA was used.

4.4.1 General Configuration

A platform was designed and constructed using 38.1mm (1.5 inch) angle iron. It is 1828.8mm (72 inch) long, 304.8mm (12 inch) wide and 914.4mm (36 inch) high. To avoid reflection from the platform, it was painted black. It was anchored to floor and leveled. The LDA optical bench (DISA 55x41/42), on which the laser and DISA 55X modular transmitting LDA optics are set, is mounted on this platform. The LDA setup without platform, is shown in Fig. 4.4.1.1. The mixhead model is fixed on a traversing table (3 axial directions traversing) whose motion in all three directions is computer controlled. The photomultiplier tube which receives the reflected light is mounted on another optical bench. The Figure also shows the relative position of the transmitting optics, mixhead and photomultiplier. The Figure does not show the frame and traversing table. The transmitting optics are fixed while the mixhead is movable. The photomultiplier (PM) is also movable in X, Y, and Z directions.

4.4.2 Optics

The laser beam (Spectra Physics model 127 35mW He-Ne Laser) first passes through a $\lambda/4$ retarder mounted on laser head and then passes to another $\lambda/4$ retarder

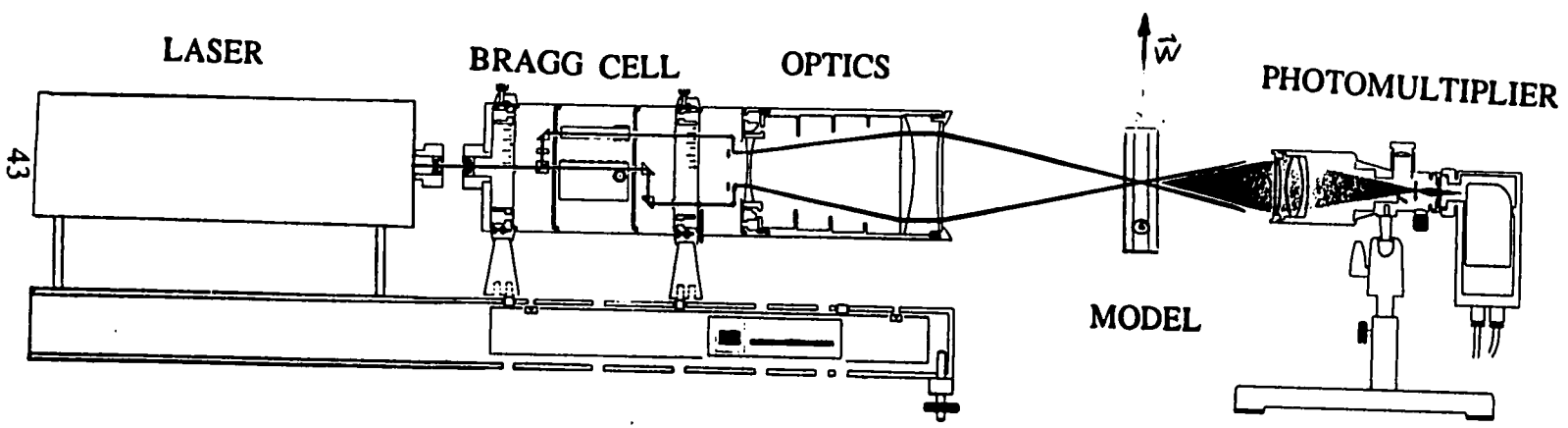

Fig. 4.4.1.1: LDA configuration (one component forward scatter mode)

mounted on the cover plate of LDA optics. The first retarder converts the linearly polarized beam to circularly polarized beam and the second converts the circularly polarized beam back to a linearly polarized beam with correct polarization direction relative to the optical axis of the optics. The beam waist is adjusted using the beam waist adjuster To optimize the fringe pattern quality in the measuring volume. This beam is divided into two beams with 50:50 ratio by a neutral beam splitter prism. The central beam is passed through the Bragg cell while the other half is passed through a glass rod to maintain the same optical path length for the two laser beams.

These two beams are passed through a backscatter section and pin hole section without any manipulation of the beam. Further, they are fed to the translator where the radial distance between the beams is controlled. Again, the beams pass through the beam expander. By expanding the laser beams they are focused into a smaller probe volume. A planoconvex front lens (focal length 80mm) is used to focus these beams into the model. The reflected light from the particle in the probe volume is collected by a photomultiplier which is mounted on an optical bench as shown in the Fig. 4.4.1.1.

LDA measurements are made for the probe volume where two converging beams from the front lens of LDA optics intersect each other inside the model. If the measurements are made in air then the probe volume is located at the optical axis f_l (focal length of the front lens) distance away from the front lens. In the present system, the laser beams travel through air, plexiglass (model material), and mineral oil (working fluid). The interfaces include plane and curved surfaces. The location of the intersection point of the beams in the model is essential. One

must know the intersection point of these beams, so that the LDA measurements (velocities) can be assigned to the proper location in the model. A method was developed and described in Appendix B to find the intersection point of these beams inside the mixhead.

4.4.3 Electronics

Besides the optical arrangements, the LDA experimental setup consists of a frequency shifter, counter processor, oscilloscope and a micro-computer. The counter processor is basically an electronic stop watch which measures the time a particle takes to cross a known number of interference fringes in the measuring volume. The distance between the fringes is known by the optics geometry and the wavelength of the laser light. The Doppler burst frequency is detected by measuring the time for a certain number of zero-crossings of the amplified and high and low pass filtered detector signal. The frequency shifter generates the combination of the optical and electronic shift with the aid of Bragg cell. The data (number of fringes and the time to pass the fringes) are collected on a micro computer which is specially equipped with a data collection board.

The block diagram for LDA setup is shown in Fig. 4.4.3.1 During the experiment, the adjustment of flow rate and focusing the reflected light on the photomultiplier tube are performed manually. The remaining operations (positioning of the model and data acquisition) are automatically controlled by a Zenith AT computer. This computer is especially equipped with a LDA data acquisition board (Model 1400 Struthers Technical Services) which is designed to communicate and collect data from Dantec 55L90a counter, and three PC21 indexer (MC

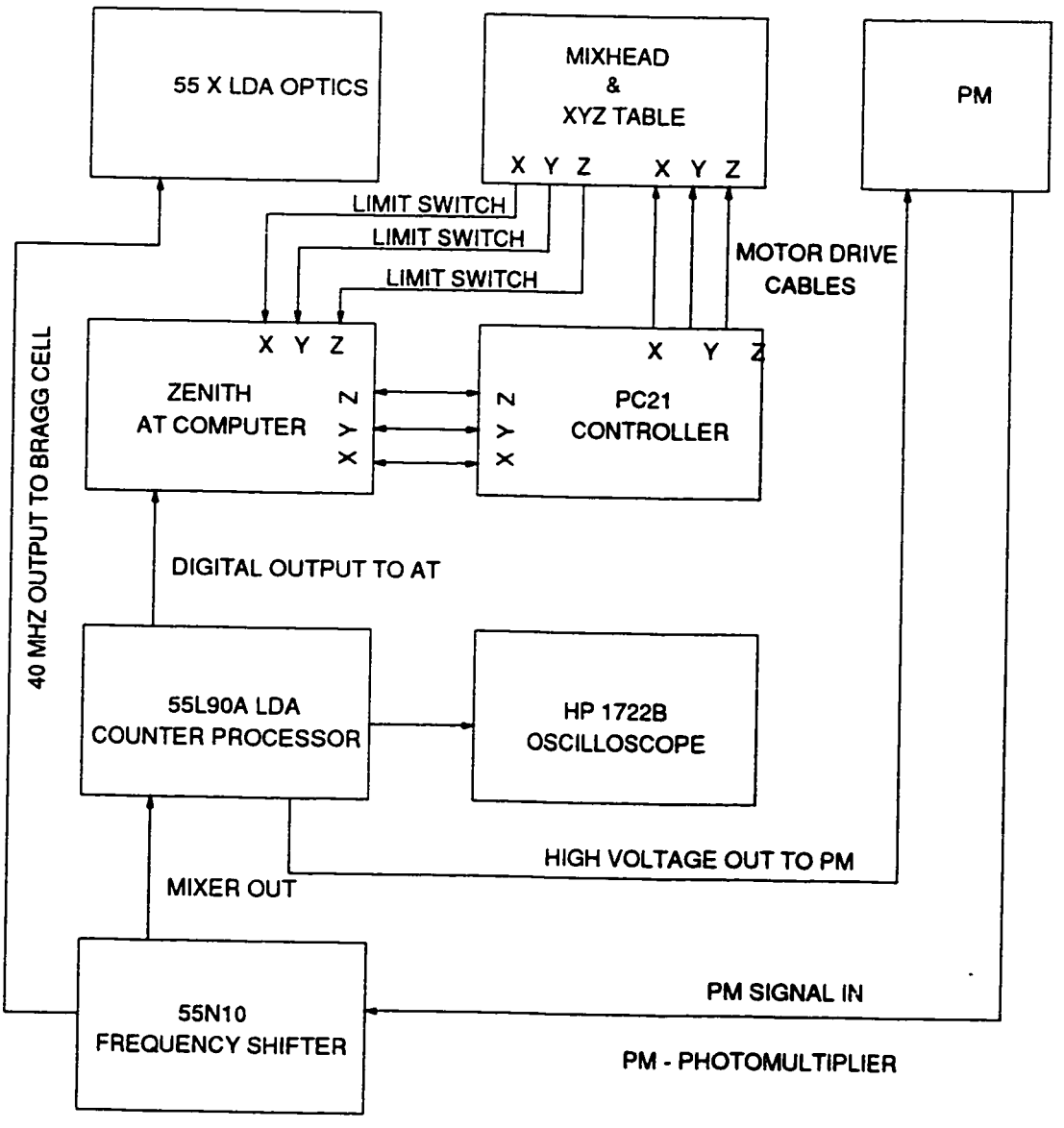

Fig. 4.4.3.1: Block diagram for LDA setup)

5000 controller from Daedal, Inc.) boards to drive motor/drive set for model positioning. Each PC21 indexer is used to move and control the mixhead positioning table (traversing table) only in one assigned direction.

The 40 MHz output signal from the frequency shifter is fed to the Bragg cell for acousto-optical shifting of one laser beam by 40 MHz. Thus, the direction of fluid motion is detectable. The reflected light coming from the particles in the fluid within the probe volume is collected by the PM tube which generates an electric signal. The high voltage to the PM tube is supplied by the counter. The electric signal from PM tube is shifted electronically to a known frequency by feeding it back to the frequency shifter. This is performed to detect near zero velocity. The mixer output from the frequency shifter is fed to the counter processor where, after proper conditioning, the signal is filtered by preassigned high and low pass filters. The digital output from the counter contains the information of the number of fringes (known distance) and time required to pass these fringes. Thus instantaneous velocity is calculated by dividing known distance with this time. This data is received by LDA data acquisition board and is stored in the computer. Also, an analog output from the counter is sent to oscilloscope where Doppler burst of LDA signal is displayed.

5 Data Acquisition and Statistical Analysis

5.1 Grid for LDA measurement

Quantitative information of the flow field generated by jet to jet impingement in the mixhead is obtained by LDA. As described in chapter 4, only one component of the velocity (U or V) can be measured at a time using the existing LDA setup. Based on the model symmetry and the conclusions derived from extensive flow visualization (chapter 6), the grid shown in Figure 5.1.1 is selected at which velocity components will be measured. Figure 5.1.1 depicts the grid projections in XY and YZ planes. The XY plane grid is generated using jet diameter (d) as the reference length. The YZ plane is formed using two reference lengths; the jet diameter (d) is kept as the reference length near the jet axis while the mixhead diameter (D) is used as a reference length beyond a half mixhead diameter (D/2) downstream of the impingement point along the jet axis.

5.2 Trigger Mode and Sampling Frequency

The LDA provides data only when small particles in the fluid cross the control volume (ellepsoid of 60x60x280 μm formed at the intersection of two laser beams). The particles (40 μm polystyrene (Tyler screen mesh -325 +400)) are uniformly distributed in the fluid. Velocity measurements from the passing of particles through the control volume can be acquired in two modes; LDA trigger and timer trigger. In LDA trigger mode, every new validated random event (data) from the counter

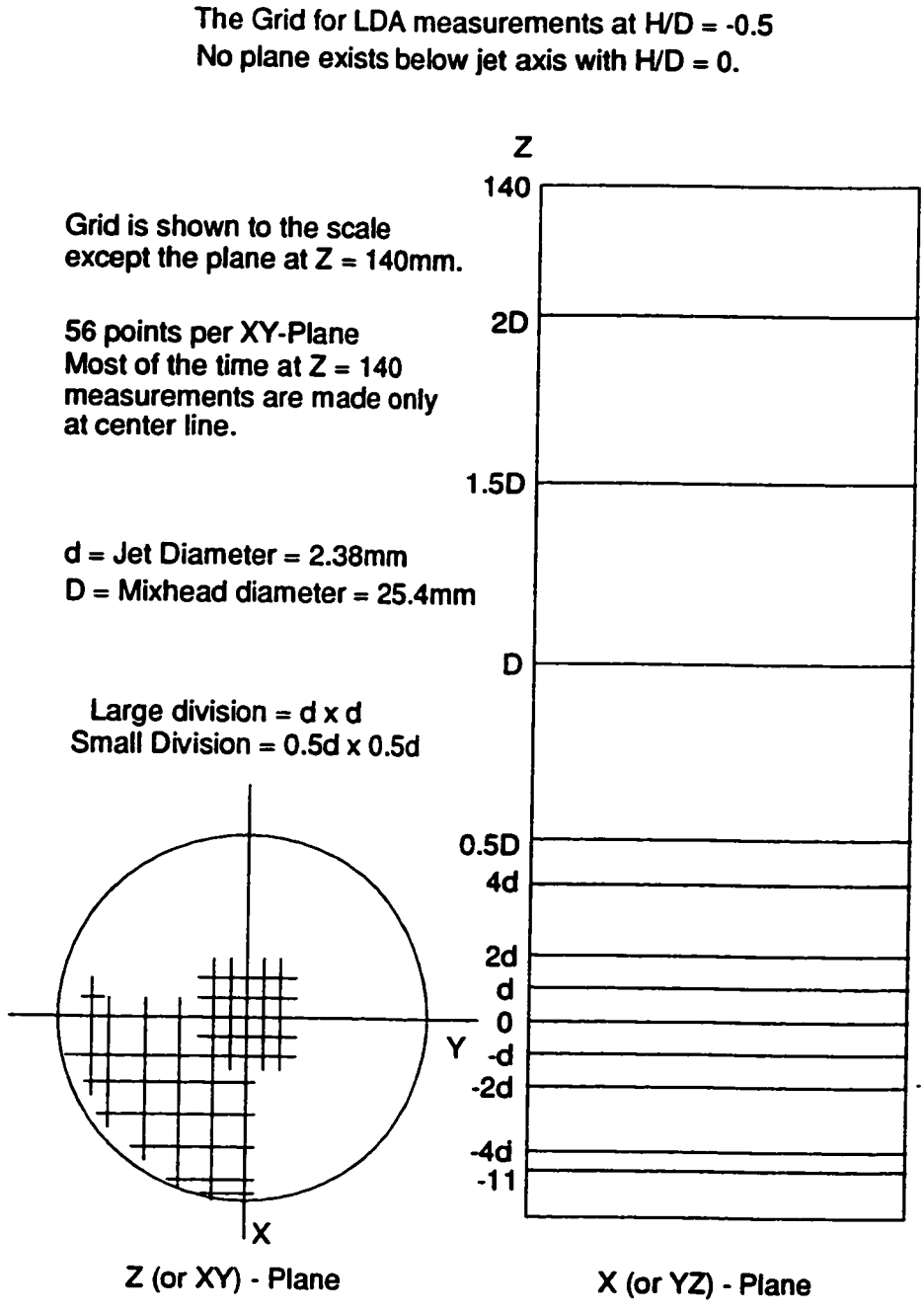

Fig. 5.1.1: Grid for LDA measurements

is collected along with the time of arrival. Hence, the time series of the velocity is unequally spaced. In the timer trigger mode, data are acquired from the counter at a prefixed sampling frequency using a "sample and hold" algorithm; thus, the time series is equally spaced. In this mode, if the counter has not received new data since the last acquisition, when the prescribed time interval has elapsed, the previous data from hold is taken as a new data. Both of these data acquisition modes have inherent advantages and disadvantages. In the LDA trigger mode, every data point in the time series is a new data point, while in timer trigger mode there may be some repetition in time series. For data analysis, the mathematics is developed best for equally spaced time series, both in time and frequency domains. The disadvantages of the timer trigger mode especially in stationary random processes are minimized to an acceptable level provided the data generation rate by particle crossings is sufficiently high and the data are collected at a suitable sampling frequency. In this work, the data generation rate is usually in kHz (~ 5kHz) with over 70% validation rate and a suitable sampling frequency is used which satisfies both required conditions to use the timer trigger mode.

The sampling frequency selected is 300 Hz. This is selected based on the Shannon's sampling theorem (Astrom and Wittenmark, 1984) and the comparison of experimental results obtained by two different modes of data collection. If ω_o is the highest frequency of interest in the system, then according to Shannon's sampling theorem, a continuous-time signal with a Fourier transform which is zero outside the interval $(-\omega_o, \omega_o)$ is given uniquely by its values in equidistant points if the sampling frequency is higher than $2\omega_o$. This is also known as Nyquist criterion. In this work, the highest frequency generated is 30 Hz due to the pump motor. Thus,

the frequency of 300 Hz which is 10 times the highest frequency generated in the system, is a suitable sampling frequency according to the above criteria and auto-oscillation up to 150 Hz can be detected.

The average velocities estimated using both modes for various flow parameter settings are shown in Figures 5.2.1 and 5.2.2 These velocities are obtained at various locations in the mixhead and jet Reynolds numbers ranging from 50 to 150. In these Figures, the average velocities obtained by LDA trigger mode are plotted against the average velocities obtained with timer trigger mode. A reference line which represents a perfect agreement between two modes, is also plotted at 45°. The mixhead axial velocities (V) obtained using timer mode are in excellent agreement with the same velocities measured using the LDA mode (Figure 5.2.1). Figure 5.2.2 shows excellent agreement between sampling methods for the radial velocity (U). Thus the selection of sampling frequency of 300 Hz seemed to be appropriate.

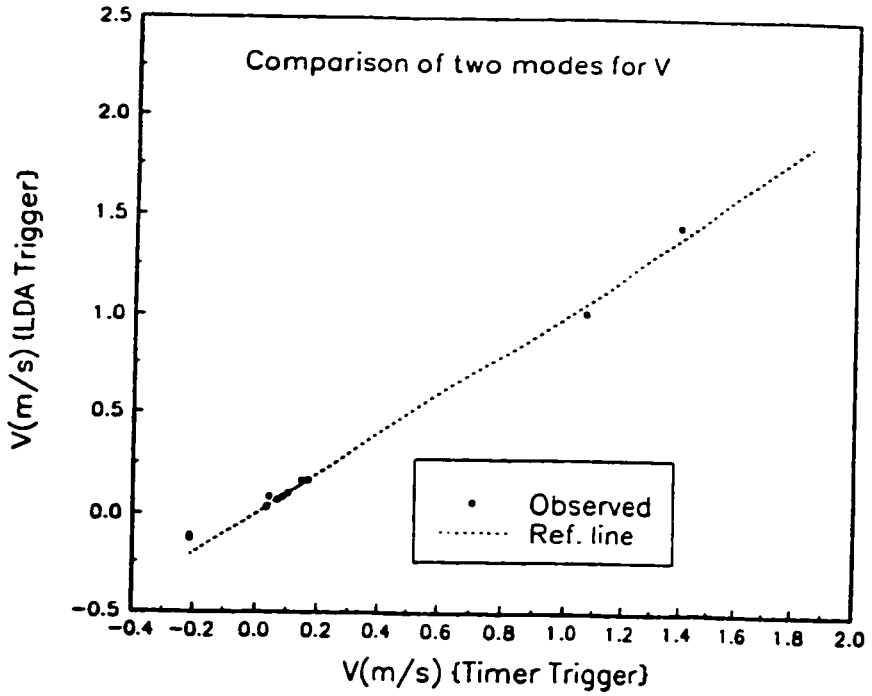

Fig. 5.2.1: LDA and timer trigger mode comparison with axial velocity (V)

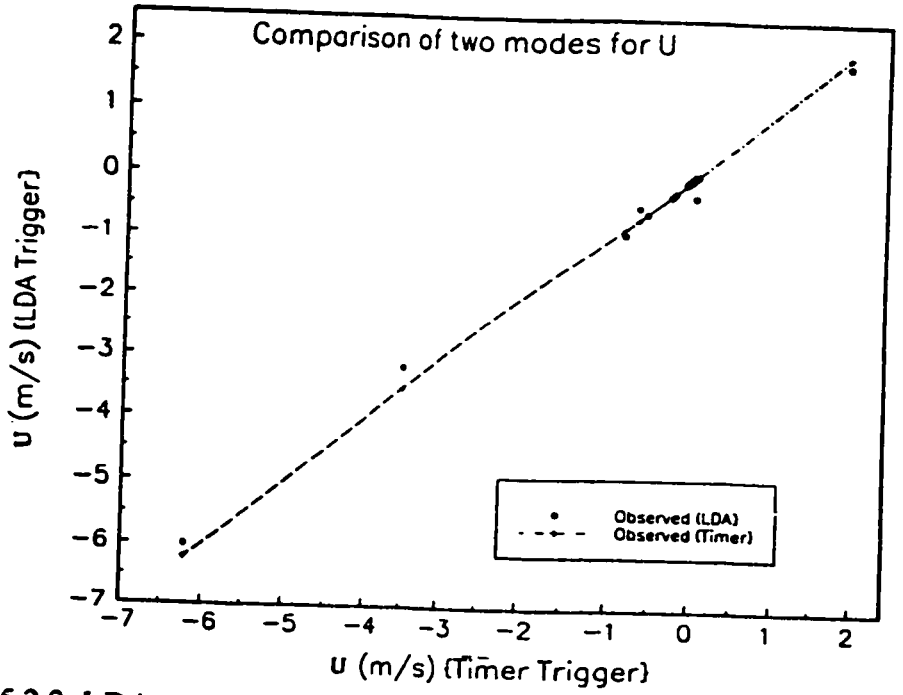

Fig. 5.2.2: LDA and timer trigger mode comparison with radial velocity (U)

6 Mixhead flow field visualization

6.1 3-D flow visualization

Investigations have been made to study the influence of fluid viscosity, jet Reynolds number (Re), and "clean-out" piston position (H/D) on the flow patterns developed by jet to jet impingement in the confined space of the mixhead. The configuration of the mixhead, origin (0, 0, 0), and X, Y, and Z axes are shown in the Figure 4.1.3.

Three different fluids; water, glycerine and mineral oils of two different viscosities ("light" (4 cp at 23°C) and "heavy" (255 cp at 23°C) have been selected. Water and glycerine as well as light and heavy mineral oils were mixed in different ratios to get a wide range of viscosities. The dye injection method is used to obtain the results described in this section. The range of H/D ratio, viscosity values, and visulization method for various Reynolds numbers are listed in Table 6.1.1.

The figures (colors and gray scale) presented in this section were prepared with the following method. A typical 35 mm color slide obtained for a flow visualization was projected on a screen. The projected image was captured on a 8 mm video camera (Cannon UC-10) and its output was fed to a computer equipped with frame-grabber (MIRO). These captured computer images were processed with Adode Photoshop (Version 3.0) software and printed on a color inkjet printer (HP 1200 300 dpi for color). In some cases, if the flow details were clear, only gray scale (600 dpi) was used for printing.

Table 6.1.1: Selected parameters settings for 3-D Flow visualization

Fluid	H/D	Viscosity (cp)	Method	Section
Water	-0.25	1.03	Dye	6.1.1
Water & Glycerine	-0.25	16.00	Dye	6.1.2
Water & Glycerine	-0.25	60.00	Dye	6.1.3
Mineral oil	-0.50	4.50	Dye	6.1.4
Mineral oil	0.00	75.00	Particles & color filter	6.1.5.1
Mineral oil	-0.50	75.00	Particles & color filter	6.1.5.2

6.1.1 Water (H/D = -0.25 & μ = 1.03 cp)

For the experiments in this section, a cylindrical tank (gravity tank) of 12 l capacity with an overflow stand pipe (constant hold-up 10 l) was kept on a higher elevation than model and was used to send the water to mixhead instead of pumps. The water flow to the model was controlled by changing the elevation of the tank and operating outlet valve at the mixhead. The experiment was conducted using water at Re = 44 and H/D = -0.25. The dye was injected from both sides. The jets bend downstream before impinging at the center (Fig. 6.1.1.1 (a)). Two vortices above the jet axis are also visible. In Fig. 6.1.1.1 (b) the vortex below the jet axis

a

b

Fig. 6.1.1.1 (a)-(b): Flow patterns with water at Re = 44 & H/D = -0.25 (f/2.8, 1/250 s) using gravity tank.

is clearly visible. Some transfer of the dye from one side to the other has also occurred. It seems that this transfer initiates at the tip of impingement plane and the impingement plane remains stationary. This may be considered as the *static stable mode* of the flow pattern.

Fig. 6.1.1.2 (a) (Re = 64) shows that the jets are not impinging on each other, while in Fig. 6.1.1.2 (b), the jets are impinging head-on. The impingement plane is oscillating and vortices are visible. It can be seen that one vortex is rotating clockwise in the upper right corner and the other one is in the bottom left corner. The bottom vortex is seen more clearly in Fig 6.1.1.2 (c) which was printed by changing contrast level of Fig. 6.1.1.2 (b). The jets are impinging (Fig. 6.1.1.3 (a) and (b) Re = 113 gray scale), both bottom vortices are visible. In Fig. 6.1.1.3 (a), the oscillating impingement plane is moved from center plane and all four different vortices are clearly visible. This impingement plane (pancake or disk shape) is captured close to center plane in the Fig. 6.1.1.3 (b). Three different vortices are also clearly visible. This flow pattern with an oscillating impingement plane and counter rotating vortices is in *dynamically stable mode*. That is, the jets impinge at a steady point but overall the impingement plane is dynamic. Further experiments were conducted at jet Reynolds numbers of 127, 170, 224, 230, 310, and 410. However, no significant change in the dynamically stable pattern of oscillating impingement plane and counter rotating vortices was observed. At these higher jet Reynolds numbers (Re > 127), the system is highly *unstable* and rapid mixing of the dye occurs. Thus the observability of a stable mode is very rare (Re > 127) because of 3-D mixing effects which obscure the visualization of the vortex structures.

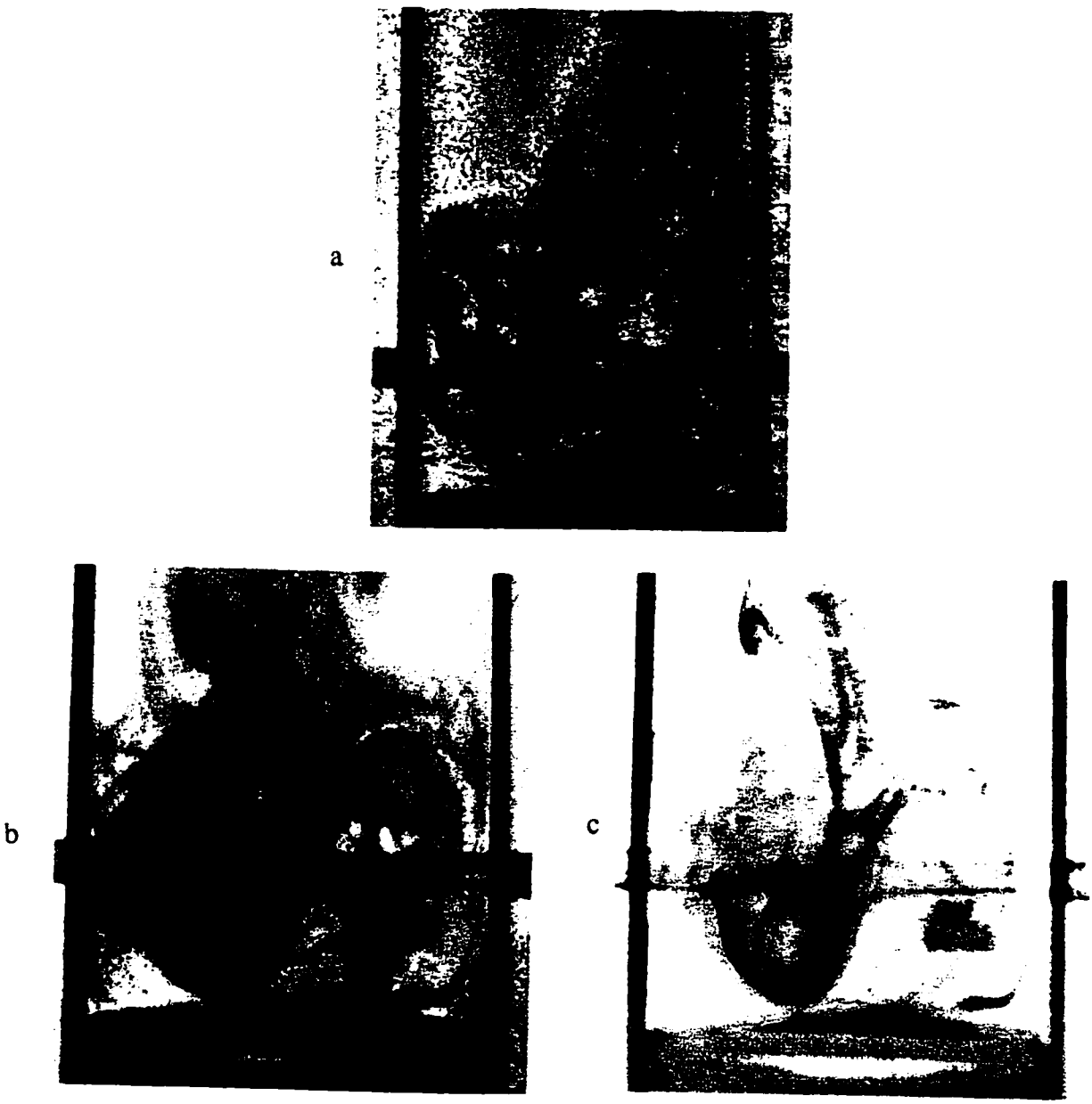

Fig. 6.1.1.2 (a)-(c): Flow patterns with water at Re = 64 & H/D = -0.25 (f/2.8, 1/250 s) using gravity tank.

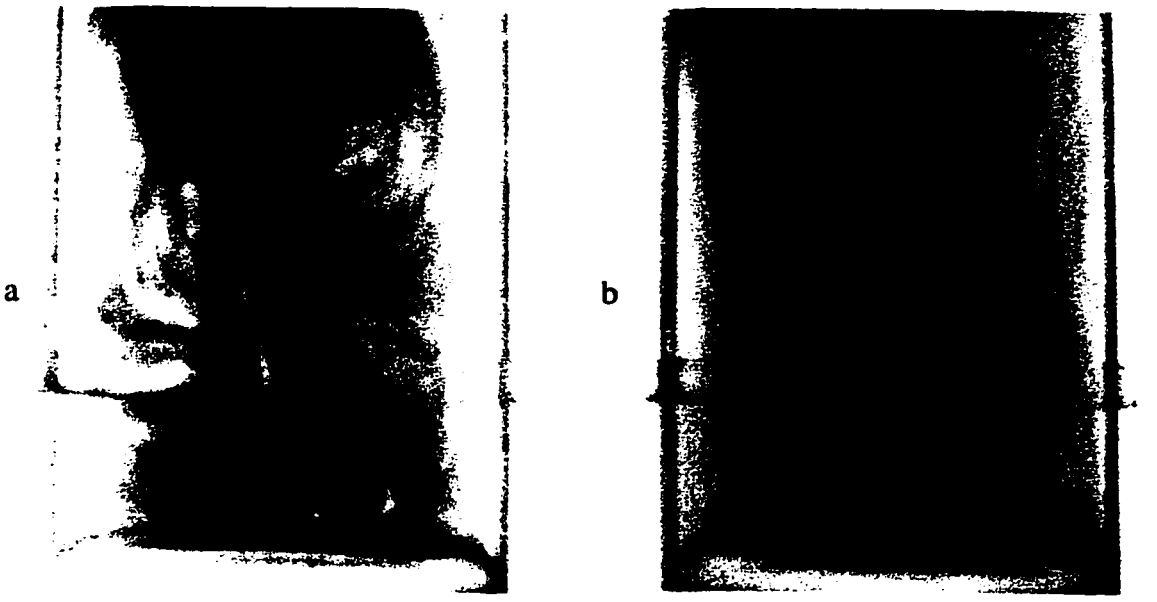

Fig. 6.1.1. 3(a)-(b): Flow patterns with water at Re = 113 & H/D = -0.25 (f/2.8, 1/250 s) using gravity tank.

6.1.2 Water and glycerine (H/D = -0.25 & $\mu = 16$ cp)

It was observed that the flow patterns obtained using water as a working fluid were highly sensitive to small perturbations (even at Re = 50). To overcome this constraint, the viscosity of the working fluid was increased to 16 cp by adding glycerine to water.

Figures 6.1.2.1 (a-c) show the flow pattern at Re = 48. The impingement plane is stable and stationary, with two pairs of counter rotating vortices clearly visible. The bottom vortices are round while the top vortices are oval in shape. This difference is due to the presence of piston head close to the bottom vortices. In Fig. 6.1.2.1 (b), the trace of blue dye is transferred to the other side of impingement plane (see upper vortex on left side). Also, path lines connecting the right side bottom and top vortices (blue) are visible. The flow seems to be one dimensional above the circulating zone of top vortices. It is also evident that the fluid mixing, if any, occurs only in the vortex region at this Re. No transfer of fluid takes place across the impingement plane above the vortices.

At a Re of 104, the oscillating impingement plane (stable mode) and mixing of fluids in the counter-rotating vortices region can be seen (Fig. 6.1.2.2 (a-d)). In Fig. 6.1.2.2 (a) and (d), the impingement plane is in the center. However, in the other two slides (b) and (c), a portion of impingement plane above the jet axis is toward the right jet of the mixhead and vice versa. In the two color slides (Fig. 6.1.2.2 (c) and (d)), dyes were injected into the both jets inlet using a syringe, however only the right hand side of jet was injected with red dye in Fig. 6.1.2.2 (a) and (b).

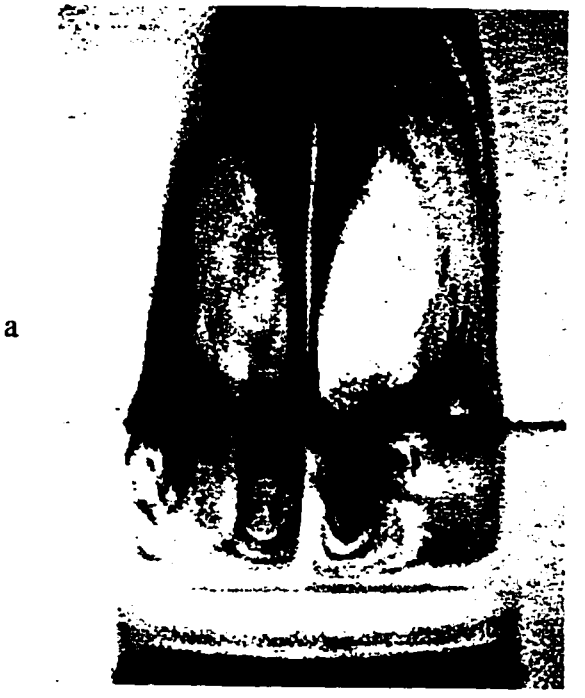

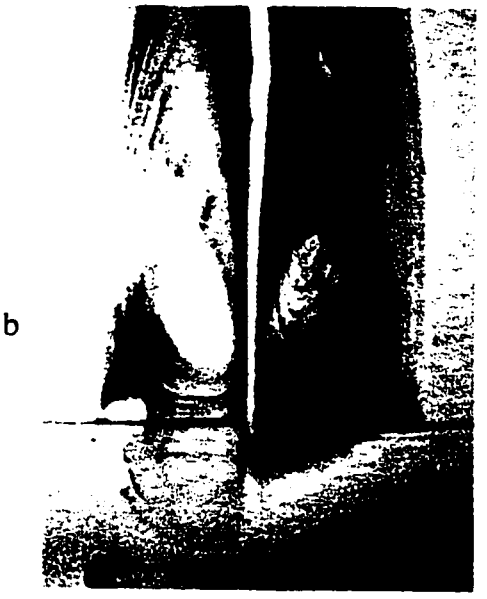

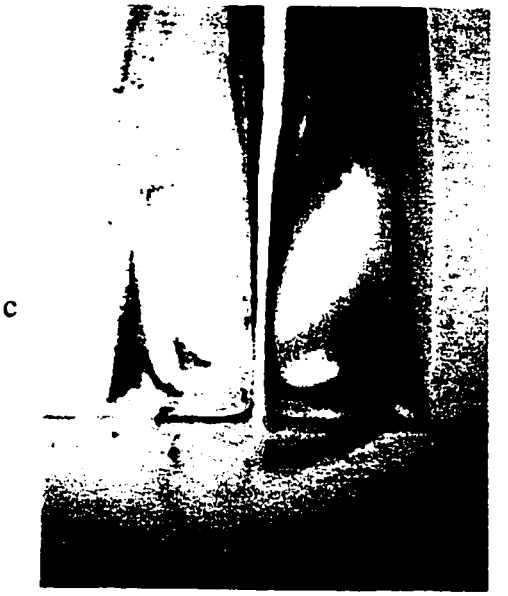

Fig. 6.1.2.1 (a)-(c): Flow patterns with water and glycerine (16 cp) at Re = 48 & H/D = -0.25 (f/2.8, 1/250 s).

Fig. 6.1.2.2 (a)-(d): Flow patterns with water and glycerine (16 cp) at Re = 104 & H/D = -0.25 (f/2.8, 1/250 s).

6.1.3 Water and glycerine (H/D = -0.25 & $\mu = 60$ cp)

The viscosity of the working fluid was further increased to 60 cp by adding more glycerine into the water. At Re = 34 (Fig. 6.1.3.1 (a)) the jets impinge head-on and the impingement plane stays stationary. Once the Re is increased to 52 (Fig. 6.1.3.1 (b)), the two vortices above the impingement point are visible and the impingement plane starts oscillating. A further increase of Re to 80 (c) enhances the oscillation of the impingement plane. The stable flow pattern of the counter rotating vortices is also seen. As mentioned earlier, with a further increase of Reynolds number beyond Re > 127, the jets miss each other and an unstable flow pattern is generated. If the jets impinge on each other, the impingement plane even at higher Re of 430 (d) is visible.

6.1.4 Mineral oil (H/D = -0.50 & $\mu = 4.5$ cp)

Since the glycerine is a hygroscopic fluid, it continuously absorbs water vapor from the atmosphere. The viscosity of the working fluid decreases with time, since the feed tank was open to the atmosphere. To overcome this limitation, mineral oil was selected as a better working fluid. Also, the refractive index of mineral oil (1.46) matches more closely that of acrylic (model material of construction, 1.48).

The figures mentioned here, are images from experiments with light mineral oil (0.85 g/cc) as the working fluid at H/D = -0.50. The shutter speed of 1/2000 sec was used with different aperture openings. The dye (Williams 300505 Ariable Scarlet supplied by Charles Tennant Co. Canada Ltd.) used is soluble in mineral oil. It was injected into the flow system by a syringe pump.

Re = 34

Re = 52

a

b

Re = 80

Re = 430

c

d

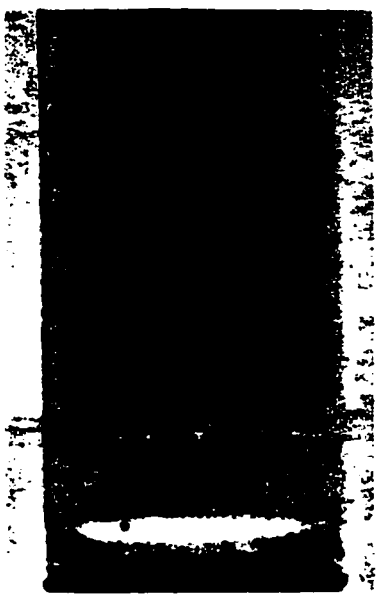

Fig. 6.1.3.1 (a)-(d): Flow patterns with water and glycerine (64 cp) at various Reynolds numbers for H/D = -0.25 (f/2.8, 1/250 s).

Figure 6.1.4.1 (a) taken at Re = 56, the impingement plane is oscillating though the flow pattern is still in a stable mode. Fluid transfer (red dye) from the right lower vortex to the right upper vortex can also be seen. Above the vortex region, the flow is unidirectional. Two consecutive slides were taken at a higher Re of 73 (b and c). Fig. 6.1.4.1 (c) was taken at the start of dye injection. The impingement plane and dispersion of dye in the X direction is visible. The impingement plane oscillation and vortices are clearly shown in Fig. 6.1.4.1 (c), after the dye injection was completed. The connection between the left side vortices above and below the jet is also clearly visible. The fluid in Fig. 6.1.4.1 (c) (see left side of impingement plane) moving towards the piston rotates clockwise from the impingement plane towards the wall. The part of this flow is then caught in the incoming jet and moves toward the impingement plane later joining the counter clockwise upper vortex. Similar flow behavior can be seen on the right side of the impingement plane though the flow directions are reversed. Fig. 6.1.4.1 (d) was taken at Re = 86. A stable flow pattern is visible. A further increase in Re produced instability and fluctuations and it was difficult to take any photographs with a discernible flow pattern.

6.1.5 Mineral oil ($\mu = 75$ cp) and particle path visualization

The preceding flow patterns were visualized using a colored dye injection technique. All the photographs were taken at shutter speeds $\leq$ 1/250 sec. Further studies of the 3-D flow patterns used a particle visualization method. Polystyrene particles were mixed with the working fluid. The paths of these particles within

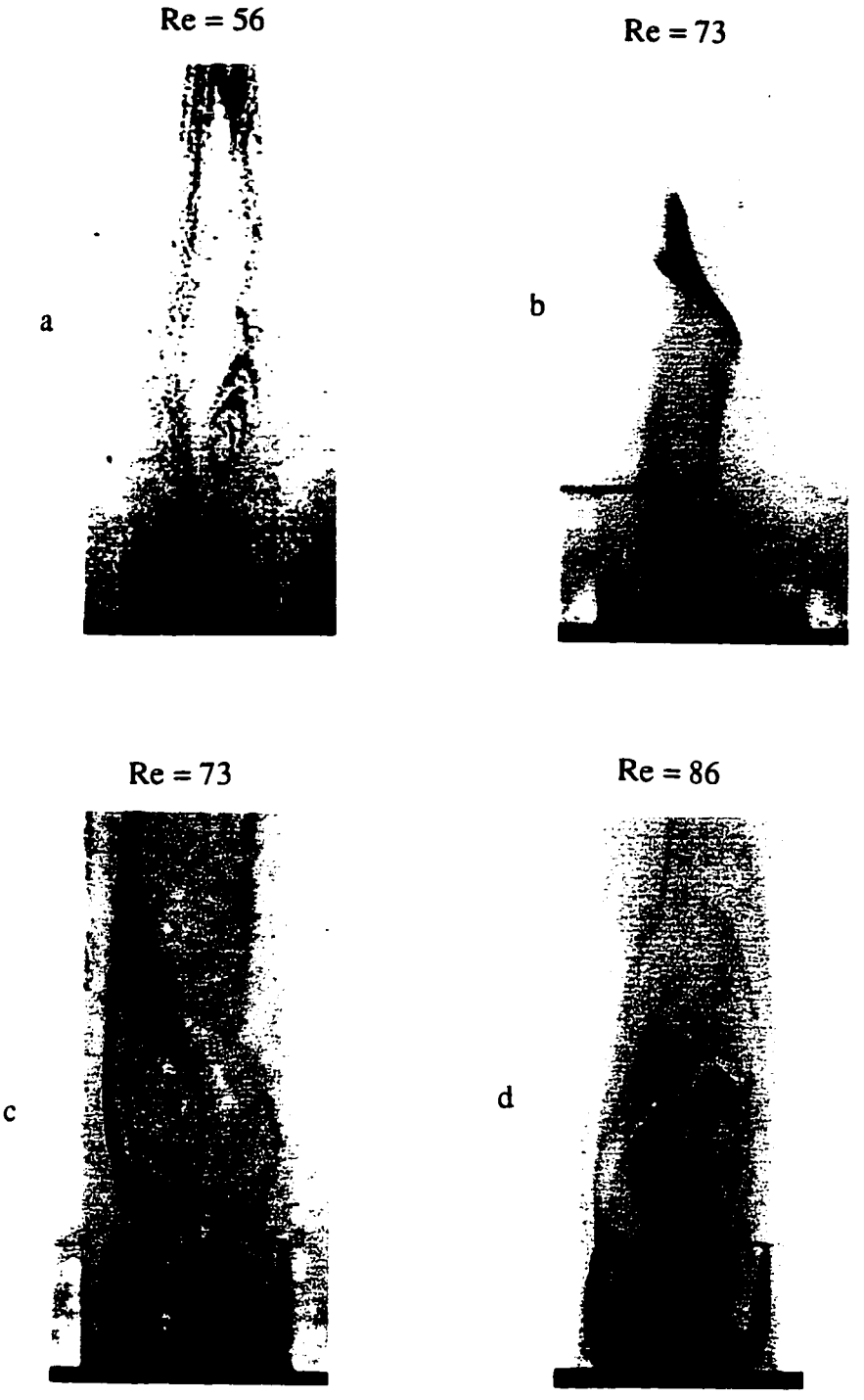

Fig. 6.1.4.1 (a)-(d): Flow patterns with mineral oil (4.5 cp) at various Reynolds numbers for H/D = -0.50.

the mixhead were captured by taking photographs of the flow field at slower shutter speeds. A color filter technique was also employed to extract some 3-D information from a 2-D picture (see chapter 4).

The figures reported in this section are the tracings of particle paths from slides. Most of the particle paths are shown with an arrow-head indicating the direction of flow. These directions are based on the observations made during the flow visualization experiments. In most cases, the flow pattern on one side of the impingement plane has been shown. The flow on the other side of the impingement plane was similar except the directions of the jet flow and vortices' rotation.

In the slides, the movement of particles in the X-direction can be identified by a change in the color of the path line. This information is lost in the tracing method. At low Re, the flow is generally 2-D (no flow in X-direction), so the 3rd dimension information loss is not that important. However, at higher Re, the particles do move in the X-direction also and this information becomes essential to confirm the 3-D nature of the flow field. Wherever the change in the color of the particle path was seen in the slides, the flow in the corresponding figures have been shown by a combination of solid and dotted lines. The dotted lines indicate that the flow had started moving in the X-direction also.

6.1.5.1 H/D = 0

At Re = 17, the left flow field is shown in Figure 6.1.5.1 (a) which is statically stable. The jets impinge on each other and two counter rotating vortices near the jet outlets are present. The particles path lines did not change color. Hence, they have been shown only by solid lines which indicates that the flow in the

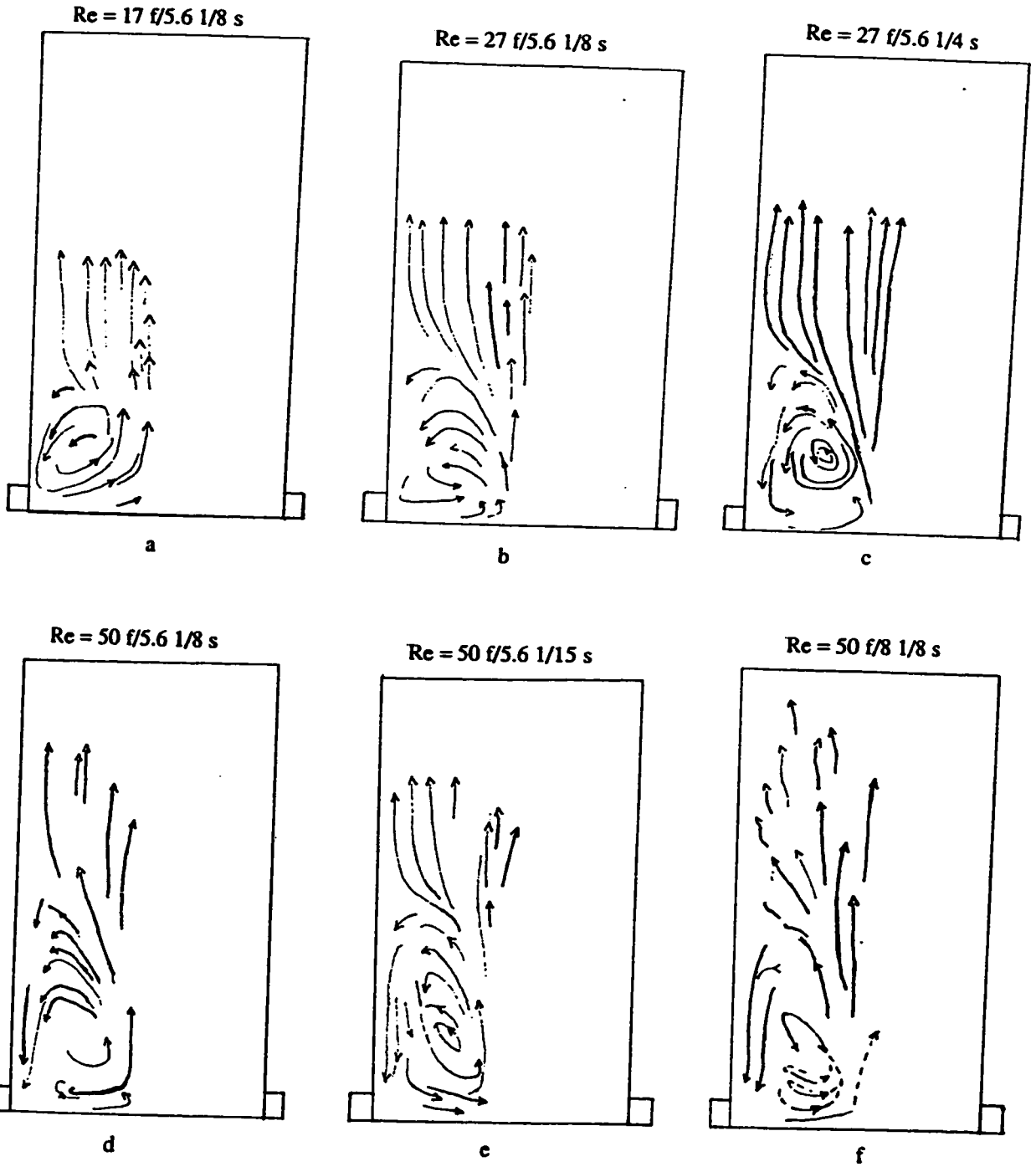

Fig. 6.1.5.1 (a)-(f): Flow patterns with mineral oil (75 cp) at various Reynolds numbers for H/D = 0.

illuminated region is 2-D. At Re = 27, the size of vortex region has increased (Fig. 6.1.5.1 (b) and (c)). The flow is still statically stable since there is no oscillation of the impingement plane. Figure 6.1.5.1 (c) is for a longer exposure time compared to Fig. 6.1.5.1 (b). Hence, the particle path lines are longer in (c). This flow pattern (except the jet flow region) resembles the flow from an abrupt expansion situated at the origin (at jet axis).

The vortex region grows further with increase in Re to 50. This is shown in figs. 6.1.5.1 (d), (e) and (f). The impingement plane is also seen to be oscillating which is indicated by the presence of slightly curved lines in the central zone. Intuitively, it seems that the vortices on the left and right side of the impingement plane start interacting dynamically with each other resulting in this oscillation. The dotted lines in the vortex region indicate the 3-D flow field. Also, the transfer of fluid from the left side of impingement plane to the right side is shown by a dotted line (Fig. 6.1.5.1 (f)).

The experiments conducted at Re = 75 show a further enlargement of the vortex region and also, the oscillations of the impingement plane. This is shown by various figs. 6.1.5.2 (a), (b), (c), (d), and (e) taken with different exposure times. As expected, the path line lengths are shown to be increasing with increasing exposure times for the same Re. The flow is always in a dynamical stable mode.

Figure 6.1.5.3 (a) - (d) show the flow patterns at Re = 100. The circulation is vigorous though the flow is still in a dynamically stable mode. The vortices and oscillating impingement plane are clearly visible. In Fig. 6.1.5.3 (d), one

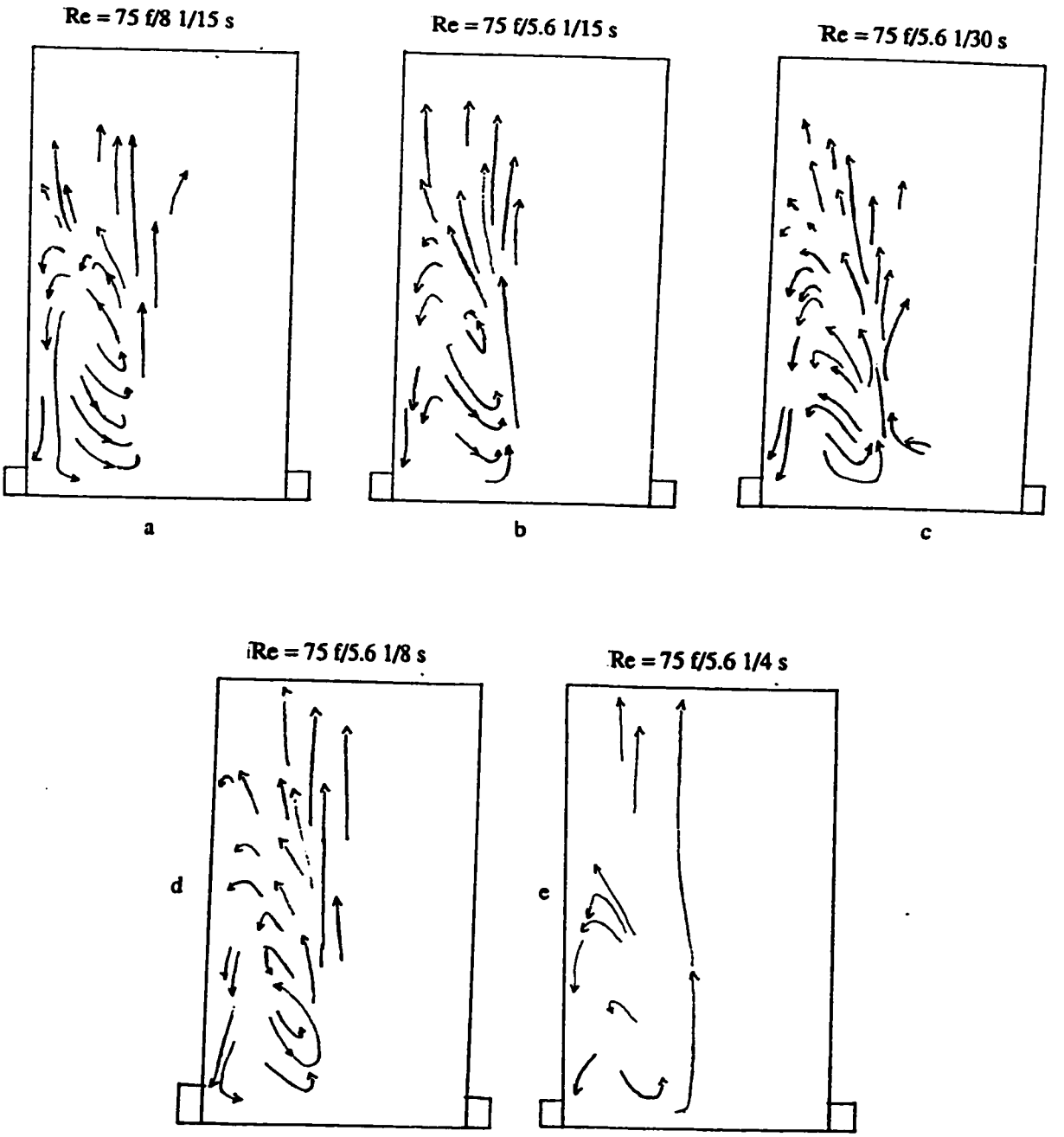

Fig. 6.1.5.2 (a)-(e): Flow patterns with mineral oil (75 cp) at Re = 75 and H/D = 0.

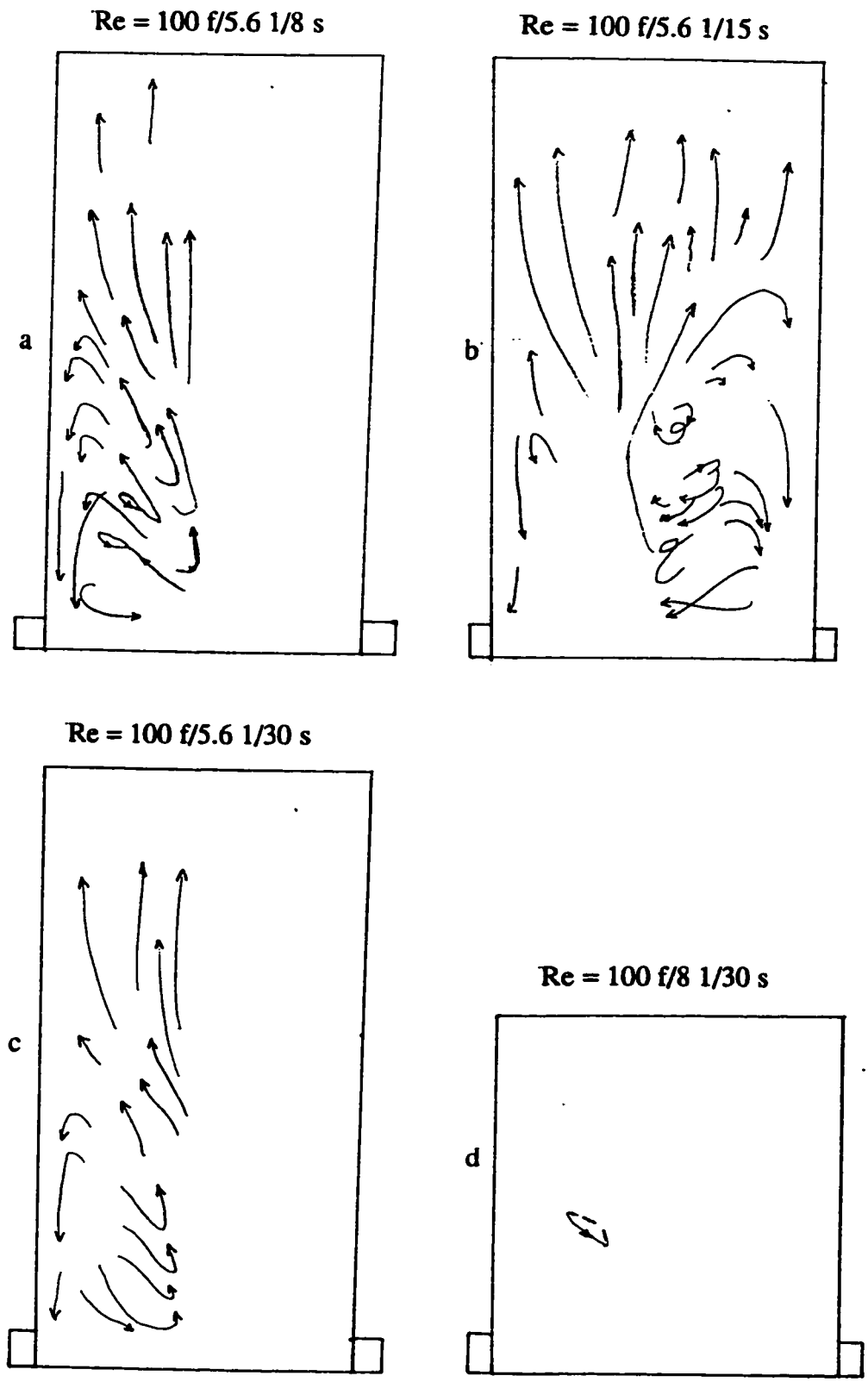

Fig. 6.1.5.3 (a)-(d): Flow patterns with mineral oil (75 cp) at Re = 100 and H/D = 0.

closed loop of a vortex is shown by a combination of solid and dotted line. This shows the 3-D nature of flow. The vortex region is also seen to be reduced at this Re which had been increasing with Re up to Re = 75.

The flow patterns are always unstable for Re ≥ 150 (figs. 6.1.5.4 (a) - (d)). In these figures, the directions of only path lines in downstream of mixhead (developed zone) are shown because these are self evident due to upward flowing fluid. The flow in the circulating zone is unstable, so the directions of the path lines are ommited since it is rather difficult to assign. The actual flow visualization (recorded on video tape) confirms that the jets do not impinge on each other but instead on the opposite mixhead walls. This is indicated by the upward path lines near the walls which converge towards the central region just above the unstable circulating zone. Downward flow is observed in the central circulating zone of the mixhead. The presence of the flow in X-direction in the central zone is also shown by a combination of solid and dotted long curved path lines. Earlier, it has been observed that for a stable flow mode (at low Re) in the circulating zone, the flow near the wall is always downward and in the central part it is upward. In the unstable flow mode; however, these directions are seen to be reversed.

6.1.5.2 H/D = -0.50

Figures 6.1.5.5 (a) and (b) show the flow patterns at Re = 50. Two pairs of counter rotating vortices (only one pair is shown in these figures) and the impingement plane are shown. The flow pattern is in the dynamically stable mode. There seems to be a dead zone, or a zone of very slowly moving fluid, at the

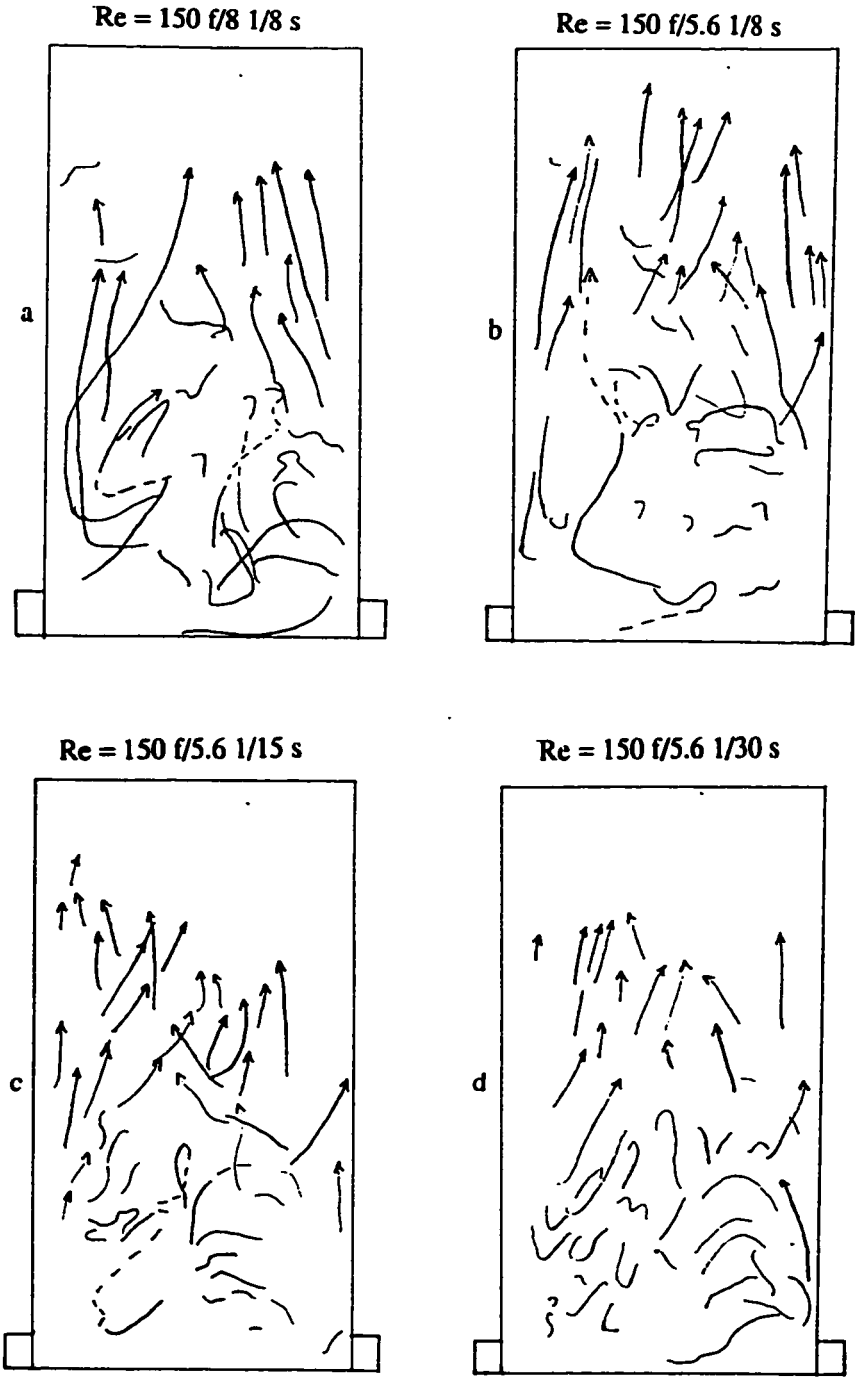

Fig. 6.1.5.4 (a)-(d): Flow patterns with mineral oil (75 cp) at Re = 150 and H/D = 0.

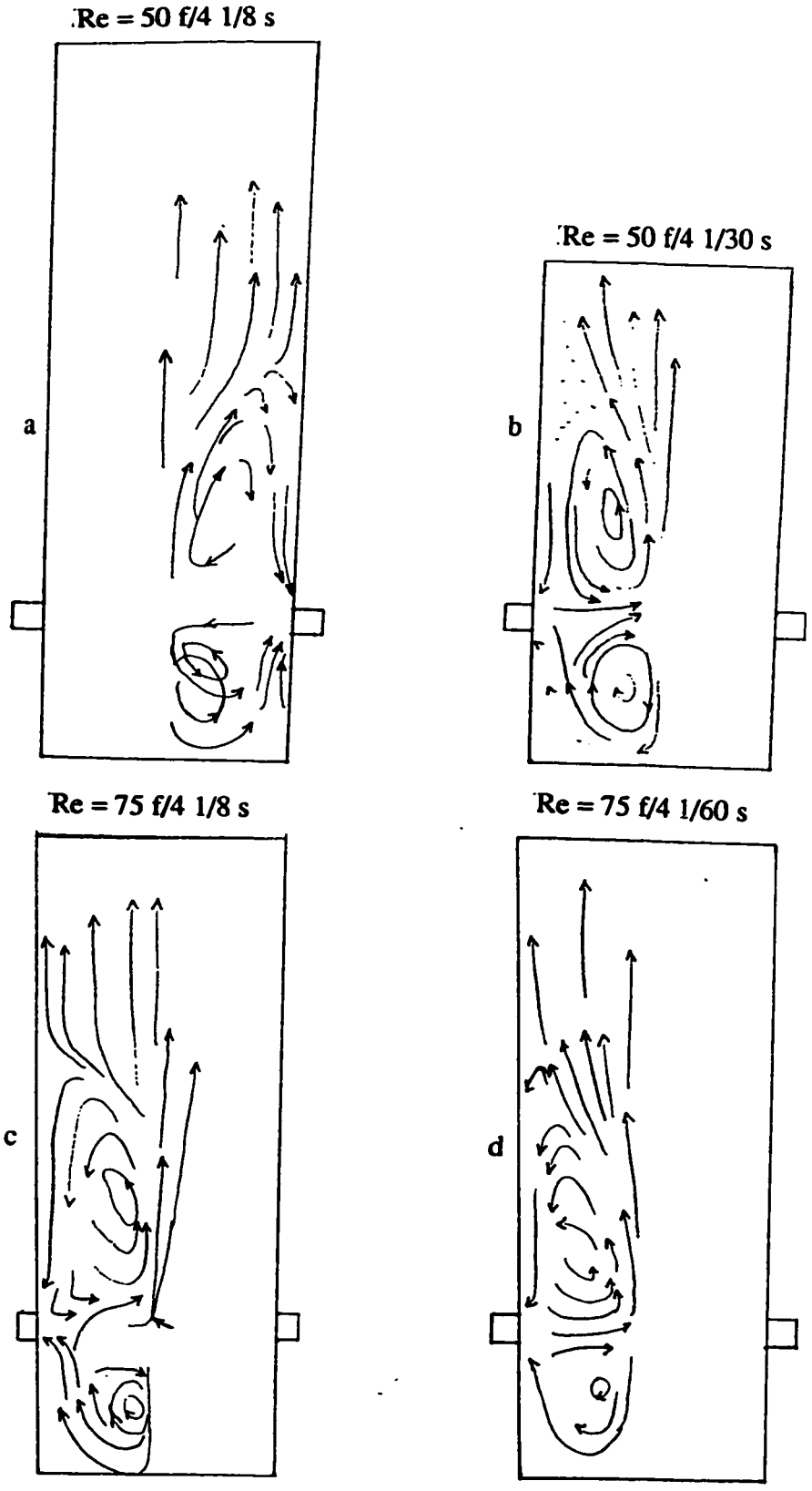

Fig. 6.1.5.5 (a)-(d): Flow patterns with mineral oil (75 cp) at various Reynolds numbers for H/D =-0.5

corner of the mixhead wall above the top of the piston. A similar slow moving zone is also observed above the vortex region near the mixhead wall. The flow in the developed zone is 1-D developed pipe flow. The vortices below the jet axis are more or less round while the top vortices are stretched in the Z-direction. This is due to the fact that fluid moving in the downward direction has to come to rest at the top of the piston while the top vortices do not face restriction.

Similar to the case H/D = 0.0, the flow pattern still remains in a dynamically stable mode at Re = 75 (Fig. 6.1.5.5 (c) and (d)). The vortex regions on either side of the jet axis have increased. The increase is more noticeable in the vortex region above the jet axis. This results in a smaller dead zone above the piston top as compared to the case of Re = 50. The path lines are also seen to be longer in Fig. 6.1.5.5 (c) compared to Fig. 6.1.5.5 (d) due to a longer exposure time.

The flow patterns at Re = 125 become unstable as shown in Figs. 6.1.5.6 (a) and (b). Also, the jets are not impinging at each other. The circulating regions have contracted. The flow is 2-D outside the circulating zone and gradually changes to 1-D downstream toward the chamber exit. In Fig. 6.1.5.6 (a), the circulating zone is not shown due to non-existence of any flow pattern and very low illumination. This section is shown in Fig. 6.1.5.6 (b). The dead zone is also observed near the piston top.

Not much difference in flow pattern is observed at Re = 150 compared to flow patterns observed at Re = 125. The flow pattern is still in unstable mode as shown in figs. 6.1.5.6 (c) and (d). This is because of the impingement of jets at

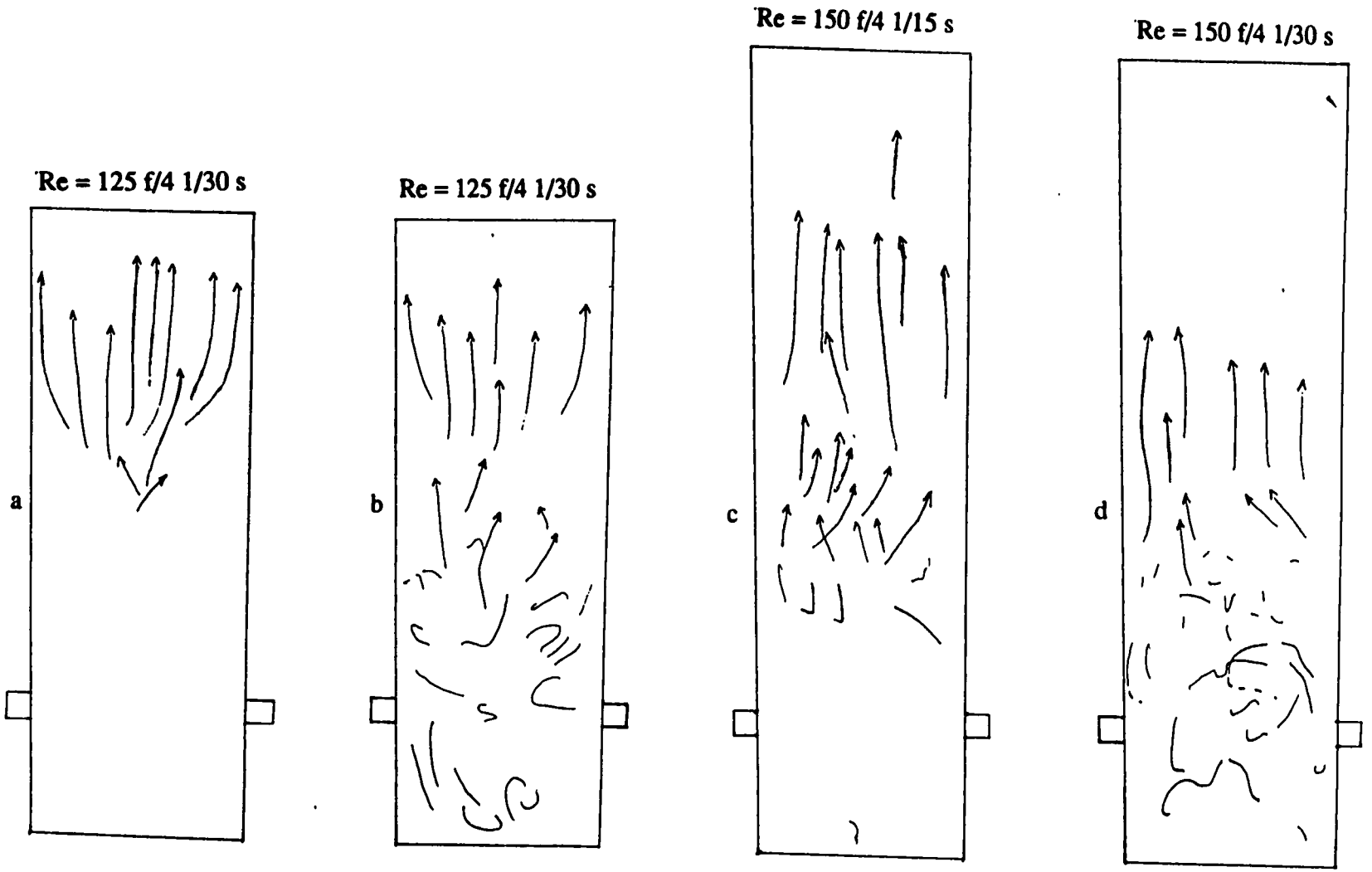

Fig. 6.1.5.6 (a)-(d): Flow patterns with mineral oil (75 cp) at various Reynolds numbers for H/D =-0.5

the wall instead-of at each other. The dead zone also exists at the top of piston near the mixhead wall. The size of the circulating zone is further reduced compared to Re = 125.

6.2 2-D flow visualization using light sheet

This section describes a method which provides the flow information in a particular plane. A plane of light was generated by passing a laser beam through a cylindrical lens. This plane was used to illuminate a plane section of the flow field inside the mixhead. During these experiments, the exposure time is relatively long since the intensity of laser light is low. Thus, the flow patterns obtained showed integrated averages of particle path within the 2-D illuminated plane.

Depending upon the orientation of the light sheet, a particular section of model can be illuminated. The three different plane types (constant X, Y, and Z respectively) in which the flow fields were studied, are shown in Figs. 4.2.3.1 and 4.2.3.2. The X-plane and Y-plane are rectangular while the Z-plane is a circle. The mixhead cross-section, in the slides taken for the Z-plane, is elliptical rather than circular due to the camera angle of 60° to 70° the Z-axis. Selected parameters for flow visualization with this method are listed in Table 6.2.1.

6.2.1 X-plane flow patterns with mineral oil ($\mu = 39$ cp)

Figures 6.2.1.1 to 6.2.1.4 identify the symmetry of the flow field about the impingement plane. The curved or wave like path lines in middle of the figures

indicate the oscillations of the impingement plane. These figures also depict the growth of vortices in Y and Z directions obtained from sectioning at different values of X.

Table 6.2.1: Selected parameters settings for 2-D Flow visualization

Fluid	Re	H/D	Viscosity (cp)	Illuminated plane	Section
Mineral oil	31-188	0.00	39.00	X = 0.00	6.2.1.1
Mineral oil	50-190	-0.50	39.00	X = 0.00	6.2.1.2
Mineral oil	50	0.00	75.00	Varying X	6.2.2
Mineral oil	9-111	-0.25	90.00	X = 0.00	6.2.3.1
Mineral oil	37 & 88	-0.25	90.00	Varying X	6.2.3.2
Mineral oil	50	-0.50	39.00	Varying Z	6.2.4.1
Mineral oil	90	-0.25	90.00	Varying Z	6.2.4.2
Mineral oil	150	-0.50	39.00	Varying Z	6.2.4.3
Mineral oil	50	-0.25	90.00	Varying Y	6.2.5.1
Mineral oil	90	-0.25	90.00	Varying Y	6.2.5.2
Mineral oil	125	-0.25	90.00	Varying Z	6.2.5.3

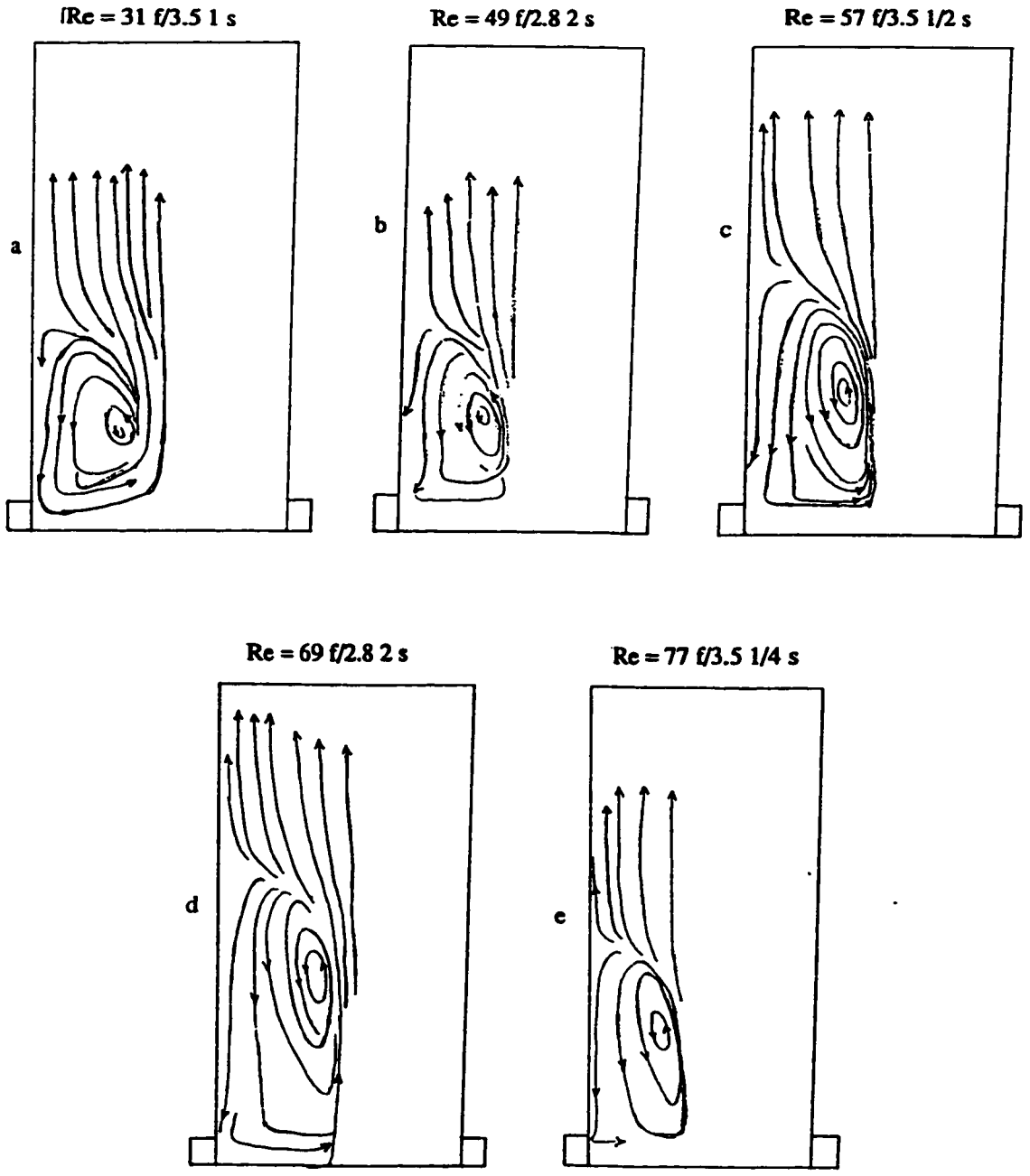

Fig. 6.2.1.1 (a)-(e): Flow patterns (X-section X = 0) with mineral oil (39 cp) at various Reynolds numbers for H/D = 0

6.2.1.1 H/D = 0 and X = 0

Figure 6.2.1.1 (a) shows the flow pattern at Re = 31. It is evident that the jets impinge head-on and the flow pattern is symmetrical about the impingement plane. The impingement plane is stationary and two counter rotating vortices areformed. The flow pattern is in a static stable mode. The flow is 2-D in the recirculating zone which quickly changes to one dimensional flow above the vortices. For Re = 49 (Fig. 6.2.1.1 (b)), the flow field reaches a dynamically stable mode. The impingement plane starts oscillating and the circulating zone increases both in Y and Z directions. At Re = 57 (Fig. 6.2.1.1 (c)), the recirculating region widens though the flow pattern still maintains a dynamically stable mode. No significant change in the flow pattern occurs at Re = 69 (Fig. 6.2.1.1 (d)). A further increase in Re to 77 (Fig. 6.2.1.1 (e)) contracts the circulating zone in Z-direction though the oscillating flow pattern still remains in the dynamical stable mode. The impingement plane is squeezed between two vortices. Thus, it can be concluded that the flow pattern changes the mode of stability from static to dynamic at Re = 50. The circulation zone expands with increasing Re to Re = 69, then contraction begins at Re = 77 (in Z-direction).

Once the Re is increased to 96 (Fig. 6.2.1.2 (a)), the flow is symmetric and dynamically stable. However, some major changes in the flow pattern result. The jets may miss one another and start to impinging on the opposite walls. The recirculating zone still develops in the center though the flow directions of the vortices and the flow near the wall are reversed. The circulating zone shrinks considerably compared to Re = 77. A quantitative description of the growth of

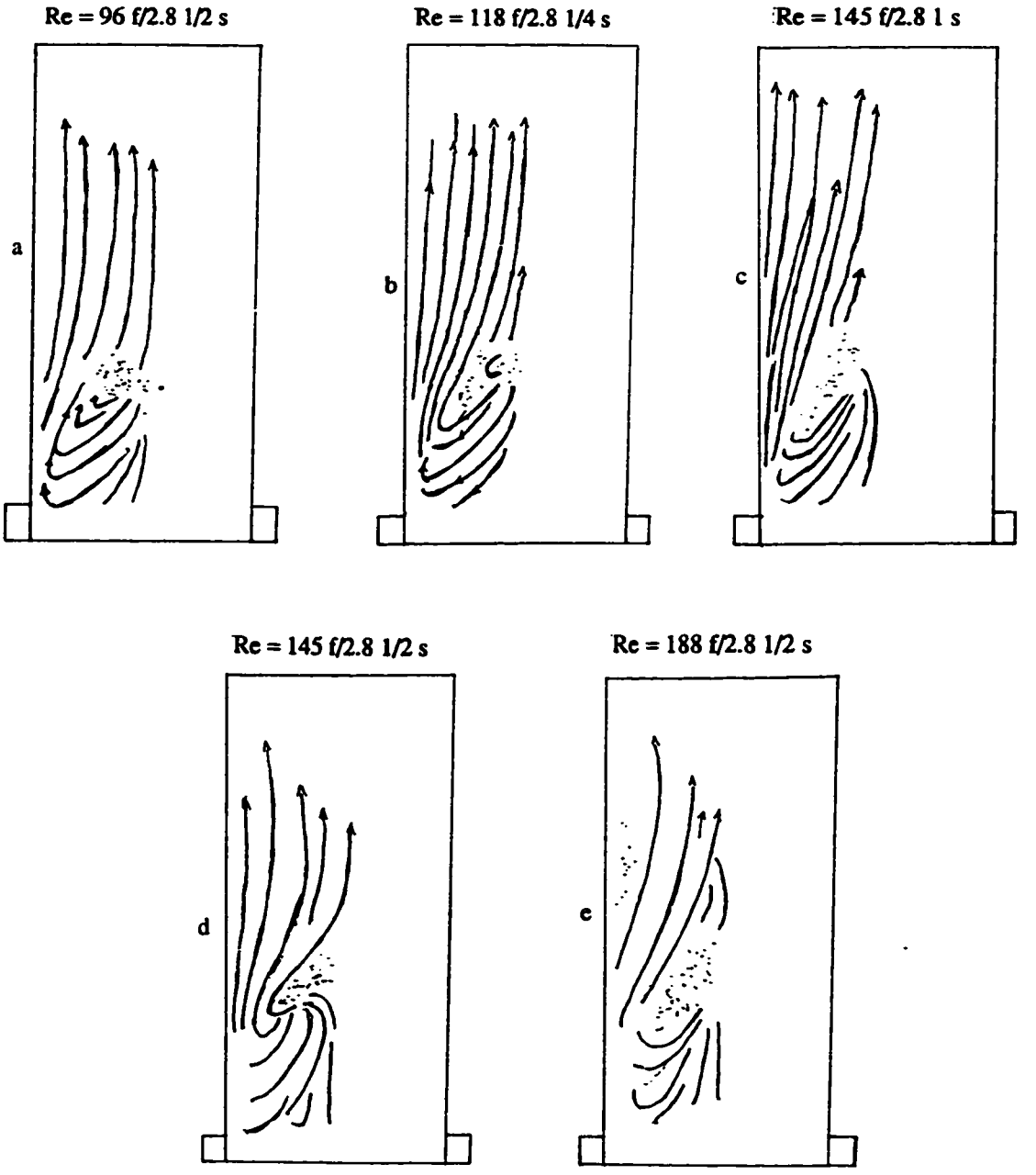

Fig. 6.2.1.2 (a)-(e): Flow patterns (X-section X = 0) with mineral oil (39 cp) at various Reynolds numbers for H/D = 0

the vortices (length, width, and the distance between vortices) is listed in the Appendix D. The flow above the circulating zone becomes one-dimensional. In fact, it will always be one dimensional above the vortices. In the center of the mixhead, a zone of very slowly moving particles is present between the circulating zone and the developing zone. This probably occurs in the region where the momentum of the particles in the developing flow and within the vortices cancel each other due to the flow in the reverse direction. This is clearly visible in the video tape. A similar flow pattern is observed at Re = 118 (Fig. 6.2.1.2 (b)).

The flow pattern becomes unstable when Re is further increased to 145. It seems that the instability in the flow disturbs the velocity field both in the region of the vortices and the developing flow region. These random and rapid changes, probably, cause the zone of slowly moving particles to grow in size. All these observations are clear from the Figures. 6.2.1.2 (c) and (d). Similar flow behavior is observed at Re of 188 (Fig. 6.2.1.2 (e)). The axial velocity at certain locations of the circulating zone may be downward (negative) in the neighborhood of the mixhead axis.

6.2.1.2 H/D = -0.50 and X = 0

Symmetric and dynamically stable flow patterns are observed at Re = 50 (Fig. 6.2.1.3 (a)). The H/D ratio has been increased from 0.0 to 0.5 to provide space between the jet axis and the piston. Thus, two more vortices are formed below the jet axis. As explained earlier, the bottom vortices are more circular in shape in comparison to the top vortices. Also, the rotation directions of the vortices on the same side of the impingement plane are opposite to each other. As shown

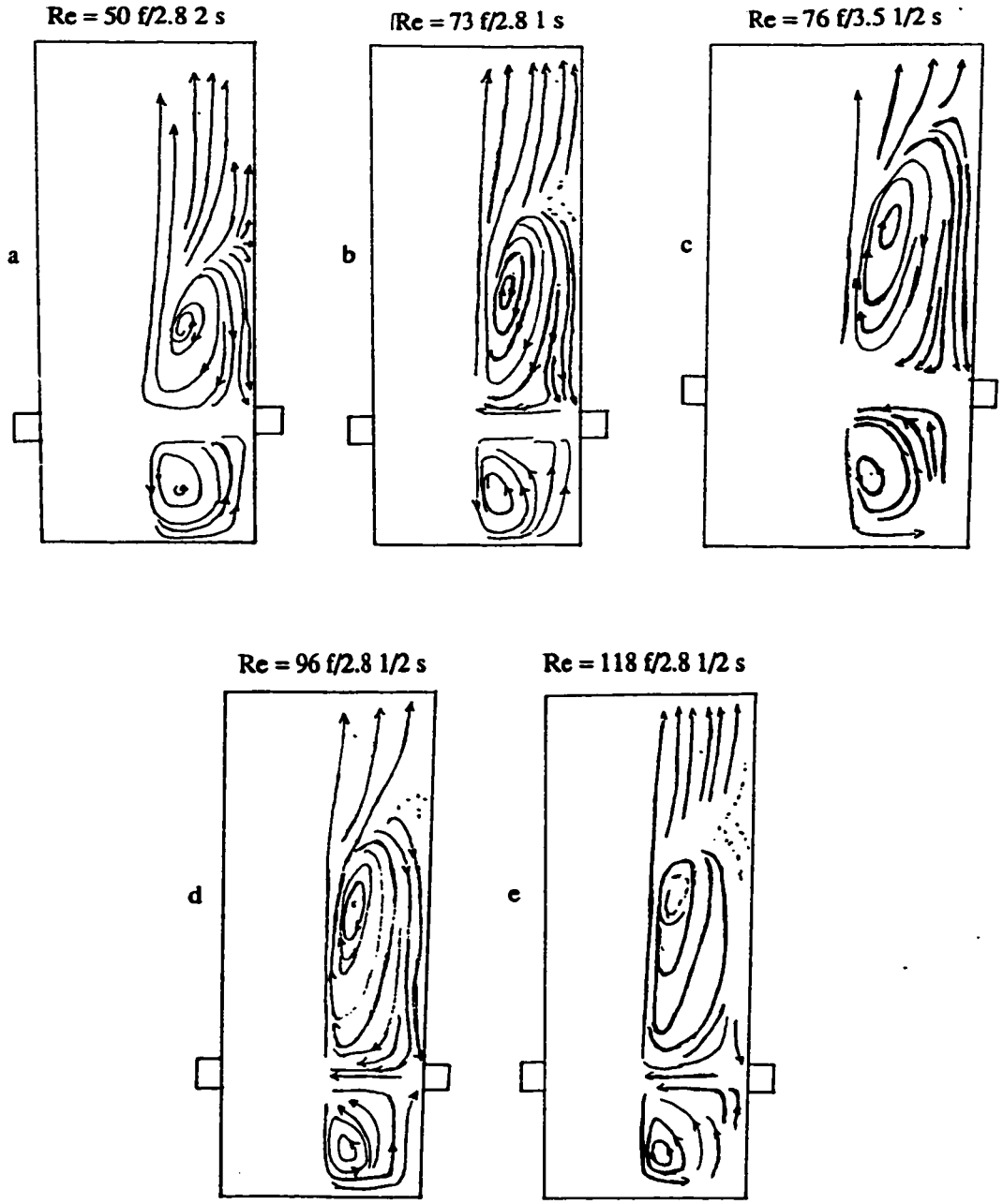

Fig. 6.2.1.3 (a)-(e): Flow patterns (X-section X = 0) with mineral oil (39 cp) at various Reynolds numbers for H/D = -0.5

in the Figure, the right top vortex is rotating clockwise while the bottom vortex is rotating counter-clockwise. An increase in Re to 73 does not change the dynamic stability of the flow. Only the recirculating regions below and above the jet axis are expanded. This change is noticeable more in the top circulating region than the bottom region (Fig. 6.2.1.3 (b)). The flow pattern remains the same even at Re = 76. Only the circulating region expands slightly more (Fig. 6.2.1.3 (c)). This expansion of the circulating zone continues until Re reaches 96 (Fig. 6.2.1.3 (d)). At Re = 118 the circulating zone reduced in height though the symmetry and dynamic stability of the flow was maintained. This is shown in Fig. 6.2.1.3 (d). The jets impinge on each other to Re = 118 when the H/D ratio is increased from 0.0 to 0.5. At H/D = 0.0, the jets started impinging on the opposite walls at a lower Re = 96 (see section 6.2.1.1).

The three flow patterns (Fig. 6.2.1.4 (a) - (c)) taken for Re = 144 at different times show that the flow keeps swinging between unstable and dynamic stable modes (the stable mode persists only for a very short time). This behavior is seen due to the change in the nature of the jet impingement. For periods of time the jets impinge on each other while at other times they impinge on the side walls. The concentrical impingement of jets generates a dynamical stable mode. Otherwise, an unstable mode is produced. At Re = 190, a totally unstable flow pattern is observed (Fig. 6.2.1.4 (d)).

In the unstable mode, all the recirculating zones contract in size, especially, in the Z-direction. The recirculating zones below the jet axis shrink more and

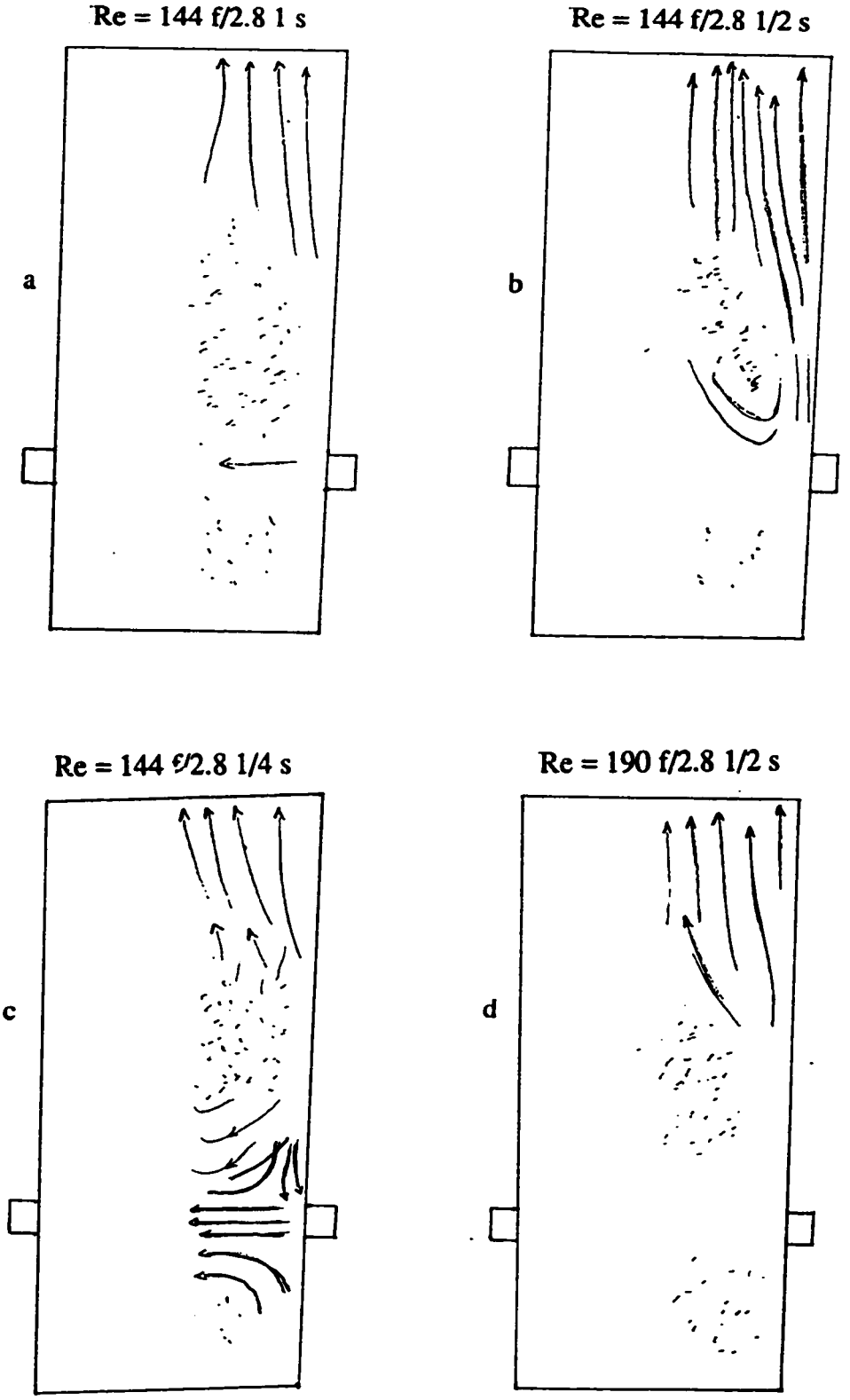

Fig. 6.2.1.4 (a)-(d): Flow patterns (X-section X = 0) with mineral oil (39 cp) at various Reynolds numbers for H/D = -0.5

become smaller than the size of the vortices observed even at a low Re = 50. The flow in the downstream direction quickly becomes one dimensional, as in the cases of low Re.

6.2.2 X-plane flow patterns with mineral oil ($\mu = 75$ cp)

These experiments have been conducted using mineral oil with a viscosity of 75cp at a fixed Re of 50. This value of Re was selected on the basis of the previous observations because the flow always transformed from static to dynamically stable mode around this Re. During the experiments, H/D = 0 and the photographs with aperture setting of f/2.8 and shutter speed of 2s, were taken at five planes with different values of X.

Figures 6.2.2.1 (a) to (c) show the anti-clockwise vortices at X = 0, 2.38, and 4.76. In all the Figures, the flow which is 2-D in the circulating zone becomes one dimensional above the vortex region. In Fig. 6.2.2.1 (c), the vortex height decreases. In a plane of X = 7.14, the recirculating zone virtually vanishes (Fig. 6.2.2.1 (d)). At a plane further close to the wall (X = 9.52), The vortex totally disappears and the flow appears to be only one dimensional (Fig. 6.2.2.1 (e)). As expected, the flow patterns in all the X-planes remain in stable mode at this low Re.

6.2.3 X-plane flow patterns with mineral oil ($\mu = 90$ cp)

6.2.3.1 H/D = -0.25 and X = 0

At Re = 9, jets impinge on each other and four small vortices are generated

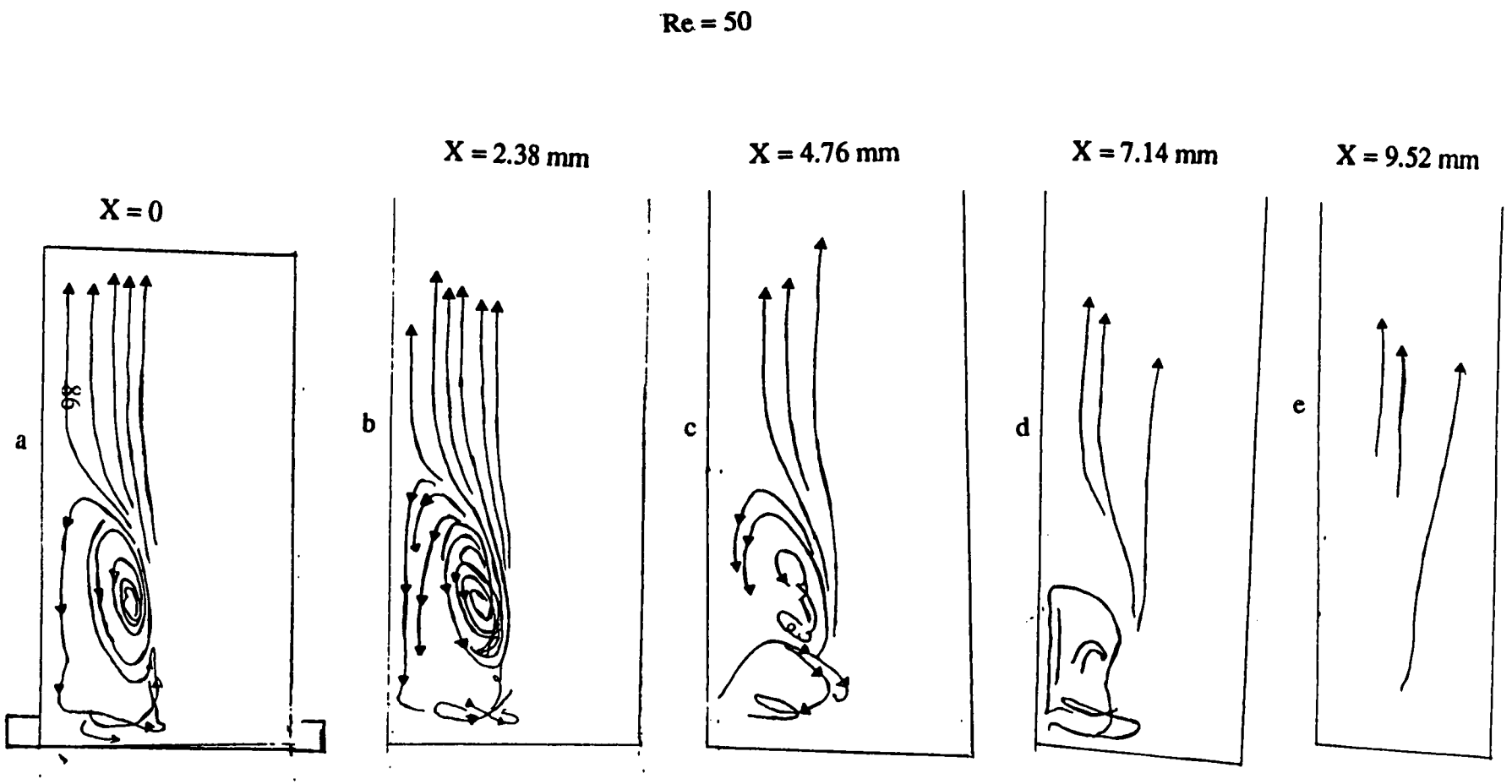

Fig. 6.2.2.1 (a)-(e): Flow patterns (X-sections) with mineral oil (75 cp) at Re = 50 and H/D = 0

(Fig. 6.2.3.1 (a)). The impingement plane is stationary and the flow pattern remains in static stable mode. At a Re of 37, larger vortices are observed (Fig. 6.2.3.1 (b)) compared to Re = 9. The vortices almost touch each other on either side of the jet axis. There is a small region between these vortices which does not take part in the recirculation. A further increase in Re to 88 further enlarges the vortices (figs. 6.2.3.1 (c) and 6.2.3.2 (a)). The crossing and curving nature of path lines in the center indicates the vigorous oscillation of the impingement plane. Figure 6.2.3.2 (a) which was taken with longer exposure time, highlights the presence of a cross closed loop in horizontal direction. This indicates that the fluid exchange between two upper vortices is occurring. The flow is symmetric about the impingement plane and remains in a dynamically stable mode. An increase in Re to 95 does not change the flow pattern. Only, a reduction in the circulating zone height occurs (Fig. 6.2.3.2 (b)). This reduction in the height of the circulating zone continues as Re is further increased to 111 (Fig. 6.2.3.2 (c)). A photograph taken with longer exposer time at this Re also shows that the fluid transfer with in the two vortices above the jet axis takes place (Fig. 6.2.3.2 (d)).

6.2.3.2 H/D = -0.25 and different X values

The study of vortex depths in X-plane are made at two different values of Re. At Re = 37, the section planes are selected at X = 2.54, 5.08, and 7.62 mm (Fig. 6.2.3.3 (a) - (c)). In the X-planes closer to the wall, vortices above and below the jet axis join together while near the jet axis (X = 0), the vortices do not join and remain on either side of the axis. At X = 7.62 the vortex zone starts diminishing (Fig. 6.2.3.3 (c)). The experiment conducted at Re = 88 shows the

(a) Re = 9; f/2; 1/2 s

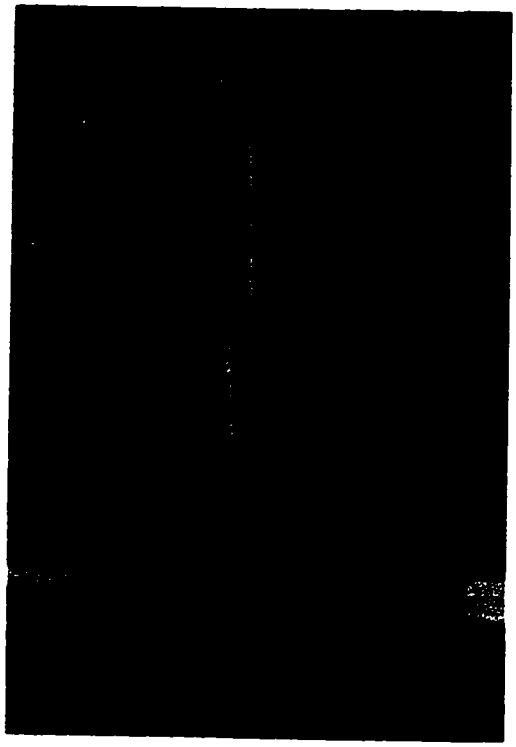

(b) Re = 37; f/2; 1 s

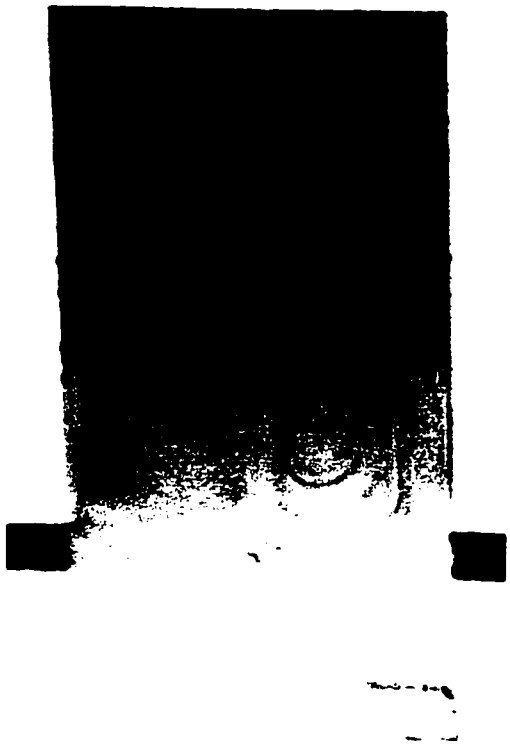

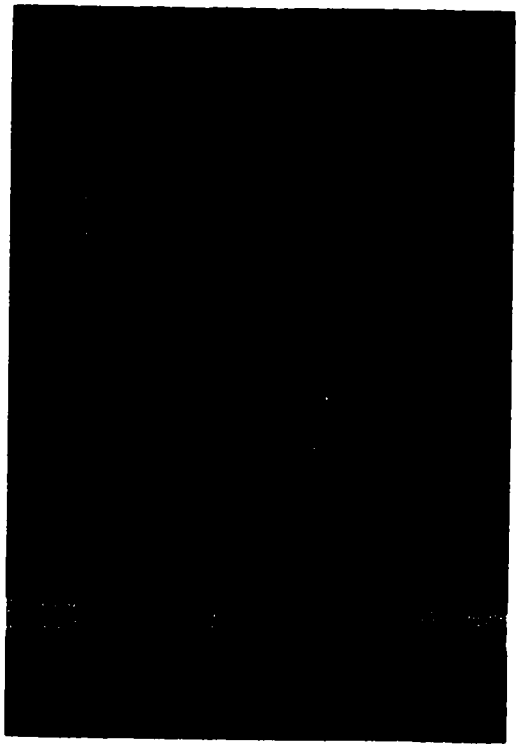

(c) Re = 88; f/2; 1 s

Fig. 6.2.3.1 (a)-(c): Flow Patterns (X-section) with mineral oil of 90 cp at various Reynolds number for H/D = -0.25

(a) Re = 88; f/2; 2s

(b) Re = 95; f/2; 2s

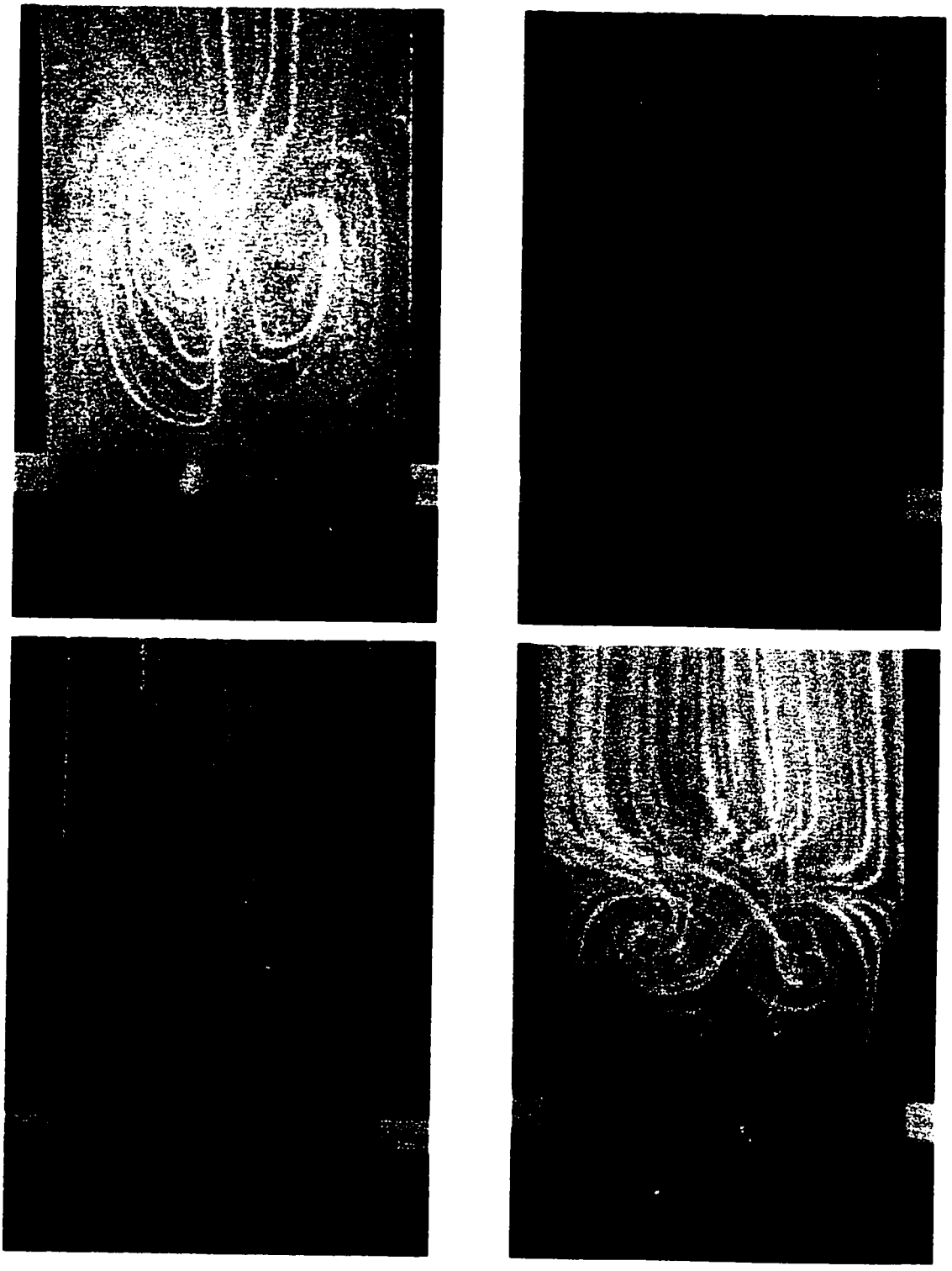

(c) Re = 111; f/2;2 s

(d) Re = 111; f/2;5 s

Fig. 6.2.3.2 (a)-(d): Flow patterns with mineral oil at various Reynolds number for H/D = -0.25

Re = 37

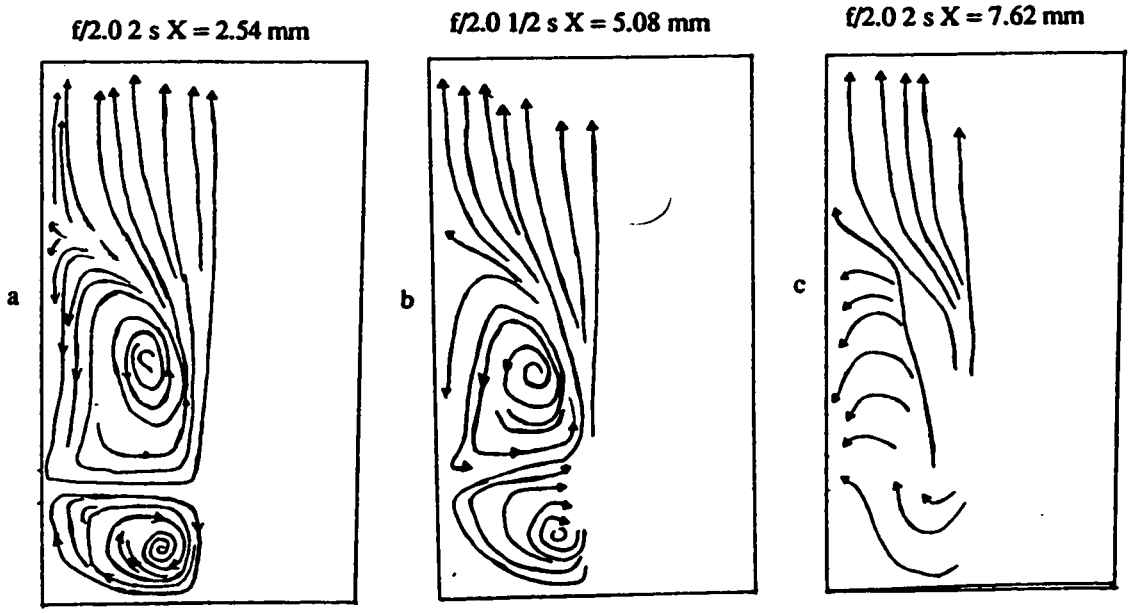

Fig. 6.2.3.3 (a)-(c): Flow patterns (X-sections) with mineral oil (90 cp) at Re = 37 and for H/D = -0.25

formation of four vortices at X = 1.27 (Fig. 6.2.3.4 (a)). The fluid transfer within the vortices above the jet axis can be seen. In other X-planes tending towards the wall (figs. 6.2.3.4 (b) -(h)), the vortices above and below the jet axis first join (see at X = 2.54, 3.21, 5.08, and 6.35 mm) and later diminish on the planes beyond X = 6.35 (see Figures at X = 8.89, 10.16, and 11.43 mm). The fluid flow direction remains the same below and above the jet axis on either side of the impingement plane. The flow is in a dynamically stable mode. During previous investigations, it was observed that at a relative low value Re = 50, the recirculating zone diminished at X > 7.14 and the flow became more or less one dimensional (Fig. 6.2.2.1). Once the Re is increased to 88, the flow does not become one dimensional even up to the depth of X = 11.43 mm but remains two dimensional. This confirms that the vortices survive up to larger depths in X-direction if the Re is increased.

6.2.4 Y-plane flow pattens with mineral oil

To further study the presence of velocity component W in the mixhead, the flow patterns have also been visualized in various Y planes. Two cases of stable flow mode and one case of unstable flow mode are presented here.

At a Re = 50 (H/D = -0.25, μ = 90 cp), the flow has been visualized at five different Y planes. In all the figures, the curved path lines can be seen traveling from the center towards the mixhead wall (Figures 6.2.4.1 (a) - (e)). These curved lines confirm the presence of a W velocity component along with the V velocity component. As mentioned earlier, only the half plane has been traced here since the flow is symmetric about the jet axis and is in stable mode. Figure 6.2.4.1 (a) shows that there is no circulation at Y = 0 which, in fact, is the impingement plane

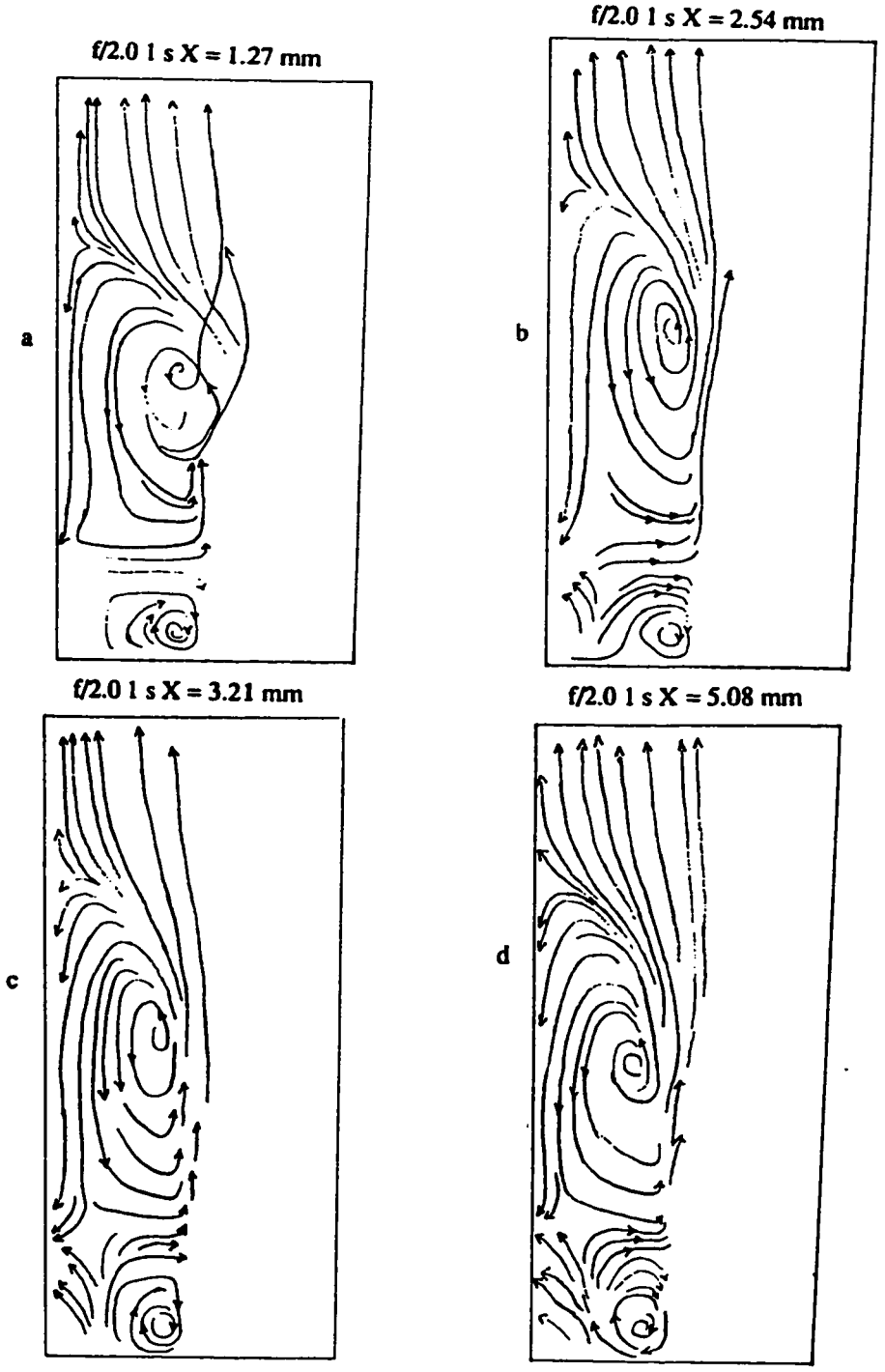

Fig. 6.2.3.4 (a)-(d): Flow patterns (X-sections) with mineral oil (90 cp) at Re = 88 and H/D = -0.25

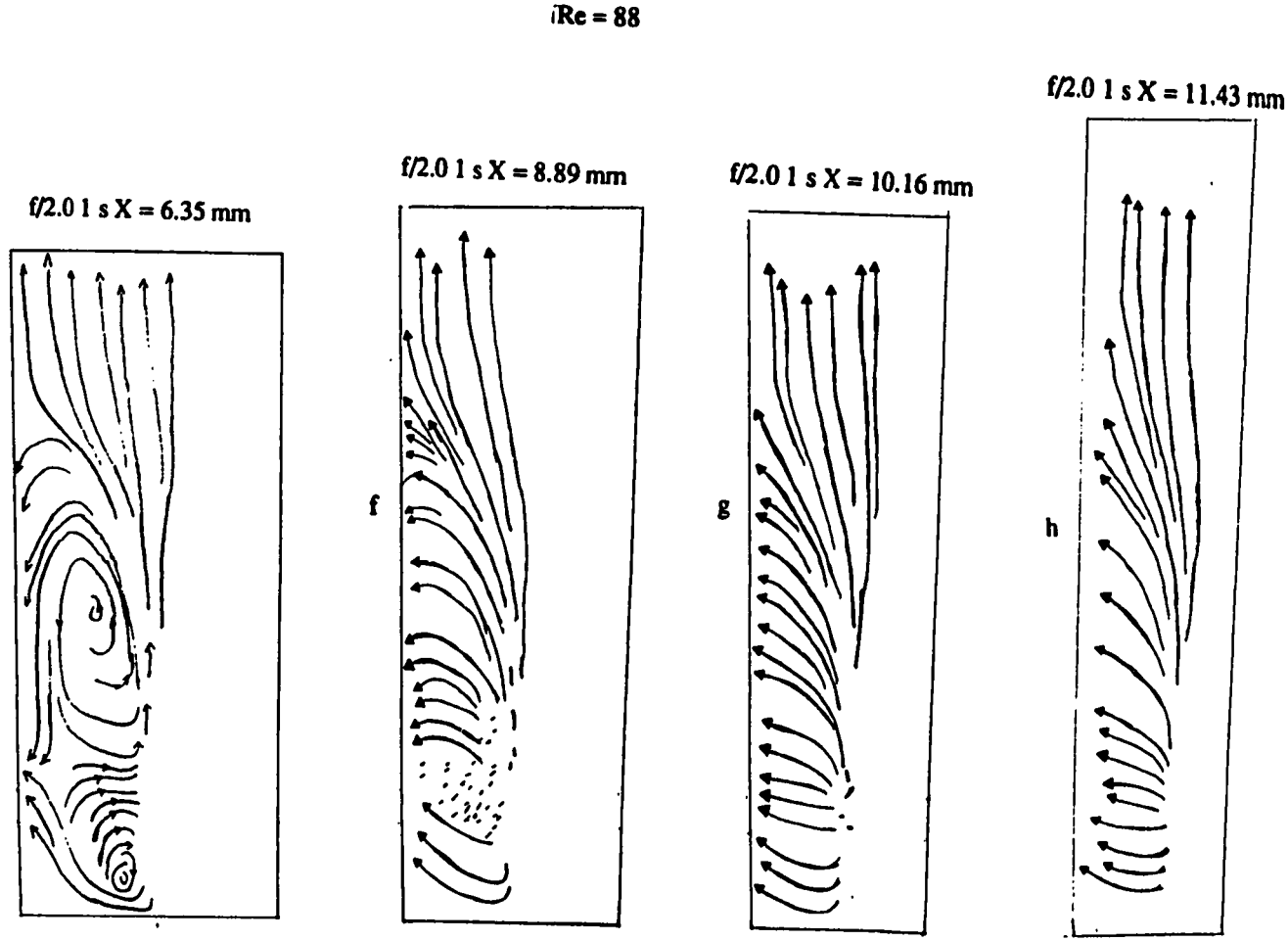

Fig. 6.2.3.4 (cont.) (e)-(h): Flow patterns (X-sections) with mineral oil (90 cp) at Re = 88 and H/D = -0.25

itself. The curved path lines indicate only the 2-D flow without any rotation. A further increase in Y to 2.40 still shows the flow in the neighborhood of the impingement plane (fig 6.2.4.1 (b)). The flow is still not rotating and is not a part of the vortex system. It seems that it is close to the interface of the impingement plane and the vortex zone. The flow patterns at planes Y = 4.95, 7.5, and 10.03 mm show the existence of the recirculation zone and the one dimensional flow above this zone. These are shown in figs. 6.2.4.1 (c) - (e).

The flow behavior at Re = 90 (H/D = -0.25, μ = 90 cp) has been visualized by taking photographs at ten different Y-planes ranging from Y = 0 to 11.43 mm. Figs. 6.2.4.2 (a) and (b) show the impingement plane and its neighborhood. These figures have been taken at Y = 0 and 1.27 mm, respectively. At Y = 0.0 flow is travelling radially outward as if it were a radial jet originating form a point source. Figure 6.2.4.2 (c) at Y = 2.54 mm shows the interface of the impingement plane and the vortex system. The vortex region starts appearing at a plane Y = 3.81 mm (fig 6.2.4.2 (d)) and persists further at all the Y-planes up to Y = 11.43. These are shown in figs 6.2.4.2 (e) - (j). In all these figures, the presence of W velocity component is strongly evident, especially in the vortex zone.

At Re = 125 (H/D = -0.25, μ = 90 cp), the flow becomes unstable. The flow patterns at different Y-planes (Y = 0, 0, 1.27, 2.54, 3.81, 5.08, 6.35, 7.62, 8.89, 10.16 and 11.43 mm) are shown in figs. 6.2.4.3 (a) - (k). The presence of W component of velocity is observable in the curved path lines. The independent existence of impingement plane is seen in figs. 6.2.4.3 (a) - (c) which are taken at Y = 0, 0, and 1.27 mm, respectively. At Y = 2.54 mm, the circulation zone consists

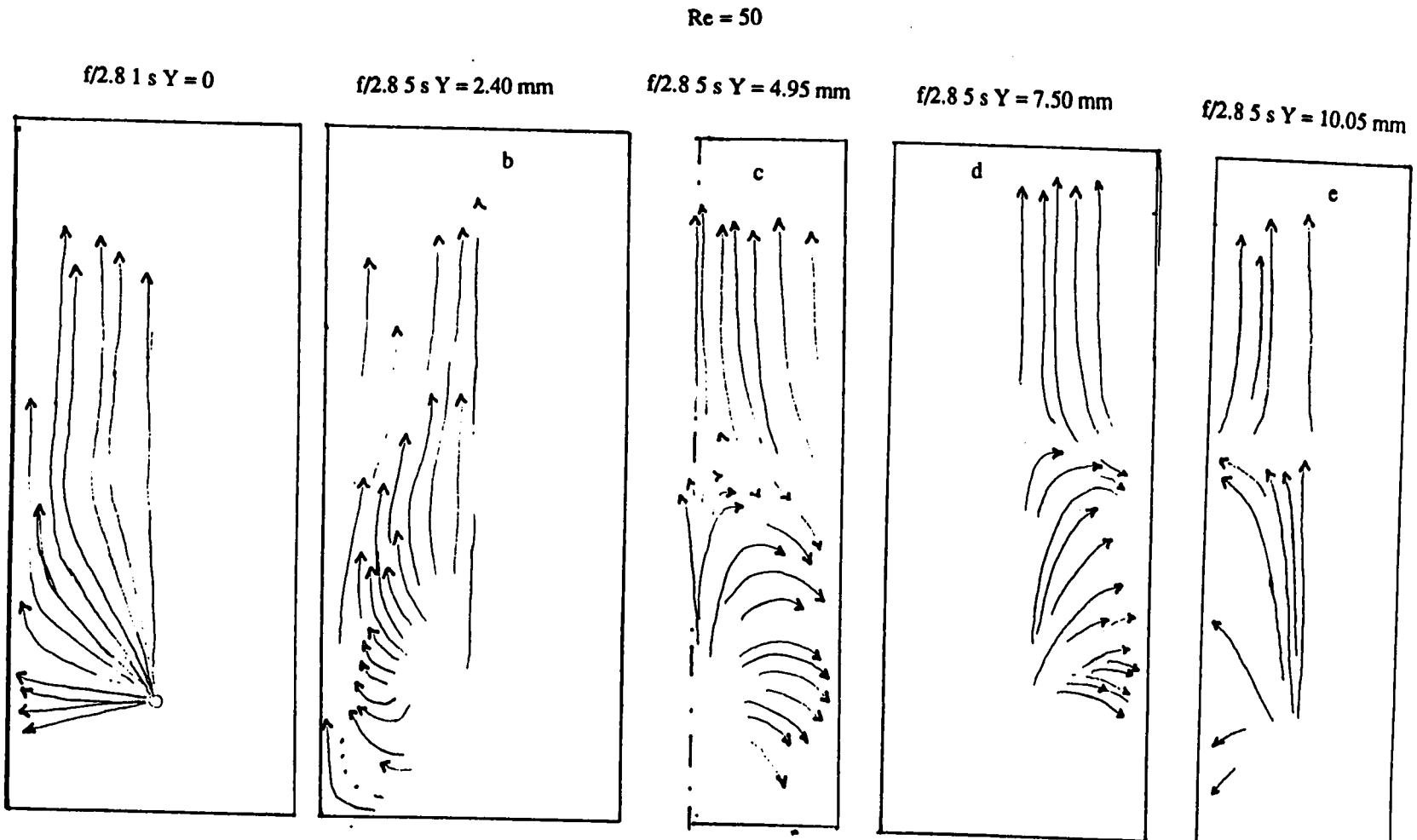

Fig. 6.2.4.1 (a)-(e): Flow patterns (Y-sections) with mineral oil (90 cp) at Re = 50 and H/D = -0.25

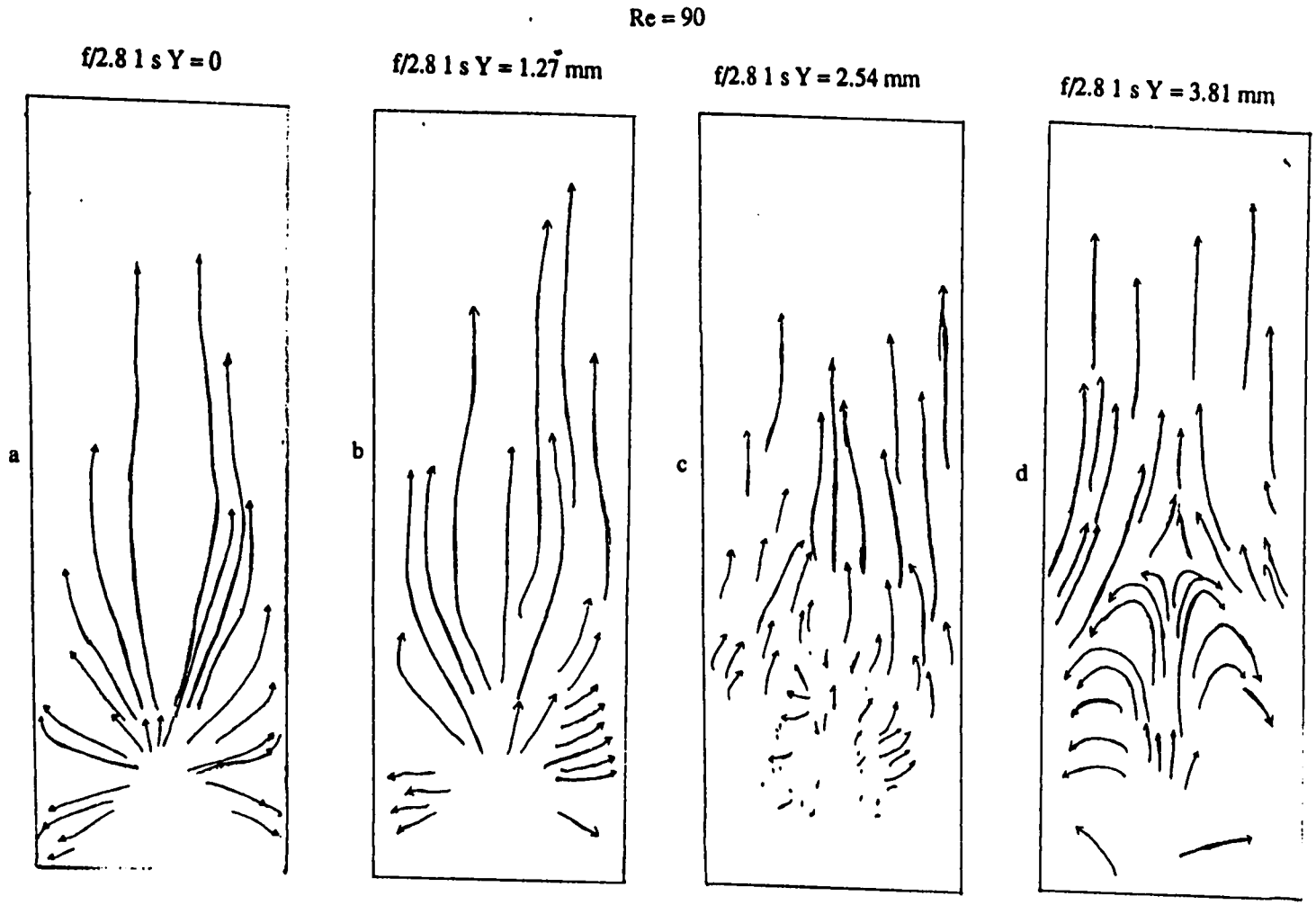

Fig. 6.2.4.2 (a)-(d): Flow patterns (Y-sections) with mineral oil (90 cp) at Re = 90 and H/D = -0.25

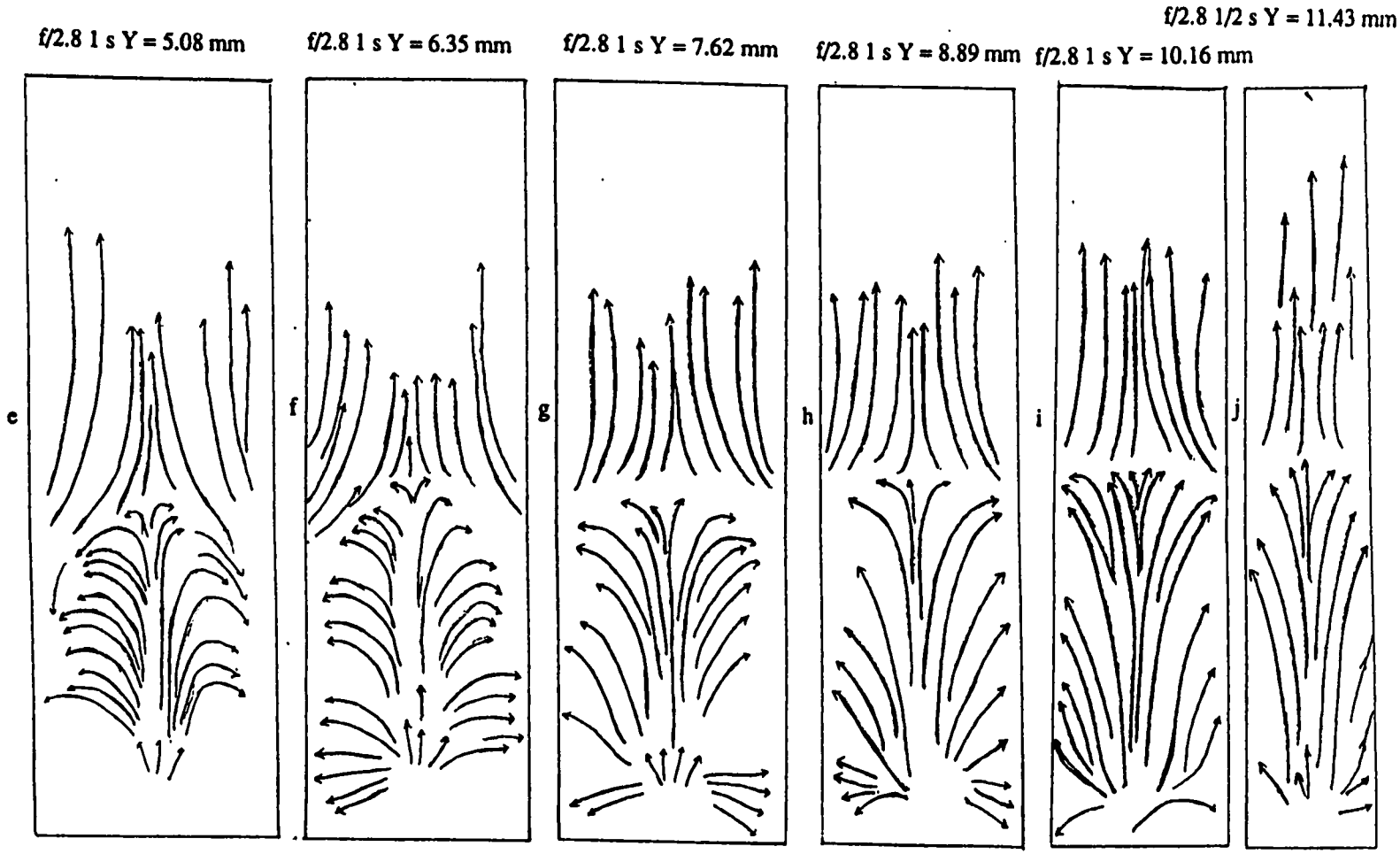

Fig. 6.2.4.2 (cont.) (e)-(j): Flow patterns (Y-sections) with mineral oil (90 cp) at Re = 90 and H/D = -0.25

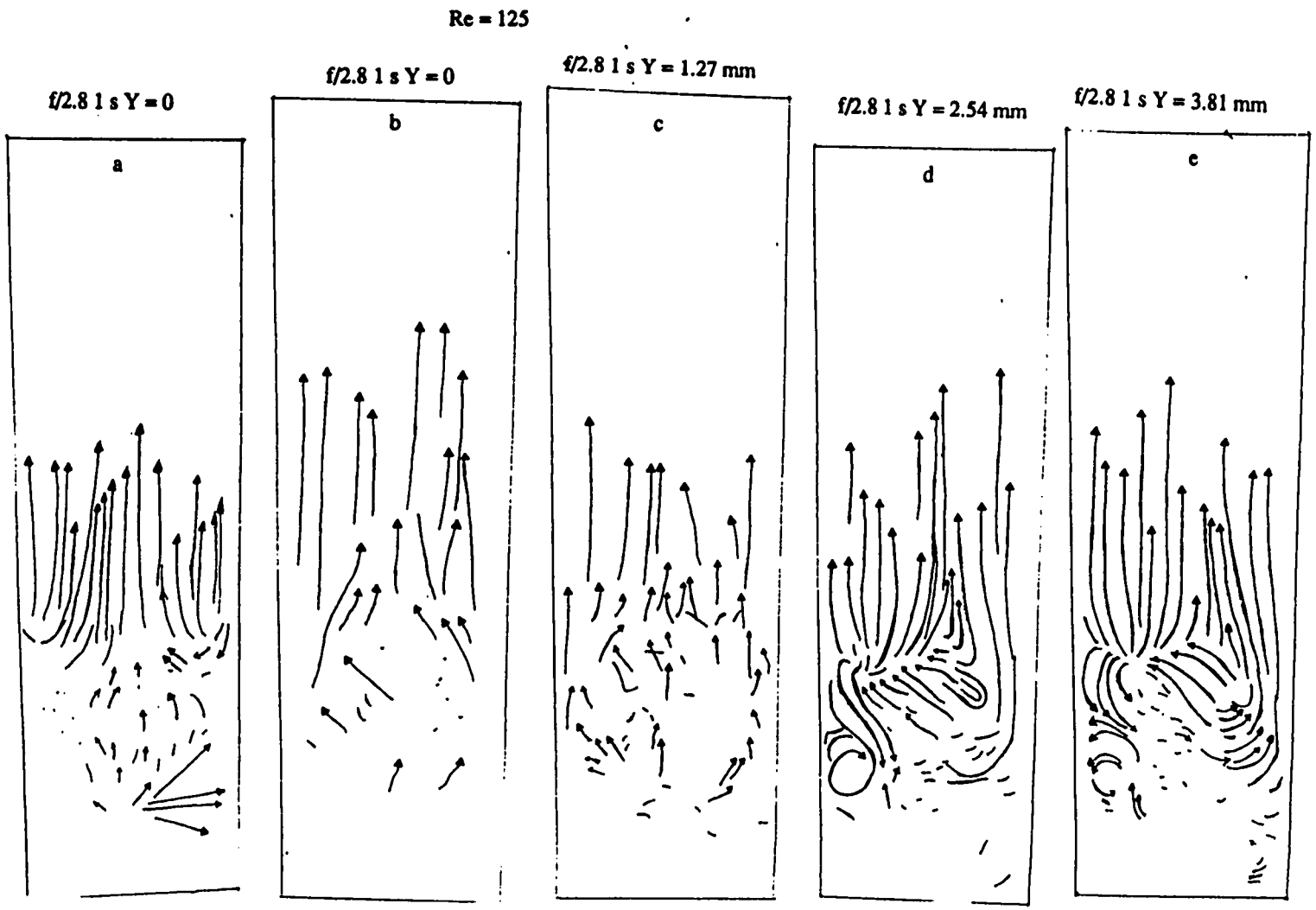

Fig. 6.2.4.3 (a)-(e): Flow patterns (Y-sections) with mineral oil (90 cp) at Re = 125 and H/D = -0.25

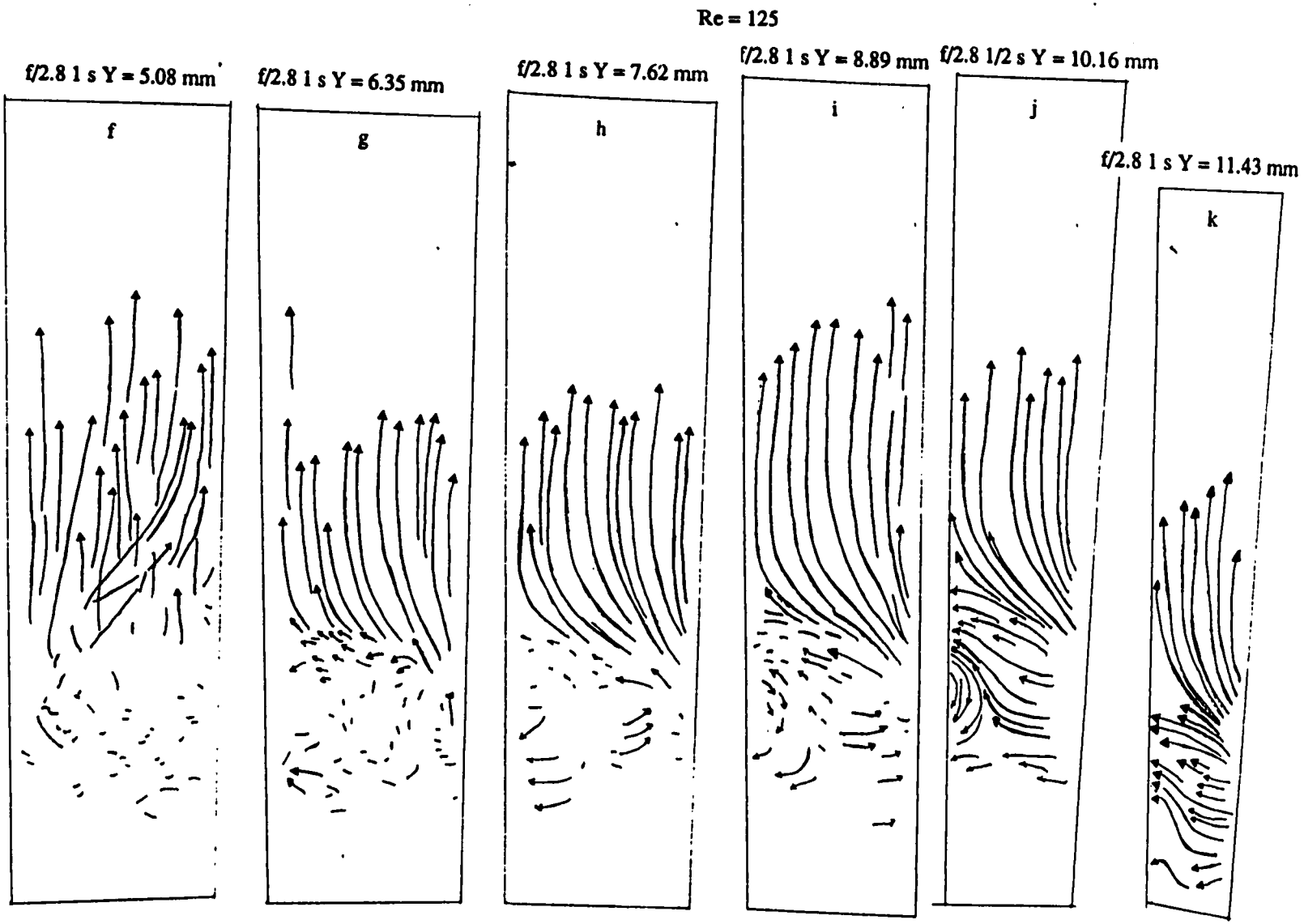

Fig. 6.2.4.3 (cont.) (f)-(k): Flow patterns (Y-sections) with mineral oil (90 cp) at Re = 125 and H/D = -0.25

of many vortices (fig 6.2.4.3 (d)). Further Figures show circulating and developing zones but due to inherent nature of unstable flow, the pattern of the flow continually changes.

6.2.5 Z-plane flow patterns with mineral oil

During the above study, the flow pattern at a plane (Y, Z) at a given $X = X_o$ of the model identified the width (Y) and height (Z) of the vortices which developed in the circulating zone. The figures showed the presence of velocity components U (in Y-direction) and V (in Z-direction) only. The presence of the third component of velocity W (in X-direction) can be studied only if the flow patterns are seen in Y and Z-sections also. To identify the extent and presence of velocity component W, the flow patterns have been obtained at different heights (Z) by illuminating the various circular cross-sections of the mixhead. Here, two cases of dynamical stable flow mode and one case of unstable flow mode are discussed.

At Re = 50 (H/D = -0.50, μ = 39 cp), four symmetrical vortices, one in each quadrant created by jet axis and impingement plane, are visible (Fig. 6.2.5.1 (a)) in the plane of Z = 0. The horizontal path lines are due to the jets. The vertical path lines are due to particles travelling away from jet axis toward wall in the impingement plane. No circulation has been detected beyond this plane (Z = 0) in both directions (increasing or decreasing Z from jet axis).

The flow patterns have been taken at various Z planes which are shown in Figures 6.2.5.1 (b) - (d) at Re = 90 (H/D = -0.25, μ = 90 cp). At all the Z-planes (Z = -2.54, 0, 2.54 mm), which are symmetrical to the jet axis, recirculation is

Re = 50; H/D = -0.5; 39cp

f/2.8 1/60 s Z = 0

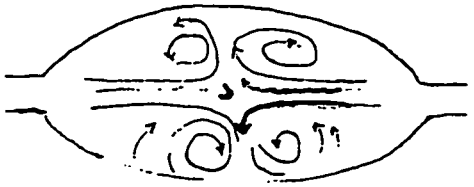

a

Re = 90; H/D = -0.25; 90cp

f/5.6 1/30 s Z = -2.54 mm

b

f/11 1/4 s Z = 0

c

f/5.6 1/30 s Z = 2.54 mm

d

Re = 147; H/D = -0.5; 39cp

f/2.8 1/125 s Z = 0

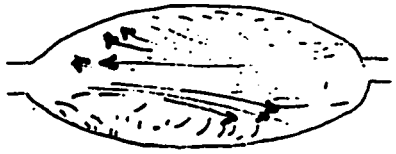

e

Fig. 6.2.5.1 (a)-(e): Flow patterns (Z-sections) with mineral oil at various Reynolds numbers.

present (Figures 6.2.5.1. (b) - (d)). The four symmetrical vortices are clearly visible at planes Z = -2.54, 0, and 2.54 mm. No vivid circulation like these figures was observed beyond Z = ±2.54 planes.

At a Re = 150 (H/D = -0.50, μ = 39 cp), the flow patterns are always in unstable mode. As expected, no symmetry along the jet axis or impingement plane is observed. Figs. 6.2.5.1 (e) shows the flow patterns at Z = 0. This figure indicates the presence of 2-D flow (several curved lines). At Z = 0, the jets do not impinge on each other, but impinge on the opposite walls. Two vortices along with an unstable flow pattern are created as shown in Figure 6.2.5.1 (e). Beyond this plane (Z = 0), circulation was not observed.

6.3 Vector & stream line plots of velocity field from LDA measurements

LDA data are obtained for both velocity components, U and V at two different Reynolds numbers which are 50 and 150. The flow patterns are in a stable mode at Re = 50 and in an unstable mode at Re = 150. These data are taken at various points of a grid as described in section 5.0. Average velocity components are computed from the instantaneous velocities measured with LDA. From these two velocity components U and V, vector and stream plots are generated in x-planes at various x values. These plots are prepared using TECPLOT (Amtek Engineering, Seattle, WA) software. In each plot, the amplitudes of the vectors are automatically scaled. The size of the arrow head indicating the direction of the vector is kept constant throughout the plot regardless of the vector amplitude. These axes represent

the solid boundaries in the mixhead. The piston position is indicated by y-axis and the z-axis represents the mixhead wall from which one jet is entering into the mixhead. Though data have also been taken at z = 140 mm, they are not shown in these plots. In fact, the flow becomes more or less one dimensional at z = 50.8mm.

Figure 6.3.1 shows vectors and stream plots at various x-planes obtained for Re = 50, H/D = 0, and viscosity of 39 cp. At x = 0, a vortex rotates counterclockwise around a point (-4.76, 12.7) as clearly visible in Fig. 6.3.1. A part of the jet flow directly reaches the impingement plane. It turns upwards and continues to move in the same direction. The remaining part of the jet flow is caught within the vortex and, after shifting towards the mixhead wall, starts moving downwards. The vortex is elongated along the z direction with slight tilting towards the mixhead wall. Similar observations were recorded with the flow visualization method. The flow near the wall tends to become one dimensional after z = 22.22 mm while it straightens around at z = 19 mm when y = -4.76. After one mixhead diameter (z = 25.4), the flow does not exhibit re-circulation at all and becomes one dimensional at Z = 50.8 mm. At x = 2.38 mm, a counterclockwise vortex is still visible and no change is observed in the flow pattern from x = 0. With a further increase in x to 4.76 mm, the counterclockwise vortex moves down and circulates around a point (-4.76, 6.35). A part of the downward circulating flow rushes towards the mixhead wall while the remaining flow joins the vortex. At x = 7.14, the circulation below z = 12.7 is clearly visible. The flow near the impingement plane moves upward. The flow between y = -2.38 and y = -4.76 moves initially upwards and then due to circulation changes direction and starts moving downwards rushing towards the mixhead wall. At x = 9.52, only a limited amount of flow has a downward trend

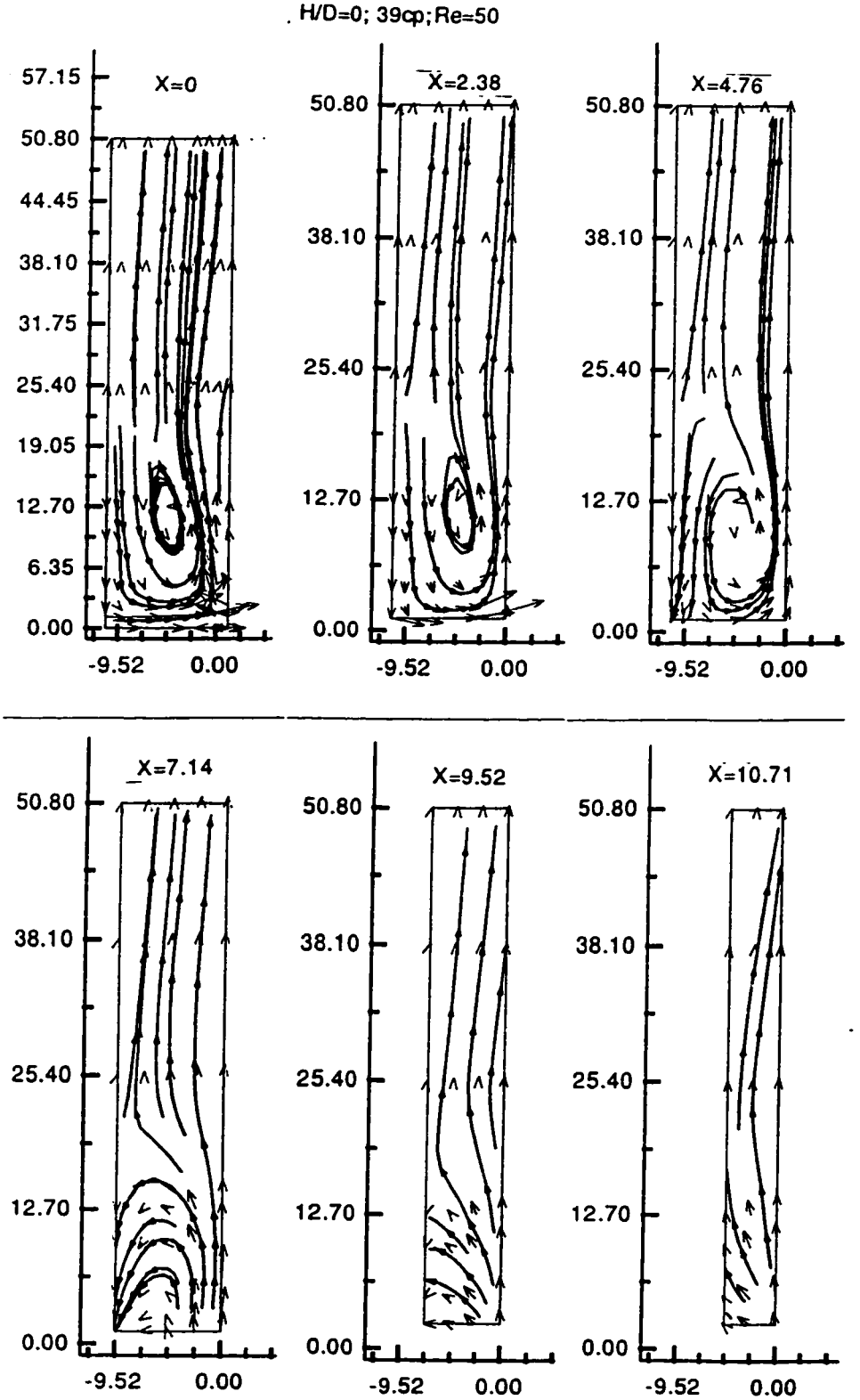

Fig. 6.3.1: Vector & stream line plots of velocity field (LDA) at various X (Re_{DH} 50; H/D = 0: 39 cp)

near the wall. This can be considered as the limit of the circulating region in x direction. No downward flow is noticed at x = 10.71 and all the flow coming from the central zone moves upward. The flow patterns observed using a fluid with viscosity of 75 cp are identical (see Figure 6.3.2).

Figure 6.3.3 shows the vector and streamline plots for Re = 50, H/D = -0.5 and the viscosity of the mineral oil as 39 cp. At x = 0, two vortices are visible. One vortex circulates counterclockwise around a point (-4.76, 19.05) above the jet axis and the other circulates clockwise around the point (-4.76, -8.0) below the jet axis. After impingement, a part of the jet flow moves upward and the remaining portion turns downward. This downward flow after nearly reaching the piston, moves towards the mixhead wall and joins the clockwise vortex. A part of the flow near the impingement plane moves directly upward while the remaining flow joins the counterclockwise vortex and moves downward. In this particular plane, no connection between the flow below and above the jet axis is apparent. The vortex above the jet axis is elongated while the bottom vortex seems more or less circular in shape. The same trend is observed in flow visualization experiments. After z = 25.4, all the flow straightens out and becomes one dimensional around z = 50.8 mm. At x = 2.38 mm, the flow pattern remains similar to the flow pattern in the x = 0 plane. Both vortices still exist at x = 4.76. The upper vortex has moved down and circulates around the point (-4.76, 12.0). Connecting streamlines are visible which show the transfer of fluid particles from the bottom circulation zone to the zone above the jet axis. A part of the flow near the mixhead wall in both circulating regions is rushing towards the jet inlet. At x = 7.14, the connecting streamlines of both vortices are seen. Some of the bottom recirculating flow joins the flow near the impingement

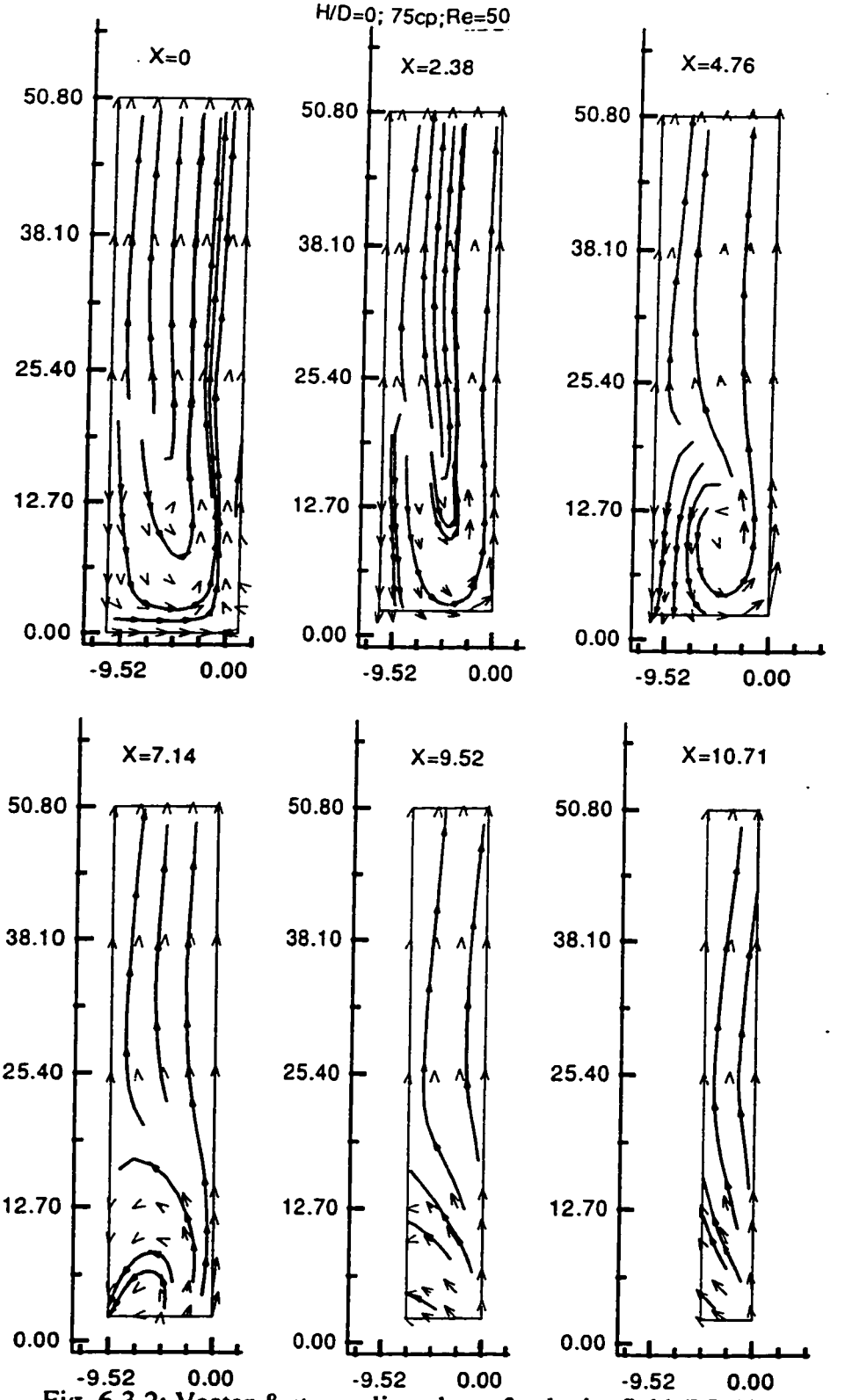

Fig. 6.3.2: Vector & stream line plots of velocity field (LDA) at various X (Re = 50; H/D = 0; 75 cp)

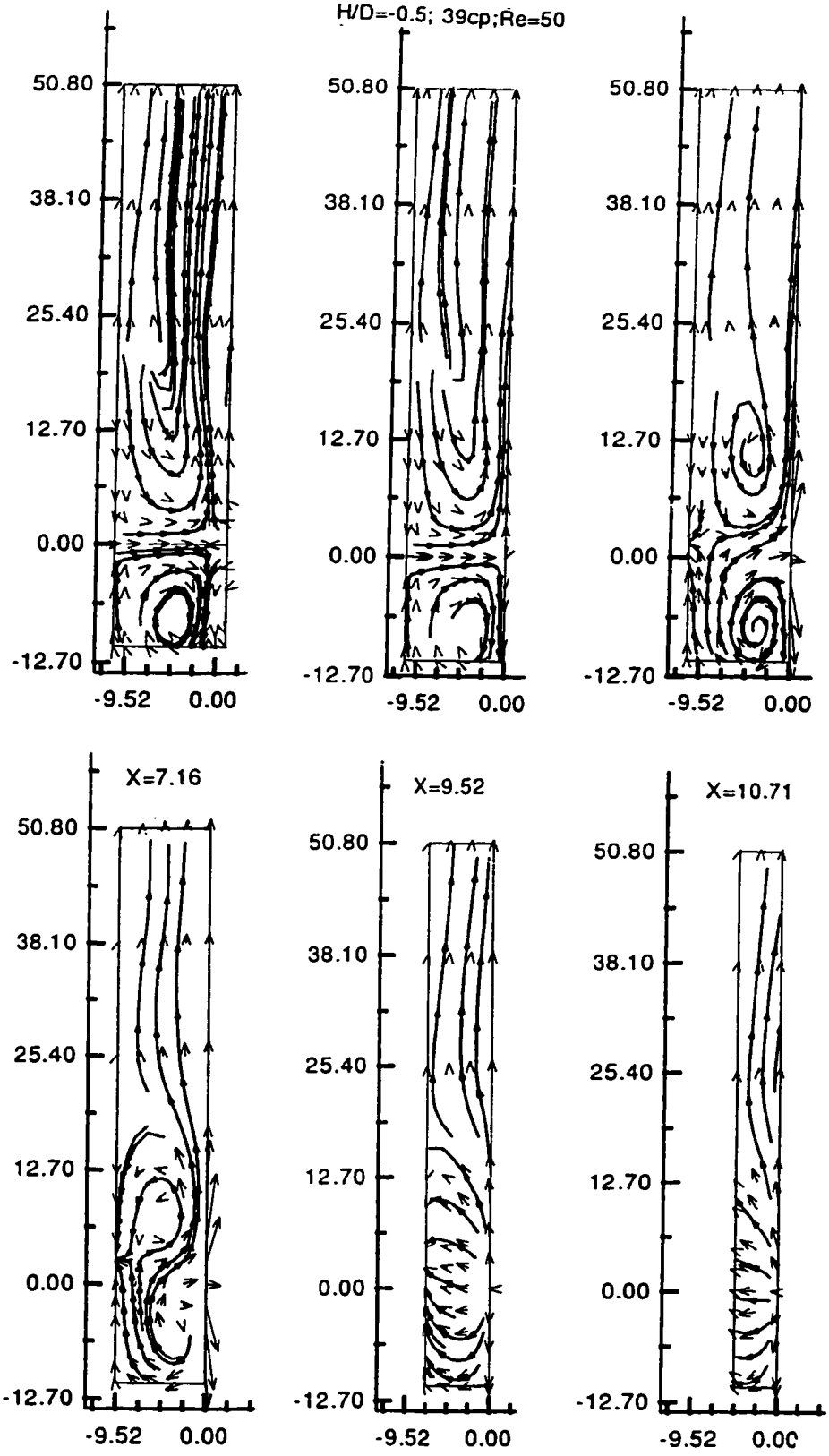

Fig. 6.3.3: Vector & stream line plots of velocity field (LDA) at various X (Re = 50; H/D = -0.50; 39 cp)

plane and moves upwards. The remaining flow joins the circulating fluid in the upper vortex. The upper vortex has further moved down. At x = 9.52, the circulating region seems to vanish. However, within the circulating region, the flow moves towards the mixhead wall from the central zone. In the bottom section, this flowturns towards the jet inlet and moves upwards. In the upper recirculating zone, the downward pattern of the flow near the wall is still in evidence. No circulation is seen at a plane x = 10.71. It seems as if the flow coming from the central region curls towards the wall and turns upward. The flow pattern remains similar for the fluid with a viscosity of 75 cp (Fig. 6.3.4). It can be concluded that lowering of the piston by a half mixhead diameter has generated another recirculating zone below the jet axis.

The vector and streamline plots for Re = 150 (unstable flow mode), H/D = 0, and viscosity of 39 cp are shown in Fig. 6.3.5. At x = 0, one vortex circulates counterclockwise around a point (-4.76, 19.05). The fluid close to the impingement plane moves upward while the remaining jet fluid enters the circulating flow. No circulation is observed beyond z = 25.4 mm. The flow pattern remains the same at x = 2.38 mm. The counterclockwise vortex moves down and closer to impingement plane at x = 4.76 mm and further moves down in case of x = 7.14 mm. Beyond x = 7.14 mm, the flow patterns are similar to the flow patterns at Re = 50 (Fig. 6.3.1).

Figure 6.3.6 shows vector and streamline plots for Re = 150, H/D = 0, and viscosity of 75 cp. These are similar to the flow patterns obtained at a viscosity of 39 cp (Fig. 6.3.5). This shows that viscosity has no effect on flow patterns. To check the symmetry of flow patterns about the jet axis at such a higher Re, the vector and

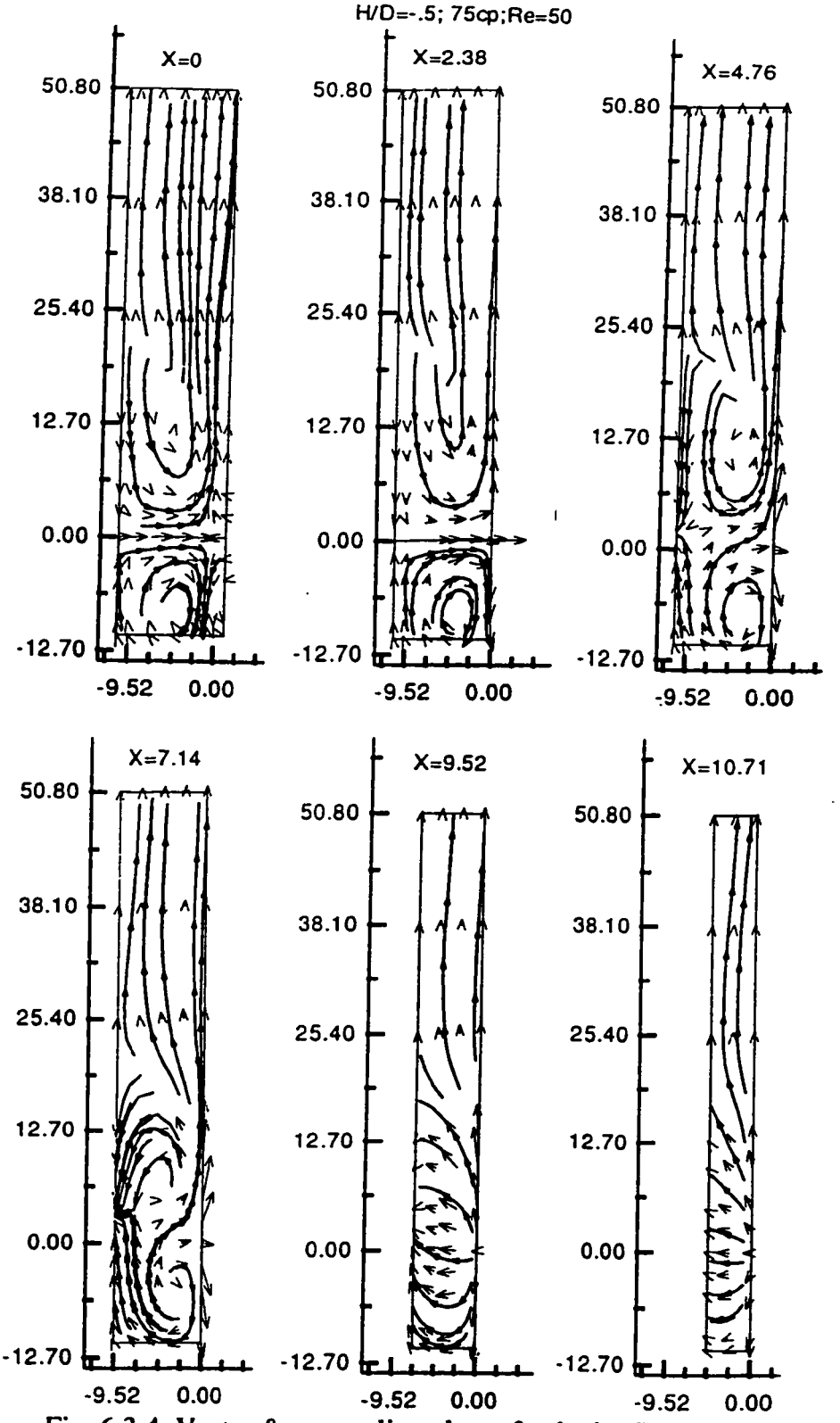

Fig. 6.3.4: Vector & stream line plots of velocity field (LDA) at various X (Re = 50; H/D = -0.50; 75 cp)

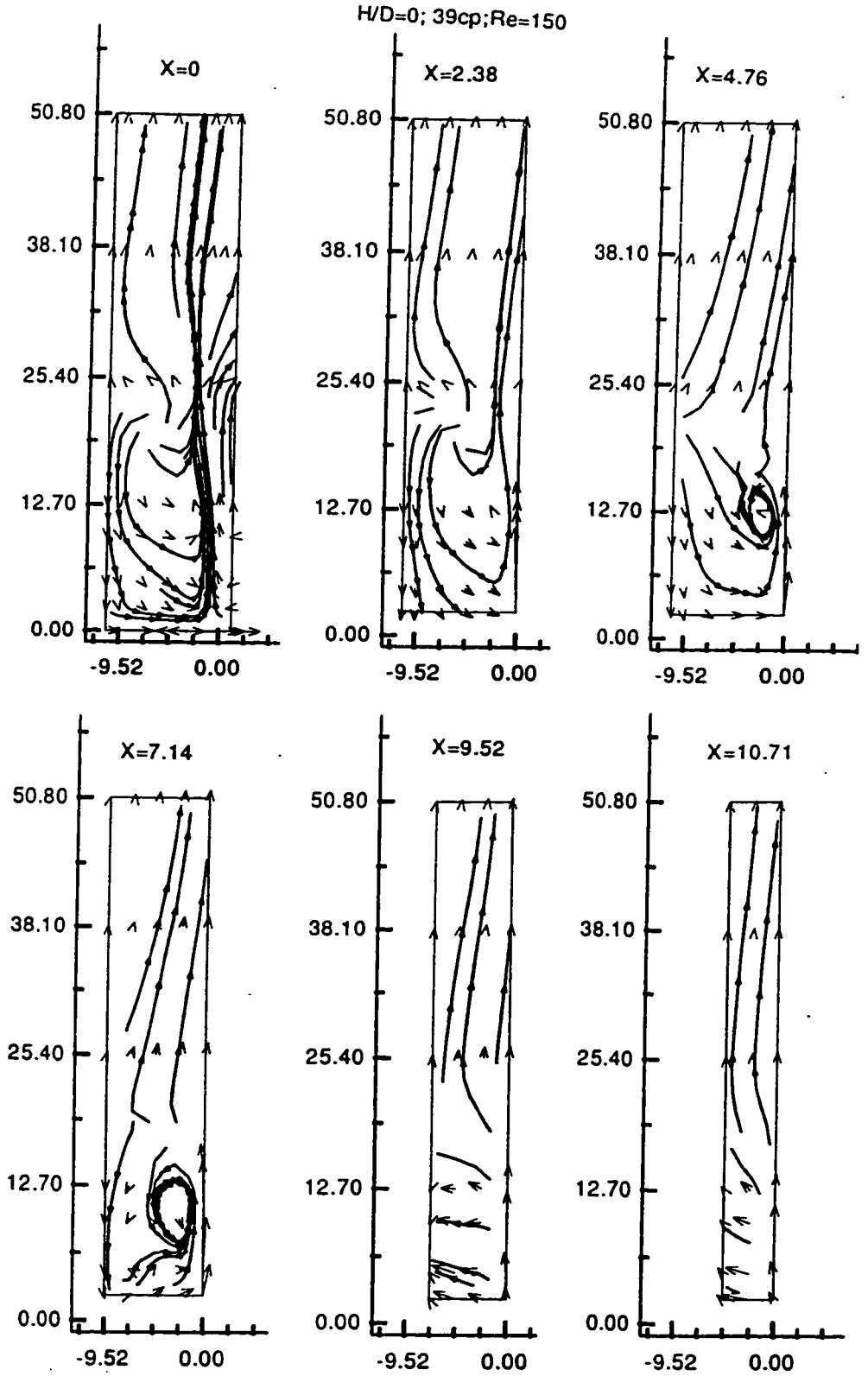

Fig. 6.3.5: Vector & stream line plots of velocity field (LDA) at various X (Re = 150; H/D = 0; 39 cp)

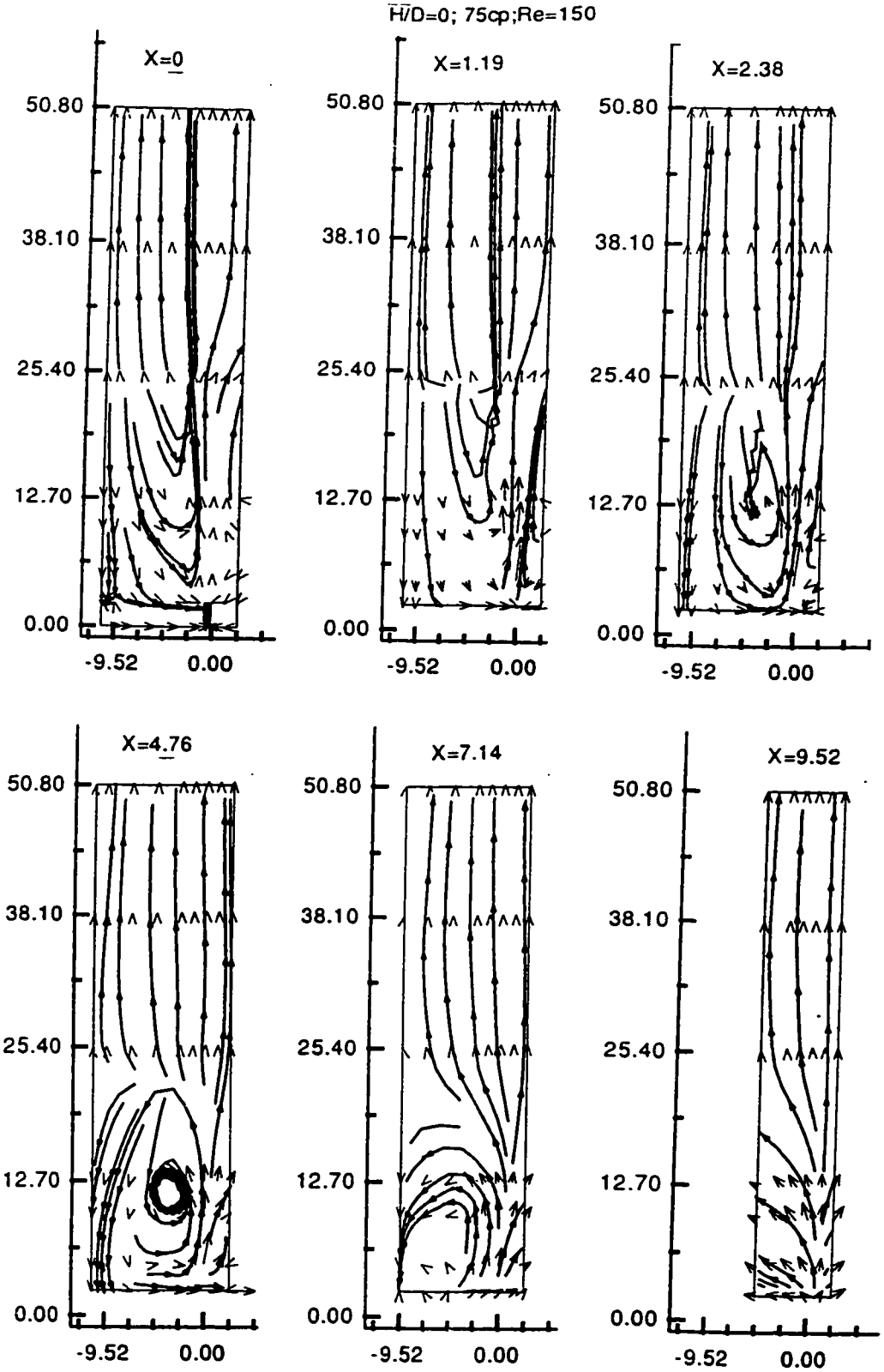

Fig. 6.3.6: Vector & stream line plots of velocity field (LDA) at various X (Re = 150; H/D = 0; 75 cp)

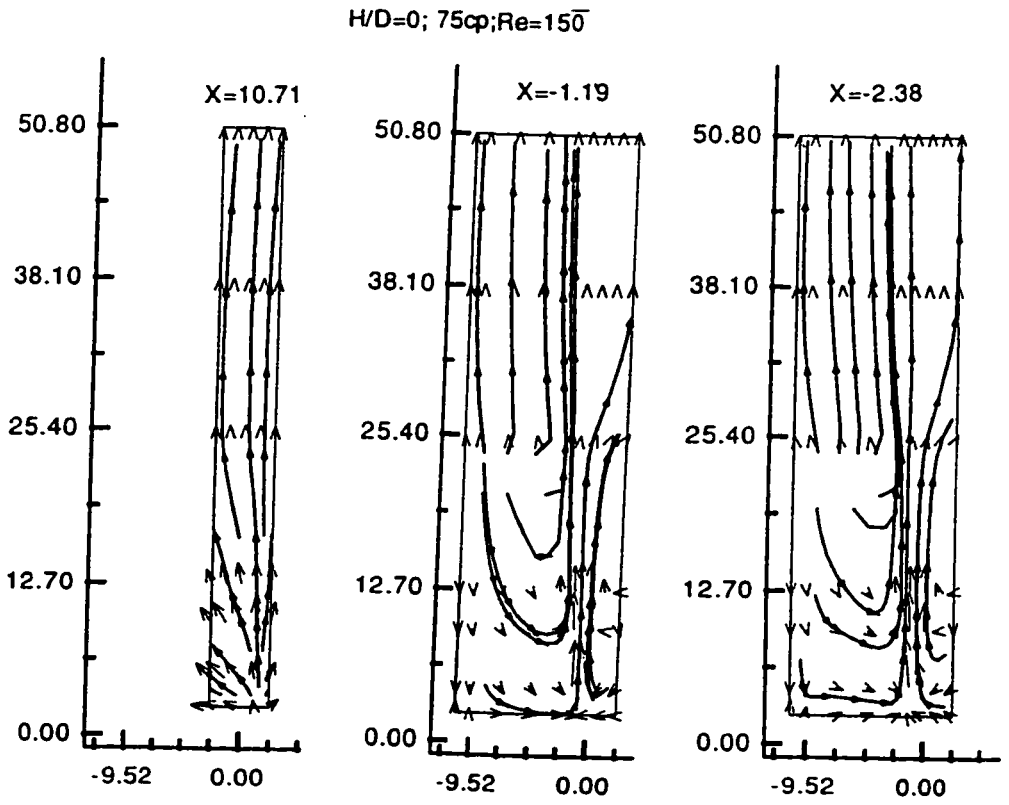

Fig. 6.3.6 (cont.): Vector & stream line plots of velocity field (LDA) at various X (Re = 150; H/D = 0; 75 cp)

streamline plots were made on either side of the jet plane. These figures show pattern symmetries for x = 1.19 mm and x = -1.19 mm, and also for x = 2.28 mm and x = -2.38 mm. Further, the data are taken and plotted for y = 1.19, -1.19 mm, and for y = 2.38, -2.38 mm which confirm the symmetry about impingement plane also. It is worth mentioning here that these are long term symmetries since plots are made using average velocities.

At a piston position of H/D = -0.5, many small vortices are visible (Fig. 6.3.7 for Re = 150 and viscosity of 39 cp) at x = 0. The lower and upper chamber circulations are also evident. No localized circulation is observable beyond x = 4.76 mm. With the increase in viscosity to 75 cp, the flow patterns remain similar to Fig. 6.3.8.

All the above figures of this section provide quantitative confirmation of the conclusions drawn with flow visualization. The flow patterns are invariant to viscosity changes and long term symmetry exists in the system.

6.4 Flow modes and vortex growth

The above study indicates that there are three distinct flow modes (static stable, dynamic stable, and unstable) which depend upon the value of Re and H/D. Fig. 6.4.1 shows the type of flow modes for a given set of Re and H/D. It can be seen that the flow mode remains static stable for all values of H/D if Re < 50. As Re is increased the static stable mode changes to a dynamic stable mode. For the present set-up, this transformation occurred at a critical value of approximately Re = 50 regardless of the value of H/D. Further increases in Re changes the dynamic stable mode to an unstable mode. The figure clearly indicates these transformations for

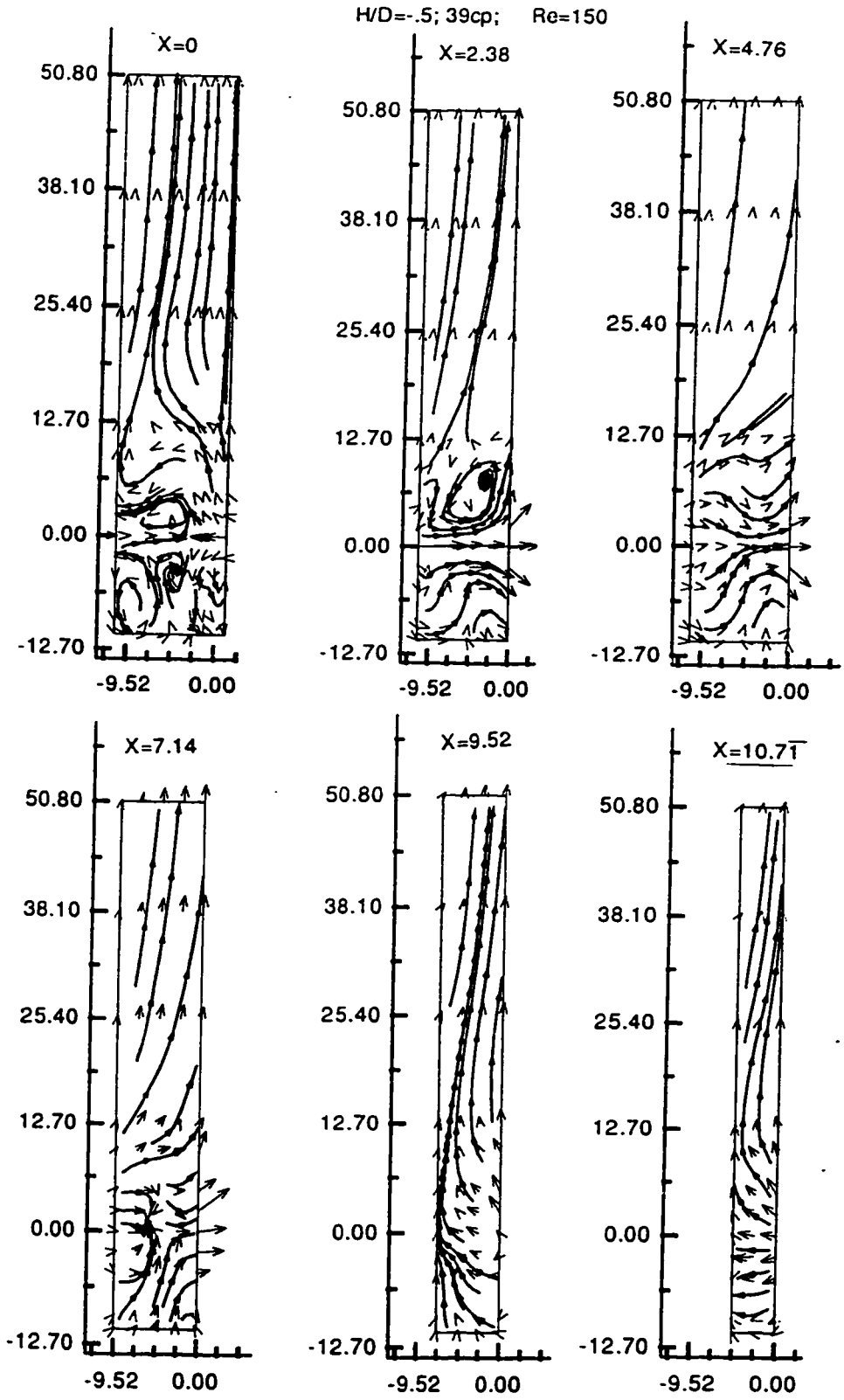

Fig. 6.3.7: Vector & stream line plots of velocity field (LDA) at various X (Re = 150; H/D = -0.5; 39 cp)

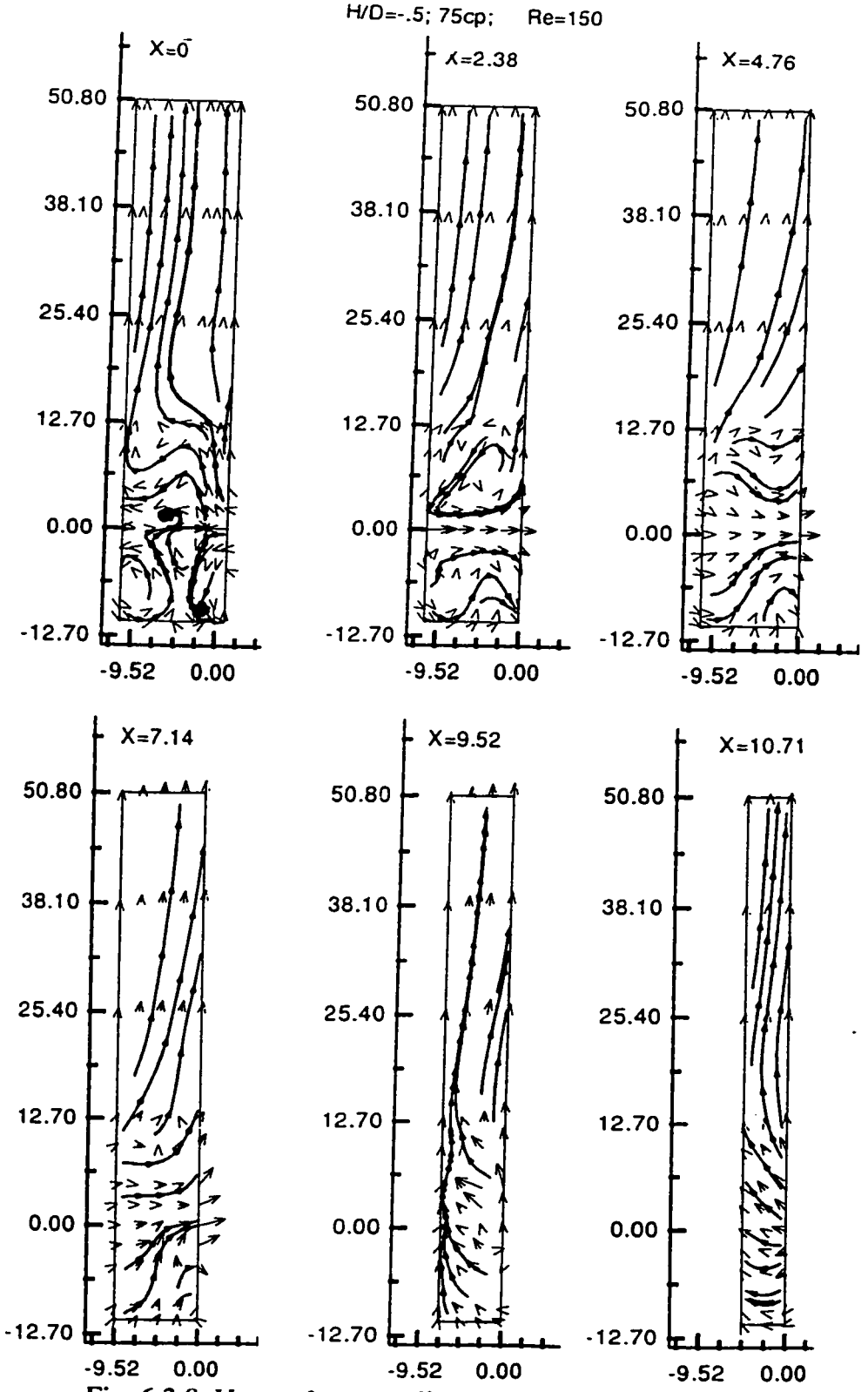

Fig. 6.3.8: Vector & stream line plots of velocity field (LDA) at various X (Re = 150; H/D = -0.5; 75 cp)

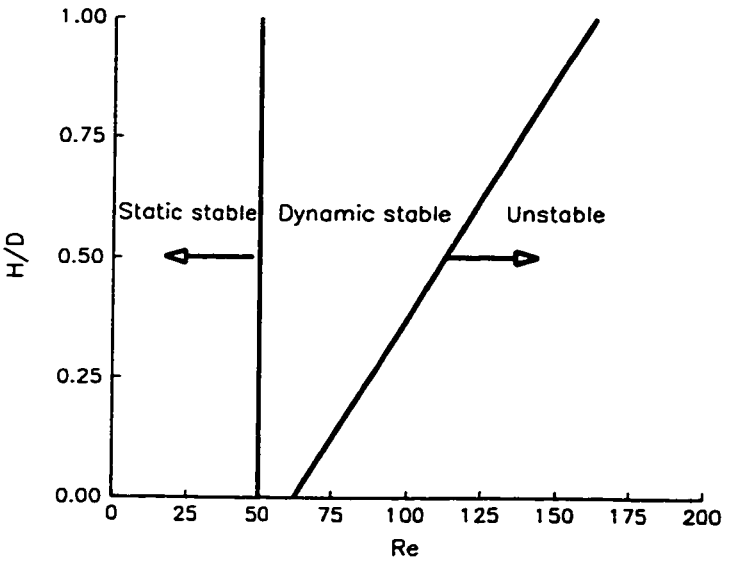

Fig. 6.4.1: Various flow mode regions as a function of Re and H/D

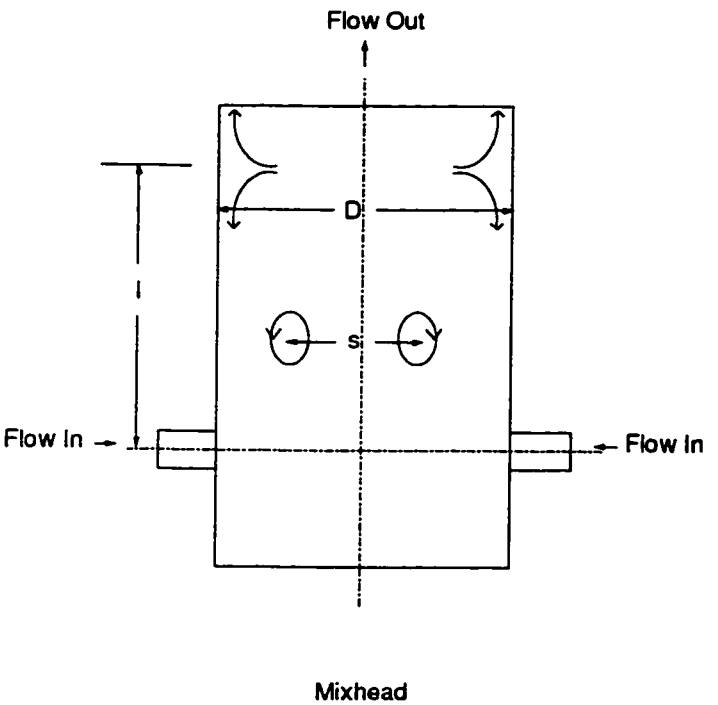

Fig. 6.4.2: Circulating zone (above jet axis) configuration

four different values of Re (approximate) = 100, 125, 150, and 200, respectively. The H/D ratio plays a significant role for this transformation to occur. For a given Re, the flow mode can be kept in a dynamically stable mode by increasing the H/D. However,the observations showed that for sufficiently high Re (approximately 200), the flow mode is always unstable. Again, the value of H/D has no influence on the flow mode. This shows that Re plays the primary role in determining the flow mode. The ratio H/D has no effect at very low (<50) or high Re ($\geq$ 200), but it has a significant effect in determining the limiting value of Re for dynamic stable mode.

During the flow visualization, it has been consistently observed that the vortices develop and grow in size with an increase in Re both in the static and dynamic stable modes. Similar observations have been reported in the work of Deshpande and Vaishnav (1982) who studied the submerged laminar jet impingement on a plane. According to Spalding (1961), the flow pattern obtained using two opposed jets is identical with that of a single fluid jet impinging on a flat plate held normal to it if the diameter, densities, and velocities of the two opposed streams are equal. Our observations do not agree with Spalding's conjecture.

The growth of the vortices is described by two dimensionless parameters l/D, and s/D where l represents the length of the recirculating zone and s is the distance between the two counter rotating vortices above the jet axis (Fig. 6.4.2). Table D 1 (Appendix D) shows s/D and l/D along with Re, H/D and viscosity of the fluid. The theoretical values of l/D = 0 and s/D = 1, when Re = 0 i.e. no flow, are also listed in the table. In no flow situation there is no vortex so l = 0 and s = D.

Figs. 6.4.3 - 6.4.5 show the growth of the vortices (variation of l/D) with Re for various combination of H/D and viscosity of the fluids. The l/D ratio always increases with increasing Re, reaches a maximum, and then a slight reduction occurs. The dynamic stable mode changes to the unstable mode if Re is further increased. Inthese figures, the curves are shown up to the dynamic stable mode limit. There are few points (Fig. 6.4.3 at Re = 125 and H/D = 0 and Re = 98 and H/D = -0.5) in the unstable mode region. Though the flow mode was unstable most of the time, it will intermittently return to dynamic stable mode. The recirculation region (l/D) slightly increases as H/D is changed 0 to -0.5 (moving piston down from jet axis) for a given Re (see Figs 6.4.3 and 6.4.4 for 39 and 75cp, respectively). This increase is more significant in the dynamic stable mode (Re > 50) compared to static stable mode (Re < 50). Fig. 6.4.6 shows the variation of s/D with Re. It sharply decreases with increasing Re within the static stable zone and then maintains a relatively constant value in the dynamic stable zone regardless of the variation in H/D. The observed data are shown with the regression curve. Models, based on a regression analysis, are proposed for the vortex growth with increasing Re.

$$\frac{l}{D} = a - be^{-cRe} \tag{6.4.1}$$

$$\frac{s}{D} = a + be^{-cRe} \tag{6.4.2}$$

The proposed models are nonlinear with respect to parameter c. The estimation of optimum parameters was obtained by iterating least squares linear analysis. For a given H/D, the observed data of l/D versus Re were linearly regressed to estimate the parameters a, b, the correlation coefficient (R^2), and F (from analysis of variation

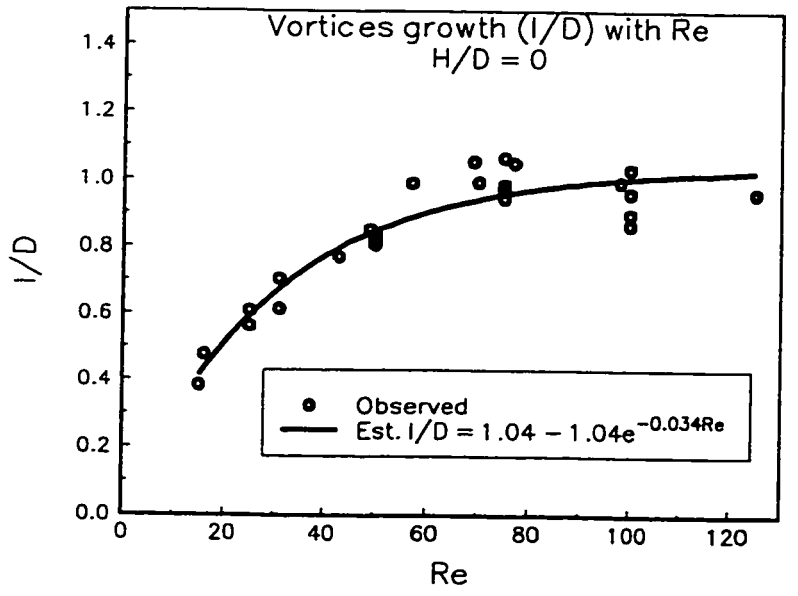

Fig. 6.4.3: Vortices growth (l/D) with Re at H/D = 0

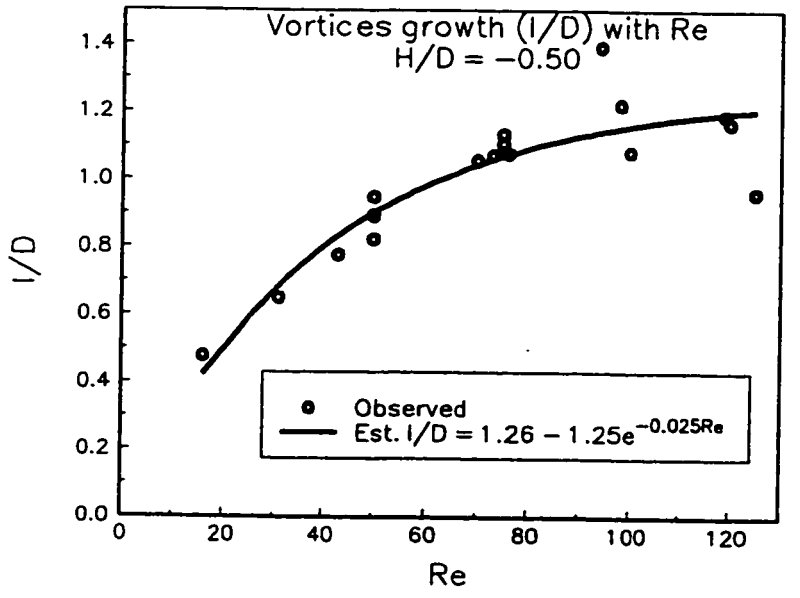

Fig. 6.4.4: Vortices growth (l/D) with Re at H/D = -0.50

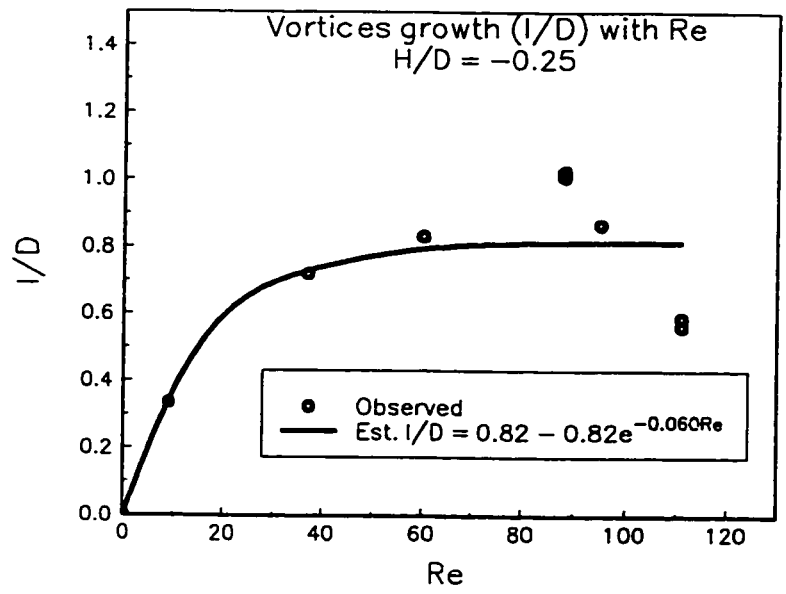

Fig. 6.4.5: Vortices growth (l/D) with Re at H/D = -0.25

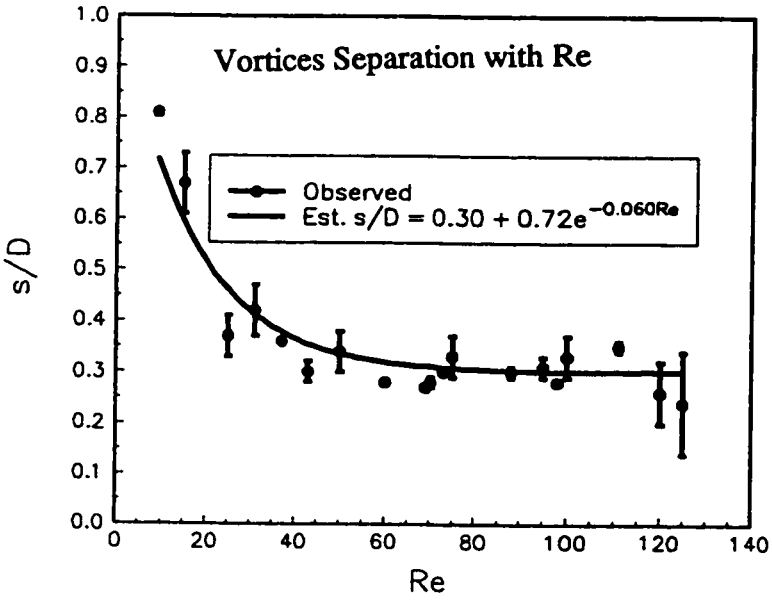

Fig. 6.4.6: Vortices sepration (s/D) with Re

table) at a selected value of parameter c in Eq. 6.4.1. The value of c was changed and the linear regression was repeated. The set of parameters that gave maximum R^2 and F was selected as optimum and are reported here (Table 6.4.1) with relevant statistical estimation.

Table 6.4.1: Coefficients of vortex growth model

Coefficients and regression analysis for vortex length estimation

$$\frac{l}{D} = a - be^{-cRe}$$

H/D	Viscosity (cp)	Data #	ID	Coefficient	Stdev	t-ratio	F	R^2
0	39 & 75	30	a	1.038	0.014	76	670	96
			b	1.038	0.040	-26		
			c	0.034				
-0.5	39 & 75	20	a	1.260	0.028	44	300	94
			b	1.249	0.072	-17		
			c	0.025				
-0.25	90	8	a	0.819	0.066	12	23	73
			b	0.819	0.170	- 5		
			c	0.060				

At the 95% confidence level all the coefficients in Eqs. 6.4.1 and 6.4.2 are significant and the regression equation accounts the significant variation. The recirculation zone length (l/D) shows some influence of H/D as

Table 6.4.1: Coefficients of vortex growth model (cont.)

Coefficients and regression analysis for vortices separation estimation

$$\frac{S}{D} = a + be^{-cRe}$$

H/D	Viscosity (cp)	Data #	ID	Coefficient	Stdev	t-ratio	F	R^2
All	All	60	a	0.300	0.007	41	941	94
			b	0.721	0.024	31		
			c	0.060				

Notes: (1) The t-ratio for each coefficient (a and b) is greater than the critical table value at 5% level. Thus the null hypothesis is rejected that the coefficient is zero.

(2) The computed F (From the analysis of variance) is greater than the tabulated value at 5% level of significance, thus the null hypothesis that all the true partial regression coefficients are equal to zero is rejected.

(3) The computed R^2 is greater than the tabulated value at 5% level of significance, it is concluded that the regression model accounts for the significant amount of variation in the dependent variable.

evident from the value of parameters listed in the Table 6.4.1 and Figs. 6.4.3 to 6.4.6. Thus, one equation for each value of H/D is proposed. For the case of s/D, the influences of H/D and viscosity were negligible; hence only one equation is proposed.

6.5 Conclusions from the flow visualization

The following conclusions can be drawn from the flow visualizations of the mixhead using various techniques:

1. From all of the experimental observations, it is evident that the viscosity has no significant influence on the flow patterns at constant Re. However, it has a definite impact on the observability of the flow patterns. At low viscosity, the flow pattern is very sensitive to any perturbation generated within the system or coming from surroundings. It is obvious that the velocity will be lower for a fluid with low viscosity when compared to a fluid with higher viscosity at a given Re. Thus, it is possible that perturbations may be of the same order as the velocity of the fluid particles at lower viscosities. This may be one of the factors for the fact that observability was very low during the experiments with low viscosity fluids. In cases of fluids with high viscosity, the perturbation will be very low compared to the velocities of fluid particles; thus, observability will be facilitated in such a case. Also, it appears that the fluids with low viscosity do not have the capacity to absorb external energy (due to the pump) and thus fluid particles activate more even at small perturbation. Probably, due to this reason also the observability of the flow patterns is diminished at low viscosities.

2. The Re has a significant effect on the flow field. At low Re (< 50), the flow is in a statically stable mode. At slightly higher Re (≥ 50), the flow pattern changes to a dynamically stable mode and the impingement plane oscillates. The flow reaches an unstable mode once $Re \geq 125$. In fact, the vortices gradually grow with increasing Re and at a critical level they dynamically interact with each other

causing the oscillation of the impingement plane. It has been found that the length of the circulating region increases in proportion $Re^{0.4}$ for both the static and dynamic stable zones as long as stability is maintained. After that, the re-circulating region shrinks a little bit before breaking into a totally unstable flow. Some traces of mixing (fluid transfer from one vortex to other) are also observed with increasing Re in dynamic stable mode.

3. As described above, the flow pattern changes from a stable to unstable mode at higher values of Re. The piston position (H/D) plays an important role in the stability of the flow pattern. The results show that the flow pattern is always unstable at Re = 150 when the mixhead aspect ratio H/D is 0 or 0.5. However, a stable flow pattern is seen at the same Re when the H/D is increased to 0.75 and above. No stable patterns could be obtained at Re = 200 up to H/D = 1.0. It appears that the flow patterns are always unstable at very high Re.

4. In the stable mode, the flow is symmetric about the impingement plane with one important exception; the flow directions on the left and right side of the circulating zone are opposite to each other.

5. Using a 2-D flow visualization technique (particle visualization with a laser sheet) , it was concluded that the actual flow is three dimensional in the vortex region. The flow patterns seen with X-sectioning confirm that the depth of the vortices reaches up to the half of the mixhead radius at Re = 50. At higher values of Re, it almost touches the wall of the mixhead. The flow study with sectioning in various Y-planes showed that there exists an irrotational flow near the mixhead axis (in the static and dynamic stable region) which, in fact, is the impingement

plane. The Z-sectioning has shown that in the neighborhood of the jet axis the flow is quadratically symmetrical. The study with the Z-sectioning also confirmed that no circulation existed beyond one mixhead diameter. The existence of W component of velocity in the circulating zone has also been established from the 2-D flow visualization technique.

6. Based on the above observations, two viscosities (39cp and 75cp), two H/D ratios (0.0 and 0.5), and two Re values (50, and 150) which represent the dynamically stable and unstable modes, were selected for mapping of the velocity components U and V and studying the flow field using the LDA technique. The flow patterns obtained from LDA experiments are qualitatively similar to those obtained with flow visualization methods.

7 Analysis of center line velocities measured using LDA

Velocity measurements were obtained using the laser Doppler anemometer for several different geometric and fluid parameters. Geometrically, the chamber diameter was fixed at D = 25.4 mm with directly opposed jets flowing from holes with diameter d = 2.38 mm. Two different "clean-out" piston positions, H, were used. These were "flush" where the clean out piston is positioned flush with the bottom of the jets, H/D = 0 and H/D = -0.5 where the piston is positioned 0.5 D back from the line joining the center of the jets. The working fluid was mineral oil and two fluids with nominal viscosities of μ = 39 cp and μ = 75 cp were used. For a fixed viscosity, the jet Reynolds number (Re) was varied by changing the volumetric flow rate flowing through the jet. Re was varied from 50 to 200 in steps of 25 for the μ = 39 cp fluid and form 50 to 150 for the μ = 75 cp fluid. Pump limitations prevented higher values of Re from being attained using the higher viscosity fluids. In this study, axial and radial velocities on the jet centre-line (X = 0; Y = 0) are presented.

The radial velocity (U) is parallel to jet axis and lies in horizontal plane. A positive radial velocity (U) indicates that the flow is from left jet to right jet, while a negative velocity indicates reverse direction (see Fig. 7.1.1). The axial velocity (V) is parallel to mixhead axis and is perpendicular to the horizontal plane. The positive axial velocity (V) indicates that the flow is upward.

Theoretically, since jets of equal strength are being impinged, the radial velocity (U) should be equal to zero at the impingement point. In addition, on the average,

the radial velocity along the center - line of chamber should also be zero. In some cases the measured radial velocity at impingement point was not zero. This could be due to a variety of reasons.

1. Alignment: It is possible that the model was not properly aligned and that readings taken at what was thought to be at the theoretical impingement point were not actually being taken at this point. This is highly unlikely since the velocity was measured on both sides of the center point and necessary adjustments in alignment were made so that the velocity approaches the theoretical zero value. Also, velocity measurements taken along a line joining the centers of the two orifices show a sudden reversal of velocity within $\pm$ 2 mm of the impingement point.

2. Jet deflection: Flow visualization experiments have shown that above a threshold value of Re (around Re = 125) the jets are deflected and may not impinge. Instead the jets impinge on the far side of the chamber and wind their way out of the chamber in a toroidal fashion.

3. Imbalanced flows: The flow input from the two jets is not exactly equal. A slight imbalance in the flow through the two orifices will result in a deviation of the U-velocity component from zero at impingement point, where the measurements are made. This imbalance is caused by the difficulty in obtaining exactly the same rotameter readings on each side. A small imbalance in the flows is the most probable cause for some no-zero U-velocity component at the mid-point.

The axial velocity (V) in the mixhead has been compared with the one-dimensional developed flow in a pipe at a particular Reynolds number in mixhead.

For H/D = 0, the minimum Z for both velocities' (U & V) measurements was equal to 1.19 mm (equal to jet radius), though the radial velocity was also measured at Z = 0. For the case of H/D = -.5 the lowest location for both measurements is Z = -11.00 mm. These limits are imposed due to the optical limitations of the experimental setup. The LDA beams below these locations are either blocked or distorted such that the photomultiplier could not be focused.

7.1 Radial and axial velocity profiles for H/D = 0 & μ = 39 cp

The radial velocity (U) profile for zero mixhead aspect ratio (H/D) for different jet Reynolds number and μ = 39cp are given in Figures 7.1.1 to 7.1.3. These plots show the average of ten thousand instantaneous velocity measurements with 95% confidence limits. A fitted cubic spline through these observed average is also drawn to show the general trend of profile. A reference line (U = 0) is also shown to highlight the axial distance (Z) where the particular velocity component has become insignificant. This distance is essential to know since it indicates the upper limit of any mixing zone due to interaction of counter-rotating vertices. If mixing is at all occurring due to fluid mechanics, it has to be in this zone since after this limit the flow is essentially one dimensional (supported by flow visualization and the axial velocity measurements with LDA) and only molecular diffusion generates mixing in one dimensional flow. Radial velocity decreases to insignificant level within one mixhead diameter (25.4 mm) from jet impingement axis.

At Re = 50 (Fig. 7.1.1), the absolute value of radial velocity starts to increase, reaches a maximum at Z = 1.19 mm (equal to jet radius) and then starts to decrease. As Z is further increased the radial velocity within one mixhead diameter vanishes

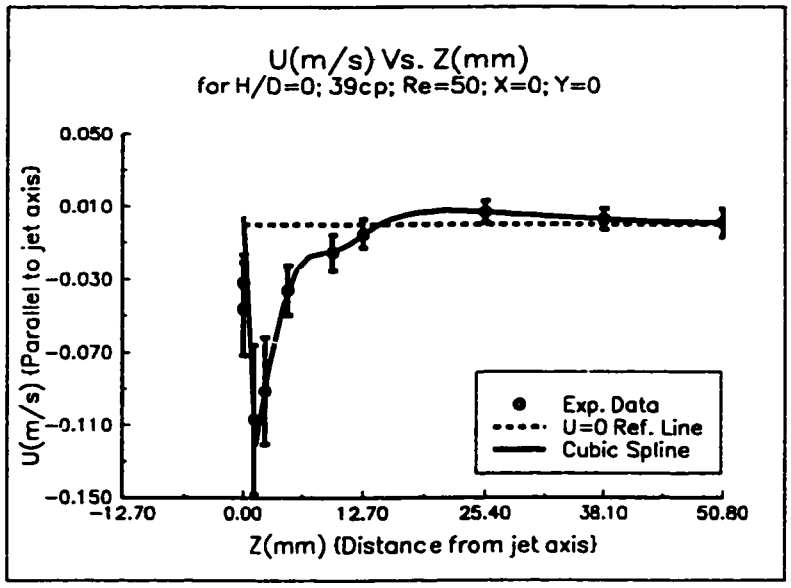

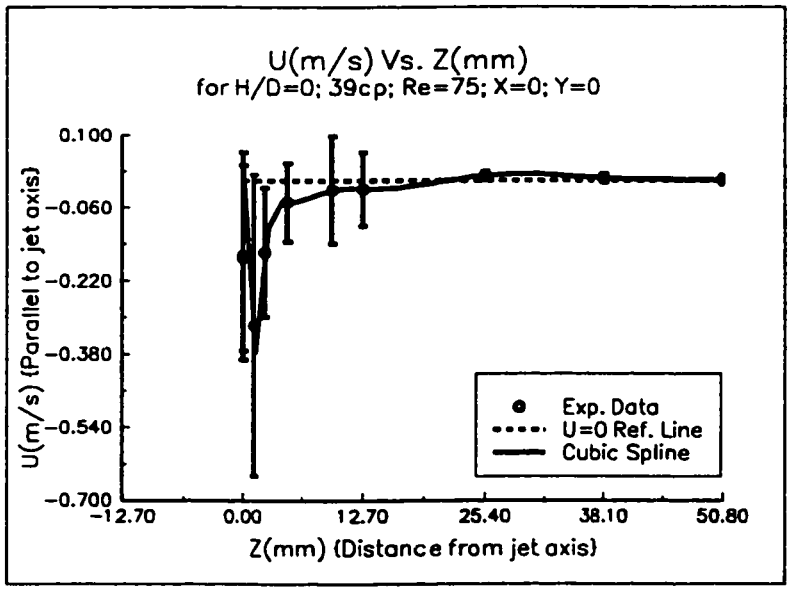

Fig. 7.1.1: Radial velocity (U) profile along mixhead axis (Z)
(Re = 50 & 75; H/D = 0; 0.39cp)

for all practical purposes. The velocity and its standard deviation after Z = 9.52 mm are less than the instrument precision of LDA. This LDA setup can precisely measure a lowest absolute velocity of 10 mm/s. The standard deviation also follow the same profile as the velocity. After Z = 9.52 mm the velocity and standard deviation are around 5 mm/s.

For Re = 75 (Fig. 7.1.1), the absolute value of radial velocity first increases to a maximum (Z = 1.19 mm) then exponentially decreases to a negligible value. The RMS of U from Z = 4.76 mm to Z = 12.7 mm is either the same order of magnitude as the U or greater than U. This indicates a vigorous fluctuating or periodic flow. From $Z \geq 25.4$ mm, U and the RMS of V vanish as in the case of Re = 50. The profile at Re = 100 (Fig. 7.1.2) follows a similar path as the previous two cases, but the RMS value at Z= 9.52 mm and Z = 12.7 mm are larger than the values for $Z < 9.52$ mm or $Z > 12.7$ mm. These RMS values of U are the order of the largest U observed at Z = 1.19 mm (.146 m/s). This indicates vigorous fluctuations. After Z = 25.4 mm the mean value of radial velocity as well as its RMS become insignificant.

The radial velocity for Re = 125 (Fig. 7.1.2) first increases as Z increases, reaches a maximum at Z = 1.19 mm then gradually decreases. It vanishes after Z = 12.7 mm. The RMS of U at Z = 9.52 mm and Z = 12.7 mm are higher than for other Z values. At Z = 0 one repeat experiment is also shown. This indicates a good reproducibility of the results since the mean radial velocity and its RMS are the almost same for these two experiments. At Re = 150 (Fig. 7.1.3) the absolute value of radial velocity decreases as Z increases. The maximum of absolute U occurs at Z = 0.0, while in previous cases the maximum was occurring at Z = 1.19 mm. One

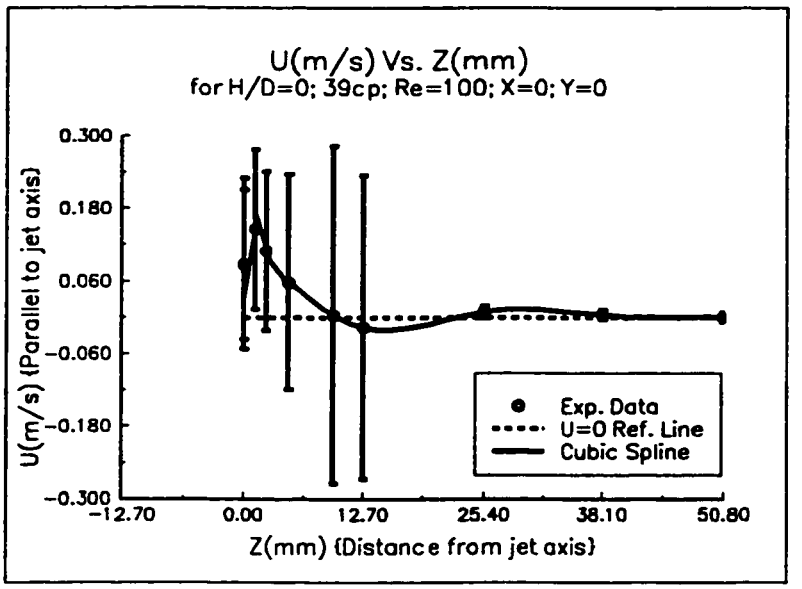

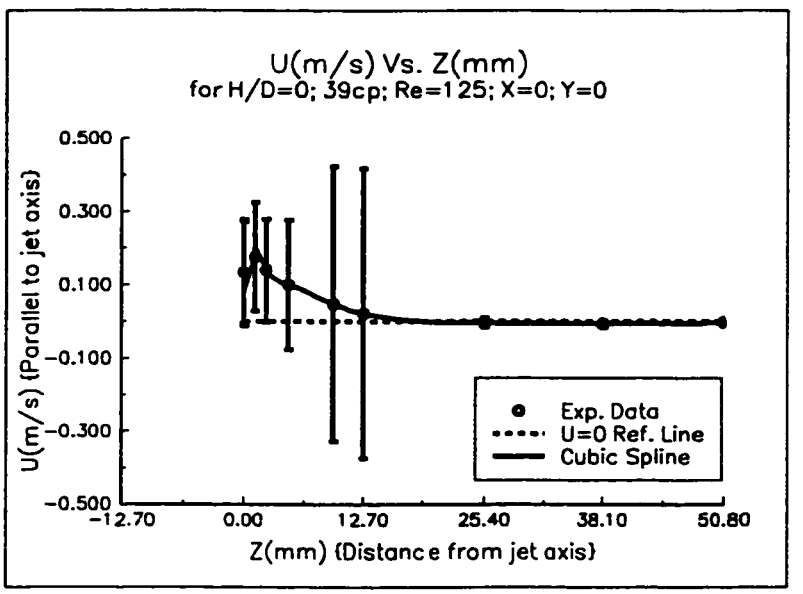

Fig. 7.1.2: Radial velocity (U) profile along mixhead axis (Z)
(Re = 100 & 125; H/D = 0; 0.39cp)

other noticeable change observed is that RMS values of U at Z = 9.52 and Z = 12.7 mm are of same order as RMS of U at Z = 0 and Z = 1.19 mm, but these values are far greater than other locations. In this figure there is one repeat experiment at Z = 0 which is also shown. The results are very well reproduced. The radial velocity profile at Re = 200 is shown in Fig. 7.1.3. The absolute radial velocity reaches a maximum at Z = 1.19 mm and then continuously decreases to a local minimum at Z = 12.7 mm. It again increases to a local maximum at Z = 25.4 mm and then continuously decreases to a nonsignificant value to Z = 50.8 mm. The RMS follows similar path. The values at Z = 9.52 and Z = 12.7 mm are not larger than other locations below Z = 9.52 mm as was the case for Re = 100 and 125.

The axial velocity (V) profile for various Reynolds number is shown in Figures 7.1.4 to 7.1.6. The observed average V is shown with the 95% confidence interval, and a fitted cubic spline is also drawn through the observed averages. In this set of figures there is no data at Z = 0 since it was not possible to sample at that plane due to optical restrictions in focusing the photomultiplier.

At Re = 50 (Fig. 7.1.4) the axial velocity sharply increases, reaches a maximum between Z = 2.38 mm and Z = 4.76 mm, then sharply decreases to its final value (0.035m/s) at Z = 25.4 mm. The rising curve is more steep than the falling curve. After one mixhead diameter the axial velocity settles to its value of developed flow in a pipe. The RMS values are higher in the sharp rising and falling section of the curve than the developed section. This indicates a periodic nature of flow, thus the mixing region of the mixhead. The axial velocity profile for Re = 75 (Fig. 7.1.4) follows a similar pattern to Re = 50. The rising curve is very steep and the maximum occurs at Z = 2.38 mm (one jet diameter), while the falling curve is

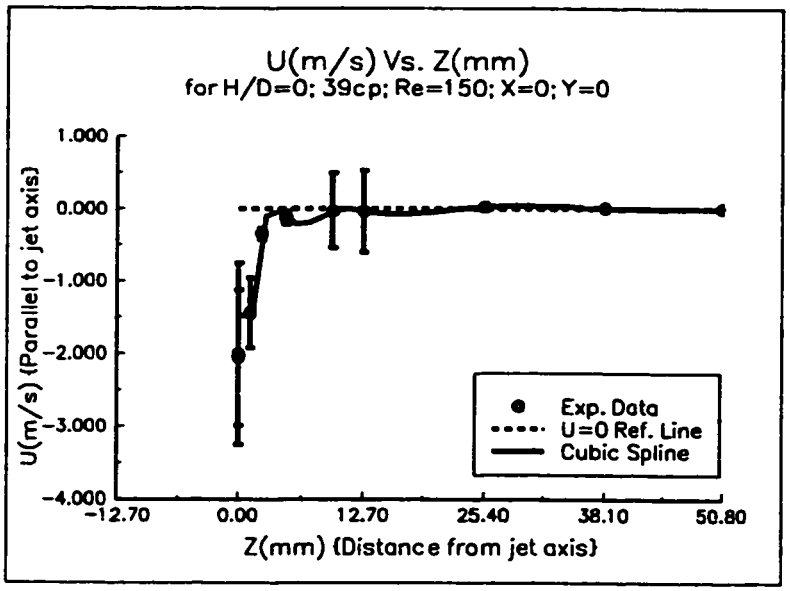

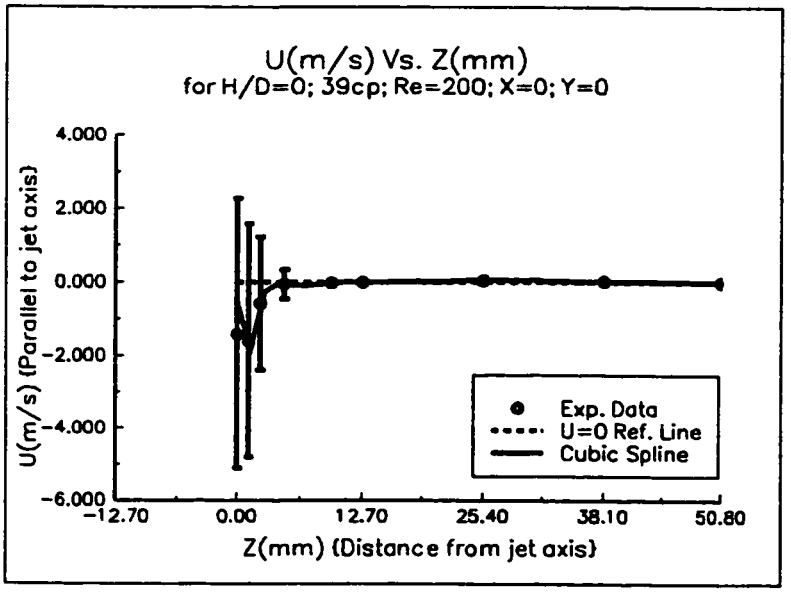

Fig. 7.1.3: Radial velocity (U) profile along mixhead axis (Z)
(Re = 150 & 200; H/D = 0; 0.39cp)

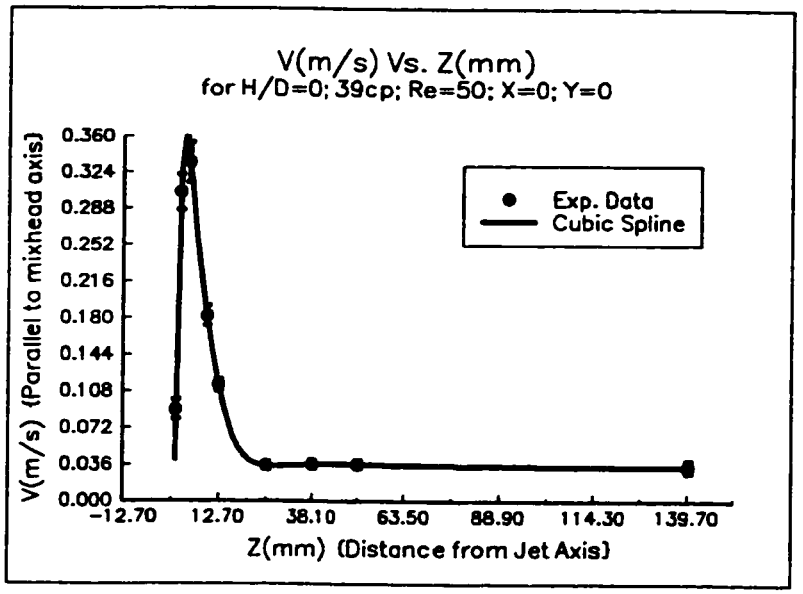

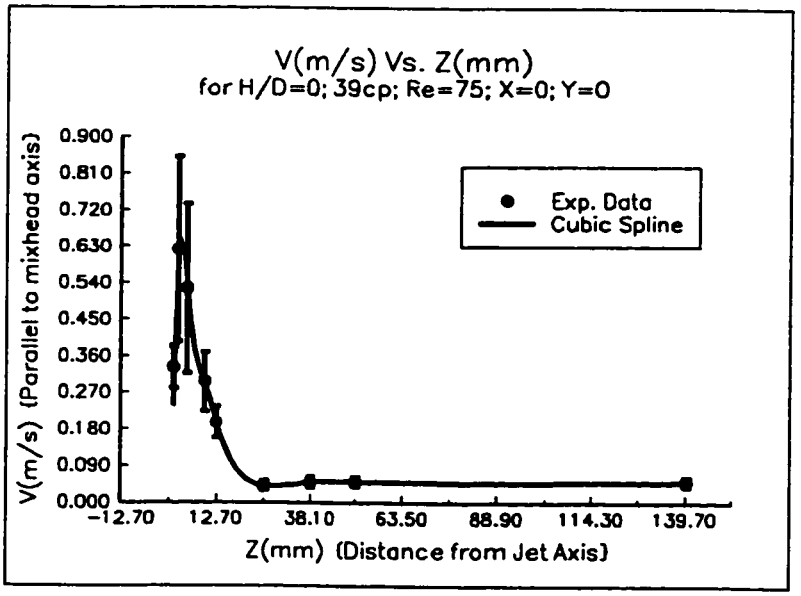

Fig. 7.1.4: Axial velocity (V) profile along mixhead axis (Z)
(Re = 50 & 75; H/D = 0; 0.39cp)

gradual. The minimum velocity is observed at Z = 25.4 mm (80% of developed velocity). The developed velocity profile is achieved at Z = 38.1 mm. Much higher RMS values are observed within one mixhead diameter of the impingement point than outside of this zone. The highest value of RMS is observed at Z = 2.38 mm. A kink is observed in the falling curve between Z = 4.76 mm and Z = 9.52 mm.

The axial velocity at Re = 100 (Fig. 7.1.5) rises to its maximum at Z = 2.38 mm and then drops to its minimum at Z = 25.4 mm. The velocity increases to the developed flow values at Z = 38.1 mm. The RMS values are higher in the vigorous mixing zone (within one mixhead diameter) than the developed zone (Z > 25.4 mm). The highest value of RMS is obtained at Z = 2.38 mm. At Re = 125 (Fig. 7.1.5) the axial velocity sharply increases to its maximum value at Z = 2.38 mm, then starts to decrease as Z is increased, reaching its minimum value at Z = 25.4 mm , after this it attains the developed profile value. As before (Re = 50 and 75), higher RMS values are evident in the mixing zone than the developed zone. In mixing zone, there is velocity direction reversal between Z = 4.76 mm and Z = 9.52 mm. This inflection point is better exhibited at Re ≥ 100 than Re < 100.

At Re = 150 the velocity increases to its maximum value at Z = 2.38 mm, but the value at Z = 1.19 mm is not that much different, especially for the one repeated case, where the values of velocities are equal (Fig. 7.1.6). The axial velocity falls to a local minimum at Z = 4.76 mm, then it slightly increases at Z = 9.52 mm. After this the velocity smoothly falls to its minimum value at Z = 25.4 mm and then rises to developed velocity value. For Re = 200 (Fig. 7.1.6) the velocity attains its maximum at Z = 1.19 mm, then continuously decreases until Z = 4.76 mm, then the velocity

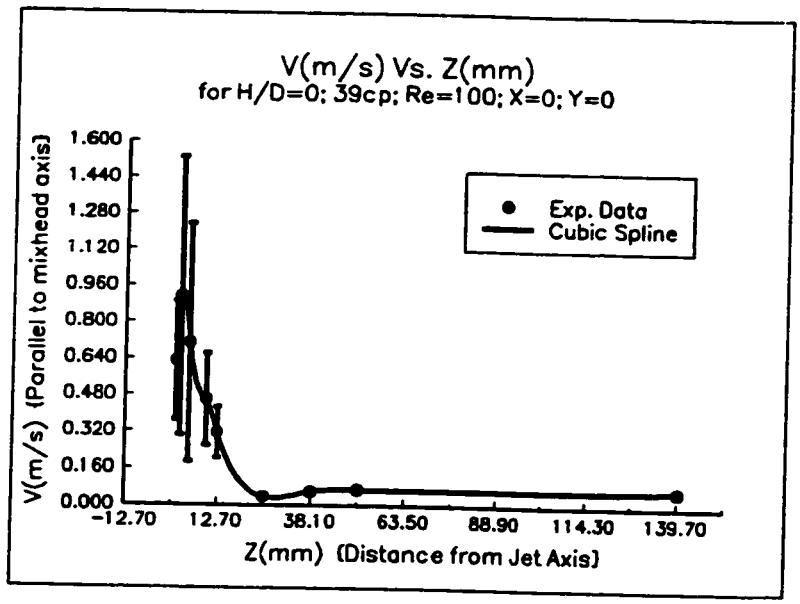

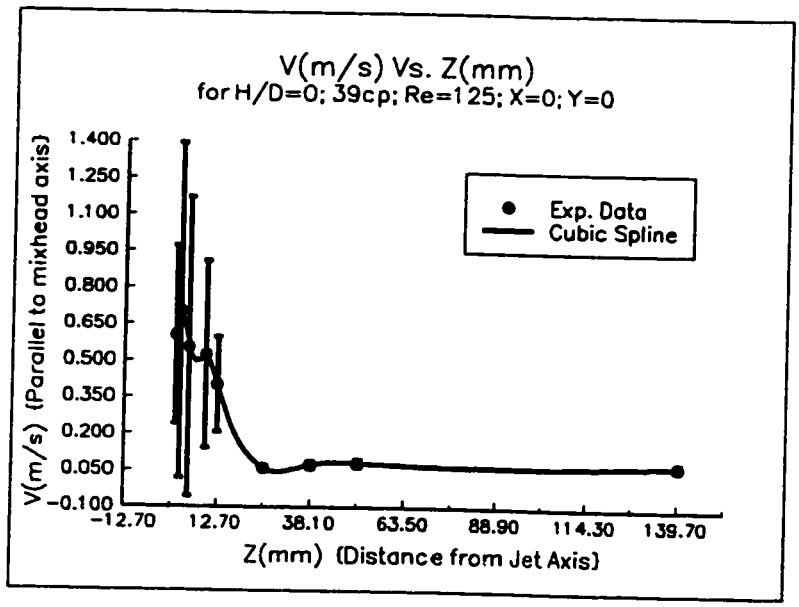

Fig. 7.1.5: Axial velocity (V) profile along mixhead axis (Z)
(Re = 100 & 125; H/D = 0; 0.39cp)

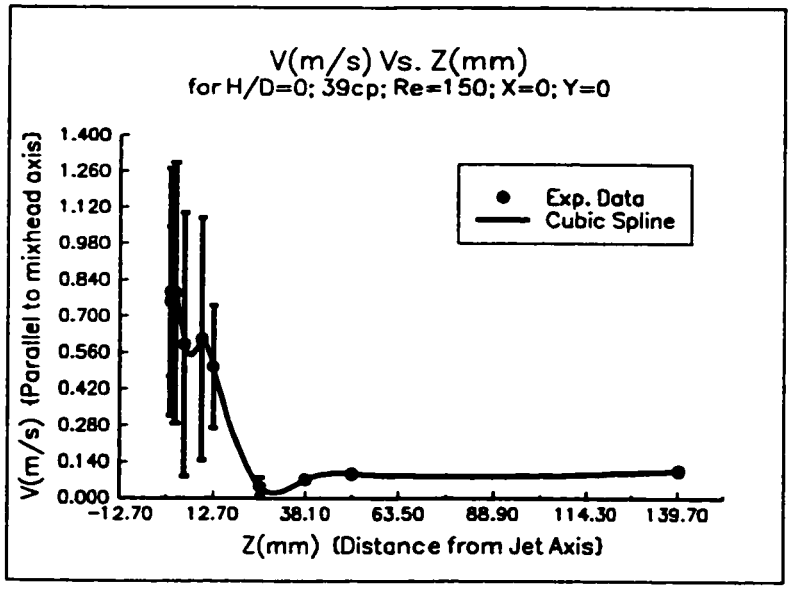

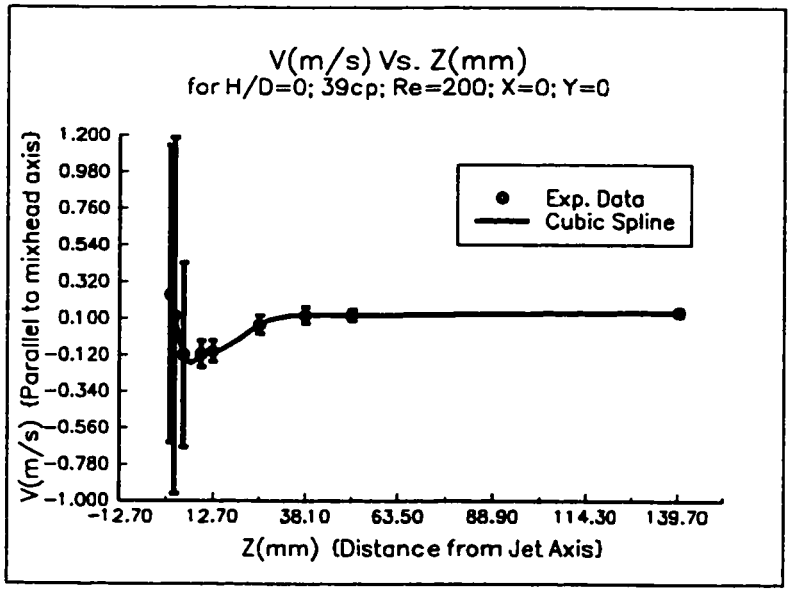

Fig. 7.1.6: Axial velocity (V) profile along mixhead axis (Z)
(Re = 150 & 200; H/D = 0; 0.39cp)

steadily increases until its reaches its developed value. Negative axial velocities were observed between Z = 4.76 mm to Z = 12.7 mm. It appears that between Z = 4.76 mm to Z = 12.7 mm strongly downward flow has been observed. This case is unusual compared to the other cases described previously with regards to the negative flow. This unusual behavior indicates that the jets are missing each other. Still RMS values of V are higher in the mixing zone than in the developed section.

7.2 Radial and axial velocities profile for H/D = 0 & μ = 75 cp

The radial velocity profile for H/D = 0 and μ = 75 cp for various jet Reynolds numbers are shown in Fig. 7.2.1 to 7.2.3. At Re = 50 (Fig. 7.2.1) the absolute value of radial velocity starts to decrease sharply from the value of 0.5m/s at Z = 0 to 0.054m/s at Z = 4.76 mm, then it is gradually reduced to a low value (0.001m/s) at Z = 12.7 mm and remains insignificant downstream from Z = 12.7 mm. The RMS value for all points are of the same order. Three repeat experiments at Z = 0 are also shown, which show the good reproducibility. The radial velocity profile for Re = 75 (Fig. 7.2.1) follows the similar pattern as the previous case, but the RMS values are higher in the mixing zone (within one mixhead diameter) than down-stream of it (Z > 25.4 mm). At Z = 0 and Z = 1.19 mm the RMS values are higher than all the other points in mixing zone. Excellent reproducibility of the result is shown at Z = 0.

For Re = 100 the absolute value of the radial velocity (Fig. 7.2.2) at Z = 0 increases to its maximum at Z = 1.19 mm, then sharply decreases from Z = 1.19 mm to Z = 4.76 mm, after Z = 4.76 mm the radial velocity gradually vanishes. The

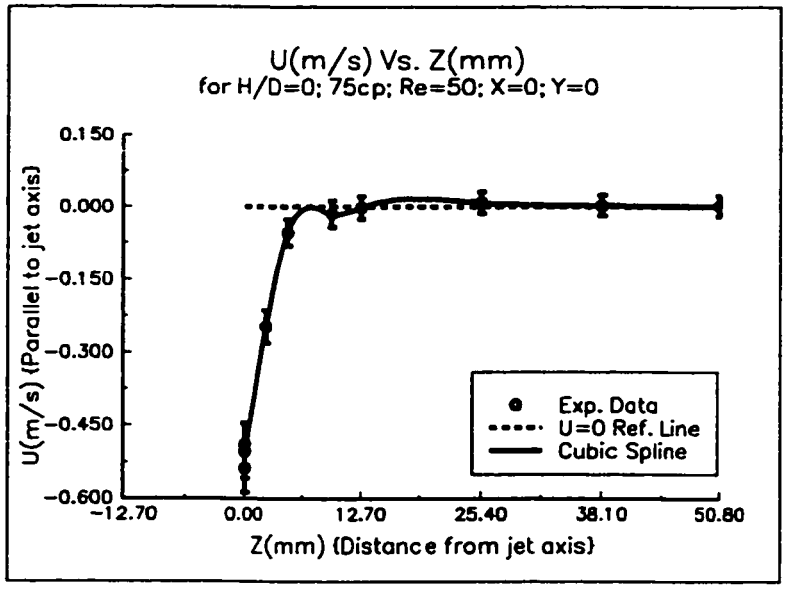

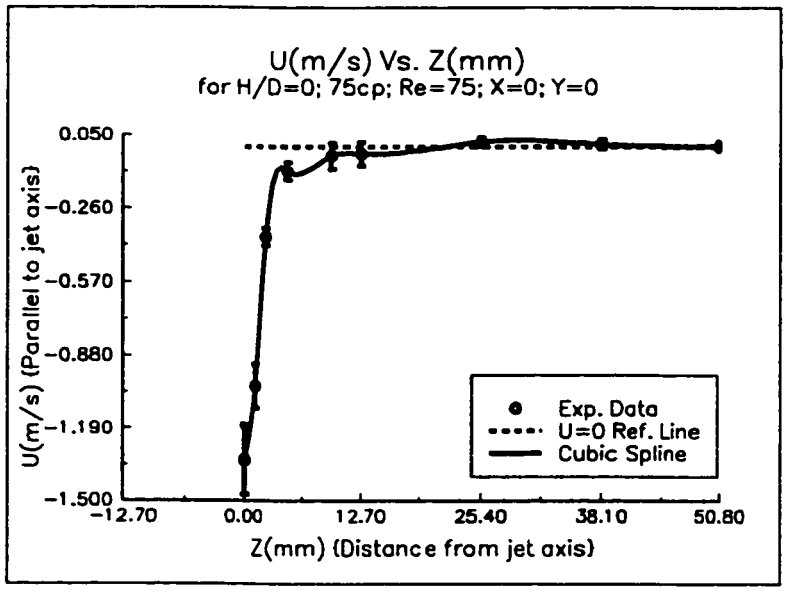

Fig. 7.2.1: Radial velocity (U) profile along mixhead axis (Z)
(Re = 50 & 75; H/D = 0; 75cp)

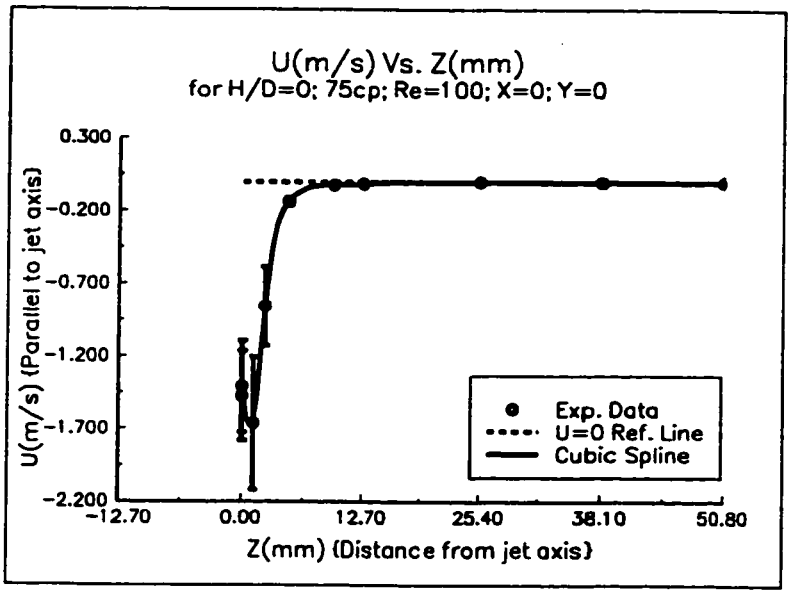

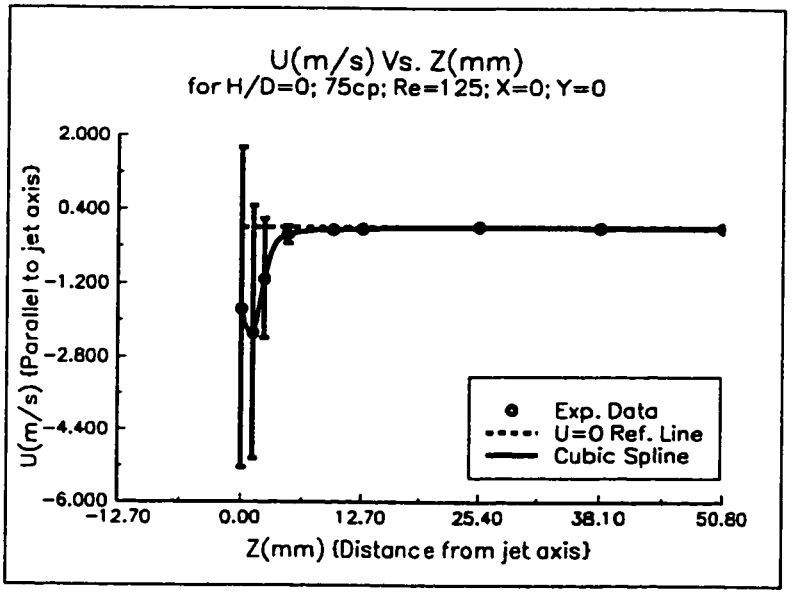

Fig. 7.2.2: Radial velocity (U) profile along mixhead axis (Z)
(Re = 100 & 125; H/D = 0; 75cp)

RMS values are very high from Z = 0 to Z = 2.38 mm compared to the remaining points downstream of Z = 2.38 mm. Two observed radial velocity averages are shown at Z = 0, which again reproduce the results. At Re = 125 the absolute radial velocity (Fig. 7.2.2) first increases from Z = 0 to its maximum at Z = 1.19 mm, then gradually decreases from Z = 1.19 mm to Z = 4.76 mm, then onward its vanishes to an insignificant value. Higher values of RMS are observed at Z = 0, Z = 1.19 mm and Z = 2.38 mm than the other observed points.

The absolute value of radial velocity for Re = 150 decreases from a high value (U = -2.699 m/s) at Z = 0 to a low value (U = -.012 m/s) at Z = 4.76 mm. It increases to .088m/s at Z = 9.52, then gradually decreases until ultimately vanishing to insignificant values at Z = 38.1 mm. The highest RMS value is observed at Z = 0. The RMS is higher at Z = 9.52 mm and Z = 12.7 mm than all remaining observed locations (Fig. 7.2.3).

The axial velocity (V) at Re = 50 (Fig. 7.2.4) sharply increases to its maximum value at Z = 2.38 mm, and, then continuously decreases from Z = 2.38 mm to Z = 25.4 mm to its lowest value in this experimental domain. A further increase in Z produces a developed velocity profile. The RMS values at Z = 2.38 mm are highest. The RMS values from Z = 1.19 mm to Z = 50.8 mm are quite significant (14% of velocity at Z = 50.8 mm compared to 1.4% of velocity at Z = 140 mm), which indicates some kind of periodicity or fluctuations. A repeat experiment at Z = 1.19 mm is also shown, which indicates good reproducibility of results.

At Re = 75 the axial velocity (Fig. 7.2.4) reaches its maximum value of 0.661m/s at Z = 2.38 mm, then it is gradually decreasing to a minimum value of

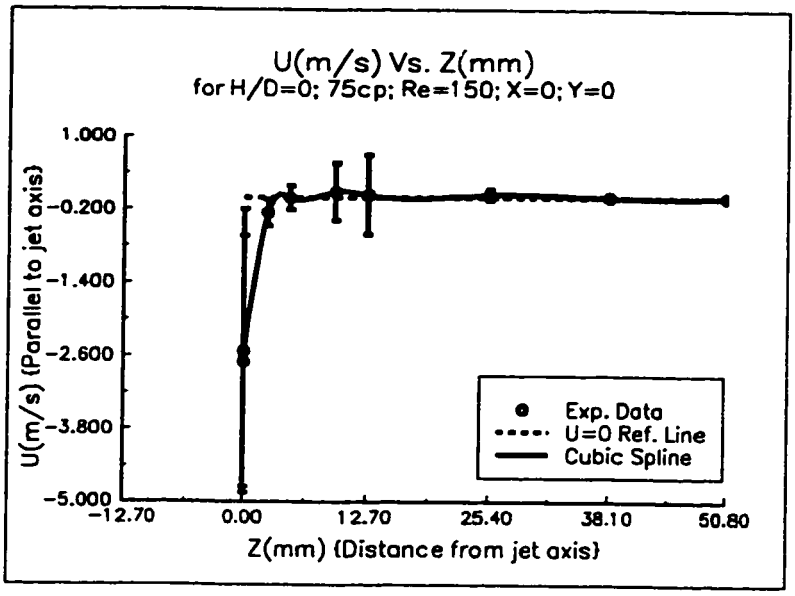

Fig. 7.2.3: Radial velocity (U) profile along mixhead axis (Z)
(Re = 150; H/D = 0; 75cp)

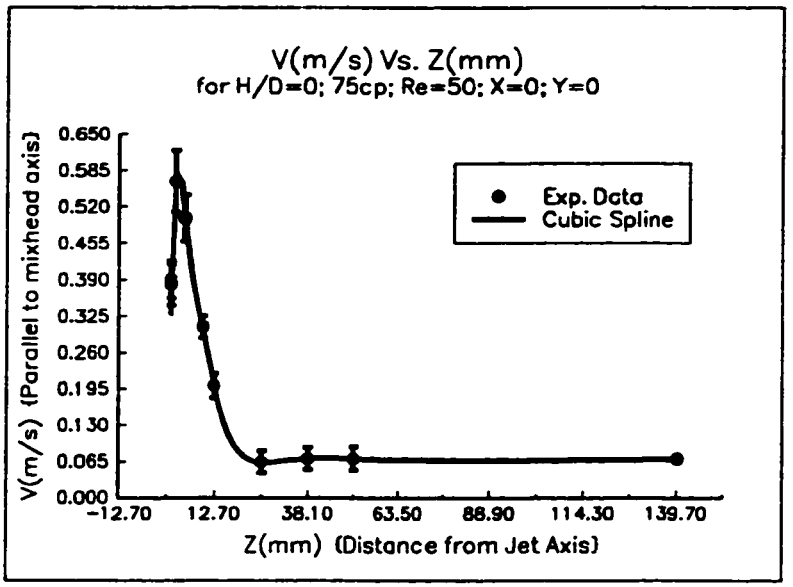

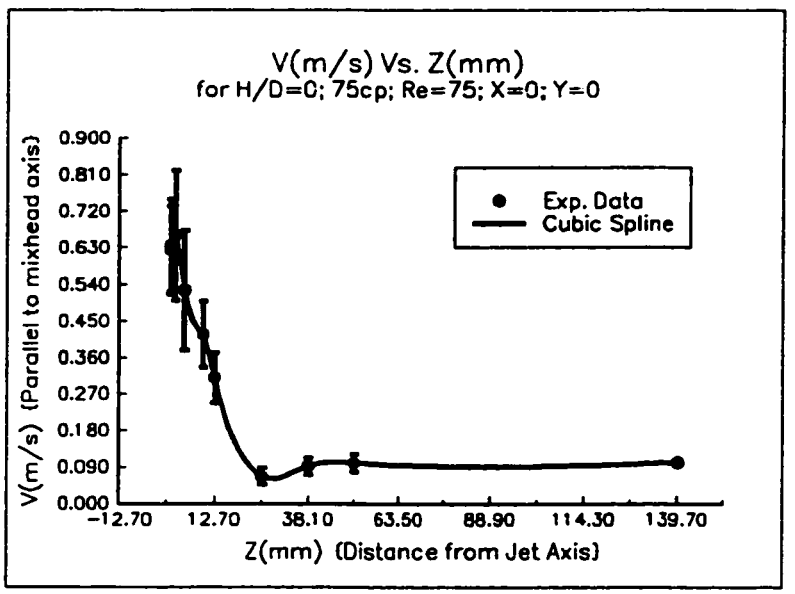

Fig. 7.2.4: Axial velocity (V) profile along mixhead axis (Z)
(Re = 50 & 75; H/D = 0; 75cp)

0.067 m/s at Z = 25.4 mm. The axial velocity profile becomes fully developed as Z is increased beyond Z = 25.4 mm. An inflection point starts to emerge between Z = 4.76 mm and Z = 9.52 mm. The higher RMS values from Z = 1.19 mm to Z = 12.7 mm suggest a fluctuating flow in this region compared with the developed region, downstream of Z = 25.4 mm. The reproducibility of the results is shown at Z = 1.19 mm. The axial velocity (Fig. 7.2.5) at Re = 100 starts to decrease from its maximum value of 0.790 m/s at Z = 1.19 mm to a local minimum at Z = 4.76 mm, then it increases to a local maximum at Z = 9.52 mm. The axial velocity decreases to its global (within sample space of this work) minimum value of 0.081m/s at Z = 25.4 mm. The axial velocity attains the developed flow profile. The inflection point, which starts to appear in the previous case (Re = 75), is clearly evident when the V starts to increase after Z = 4.76 mm. From Z = 1.19 mm to Z = 9.52 mm higher values of RMS are observed than downstream of Z = 9.52 mm. A repeat experiment at Z = 1.19 mm is also shown.

The upward axial velocity for Re = 125 (Fig. 7.2.5) at Z = 1.19 mm quickly reverses the direction to downward flow and attains its lowest value of -0.195 m/s at Z = 4.76 mm, Then the velocity starts to increase and becomes upward again between Z = 12.7 mm to Z = 25.4 mm. Downstream of Z = 25.4 mm velocity attains the fully developed profile. The negative or downward flow is observed between Z = 2.38 mm to Z = 12.7 mm. The vigorous fluctuations are observed at Z = 1.19 mm and Z = 2.38 mm. The reproducibility is shown at Z = 1.19 mm.

At Re = 150 negative axial velocity (Fig. 7.2.6) is observed at Z = 1.19 mm and Z = 2.38 mm, it increases to a positive value between Z = 2.38 mm and Z = 4.76 mm and attains its maximum between Z = 4.76 mm and Z = 9.52 mm. The

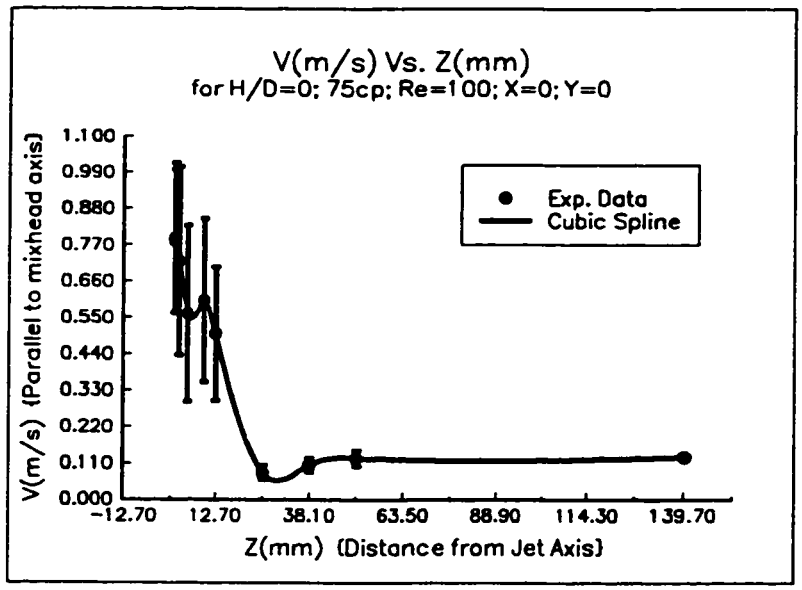

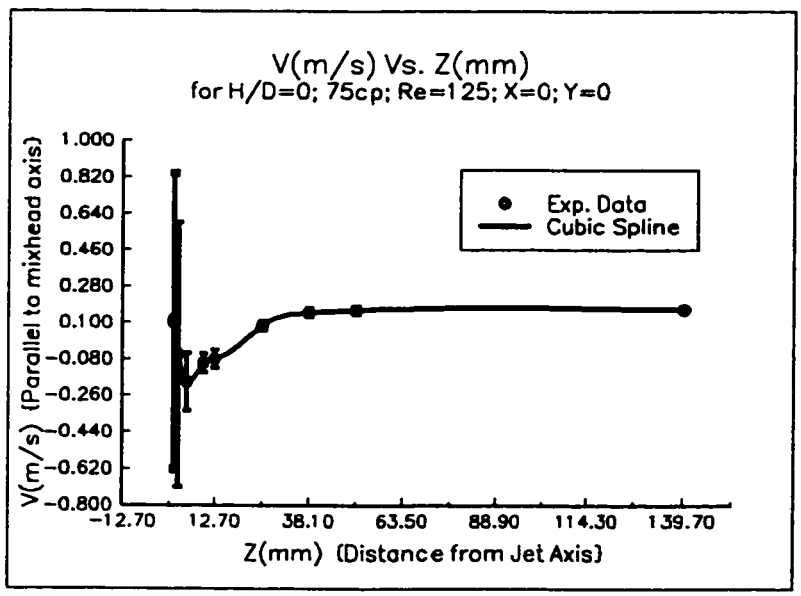

Fig. 7.2.5: Axial velocity (V) profile along mixhead axis (Z)
(Re = 100 & 125; H/D = 0; 75cp)

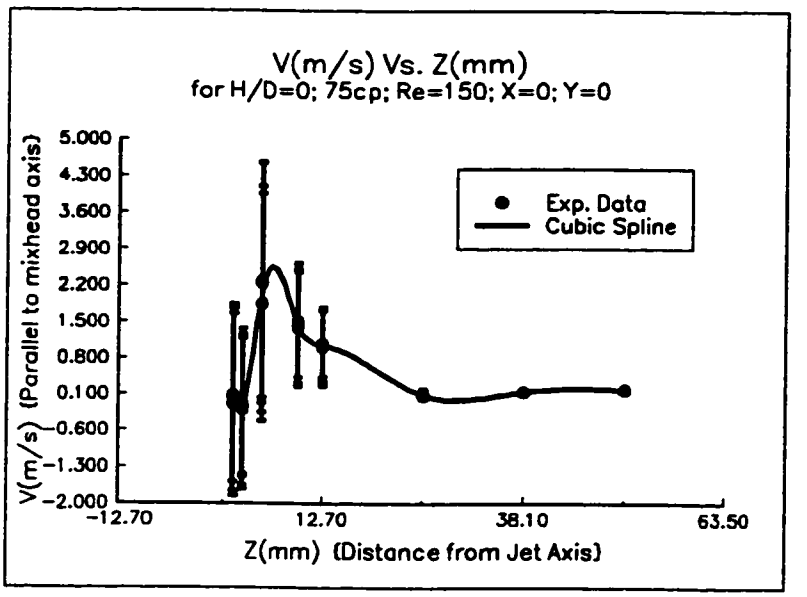

Fig. 7.2.6: Axial velocity (V) profile along mixhead axis (Z)
(Re = 150; H/D = 0; 75cp)

axial velocity continuously decreases from Z = 4.76 mm to Z = 25.4 mm, downstream of Z = 25.4 mm, attains the fully developed value. Higher RMS values are observed from Z = 1.19 mm to Z = 12.7 mm compared to other Z locations, indicating fluctuating flows. Due to vigrous fluctuation and missing of jet to jet impingement, observations of negative axial velocities in mixing zone for Re = 125 and 150 indicate the presence of downward recirculating regions at the center line.

7.3 Radial and axial velocities profile for H/D = -0.5 & μ = 39 cp

The radial velocity (U) profile at Re = 50 (Fig. 7.3.1) is symmetric about the jet axis. The radial velocity and associated RMS at one and two jet diameters locations below the jet axis are almost equal to respectively corresponding locations above jet axis. The radial velocity changes direction between Z = -4.76 mm and Z = -9.52 mm and keeps on increasing as the observation location moves toward the piston head. As we know this velocity will become zero at the piston head, so the increase in the radial velocity, as the location moves towards the piston head, will reach a maximum and then will start to decrease and finally will become zero at the piston head. Above the jet axis the absolute value of radial velocity keeps decreasing as the location moves toward the mixhead outlet. After half a mixhead diameter (12.7 mm) this velocity vanishes to an insignificant value. The RMS on both sides of the jet axis is also symmetric in the mixing zone, which lies from the piston head to Z = 12.7 mm. The highest RMS value is observed at Z = 0, which indicates the fluctuations and thus periodic flow. The repeat of the experiment at Z = 0 confirms the reproducibility of the results.

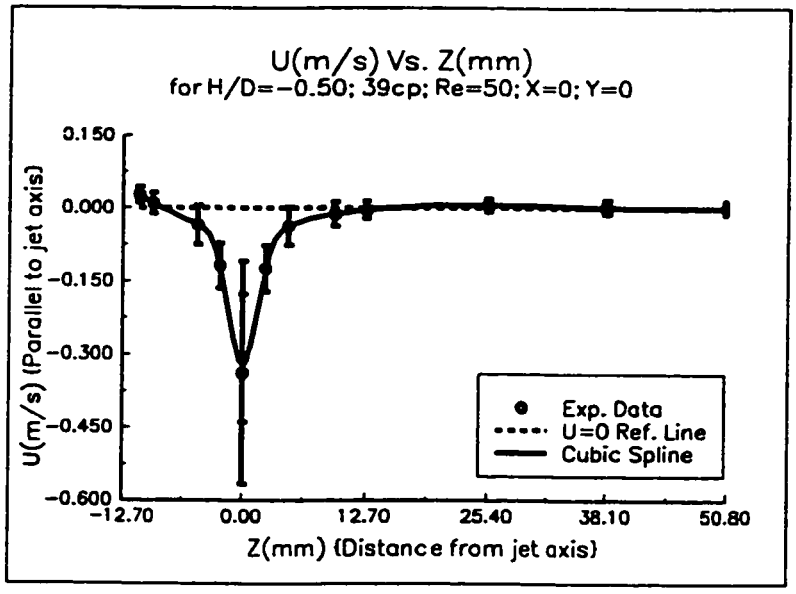

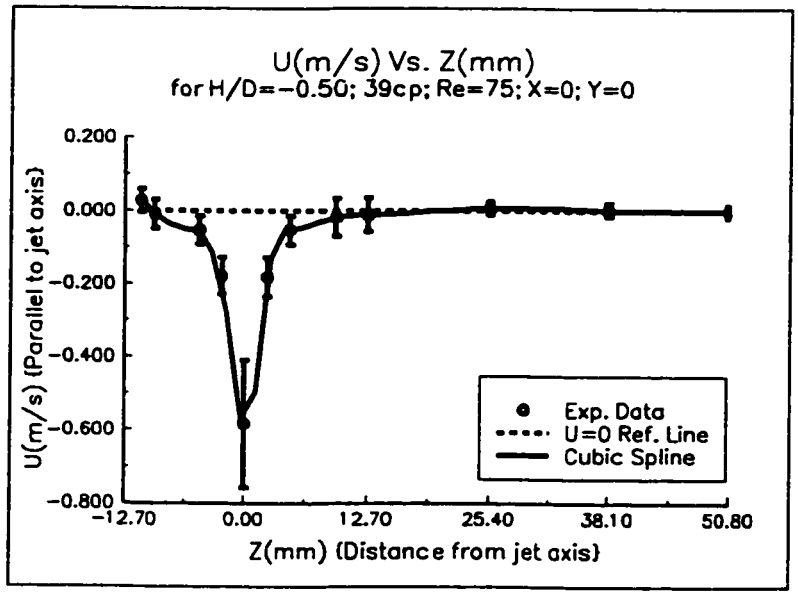

Fig. 7.3.1: Radial velocity (U) profile along mixhead axis (Z)
(Re = 50 & 75; H/D = -0.50; 39cp)

At Re = 75 (Fig. 7.3.1) the radial velocity follows a similar profile to the previous case. The symmetry of the radial velocity about the jet axis is further increased from Z = -9.52 mm to Z = 9.52 mm instead of Z = -4.76 mm to Z = 4.76 mm. The radial velocity direction reversal occurs between Z = -9.52 mm and Z = -11 mm. It vanishes to an insignificant value between Z = 12.7 mm and Z = 25.4 mm and remains insignificant downward from one mixhead diameter. The highest RMS is observed at Z = 0. Higher RMS values are obtained in the mixing zone than other zones. The radial velocity profile at Re = 100 (Fig. 7.3.2) is similar to the previous two cases. The symmetry of the radial velocity about jet axis exists from Z = -9.52 mm to Z = 9.52 mm. The reversal of the direction of velocity occurs between Z = -9.52 mm and Z = -11 mm. It becomes insignificant after one mixhead diameter. A higher RMS of the U velocity component is observed at Z = 9.52 mm and Z = 12.7 mm than at other locations except Z = 0 where the RMS is largest. At Re = 125 the radial velocity profile is also similar to previous cases (Fig. 7.3.2). The symmetry is intact, though the absolute values of radial velocity above the jet axis are higher than their respective counterparts below the jet axis. But the directions are identical. The velocity reversal occurs between Z = -9.52 mm and Z = -11 mm. Again the largest RMS is observed at Z = 0, and also larger RMS values are observed at Z = -11 mm, Z = -9.52 mm, Z = 9.52 mm and Z = 12.7 mm than other locations. A reversal of the direction of the radial velocity is also evident between Z = 12.7 mm and Z = 25.4 mm. It eventually reduces to an insignificant level after Z = 38.1 mm, i.e. one and half mixhead diameters.

The radial velocity at Re = 150 (Fig. 7.3.3) is symmetric about the jet axis, but this envelope extends to one jet diameter from the jet axis in both directions.

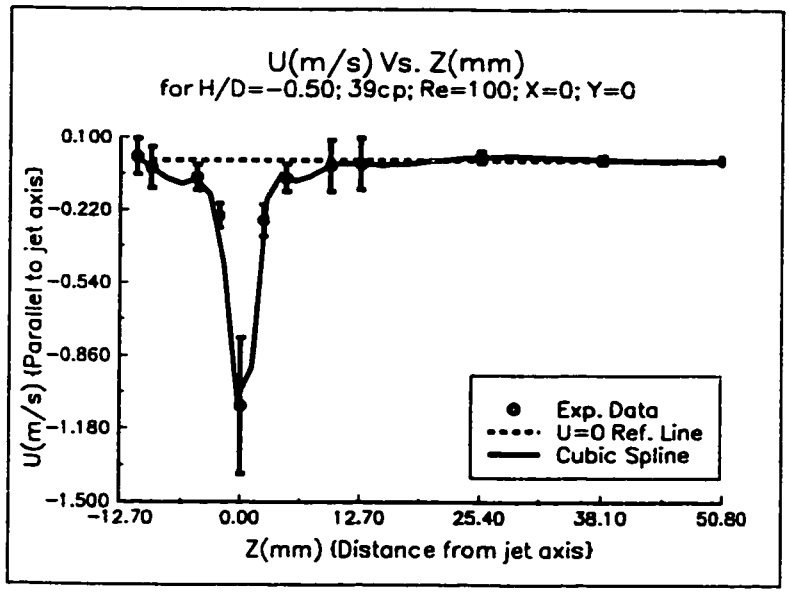

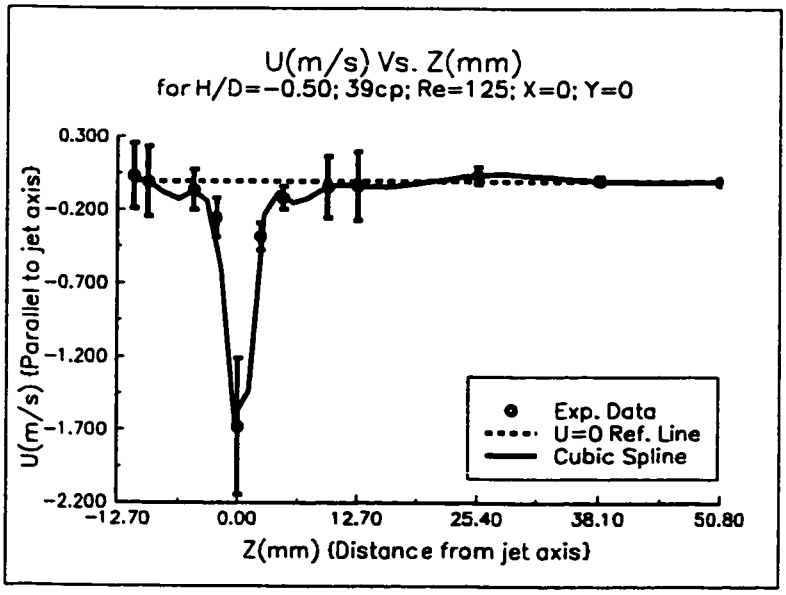

Fig. 7.3.2: Radial velocity (U) profile along mixhead axis (Z)
(Re = 100 & 125; H/D = -0.50; 39cp)

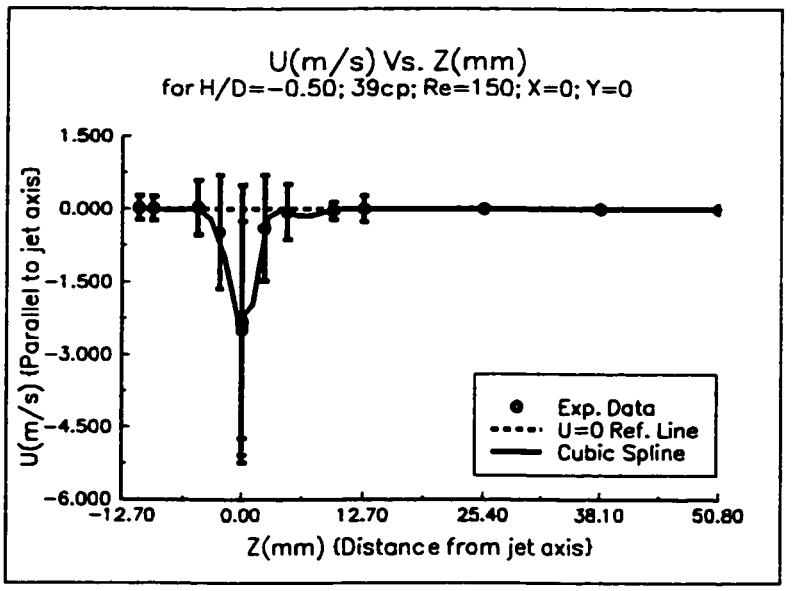

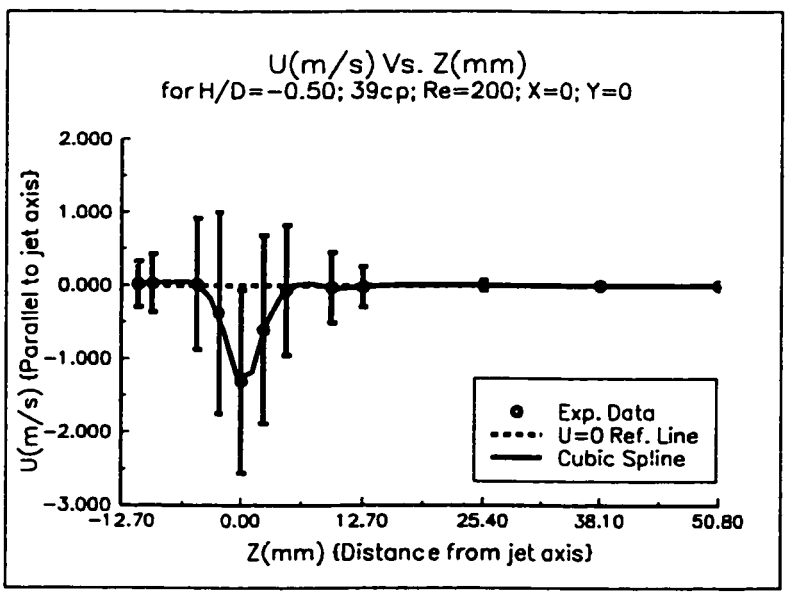

Fig. 7.3.3: Radial velocity (U) profile along mixhead axis (Z)
(Re = 150 & 200; H/D = -0.50; 39cp)

The reversal of the velocity occurs between Z = -2.38 mm and Z = -4.76 mm. At Z = 0, three experimental results are shown, where the RMS is very high, with good reproducibility. The high RMS values are again found in the mixing zone. The velocity vanishes to an insignificant value after Z = 12.7 mm. For Re = 200, the radial velocity (Fig. 7.3.3) symmetry about the jet axis is limited to only one jet diameter in both directions, though the mirror image symmetry of direction is still followed from Z = -9.52 mm to Z = 9.52 mm. The RMS values are higher in the mixing zone than the developed zone. In both directions from the jet axis the RMS values are very high and of same order within two jet diameters. A consistent decrease is observed in the RMS as one moves away from the jet axis in both direction.

The axial velocity (V) at Re = 50 (Fig. 7.3.4) from impingement point (X = 0, Y = 0, Z = 0) decreases sharply as observer travels from jet axis to piston head, reaches its minimum (-0.261 m/s) at Z = -2.38 mm and starts to increase and will be zero at the piston head (theoretical). On the other side of the impingement point, the axial velocity sharply increases to its maximum value of 0.276 m/s at Z = 2.38 mm, when the observer moves from jet axis to mix head outlet. The velocity then smoothly reduces to its developed flow velocity (.036 m/s at Z = 140 mm). The axial velocity completely attains its developed velocity value at Z = 25.4 mm (one mix head diameter). The high RMS values are observed at one and two jet diameter below and above the jet axis. There is also symmetry of absolute axial velocities about jet axis with in 2 jet diameter from jet axis. High RMS values are obtained around both inflection points. At Re = 75 (Fig. 7.3.4) the axial velocity profile is similar to the previous case. A breakdown in the

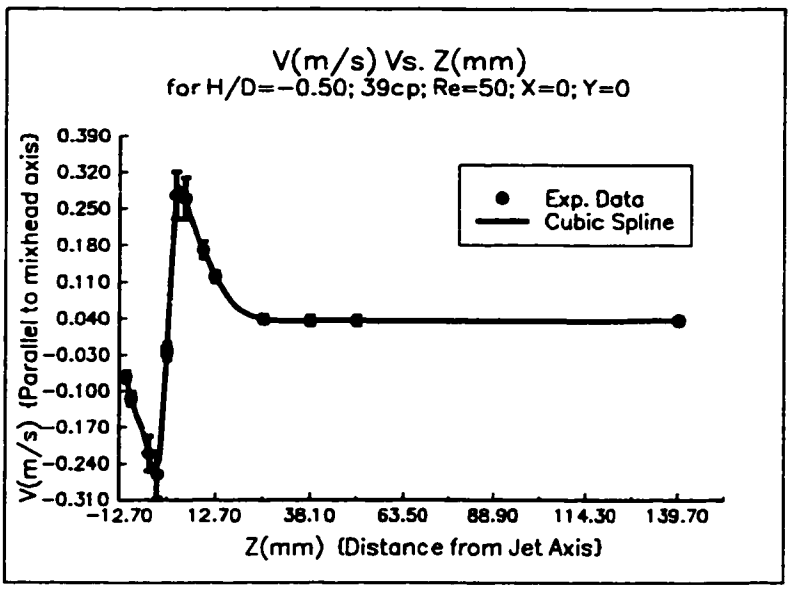

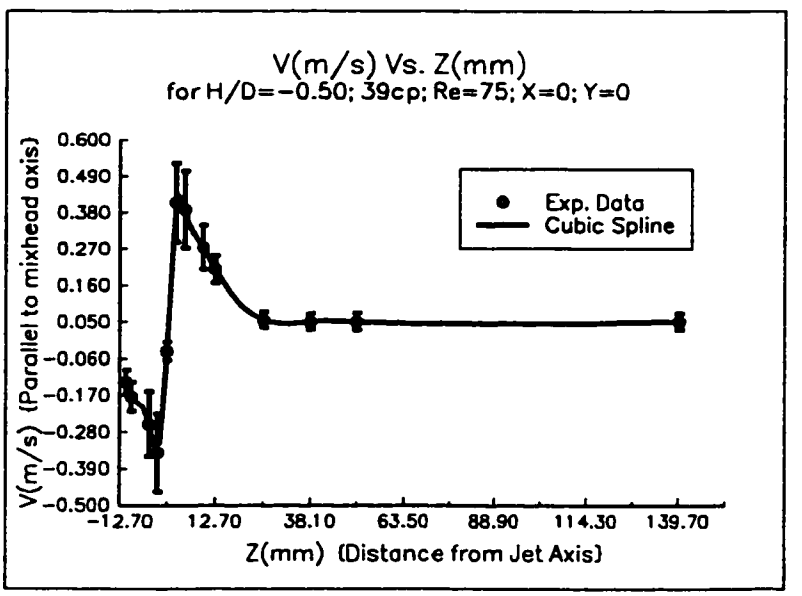

Fig. 7.3.4: Axial velocity (V) profile along mixhead axis (Z)
(Re = 50 & 75; H/D = -0.50; 39cp)

smoothness is observed between Z = -4.76 mm and Z = -9.52 mm, a similar observation is also clear on the other side of jet axis, i.e. between Z = 4.76 mm and Z = 9.52 mm. The RMS values are again high from Z = -4.76 mm to Z = 4.76 mm except Z = 0, which indicates a fluctuating flow in this region.

At Re = 100 the axial velocity profile (Fig. 7.3.5) is similar to the previous cases, but breaking of smoothness of ascending curve below the jet axis and breaking of smoothness of descending curve above the jet axis are more clear than for Re = 75. Inflection points occur between Z = -4.76 mm and Z = -9.52 mm for ascending curve and between Z = 4.76 mm and Z = 9.52 mm in the descending curve. The axial velocity attains the developed velocity profile at one and half mixhead diameters (38.1mm) downstream from jet axis. High values of RMS are limited to within a half mixhead diameter (12.7mm) on both sides of the jet axis. The axial velocity (V) for Re = 125 (Fig. 7.3.5) starts to decrease as the observer moves downward (toward the piston head from jet axis), reaches its minimum at Z = -9.52 mm and then starts to increase. This velocity will eventually vanish at piston head. On the other side of the jet axis, the velocity reaches its maximum at Z = 2.38 mm and then starts to decrease as Z is increased, until it attains its developed velocity profile after one and half mixhead diameters downstream of the jet axis. There is a break in the smoothness of the descending curve between Z = 4.76 mm and Z = 9.52 mm. High RMS values are limited to half a mixhead diameter (12.7 mm) on both sides of the jet axis.

The axial velocity at Re = 150 sharply decreases as Z decreases, reaches its minimum at Z = -2.38 mm (Fig. 7.3.6), then sharply increases and then slowly starts to vanish. The axial velocity, as the observer moves toward the mixhead outlet from

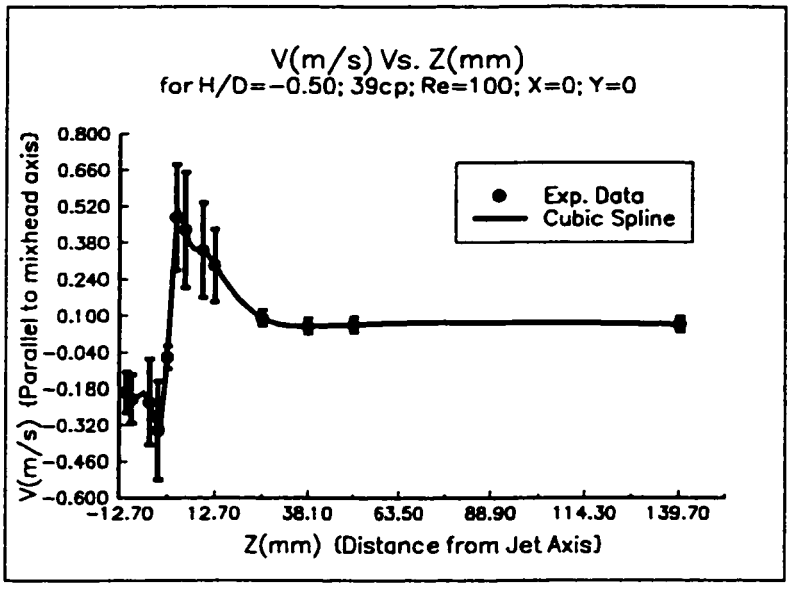

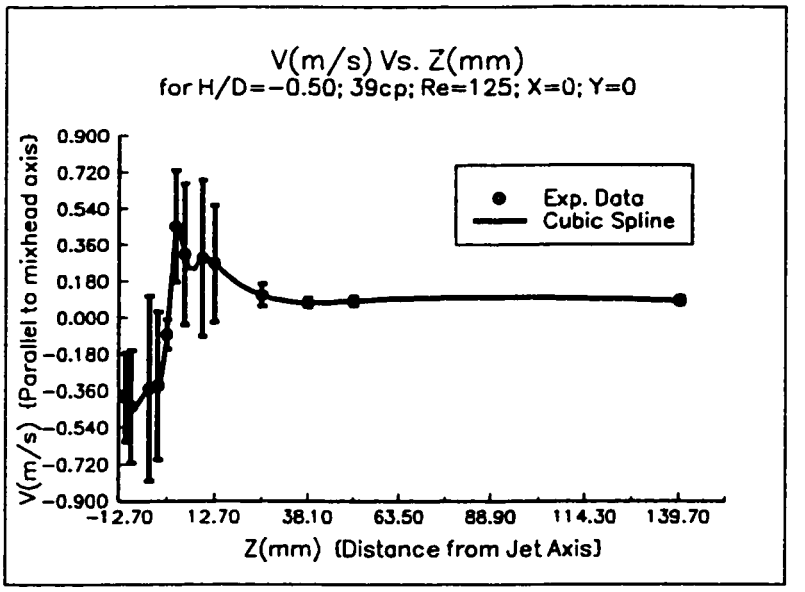

Fig. 7.3.5: Axial velocity (V) profile along mixhead axis (Z)
(Re = 100 & 125; H/D = -0.50; 39cp)

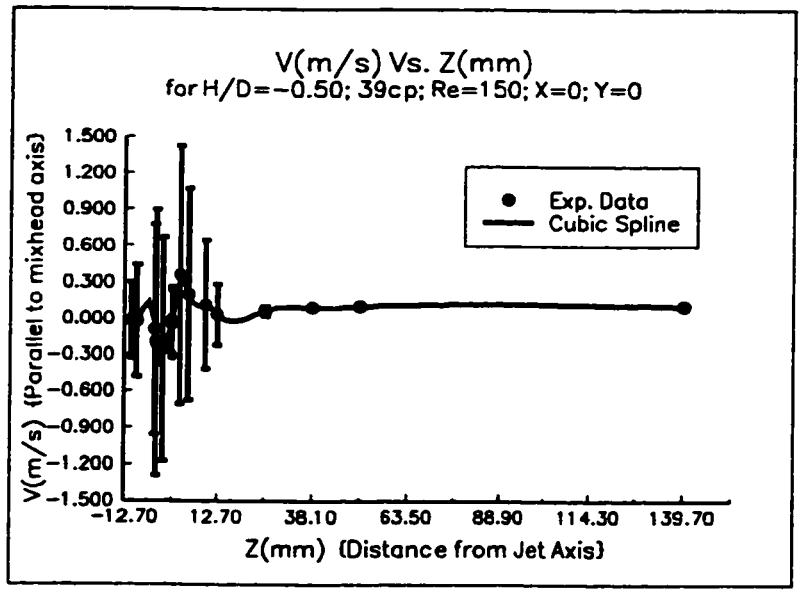

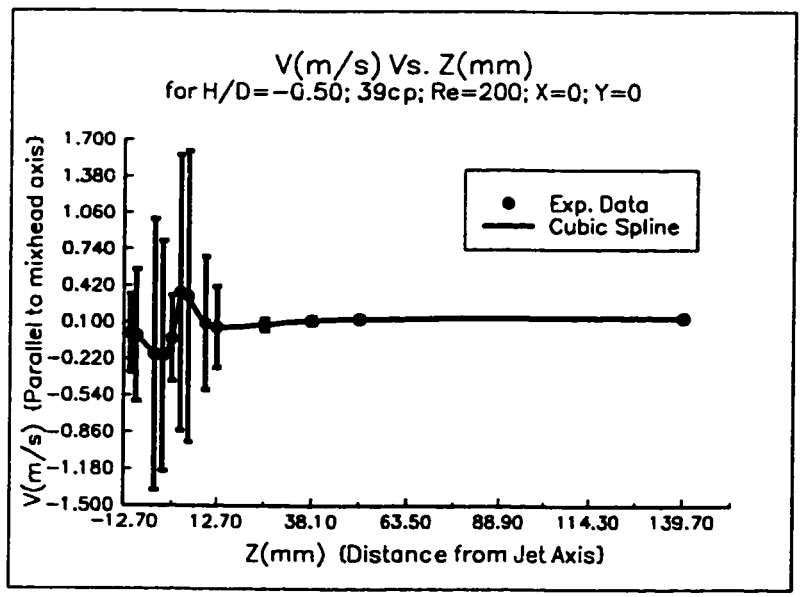

Fig. 7.3.6: Axial velocity (V) profile along mixhead axis (Z)
(Re = 150 & 200; H/D = -0.50; 39cp)

the jet axis, increases and attains its maximum at Z = 2.38 mm, then decreases until Z = 12.7 mm. Somewhere between Z = 12.7 mm and Z = 25.4 mm, the local minimum of axial velocity is achieved. After this location (Z = 25.4 mm), the velocity starts to attain its developed flow profile, which is achieved between Z = 38.1 mm and Z = 50.8 mm. High RMS values are observed within half a mixhead diameter on both sides of the jet axis. A repeat observation at Z = 0 is also shown, which reproduces the result well.

At Re = 200 the axial velocity (Fig. 7.3.6) smoothly decreases as one moves downward from the jet axis, reaches its minimum at Z = -2.38 mm, then starts to increase smoothly and vanishes at the piston head. The profile above the jet axis attains a maximum at Z = 2.38 mm and then smoothly descends to a local minimum at Z = 12.7 mm. The developed velocity is attained at Z = 50.8 mm. Very high RMS values are found in the neighborhood of global maximum (Z = 2.38 mm) and minimum (Z = -2.38 mm). Though the very high RMS values are observed within half a mixhead diameter in this case compared to the profile for Re = 50 (Fig. 7.3.4), the smoothness of the profile curve are similar.

In all the previously described profiles of the axial velocities (Fig. 7.3.4 to Fig. 7.3.6), there is a symmetry in the absolute axial velocities within a half mixhead diameter (12.7 mm) about the jet axis. The absolute axial velocity component at locations above the jet axis are greater than their respective locations below the jet axis. This is due to the fact that while the velocities below jet axis have to vanish at piston head, the velocities above jet axis attain the developed flow values. If this

value of axial velocity of developed flow at center is subtracted from the observed axial velocities above jet axis, then symmetry in absolute axial velocities is further evident.

7.4 Radial and axial Velocities profile for H/D = -0.5 & μ = 75 cp

The radial velocity at Re = 50 is shown in Figure 7.4.1. The radial velocity sharply increases from the minimum value at Z = 0 (-0.619 m/s) on both sides of the jet axis. After two jet diameters above the jet axis the radial velocity gradually vanishes to an insignificant level, while the radial velocity below jet axis continuously increases though the slope has flattened after Z = -4.76 mm. This steepness of the curve again increases after Z = -9.52 mm. Though in the experimental space this radial velocity below jet axis keeps increasing, it will vanish sharply to zero at the piston head, which is less than 3 mm from the last observed point. The velocities are symmetrical about the jet axis within two jet diameter from the jet axis. High RMS values are obtained within mixing zone which lies within one half mixhead diameter on both side of the jet axis. Many repeat results are shown at different locations, which show good reproducibility.

At Re = 75, the radial velocity (Fig. 7.4.1) profile is similar to the profile at Re = 50. The profile curve is smoother in this case than the previous one. Also the symmetry about the jet axis extends from Z = -9.52 mm to Z = 9.52 mm instead from Z = -4.76 mm to Z = 4.76 mm as in the previous case. The radial velocity below the jet axis after Z = -2.38 mm approaches an inflection point just before Z = -4.76 mm and one more inflection point between Z = -4.76 mm and Z = -9.52 mm. One inflection point is also observed just before Z = 4.76 mm above the jet

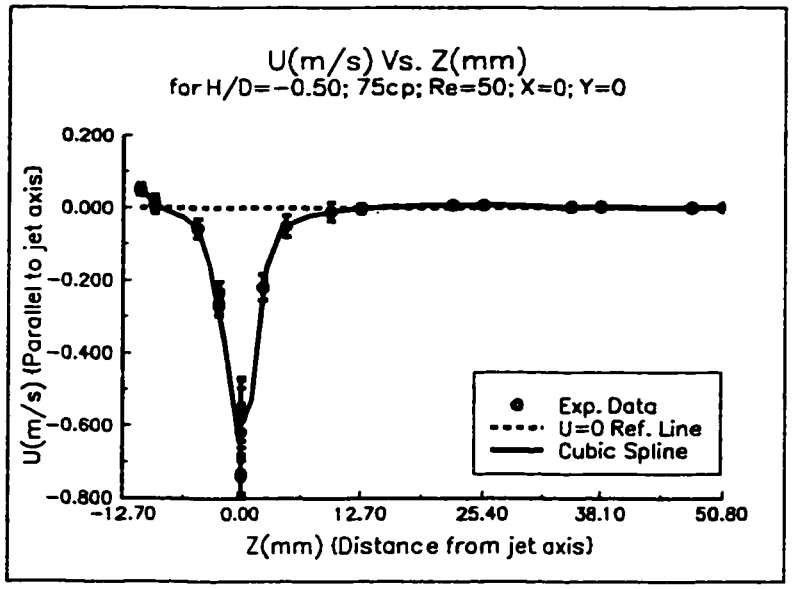

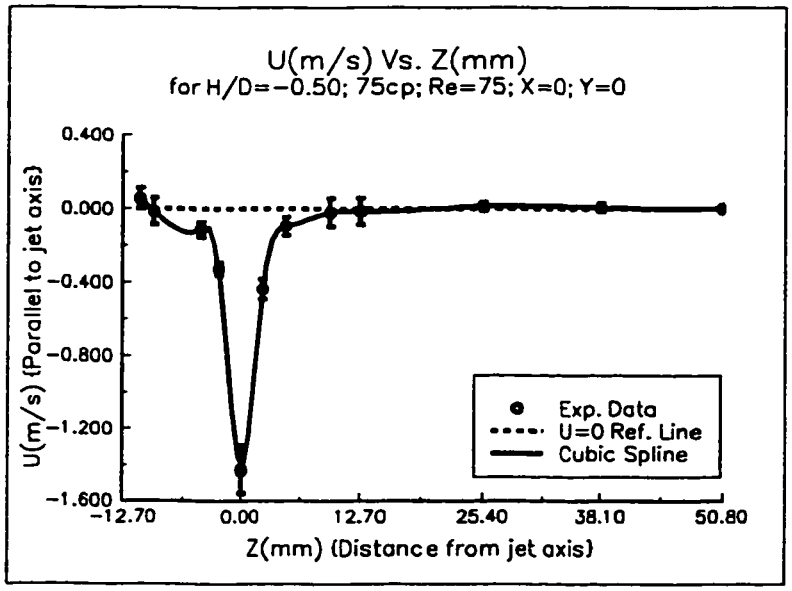

Fig. 7.4.1: Radial velocity (U) profile along mixhead axis (Z)
(Re = 50 & 75; H/D = -0.50; 75cp)

axis. The radial velocity vanishes to an insignificant level after Z = 25.4 mm. High RMS values are observed at Z = 0, Z = ±9.52 mm, Z =-11 mm and Z = 12.7 mm which indicates more fluctuating flow than the other observation locations in the experimental domain. A repeat experiment, is shown at Z = 0, indicating reproducibility of the results. The radial velocity at Re = 100 (Fig. 7.4.2) shows a similar pattern to the previous case. Beside the inflection point at Z = 0, the other four inflection points (2 below jet axis and 2 above jet axis) are more vividly apparent. The symmetry about the jet axis is evident, even for the inflection points. Again high RMS values are observed at Z = 0, Z = ±9.52 mm, Z = -11 mm and Z = 12.7 mm. The velocity (U) vanishes to an insignificant level beyond Z = 25.4 mm above the jet axis. At Z = 0 reproducibility of the results is shown. The radial velocity profile for Re = 125 (Fig. 7.4.2) is similar to the last case. The inflection points below and above jet axis are further evident. The radial velocity vanishes after Z = 38.1 mm.

The radial velocity (Fig. 7.4.3) at Re = 150 increases from its minimum value (-4.02 m/s) at Z = 0 as the observer moves toward the piston head, after Z = -4.76 mm it smoothly increases to -0.011m/s at Z = -11 mm. Similarly the radial velocity above the jet axis sharply starts to increase from its value at Z = 0 till Z = 2.38 mm, then it is gradually increases as Z increases to 12.7 mm, after this location it vanishes to an insignificant level. Many repeat experiments are shown for each locations, indicating good to excellent reproducibility of the results. The largest RMS is observed at Z = 0. In general the RMS values are large in the mixing zone (within half mixhead diameter for this case).

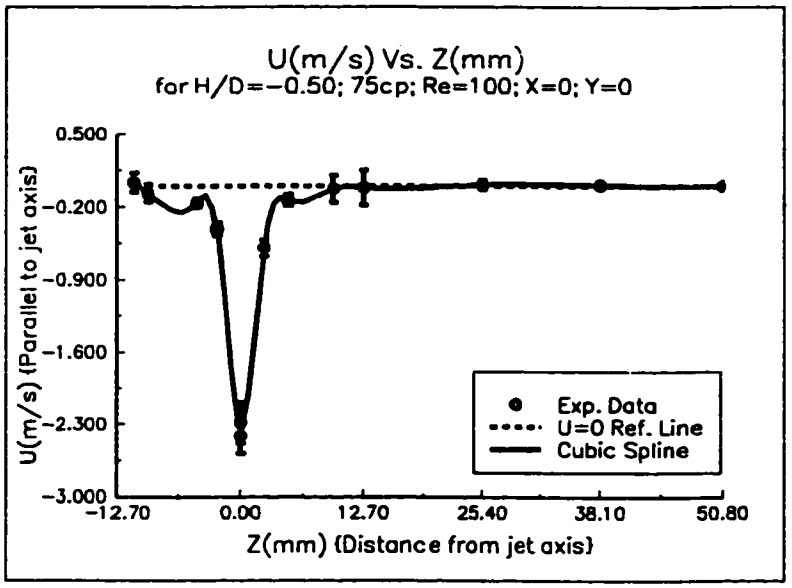

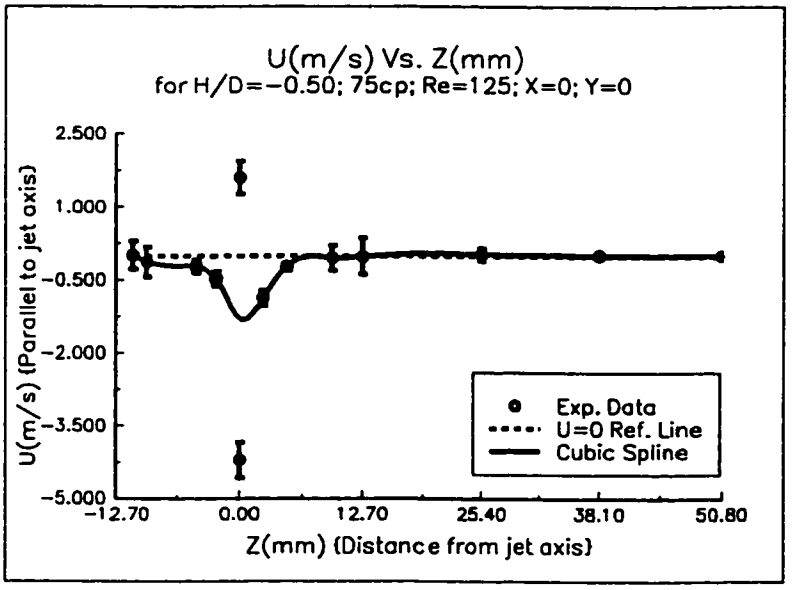

Fig. 7.4.2: Radial velocity (U) profile along mixhead axis (Z)
(Re = 100 & 125; H/D = -0.50; 75cp)

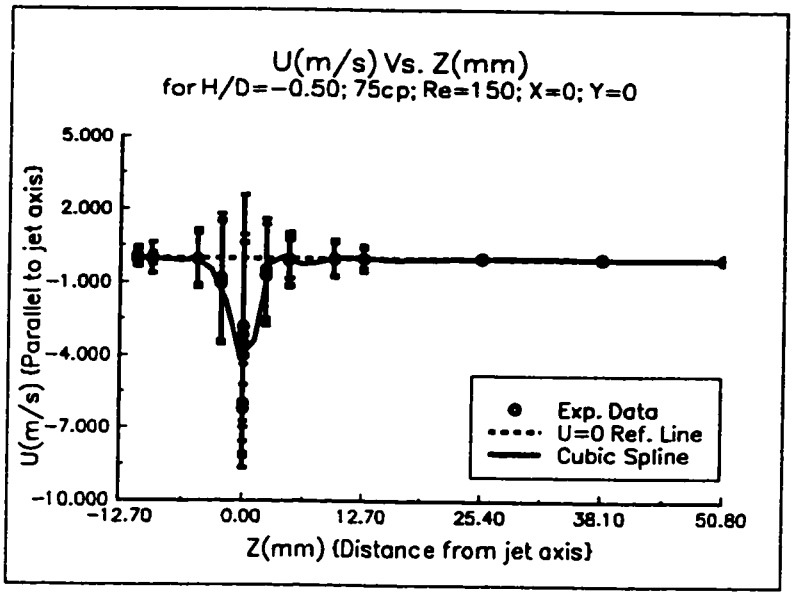

Fig. 7.4.3: Radial velocity (U) profile along mixhead axis (Z)
(Re = 150; H/D = -0.50; 75cp)

The axial velocity (V) at Re = 50 (Fig. 7.4.4) decreases sharply from its value of -0.021 m/s at Z = 0 to its minimum -0.402 m/s at Z = -2.38 mm, then it starts to increase gradually as the measurement location moves towards the piston head. On the other side of the jet axis, the axial velocity sharply increases to its maximum 0.448 m/s at Z = 2.38 mm, then it gradually decreases to its developed flow values. This value of one dimensional developed flow velocity is achieved between Z = 12.7 mm and Z = 25.4 mm. Some repeat results are shown at Z = 0, while the average velocity results reproduce satisfactorily, in one case the RMS value is much larger than the others. In the neighborhood of both inflection points below and above jet axis the RMSs' values are larger than the remaining observation locations except one experiment at Z = 0. The absolute axial velocities are symmetric about the jet axis, usually the absolute values above the jet axis are larger than their respective counter-parts below the jet axis. If the developed central line velocity of one dimensional flow is subtracted from the absolute axial velocities above the jet axis, then the symmetry is enhanced.

At Re = 75, the axial velocity (Fig. 7.4.4) below the jet axis sharply decreases to its global minimum (-.32 m/s) at Z = -2.38 mm, and then gradually increases until it vanishes at the piston head. There are two more direction changes till Z = -11 mm. A local maximum occurs at Z = -4.76 mm, and a local minimum at Z = -9.52 mm. Thus there are three inflection points (at Z = -2.38 mm, -4.76 mm and -9.52 mm) below the jet axis. The axial velocity above the jet axis sharply increases to its global maximum (0.50 m/s) at Z = 2.38 mm, then gradually decreases to its developed flow values after two change of direction at Z = 4.76 mm and Z = 9.52 mm. Similar to the profile below the jet axis there are three inflection points (at Z

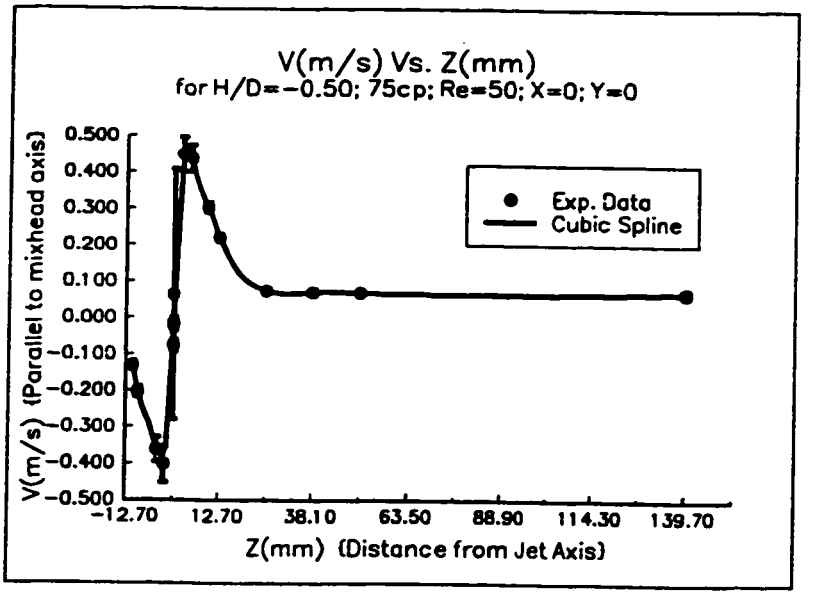

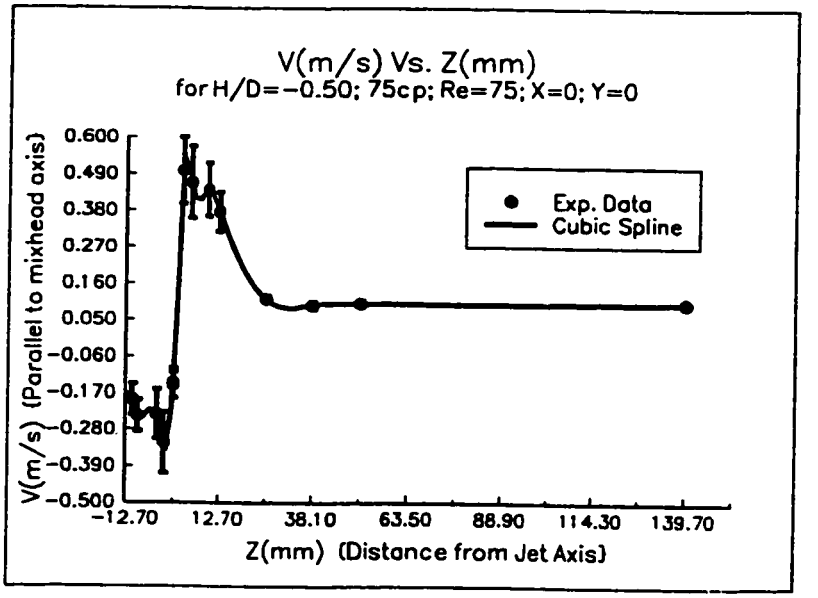

Fig. 7.4.4: Axial velocity (V) profile along mixhead axis (Z)
(Re = 50 & 75; H/D = -0.50; 75cp)

= 2.38 mm, 4.76 mm and 9.52 mm) in this side. From the piston head to Z = 12.7 mm larger RMSs' values are observed than in the developed zone section. A repeat experiment at Z = 0 shows excellent reproducibility of the results. Symmetry in absolute axial velocity about jet axis is also evident, even the inflection points are also symmetrically distributed. The axial velocity profile at Re = 100 follows a similar form to the previous case. The change in direction at all three above mentioned inflection points are more clear than the previous case especially below the jet axis (Fig. 7.4.5). One more inflection point is evident between Z = 12.7 mm and Z = 25.4 mm in this case. A repeat observation at Z = 0 is also shown. At Re = 125, the axial velocity profile (Fig. 7.4.5) is similar to the last two cases including symmetry, inflection points and repeatability. Very large RMS values are observed at Z = -11 mm, ± 9.52mm and 12.7mm, which indicate highly fluctuating flow.

The axial velocity (Fig. 7.4.6) at Re = 150 from its value at Z = 0 decreases to its minimum at Z = -2.38 mm, then gradually increases till Z = -11 mm (the last observation point). On the other side of the jet axis the axial velocity increases to its maximum at Z = 2.38 mm, then gradually attains its one dimensional developed pipe flow velocity value after going through three inflection points at Z = 4.76 mm, 9.52 mm and point between Z = 12.7 mm and Z = 25.4 mm. Many repeat experiments for all locations are also shown, and indicate good reproducibility of the results. Very large RMS values are observed at inflection points. Symmetry of absolute axial velocities about jet axis is also evident. The discussion, about symmetry of absolute axial velocity about jet axis, of the last paragraph of section 7.3 also applies for this section.

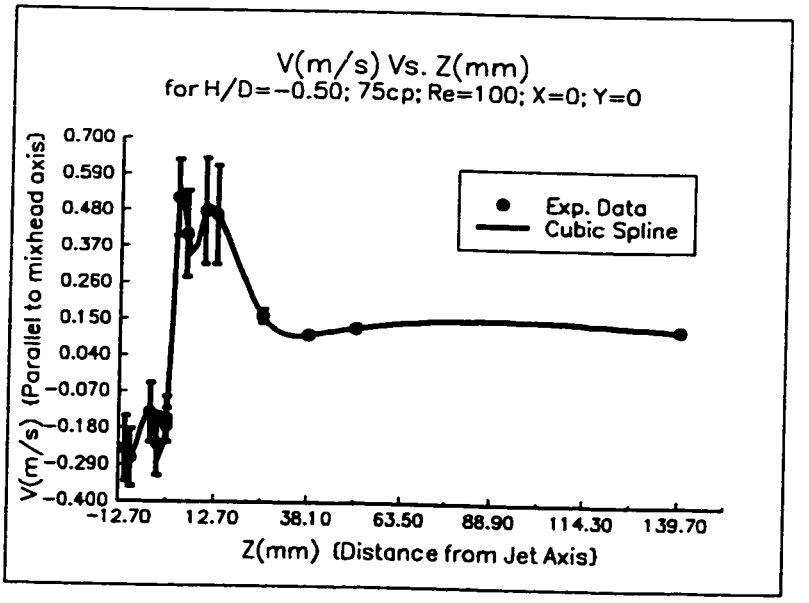

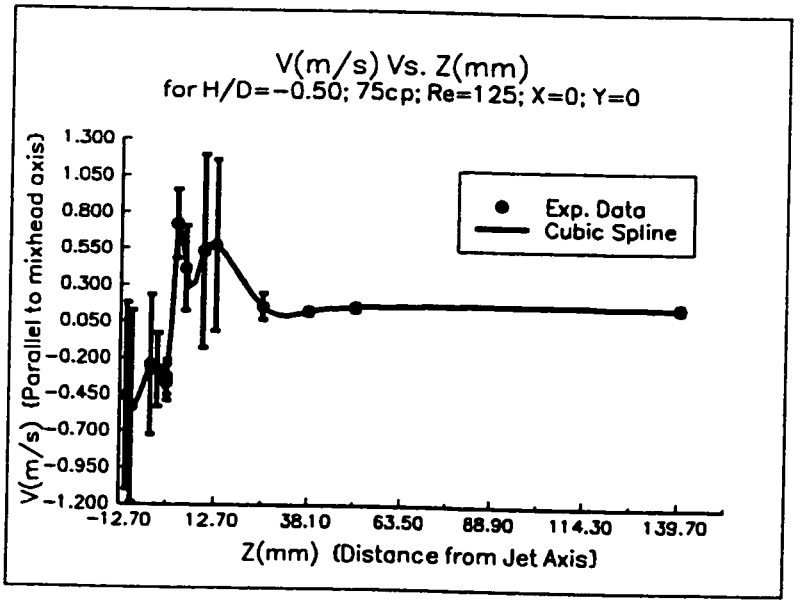

Fig. 7.4.5: Axial velocity (V) profile along mixhead axis (Z)
(Re = 100 & 125; H/D = -0.50; 75cp)

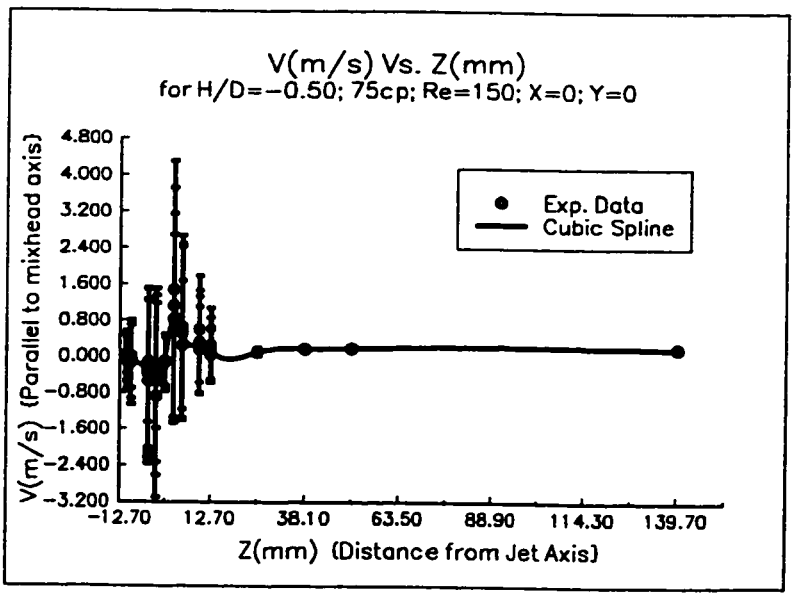

Fig. 7.4.6: Axial velocity (V) profile along mixhead axis (Z)
(Re = 150; H/D = -0.50; 75cp)

7.5 Effects of jet Reynolds number on radial and axial velocities

In the four previous sections the radial and axial velocity profiles were described. In general, an increase in jet Reynolds number produces increased magnitudes of radial and axial velocities. If an increase in Re only produces proportional increase in magnitudes of the average velocities, then the effect of Re is linear and well understood. It is clear from the flow visualization experiments that a change in Re considerably alters flow field pattern and its mode. To analyze the effects of jet Reynolds number on the velocities, plots have been prepared for the variation of dimensionless radial and axial velocities along the central axis.

The dimensionless radial velocity (u) is the ratio of actual radial velocity (U) and average jet velocity (Uavg_jet), and dimensionless axial velocity (v) is the ratio of measured axial velocity (V) and average velocity of mixhead (Vavg_MH) at a particular Re. In this calculation the direction signs of the actual radial and axial velocities are maintained by using only the absolute values of Uavg_jet and Vavg_MH. To maintain the clarity of the Figures only velocities at Re = 50 and 150 are connected by cubic spline.

In the profiles of the radial velocity (u), a reference line at u = 0 is drawn to identify the location, where u has vanished. This velocity will become zero for every Re because flow is one dimensional after the mixing zone. Usually the radial velocity U becomes insignificant in the neighborhood of half mixhead diameter (12.7 mm) above jet axis. A pattern shown from data above Z = 12.7 mm should

not be given much weight. At these locations, u is more susceptible of numerical and experimental errors than other locations. This does not mean that the results are not valid for these locations.

The radial velocity u profiles were not clear enough to show the influence of the jet Reynolds numbers (Fig. 7.5.1), even zooming in on the particular section (fig 7.5.2) did not help. There are two basic reasons. One is that u vanishes to an insignificant level very quickly and second is the location, i.e. the axis itself. Theoretically we know that u must vanish on impingement plane (X = 0 and Y = 0). Even on those locations for which u is sufficiently large, the direction of u kept changing from one location to other. To overcome these problems, plotting of profiles like Fig. 7.5.1 is abandoned, and profiles are prepared with logarithm of the absolute value of u instead of u. This facilitates the representation of larger ranges of u at the cost of losing the direction information of the velocity.

For axial velocity profiles two reference lines v = 0 and v = 2.0 are drawn. The first reference line (v = 0) is shown to facilitate the quick identification of the location, where the axial velocity is negative, i.e. flow is toward the piston head. The second reference line (v = 2.0) identifies locations of developed flow, since in developed one dimensional pipe flow central line axial velocity is twice the average velocity. This line is drawn from Z = 25.4 mm (one mixhead diameter) to Z = 50.8 mm (two mixhead diameter) to maintain the clarity of the Figures.

The influence of a change in jet Reynolds number is easily evident from such profiles of dimensionless velocities. If the change in the Re has no influence on the

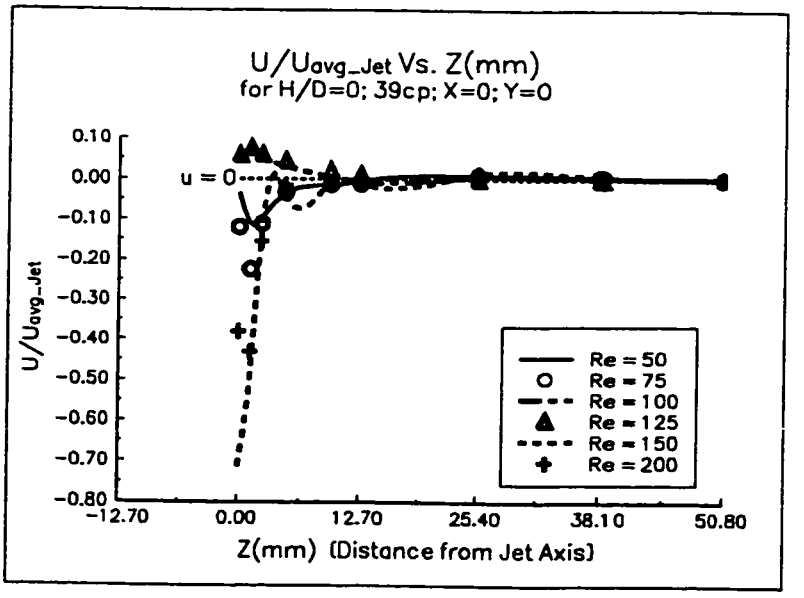

Fig. 7.5.1: Radial velocities (u) profile along mixhead axis (Z)
(Re = 50 to 200; H/D = 0; 39cp)

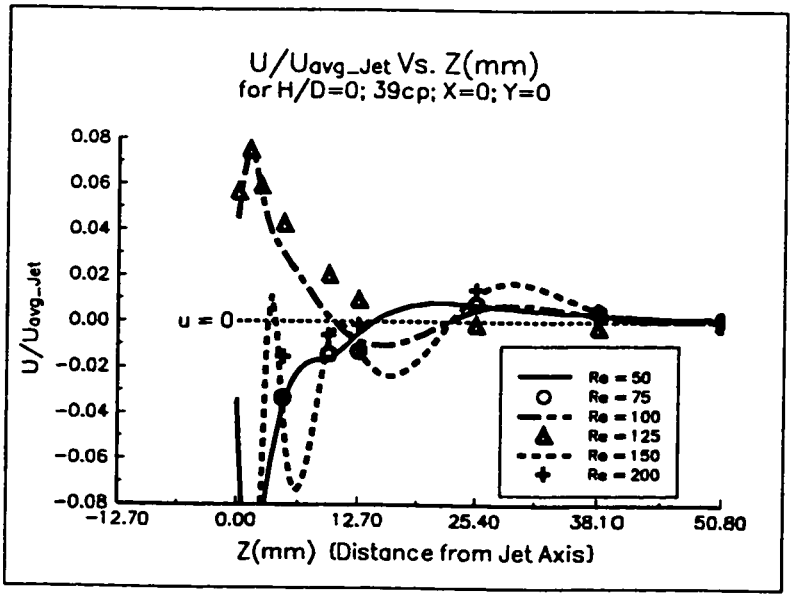

Fig. 7.5.2: Radial velocities (u) profile along mixhead axis (Z)
(Re = 50 to 200; H/D = 0; 39cp; zoomed portion of Fig. 7.5.1)

flow field, one expects that at each location all observations (one v for one Re) must overlap each other or be closely distributed in a narrow range; this range should be less than the spread due to experimental errors.

7.5.1 Radial velocities (u) for H/D = 0 & -0.5 and μ = 39 & 75 cp

The radial velocity profiles for H/D = 0 and viscosities of 39cp and 75cp are shown in Fig. 7.5.1.1. For H/D = -0.5 and viscosities of 39cp and 75cp, radial velocity profiles are shown in Fig. 7.5.1.2.

In the above Figs., the absolute u attains its global maximum usually at Z = 1.19 mm for H/D = 0 and at Z = 0 for H/D = -0.5. It seems (also supported by flow visualizations experiments) that jets are slightly bent upward with H/D = 0 case. This is due to the presence of the piston head 1.19 mm below the jet axis. The jet flow coming out of the nozzles is one dimensional and its profile is symmetrical regardless of shape (in our case it is parabolic). For the case of H/D = 0, as the jet travels in the mixhead its profile starts to become skewed due to higher velocity at Z = 1.19 mm than at Z = -1.19 mm where it is zero (wall effects due to piston head). Thus symmetry is broken. This results in having a global maximum at Z = 1.19 mm with H/D = 0. In the case H/D = -0.5 the jet symmetry is maintained (no wall effects) and global maximum is at Z = 0.

After achieving the global maximum, the absolute radial velocity continuously decreases along the positive Z axis as long as it is significant (below Z = 12.7 mm). For Z is greater than 12.7 mm, this decreasing pattern is lost, but it is irrelevant

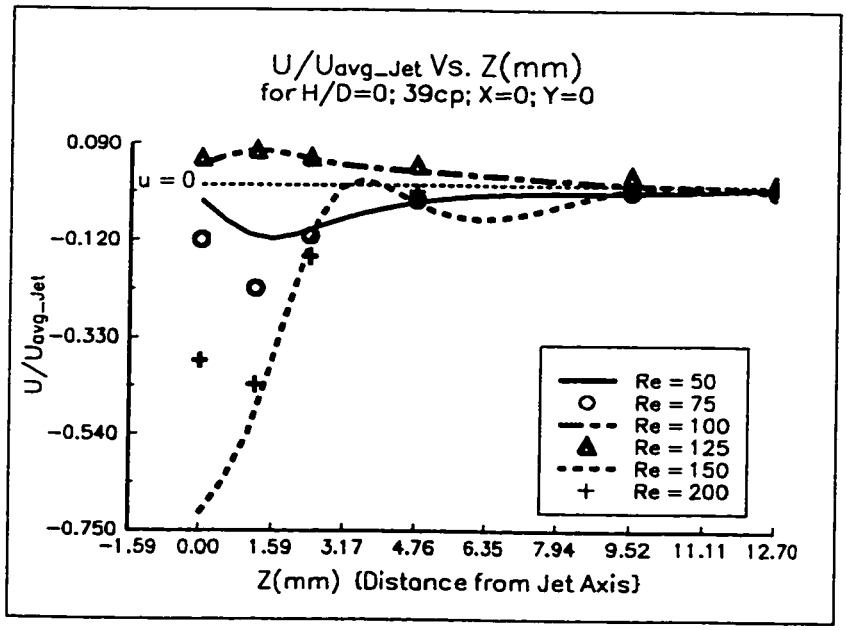

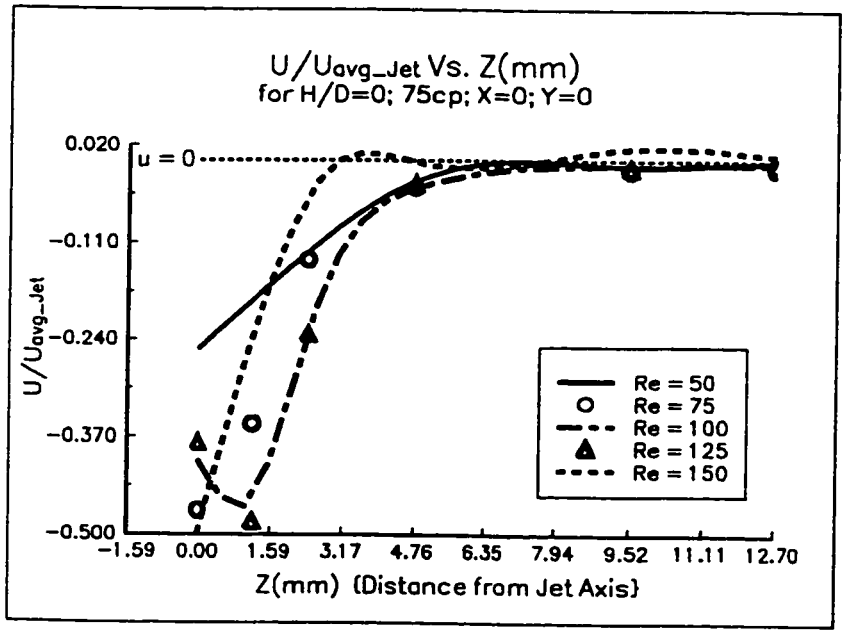

Fig. 7.5.1.1: Radial velocities (u) profile along mixhead axis (Z)
(Re = 50 to 200; H/D = 0; 39 & 75cp)

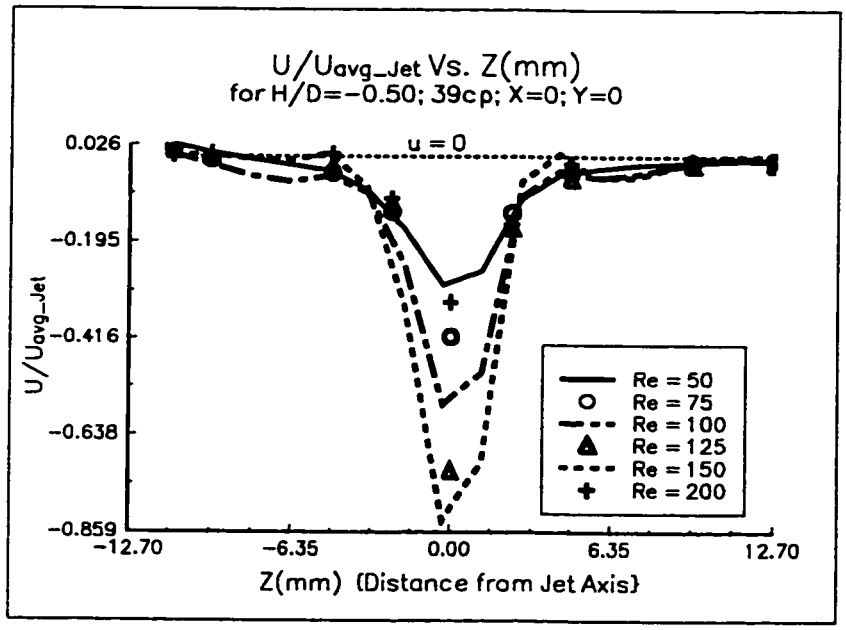

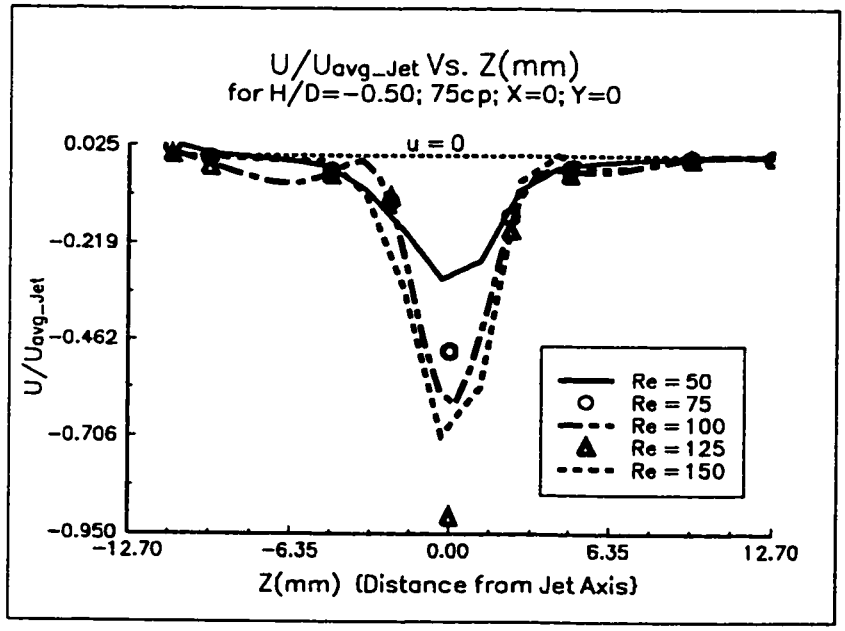

Fig. 7.5.1.2: Radial velocities (u) profile along mixhead axis (Z)
(Re = 50 to 200; H/D = -0.50; 39 & 75cp)

since u for practical purposes has vanished. Below the jet axis for H/D = -0.5 (Fig. 7.5.1.2) the absolute radial velocity from its global maximum at Z = 0 starts to decrease and reaches its local minimum around Z = -9.52 mm. The absolute radial velocity below this value of Z usually again increases.

7.5.2 Axial velocities (v) for H/D = 0 & -0.5 and μ = 39 & 75 cp

The axial velocity profiles for various Re at H/D = 0 and viscosity of 39 cp are shown in Fig. 7.5.2.1. On examining the Fig. 7.5.2.1, it is concluded that the increase of Re had altered the flow structure since the differences in axial velocity values are significant till Z = 25.4 mm (one mixhead diameter). The lowest v for all Re is found at Z = 25.4 mm, except in the case of Re = 200. It is the absolute v which is lowest in the case of Re = 200 at Z = 25.4 mm, since some negative flows are observed for this case which supports the observation that at this Re jets are not impinging on each other.

In the developed zone, as the Re increases, it takes longer for v to attain its developed flow value. In the case of Re = 50 the v_d (one dimensional developed velocity in a pipe and is equal = 2) is achieved at Z = 25.4 mm, for Re = 200 it is attained after Z = 50.8 mm (The location to attain v_d (or within 5% of v_d) is 25.4 mm for Re = 50, 38.1 mm for Re = 75 and 50.8 mm for Re = 100 and 125. For Re = 150 velocity is approximately 92% of v_d at Z = 50.8 mm, while for Re = 200 it is 90% at Z = 50.8 mm).

In the mixing zone (0 < Z < 25.8 mm), axial velocities are in ascending order of Re at Z = 12.7 mm (Fig. 7.5.2.1). The only exception to this

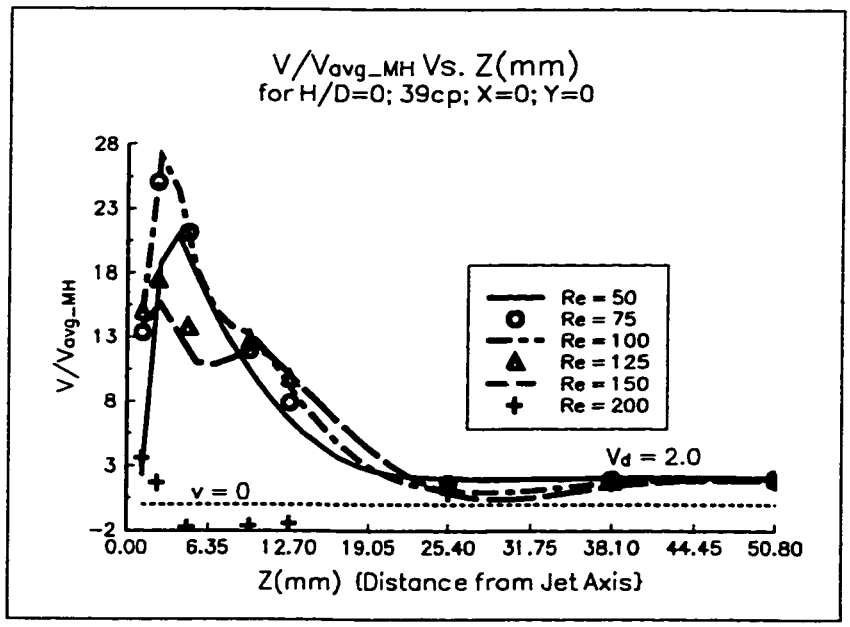

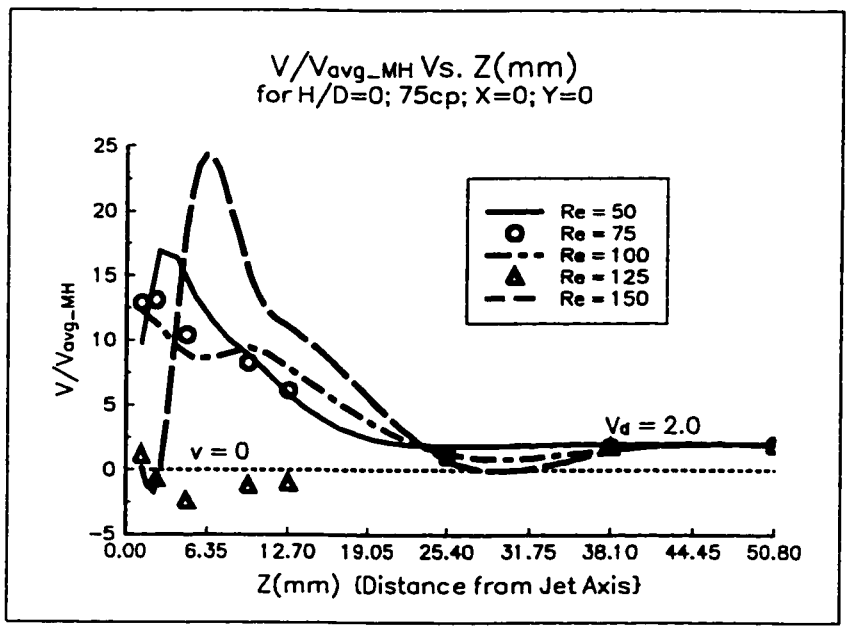

Fig. 7.5.2.1: Axial velocities (v) profile along mixhead axis (Z)
(Re = 50 to 200; H/D = 0; 39 & 75cp)

velocity at Re = 200. The axial velocity sharply increases to a respective maximum (except at Re = 50) for each Re at Z = 2.38 mm i.e. one jet diameter and then starts to decrease. For Re = 50, this maximum occurs at 2 jet diameters downstream. Usually, the axial velocities for the three lower jet Reynolds numbers of 50, 75 and 100 bunch together and their values are higher than the velocities at Re = 125 and 150. For these three values of Re, the decrease in velocities along the Z is gradual and smooth. However, for Re = 125 and 150 the behaviour seems to be fluctuating which indicates that the flow structure is not the same after Re = 100. The flow visualization has already shown that the flow patterns change from the static stable to dynamic stable to the unstable mode as Re increases from 50 to 200. The dynamic stable mode changes to unstable mode around Re = 125. The present analysis confirms the previous observations. One specific observation here is that once the flow has changed to an unstable mode the axial velocity in the mixing zone reduces with increasing Re.

For Re = 200 at three locations (Z = 4.76, 9.52, and 12.7 mm) negative axial velocities are obtained which indicates the presence of downward flow even in the central section of the mixhead (this occur due to missing of jet to jet impingement).

The axial velocity v for H/D = 0 and viscosity of 75cp profile is shown in Fig. 7.5.2.1. The spread increasing of the velocity profile at each location is sufficient to conclude that flow structure has an influence due to Re. The lowest v is found at Z = 25.4 mm (Re = 125 is an exception).

In the developed zone (Z > 25.4 mm) v_d is achieved at Z = 38.1 mm for Re = 50 and at Z = 50.8 mm for Re = 75, 100, 125 and 150. It appears that the increase of the viscosity from 39 cp to 75 cp has moved the recovery location downstream, specifically with case of Re = 50 and 75. However, v_d is attained within two mixhead diameters (Z = 50.8 mm) for all jet Reynolds numbers examined.

The mixing zone data show the same behaviour of axial velocities as observed with a fluid of viscosity 39 cp. Negative velocities are observed for Re = 125 and only at one point for Re = 150 (Z = 2.38 mm).

The profile of the axial velocity v for H/D = -0.5 and viscosity of 39 cp with Z is shown in Fig. 7.5.2.2. The minimum in the developed zone (equal or greater than one mixhead diameter) occurs at Z = 38.1 mm for Re = 50, 75, 100 and 125 and at 25.4 mm for Re = 150 and 200. The v_d is achieved at Z = 38.1 mm for Re = 50 and 75, Z = 50.8 mm for Re = 100, 125, 150 and 200. This distance to achieve fully developed flow has increased for lowest Re (50) but has decreases for High Re (150 and 200) in comparison with the case of H/D = 0 and 39 cp.

In the mixing zone above the jet axis, v increases to its maximum at Z = 2.38 mm for each Re after which it continuously decreases to a minimum and then gradually converges to v_d. As in the previous cases, the data at each location for the lower three jet Reynolds numbers of 50, 75 and 100 stay in one cluster and data for higher two jet Reynolds numbers of 150 and 200 stay in second cluster. These two clusters are separated by the data for Re = 125. This again supports the idea that a change of flow structure occurs around Re = 125. No negative axial velocities are observed in the unstable flow mode.

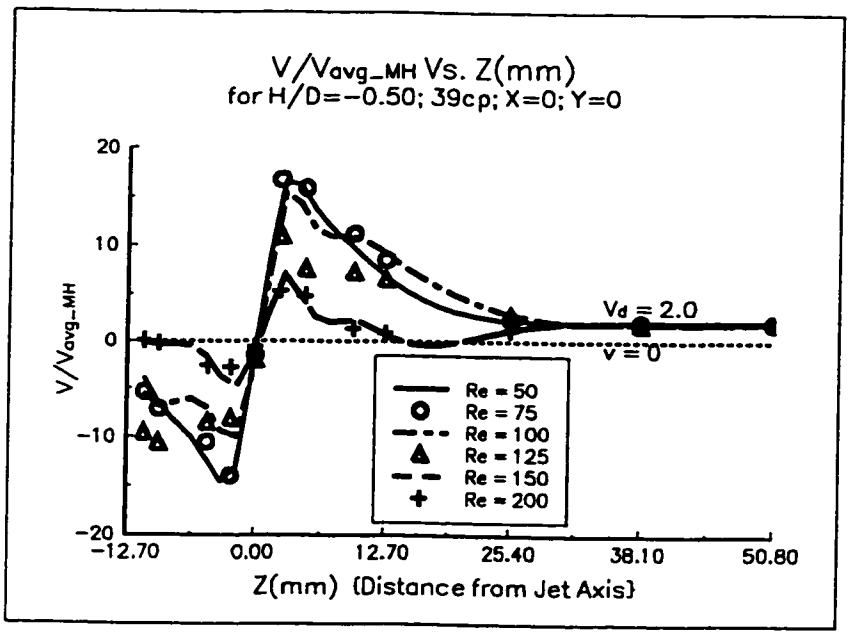

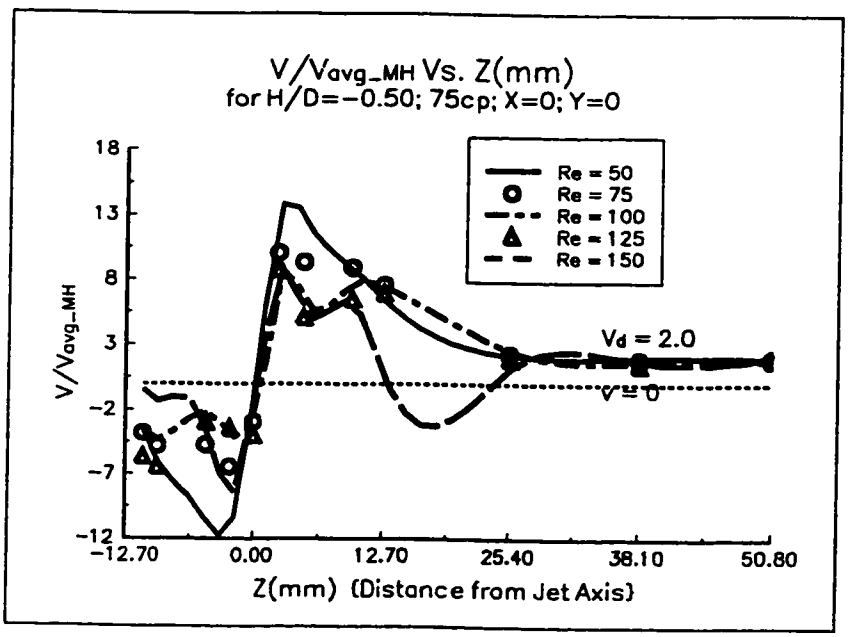

Fig. 7.5.2.2: Axial velocities (v) profile along mixhead axis (Z)
(Re = 50 to 200; H/D = -0.50; 39 & 75cp)

In the lower mixing zone (below jet axis), v decreases with decrease in Re. The magnitude of the velocities follows a behavior similar to the upper mixing zone. If one considers absolute velocities. Similarly there are clusters like the upper mixing zone separated by data from Re = 125. Again there are a few exceptions for Re = 125, these occur in the vicinity of the piston head. While the velocities above the jet axis smoothly converge to v_d, the velocities below the jet axis have to vanish to zero at piston head. This fact alone has a major influence for these exceptions and thus some of the symmetry between lower and upper zone of mixing is lost. Theoretically there will be no difference in these two sections if the lower section, like its counter-part upper section, is also open.

The axial velocity v profile along central axis for H/D = -0.5 and viscosity of 75 cp is shown in Fig. 7.5.2.2. The developed velocity v_d is attained at Z = 38.1 mm for Re = 50 and 75 and Z = 50.8 mm for Re = 100, 125 and 150. These values are identical for the lower viscosity case μ = 39 cp.

In the upper mixing zone the behaviour is same as described earlier. In the lower mixing zone, the axial velocity v usually attains its minimum at Z = -2.38 mm, then gradually increases as one moves towards the piston head. For Re = 100 and 125 the minimum is attained at Z = -9.52 mm. A rough symmetry exists between the lower and upper sections. This symmetry is further enhanced if one makes a correction (subtracting the value of v_d from the velocity above jet axis) for the fact that in the lower section the velocity has to vanish while in the upper section it becomes v_d.

7.6 Effects of H/D and viscosity on radial velocities

The radial velocity along the central axis of the mixhead vanishes completely or reduces to an insignificantly low number after half mixhead diameter (12.7 mm) from the jet impingement axis. The figures in this section are drawn from Z = -12.7 mm to Z = 12.7 mm and only average velocities without confidence limits are plotted to maintain clarity. Further more, the point at Z = 0 is also not shown in the Figures due to two reasons. It is the largest absolute radial velocity. Inclusion of this point will increase the range of y-axis in the figures, which will hide the differences of radial velocities (if any) due to H/D and or viscosities changes at other locations. The second difference at Z = 0 in radial velocities is more due to experimental (influence of rotameter settings) than the influences of H/D and or viscosity changes.

It is clear from Figures 7.6.1 to 7.6.3 that H/D and viscosity changes, either individually or collectively, do not influence the radial velocity with all jet Reynolds numbers. For some cases in the figures there seems to be some influence. An examination of the Figures 7.6.1 to 7.6.3 indicates that the largest absolute difference in average velocities are at Z = 0. On all the other locations this difference is small until it vanishes and the velocity becomes insignificant. It is highly probable that the differences in the radial velocities at other locations are due to initial difference at Z = 0 than the influence of H/D and or viscosity changes. At the best influences are marginal, even than it is insignificant since the radial velocities usually after two jet diameters are insignificant. It is concluded that Re is an adequate measure to explain the changes in radial velocity.

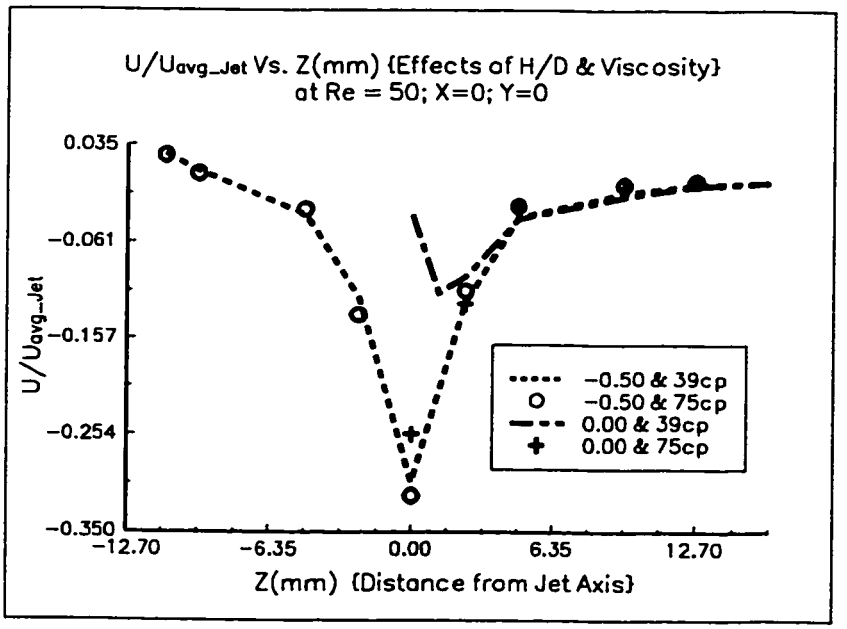

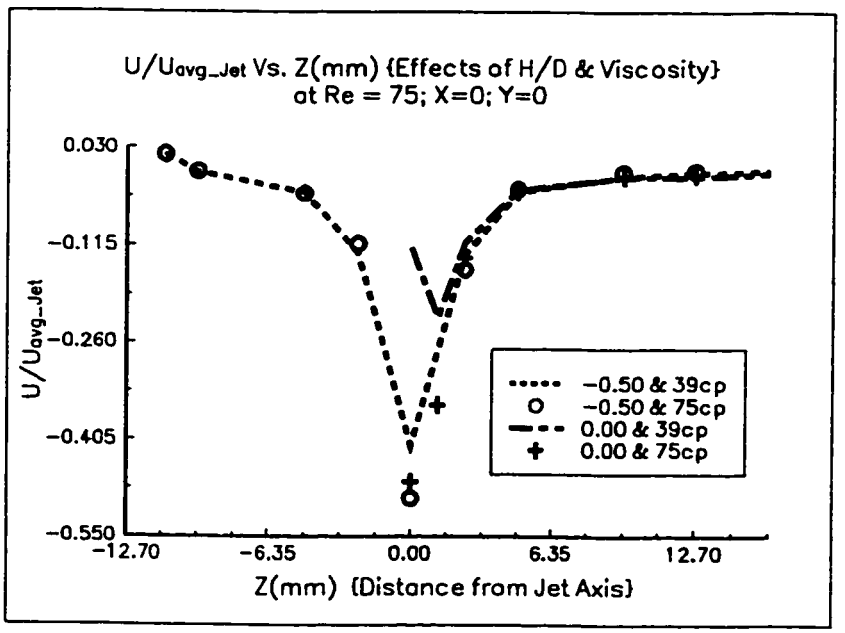

Fig. 7.6.1: Effects of H/D and viscosity on radial velocity for Re = 50 & 75

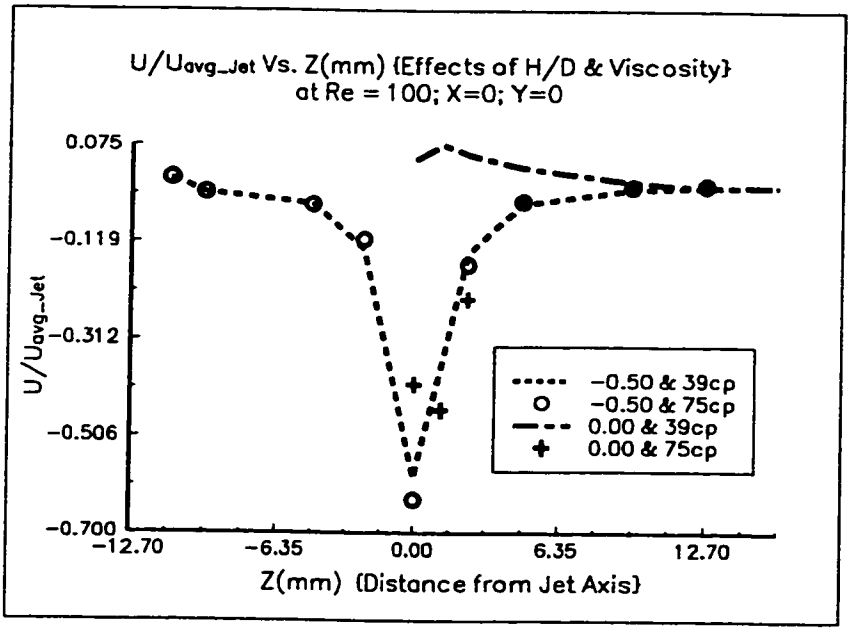

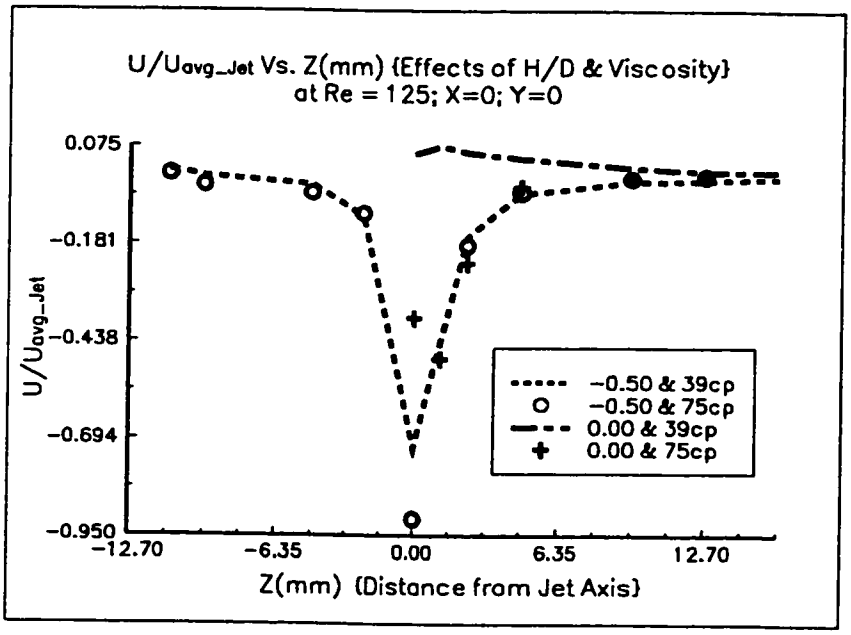

Fig. 7.6.2: Effects of H/D and viscosity on radial velocity for Re = 100 & 125

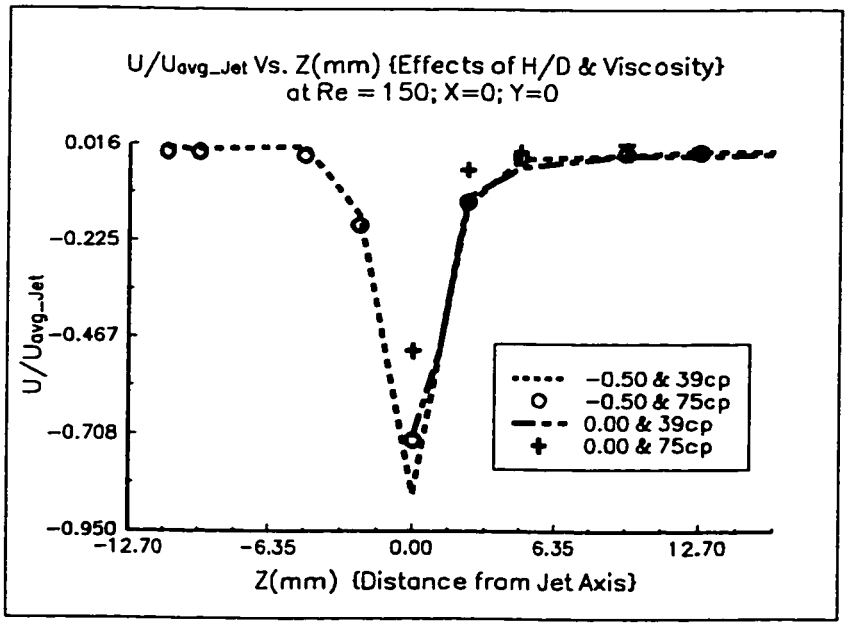

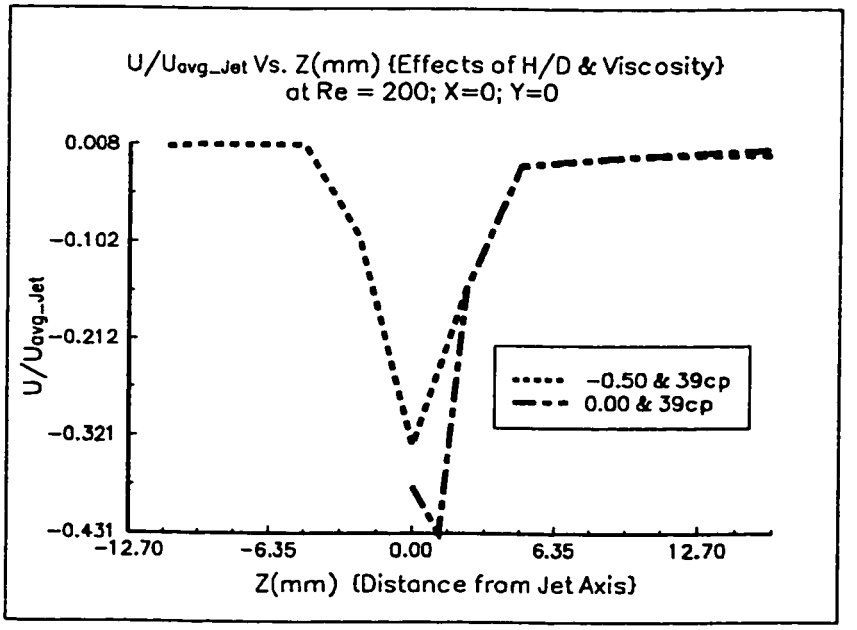

Fig. 7.6.3: Effects of H/D and viscosity on radial velocity for Re = 150 & 200

7.7 Effects of H/D on axial velocities

The effects of H/D on axial velocity for different jet Reynolds numbers is highlighted in the axial velocity profile with distance (Z) from jet impingement axis in Figures 7.7.1 to 7.7.3. The axial velocity component decreases as H/D decreases from 0.0 to -0.5. The difference between two velocities (higher at H/D = 0 than H/D = -0.5) is gradually diminishing as Z is increasing. This difference is usually a minimum around Z = 9.52 mm. At the end of mixing zone (around Z = 12.7 mm)usually higher axial velocities are observed at the lower H/D = -0.5 than for H/D = 0 and this trend is followed until v_d is attained. This distance of changing of direction keeps moving farther away from jet impingement axis with increasing Re. For Re = 50 and 75 this point is between 9.52 mm and 12.7 mm (crossing of lines in Fig. 7.7.1); for Re = 100 (Fig. 7.7.2) it is after 12.7; for Re = 125 (Fig. 7.7.2) it is between 12.7 and 25.4; for Re = 150 (Fig. 7.7.3) it is at 25.4 mm. There are two exceptions for this behavior. One is at Re = 125 and viscosity 75 cp (Fig. 7.7.2) and other is at Re = 200 and viscosity 39 cp (Fig. 7.7.3). Axial velocity stays lower at higher H/D (= 0.0) until v_d is attained in the developed zone. In these two cases actually negative axial (downward) velocities are observed for H/D = 0.

The jet flow, which is one dimensional, is vertical to mixhead axis. All the jet velocity is converted from radial velocity to axial velocity. In case of H/D = 0 this is achieved only in the upper section of the mixhead, while with H/D = -0.5 this flow is divided in half between the upper and lower sections of mixhead. Thus this conversion of the radial to axial velocity is smoother with H/D = -0.5 than for H/D = 0. This results in higher axial velocity in mixing zone at H/D = 0 than H/D = -0.5.

Again in developing zone, the attainment of v_d is smoother with H/D = -0.5 than for H/D = 0. The axial velocity from the mixing zone at H/D = -0.5 has less to change to be v_d than with H/D = 0. This results in a lower axial velocity with H/D = 0 than with H/D = -0.5.

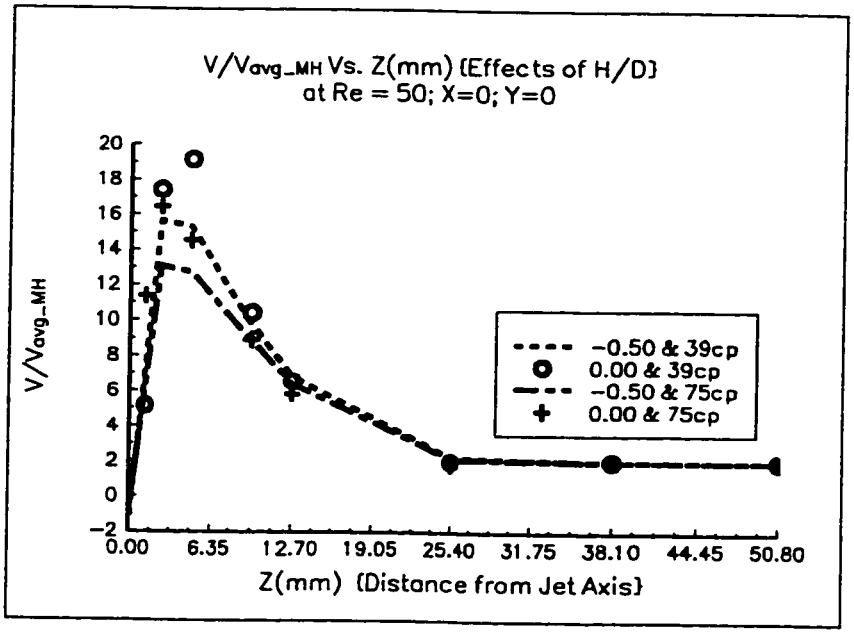

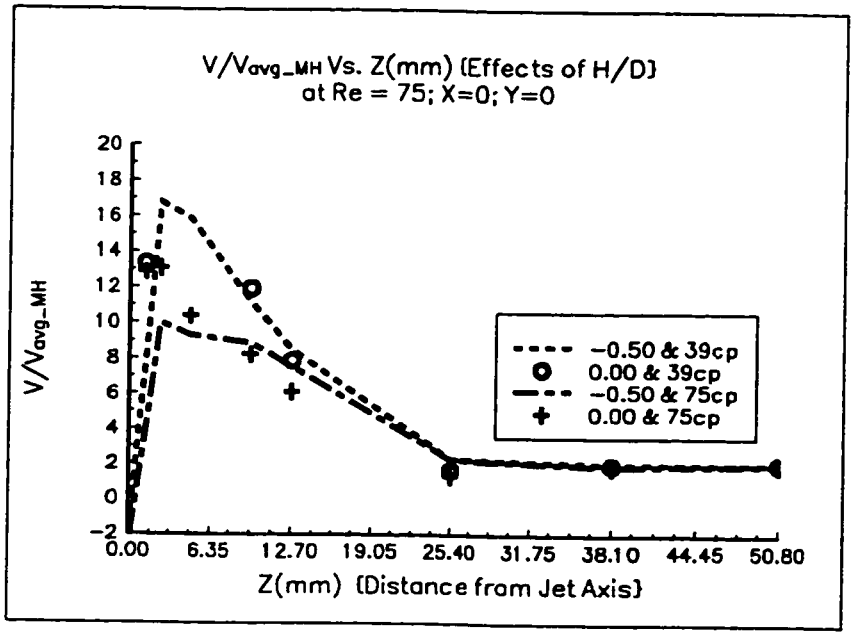

Fig. 7.7.1: Effects of H/D on axial velocity for Re = 50 & 75

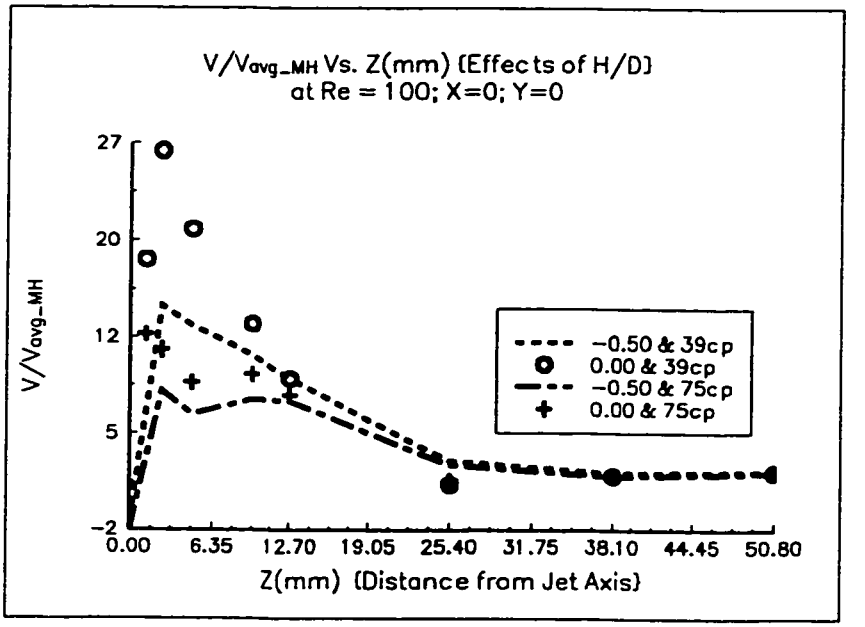

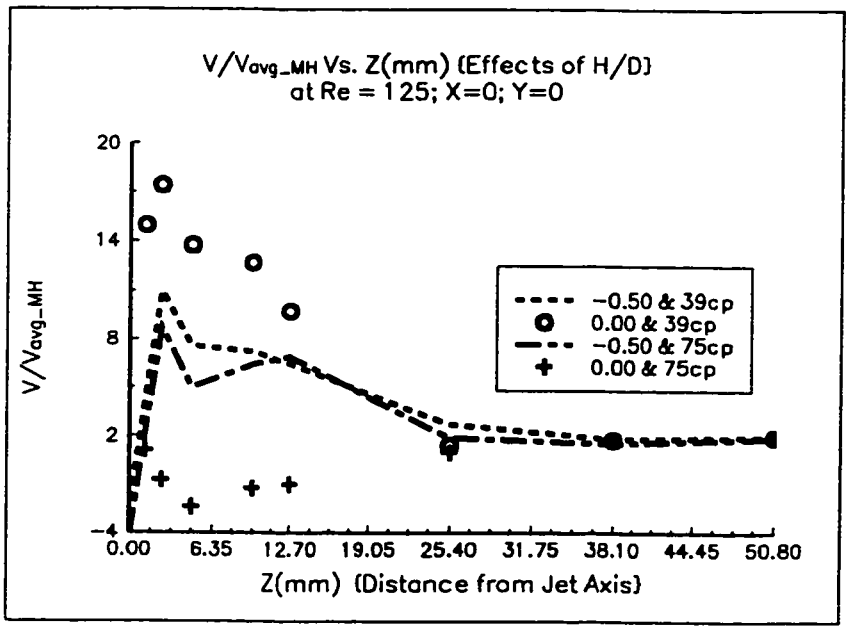

Fig. 7.7.2: Effects of H/D on axial velocity for Re = 100 & 125

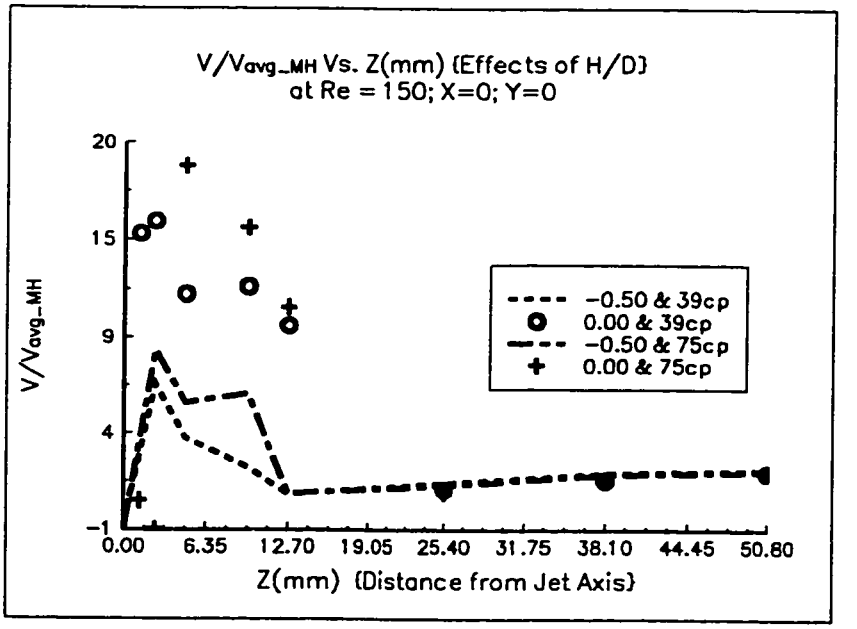

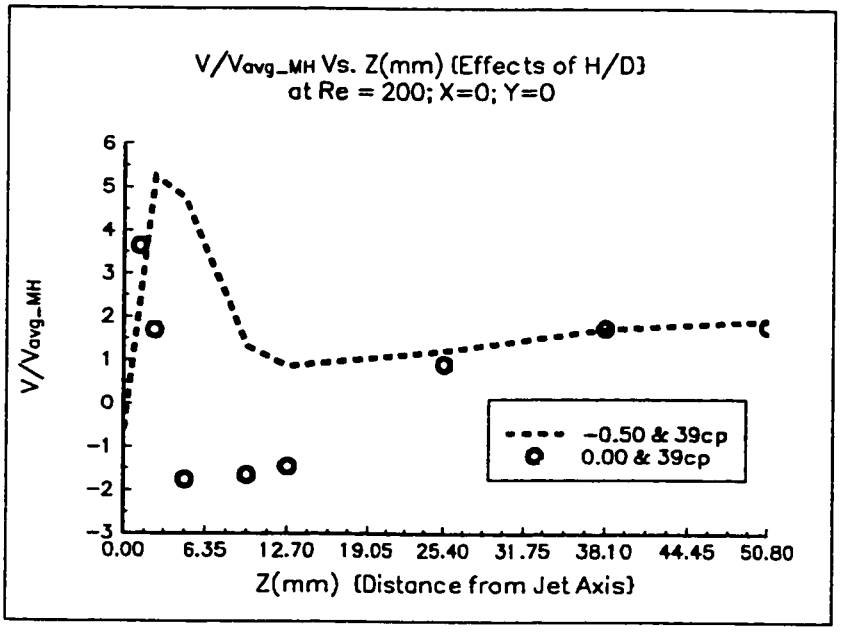

Fig. 7.7.3: Effects of H/D on axial velocity for Re = 150 & 200

7.8 Effects of viscosity on axial velocities

The influence of viscosity is stronger in the mixing zone than in the developing and developed zone. Here plots are limited to one mixhead diameter (25.4 mm) for clarity. The average velocities are plotted with their respective confidence level (95%).

7.8.1 H/D = 0

The axial velocity and confidence limits are plotted versus Z to highlight the viscosity effects are shown in Figures 7.8.1.1 to 7.8.1.3, one for each Re.

The average velocity decreases as viscosity increases in the mixing zone (Fig. 7.8.1.1 to 7.8.1.3) for a given Re except at Z = 1.19 mm. This difference in the average velocities keeps decreasing with increasing Z. At one mixhead diameter (Z = 25.4) both of the axial velocities converge to a similar value. Usually it is v_d. Any difference after that is due more to experimental differences and error than a viscosity influence. At lower viscosity (39 cp) variances are also higher than at higher (75 cp). The values at Z = 1.19 mm are more prone to error in rotameter settings i. e. the error in rotameter settings to achieve a specific Re, let say Re = 75, at two different viscosities affects the value at Z = 1.19 mm more than the other point farther away from jet impingement axis. The behavior at Re = 150 is reversal of general trend at Z = 4.76 mm and Z = 9.52 mm.

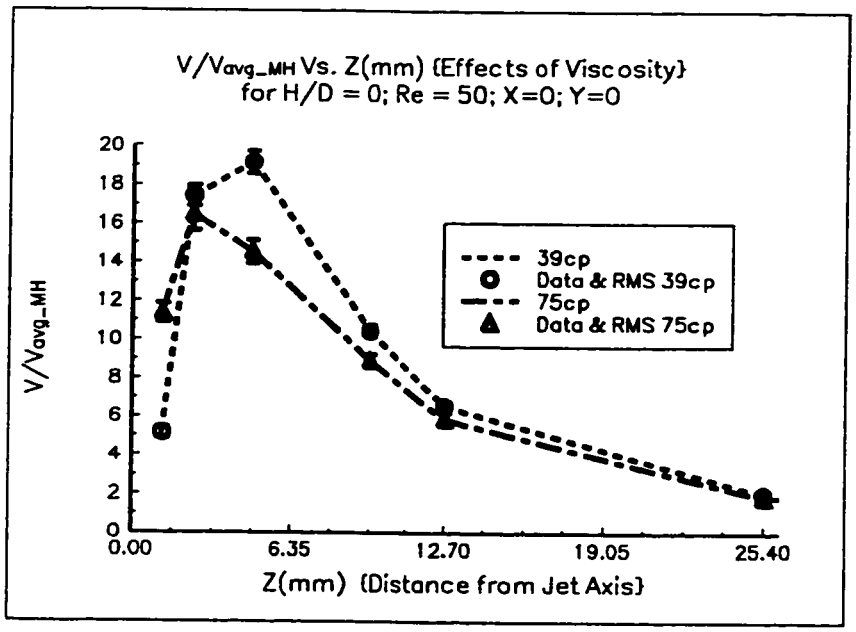

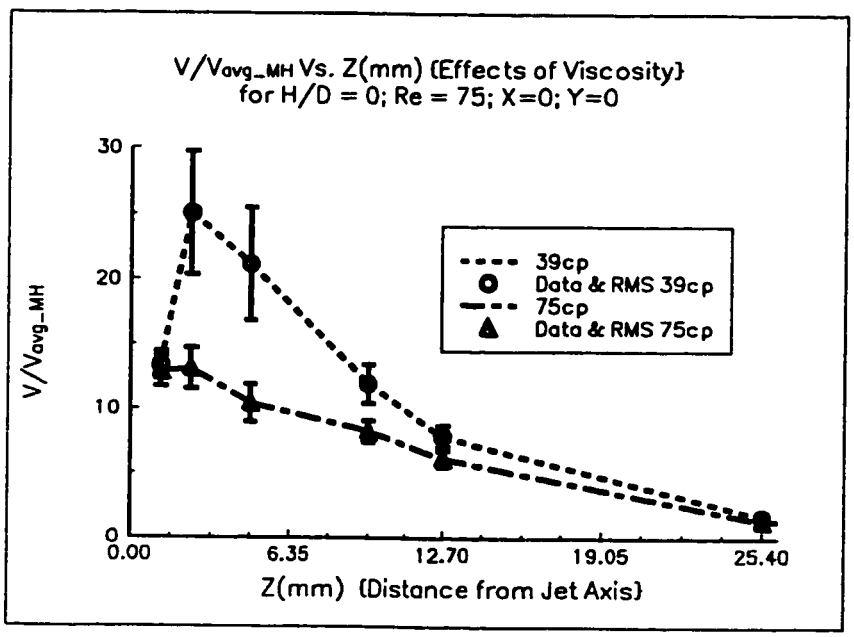

Fig. 7.8.1.1: Effects of viscosity on axial velocity for Re = 50 & 75

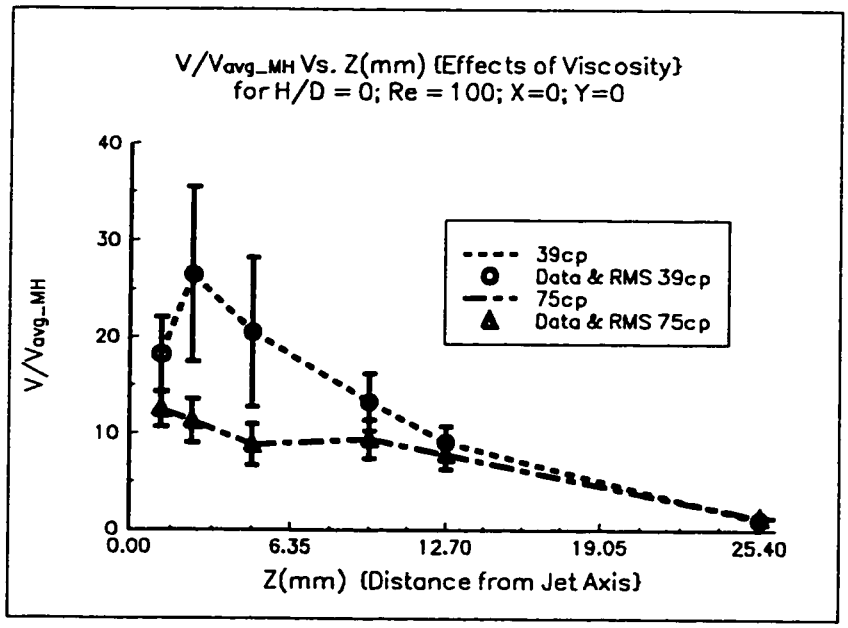

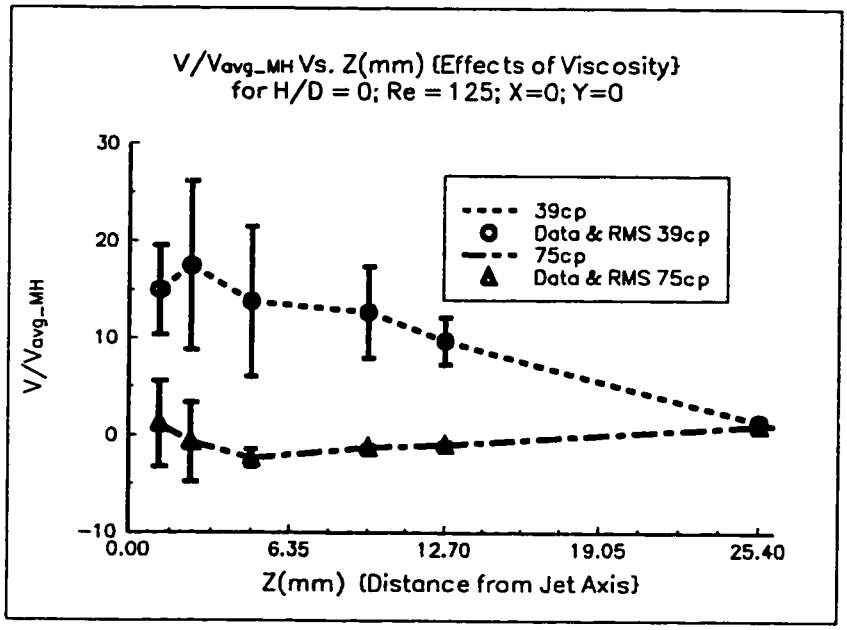

Fig. 7.8.1.2: Effects of viscosity on axial velocity for Re = 100 & 125

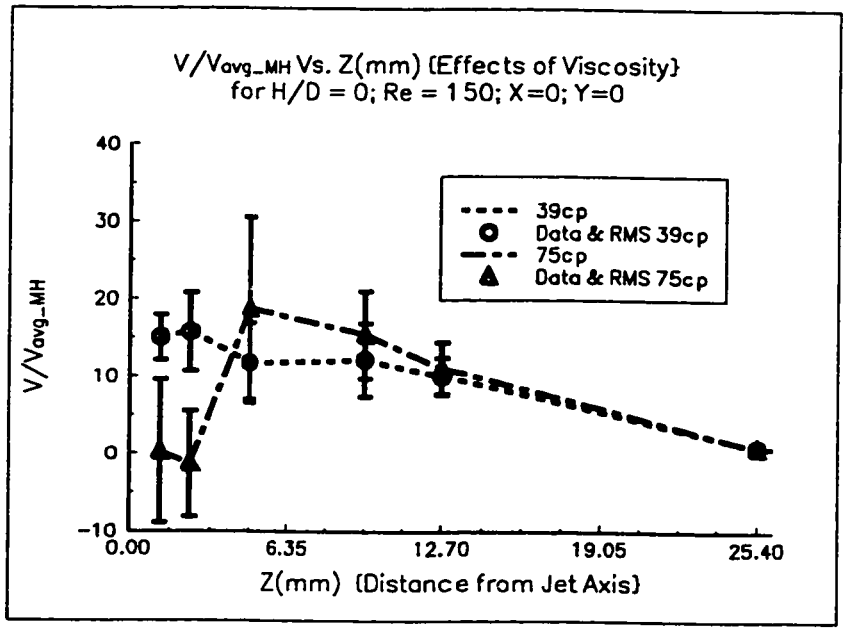

Fig. 7.8.1.3: Effects of viscosity on axial velocity for Re = 150

7.8.2 H/D = -0.5

From Re = 50 to 125 axial velocity increases as viscosity decreases on both sides of the jet axis (Figs. 7.8.2.1. and 7.8.2.2). This increase in the absolute axial velocity along with the standard deviation gradually diminishes as the absolute value of Z increases. In the upper mixing zone, difference between axial velocities with different viscosities becomes insignificant at Z = 25.4 mm. Once v_d is attained the influence of viscosity has vanished.

In the lower mixing zone, convergence (*at same Re, an insignificant velocities difference with two viscosities*) of different axial velocities for two viscosities at Z = -11 mm (last location for observed data) is achieved at low Re = 50, but for Re = 75, 100 and 125 the convergence of axial velocities for two viscosities does not occur. Low viscosity gives higher absolute velocity than high viscosity just like in the upper mixing zone. There is no convergence of axial velocities for two viscosities in the sample space of lower mixing zone. This different behavior of lower mixing zone compared to upper mixing zone is due to fact that in lower mixing zone all velocities have to come to zero at piston head due to fixed boundary while in upper zone velocities are smoothly converging to v_d.

At Re = 150 (Fig. 7.8.2.3) in both mixing zones the effects of viscosity are opposite to effects at low jet Reynolds numbers described in last two paragraphs. In this case absolute axial velocity increases as the viscosity increases, but this change in velocities and variances are marginal. This difference after becoming

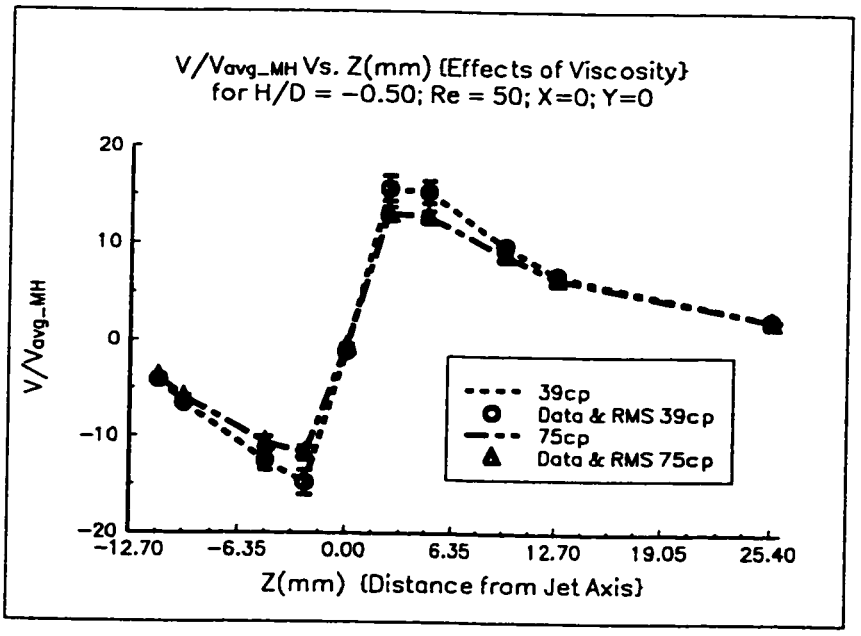

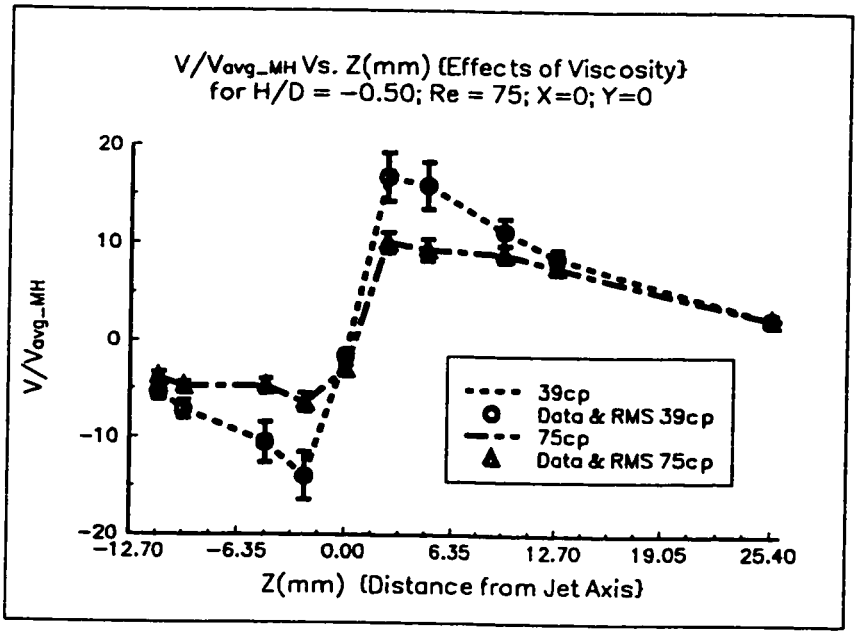

Fig. 7.8.2.1: Effects of viscosity on axial velocity for Re = 50 & 75

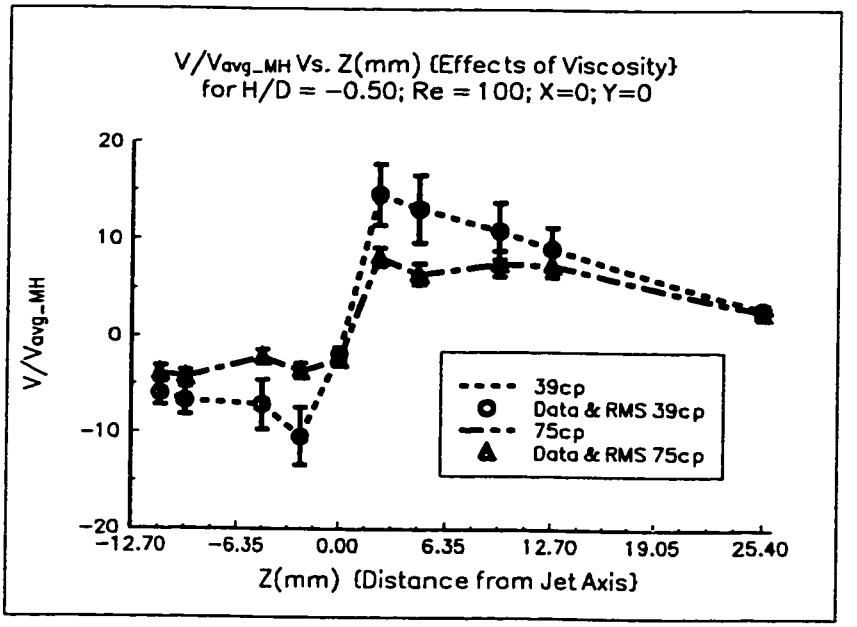

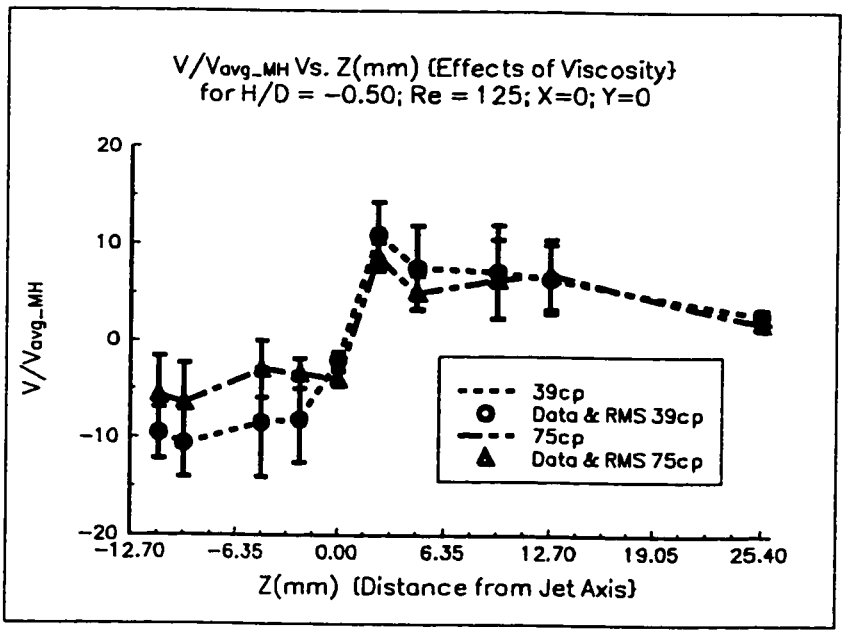

Fig. 7.8.2.2: Effects of viscosity on axial velocity for Re = 100 & 125

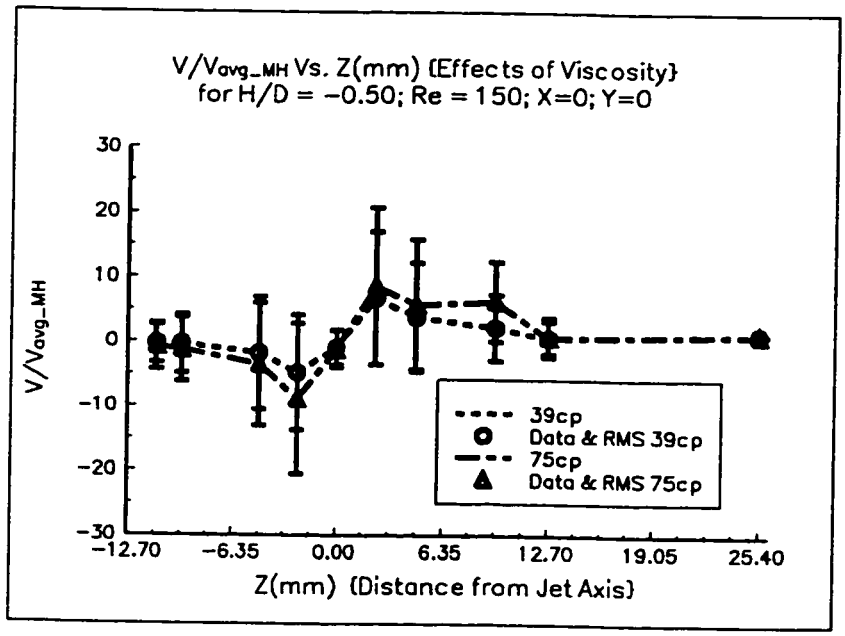

Fig. 7.8.2.3: Effects of viscosity on axial velocity for Re = 150

maximum within one or two jet diameters from the jet impingement axis gradually diminishes converges to each other. This convergence is achieved in both mixing chambers. The convergence of axial velocities in lower mixing chamber is also reversal of the behavior at low jet Reynolds numbers.

It is concluded that the increase in viscosity from 39 cp to 75 cp influences axial velocity inversely at a given location in mixing zone and Re. This effect of viscosity change is diminished as Re is increased to a certain value. This value lies after Re = 100. The close examination of the figures indicates that once Re = 125 the difference in axial velocities at two viscosities usually never grows more than the difference of at Z = 0. The conclusion of this paragraph applies for both cases of H/D ratios (H/D = 0 and -0.5).

8 Frequency Analysis

During the flow visualization experiments, it is observed that the impingement plane shows some oscillations. Similar observations have also been reported in the literature (Sandell et. al, 1985, and Tucker et. al 1980). The time series obtained for instantaneous velocity components using LDA are analyzed in the time and frequency domains. In the time domain, statistical functions such as the autocorrelation function (ACF) and partial autocorrelation function (PACF) are obtained while in the frequency domain, the power spectrum density (PSD) is computed. In the next section, the results are reported for data taken along the center line (0,0,Z) of the mixhead for various cases.

8.1 Effects of Re, H/D, and Viscosity

Tables 8.1.1 and 8.1.2 show the significant frequencies estimated by using Fisher test and Whittle's suggested extension of this test on the PSD data (Wei, 1989). Table 8.1.1 provides data for H/D = 0 and Table 8.1.2 shows data for H/D =-0.5. The significant frequencies are reported for various Reynolds numbers along the central axis of mixhead for viscosities of 39 cp and 75 cp. The data in the tables have been represented in the form of binary codes which indicate the presence or absence of the harmonics and its higher harmonics at a particular location for a given set of parameters. Thus, the presence of a particular harmonics is indicated by 1 and absence by 0. To give an example, the bit code for velocity component U in Table 8.1.1. at z = 0, Re = 125, and viscosity = 39 cp, is denoted as 101011 which indicates the presence of fundamental harmonics along with its second, fourth, and

Table 8.1.1: Significant frequencies estimated from PSD for H/D = 0

(A) Radial velocity (U) at (0,0,Z) for 39 cp; Fundamental frequency = 14.65 Hz

Z(mm)	0.00	1.19	2.38	4.76	9.52	12.70	25.4	Freq(Hz)
Re								
50	1	1	11	1	1	1		
75	111	1111	1111	1111	111	11		
100	1011	1111	1111	1111	1111	111	1	
125	101011	1111	11111	111111	11111111	11111	1	
150	111111	111111	111111	111111	111111	1111111	11	

(B) Axial velocity (V) at (0, 0, Z) for 39 cp; Fundamental frequency = 14.65 Hz

Z(mm)	0.00	1.19	2.38	4.76	9.52	12.70	25.4	Freq(Hz)
Re								
50		1	1	11	1	1		
75		111	11	111	111	11		
100		1111	111	1111	11111	111		
125		1111	1111	1111	1111111	11111		
150		1011	1111	1111	11111	111111	1	

(C) Radial velocity (U) at (0, 0, Z) for 75cp; Fundamental frequency = 15.82 Hz

Z(mm)	0.00	1.19	2.38	4.76	9.52	12.70	25.4	Freq(Hz)
Re								
50	11		11	11	11	11		
75	101111	101111	1011	101011	11	11		21.97
100	11	11	11	10				21.97
125	1							52.19
150	11		11	11	11	111	1	61.00

(D) Axial velocity (V) at (0, 0, Z) for 75cp; Fundamental frequency = 15.82 Hz

Z(mm)	0.00	1.19	2.38	4.76	9.52	12.70	25.4	Freq(Hz)
Re								
50		11	11	11	11			
75		1011	1111	1011	1011	1011		
100		1111	101111	101111	101111	1111		
125		1	1	1				48.05
150				1011	11110	1010	1	

Note: In column (9) {Freq. (Hz), no entry means that "1" represents the fundamental frequency and its higher harmonics at that Reynolds number and location. But in case of entry (with 75cp) in this column "1" represents the listed frequency and its higher harmonics for that row.

Table 8.1.2: Significant frequencies estimated from PSD for H/D = -0.50

(A) Radial velocity (U) at (0,0,Z) for 39 cp; Fundamental frequency = 14.65 Hz

Z(mm)	-11.00	-9.52	-4.76	-2.38	0.00	2.38	4.76	9.52	12.7	25.4	Hz
Re											
50	1	11	111	111	1111	11	111	11	1		
75	11	11	11	11	11	11	11	11	11		
100	1111	1111	1111	1011	1011	11	1111	1111	1111	1	
125	1111	1111	1111	1011	1011	111	1111	1111	1111		

(B) Axial velocity (V) at (0, 0, Z) for 39 cp; Fundamental frequency = 14.65 Hz

Z(mm)	-11.00	-9.52	-4.76	-2.38	0.00	2.38	4.76	9.52	12.7	25.4	Hz
Re											
50	1	1	11	11	1	11	11	1	1		
75	1	11	11	11	1	11	11	11	1		
100	11	1111	111	1111	11	1111	1111	1111	11	1	
125	11	11	1011	1111	11	1111	1111	1111	11		

(C) Radial velocity (U) at (0, 0, Z) for 75cp; Fundamental frequency = 15.82 Hz

Z(mm)	-11.00	-9.52	-4.76	-2.38	0.00	2.38	4.76	9.52	12.7	25.4	Hz
Re											
50	11	11	1011	11	1111	1011	1011	11	11		
75	111	111	101111	111	101111	111	1111	1111	1111		21.97
100	1111	1111	101110	10	1111	11	101111	101111	101111	11	21.97
125	11	11	11	11	111	1	11	1011	1011	1	21.97

(D) Axial velocity (V) at (0, 0, Z) for 75cp; Fundamental frequency = 15.82 Hz

Z(mm)	-11.00	-9.52	-4.76	-2.38	0.00	2.38	4.76	9.52	12.7	25.4	Hz
Re											
50	11	11	11	1011		11	11	11	11		
75	1111	1111	1011	1111	11	1011	1011	11	11		
100	11111	1111	111	1111	11	11	11	1111	1111	11	
125	11	11	11	111	11	111	11	11	11	11	21.97

Note: In column (12) {Hz}, no entry means that "1" represents the fundamental frequency and its higher harmonics at that Reynolds number and location. But in case of entry (with 75cp) in this column "1" represents the listed frequency and its higher harmonics for that row.

sixth higher harmonics. The third and fifth higher harmonics are absent. No code is indicated for axial component V at z = 0 for H/D = 0 since LDA data at this location has not been collected due to physical obstruction in the paths of beams.

For all cases beyond z = 25.4, no oscillations are detected. In only a few cases are harmonics present at z = 25.4. These cases are observed at higher Reynolds numbers where unstable flow modes exist (chapter 7). For a specified viscosity at a particular location, the observed number of significant higher harmonics increases as Re is increased. This pattern continues up to a certain value of increasing Re. After which no significant harmonics are detected. With H/D = 0, this limiting value of Re is 150 and for H/D = -0.5, this limit is Re = 125. The decrease in limiting Re probably occurs due to the lower localized Re number generated due to lower piston position. In this situation, the flow after the jet to jet impingement divides into two streams in opposite directions which leads to a decrease in the local Re. Within the oscillation region, the number of significant harmonics at a given Re is rarely influenced by the location along the central axis (z). The fundamental harmonics detected for all cases with viscosity of 39 cp is 14.65 Hz. At a viscosity of 75 cp, two different frequencies of 15.82Hz and 21.97 Hz are detected as fundamental frequencies during various settings. The frequency of 21.97Hz is the commensurate multiple of 14.65Hz (1.5 times) which is the detected fundamental frequency for all the cases with 39 cp and thus, may be its higher harmonics. The frequency of 15.82Hz is also close to the fundamental frequency of 14.65Hz. In the author's opinion, this difference is probably due to variation in the experimental settings in

place of viscosity effects. Thus, it appears that viscosity has no effect on the fundamental harmonics at constant Re and H/D. Further discussion of frequency analysis is concentrated for a specific location of z = 9.52.

8.2 ACF, PACF, and PSD at (0, 0, 9.52)

Figure 8.2.1 shows the ACF and PACF. Corresponding PSD are shown in Figure 8.2.2. These are for the U velocity component, measured at various Reynolds numbers for H/D = 0 and viscosity of 39 cp. Figures 8.2.3 and 8.2.4 show the ACF, PACF, and PSD for the V velocity component for same parameter settings. The PSD are shown on a semi-logarithmic graph instead of log-log graph. This selection is made since it is easy to identify the higher harmonics on the linear scale. On the PSD plot, other identifiable harmonics are also marked along with the significant harmonics. At Re = 50, the process is periodic with a frequency of 14.68 Hz (Figs. 8.2.1 and 8.2.2). As the Re is increased to 75, second harmonics whose amplitude is a little greater than fundamental harmonics is also visible. With further increases of Re up to 150, more and more higher harmonics are clearly evident. The amplitude of second harmonics once seen at Re = 75 remains more or less constant. The amplitude of fundamental harmonics keeps decreasing and all the other harmonics amplitudes are increasing. At Re = 200, this periodic structure is completely broken. The ACF, PACF, and PSD of velocity component V (Figs. 8.2.3 and 8.2.4) when analyzed, provide the same information. The sets of Figures 8.2.5 and 8.2.6 for U, and Figures 8.2.7 and 8.2.8 for V at H/D = -0.5 also show similar patterns. In this case, the periodic nature of the process breaks down at Re = 150. This is probably due to system energy is absorbed by the extra space created below the jet axis. In

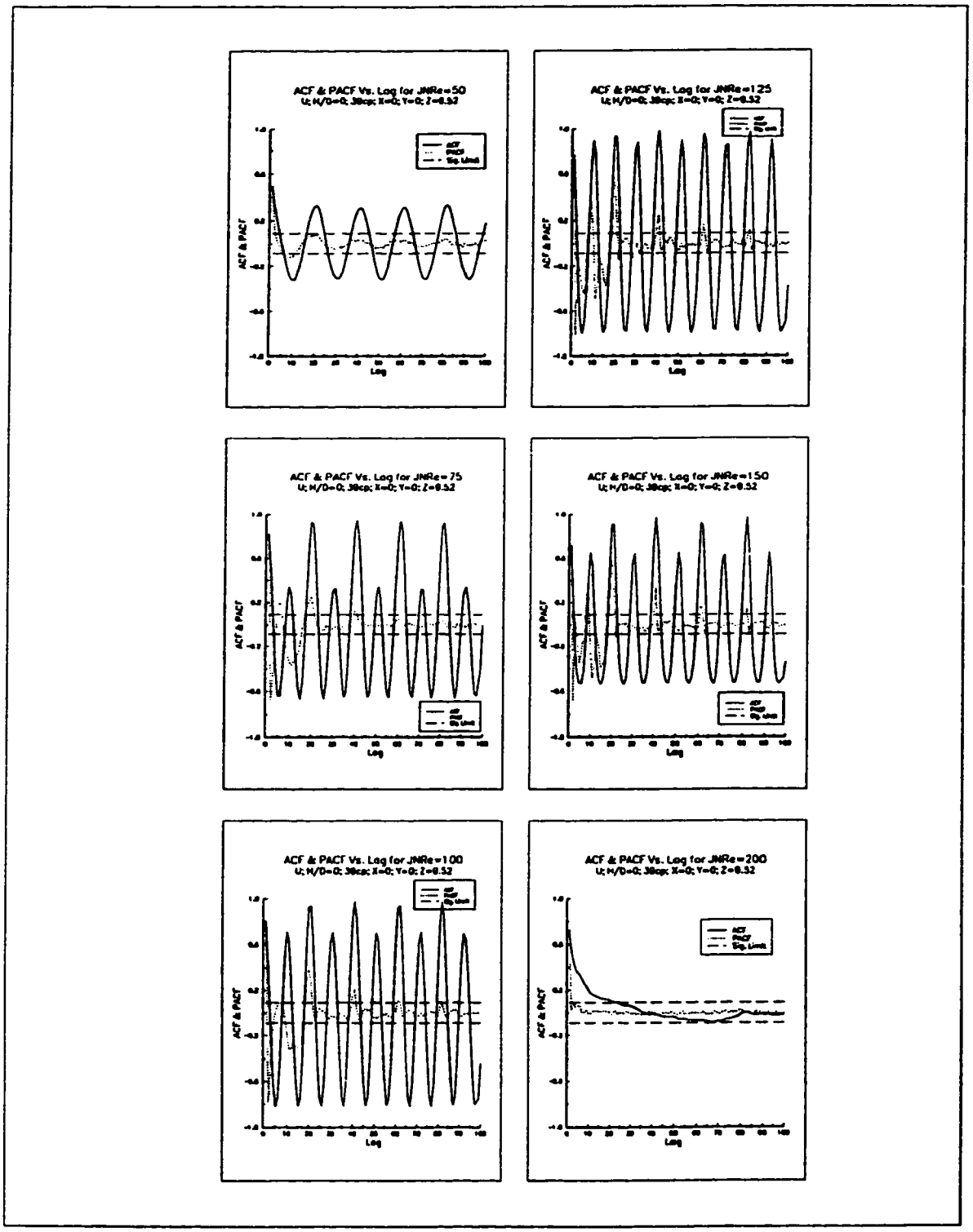

Fig. 8.2.1: ACF and PACF of radial velocity (U) at (0, 0, 9.52) for various Reynolds number with 39 cp and H/D = 0

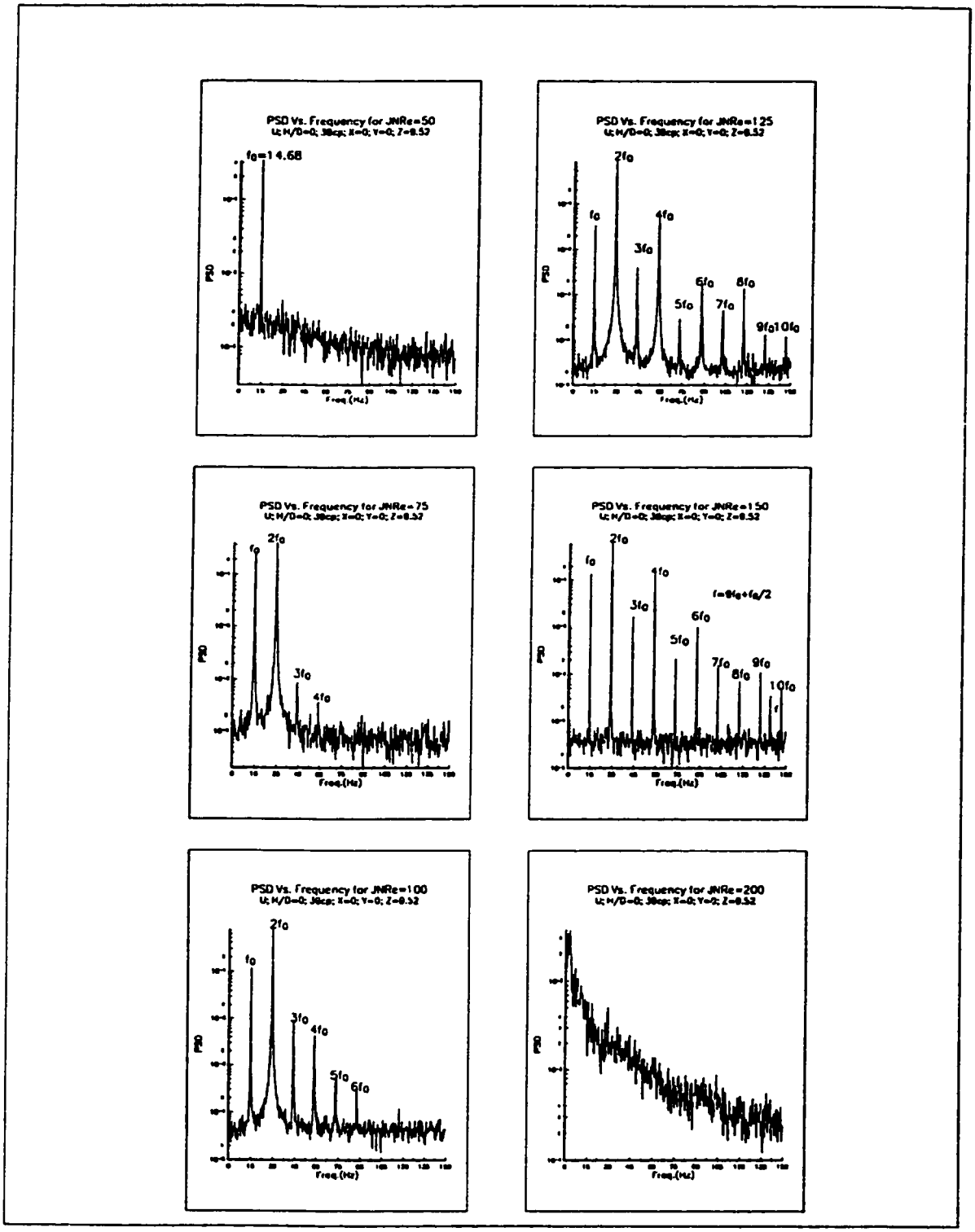

Fig. 8.2.2: PSD of radial velocity (U) at (0, 0, 9.52) for various Reynolds number with 39 cp and H/D = 0

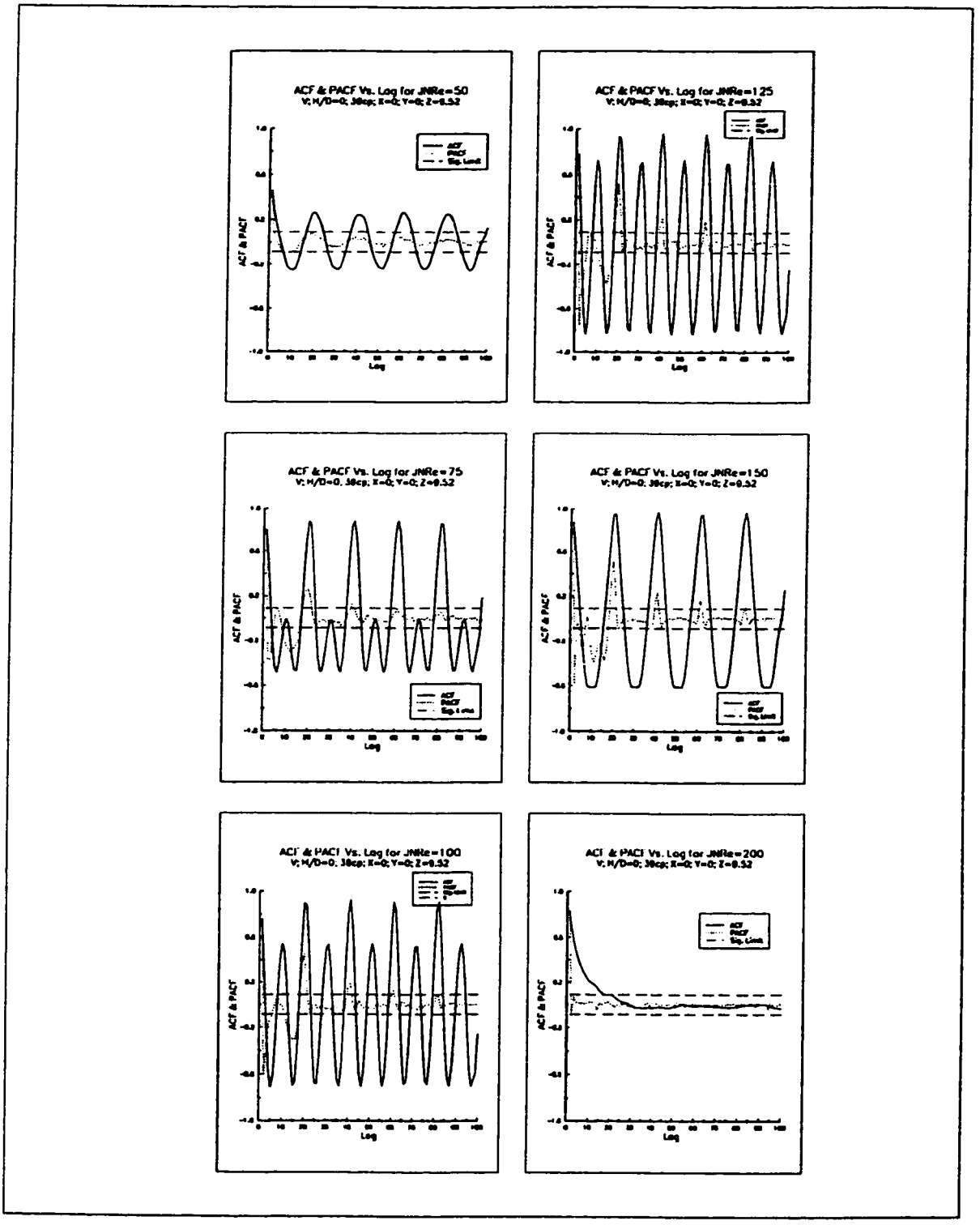

Fig. 8.2.3: ACF and PACF of axial velocity (V) at (0, 0, 9.52) for various Reynolds number with 39 cp and H/D = 0

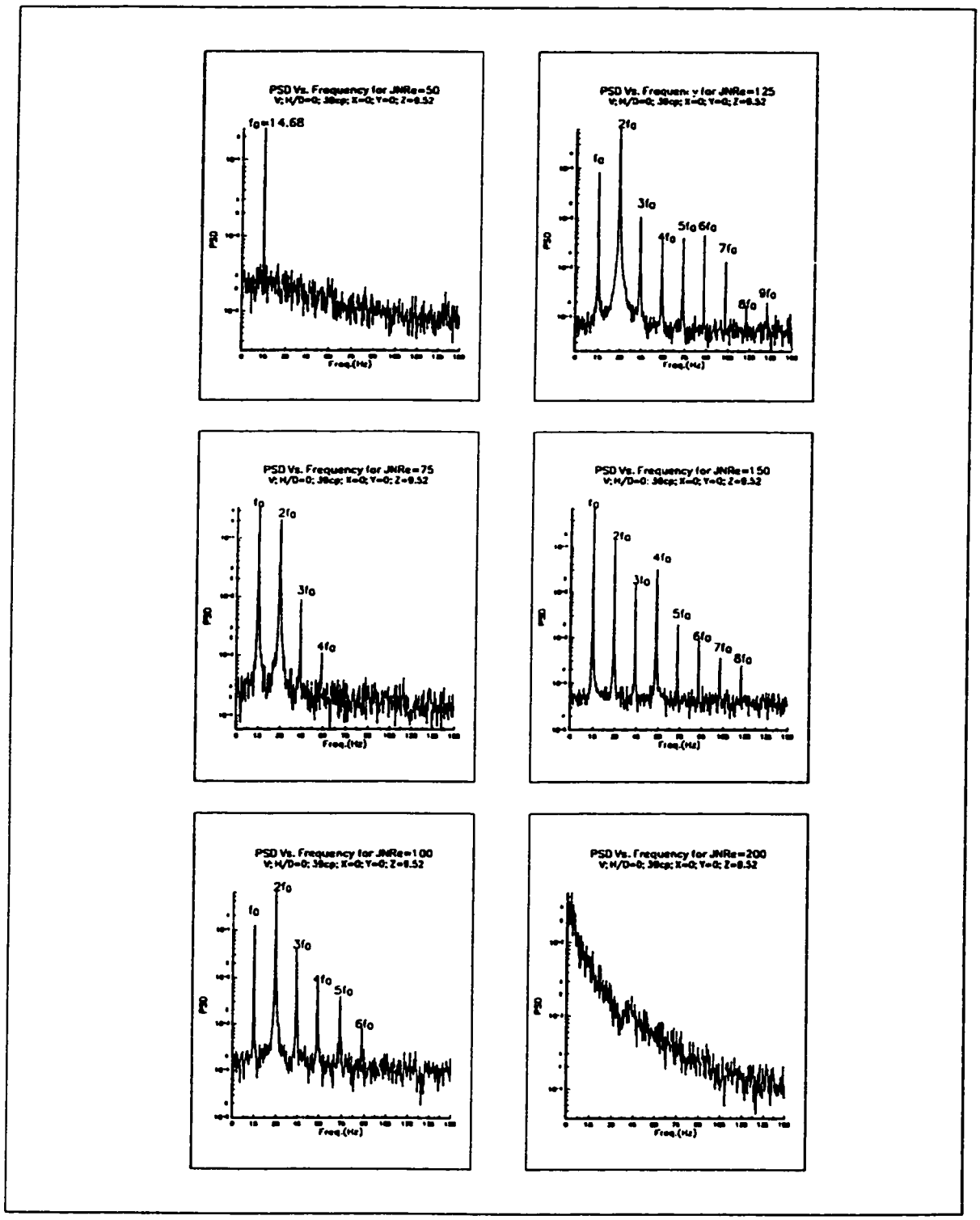

Fig. 8.2.4: PSD of axial velocity (V) at (0, 0, 9.52) for various Reynolds number with 39 cp and H/D = 0

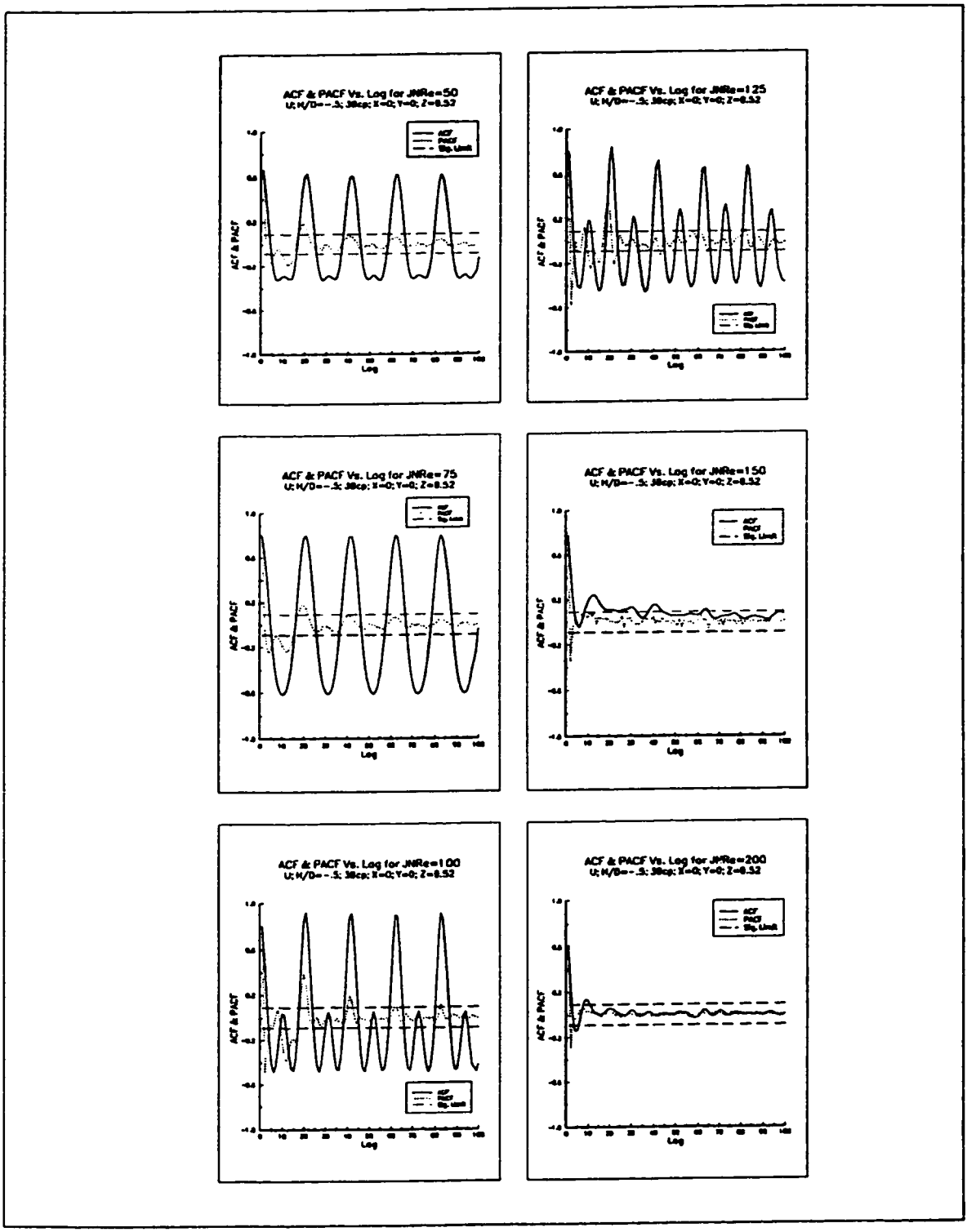

Fig. 8.2.5: ACF and PACF of radial velocity (U) at (0, 0, 9.52) for various Reynolds number with 39 cp and H/D = -0.5

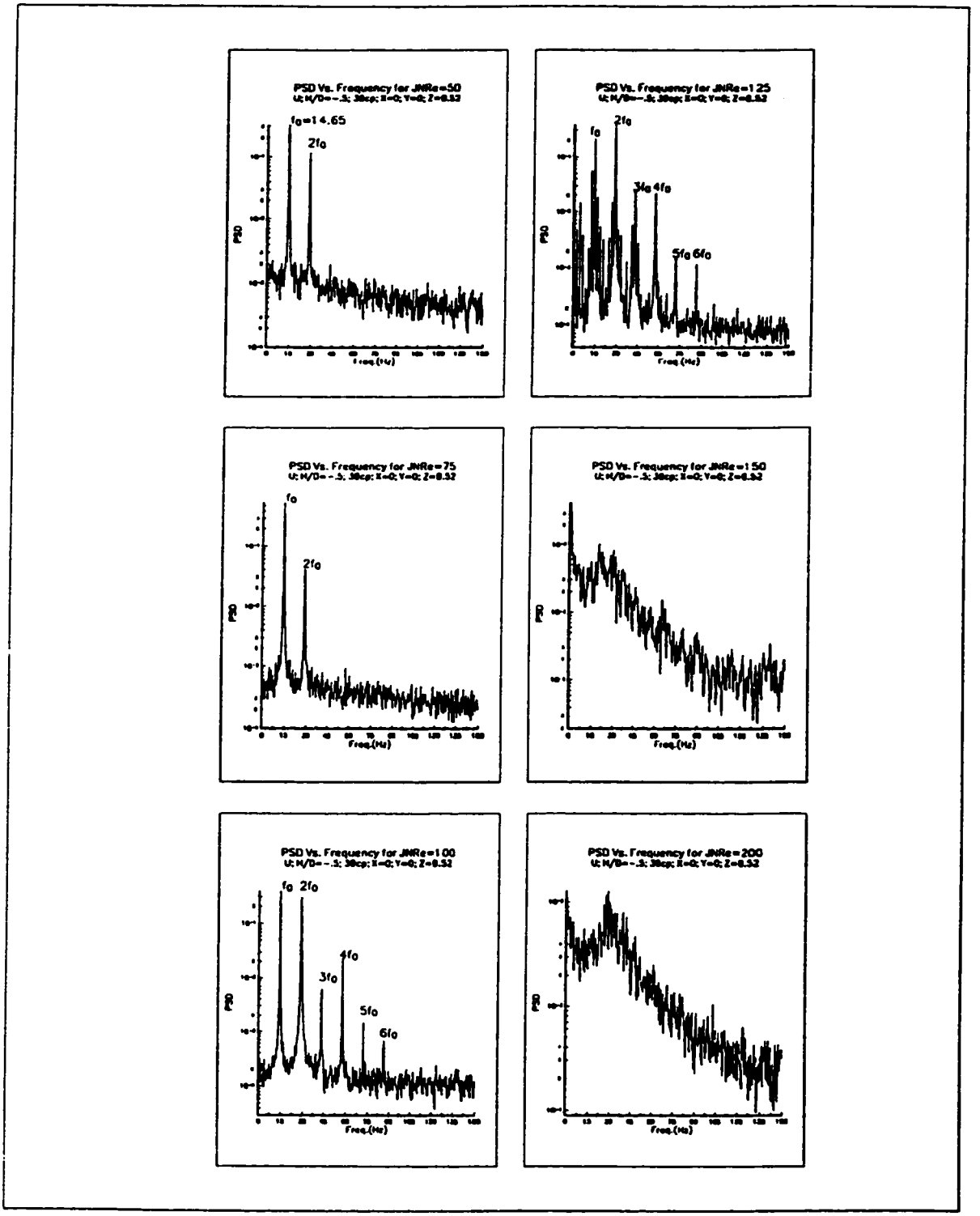

Fig. 8.2.6: PSD of radial velocity (U) at (0, 0, 9.52) for various Reynolds number with 39 cp and H/D = -0.5

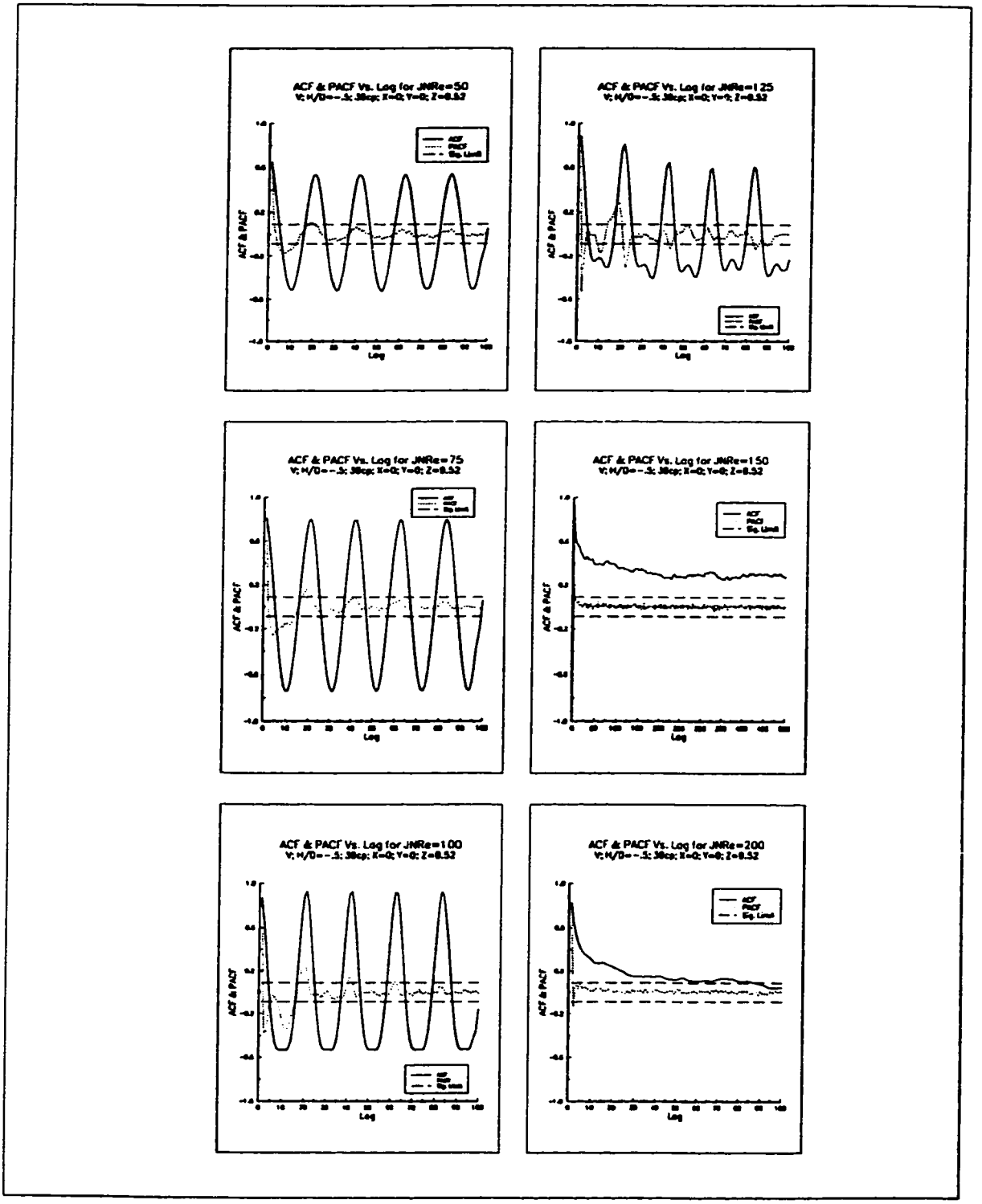

Fig. 8.2.7: ACF and PACF of axial velocity (V) at (0, 0, 9.52) for various Reynolds number with 39 cp and H/D = -0.5

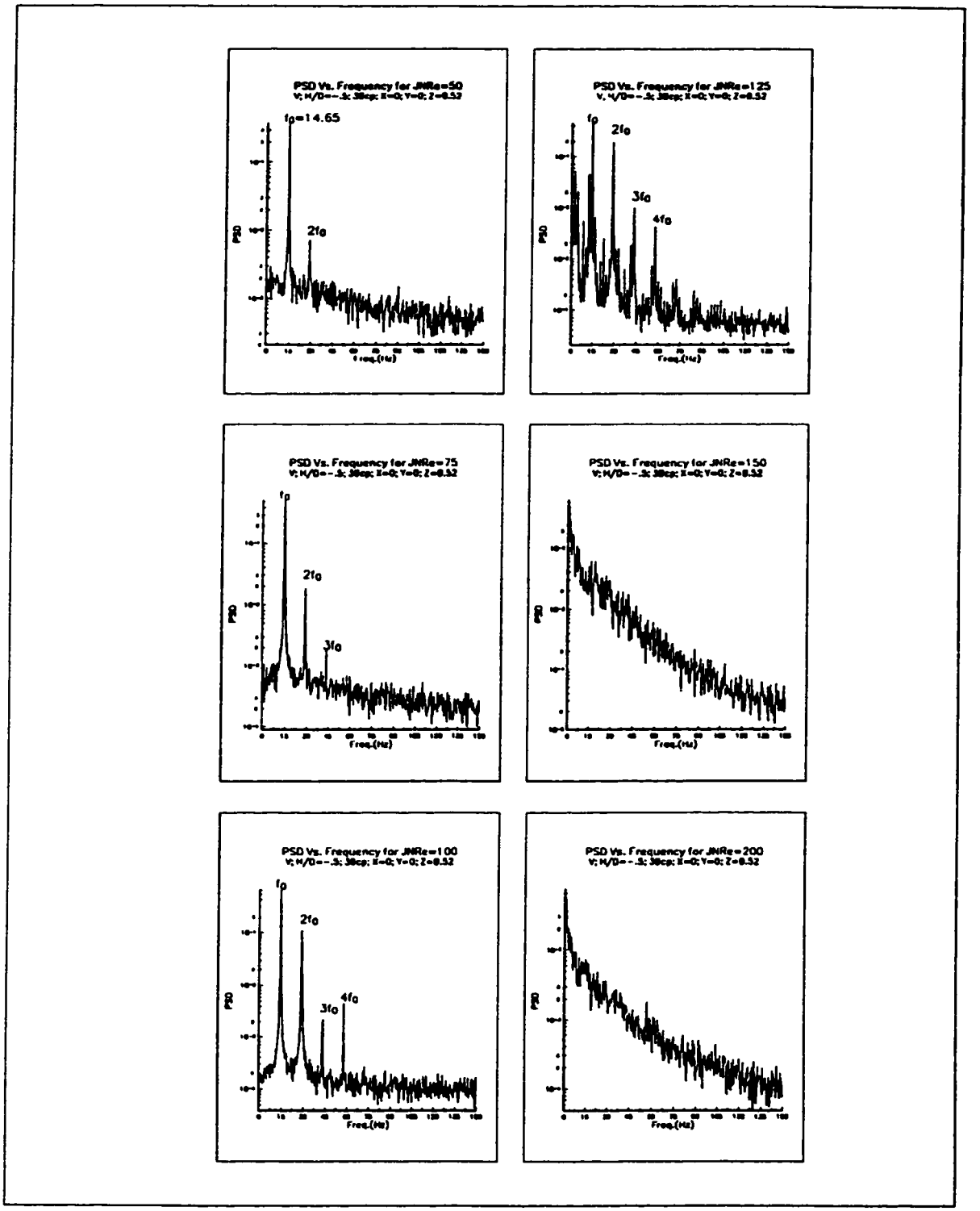

Fig. 8.2.8: PSD of axial velocity (V) at (0, 0, 9.52) for various Reynolds number with 39 cp and H/D = -0.5

these cases second harmonic is also visible at Re = 50.

Figures 8.2.9 to 8.2.16 show the similar plots obtained with 75 cp viscosity at the same point. As indicated earlier, the change in viscosity has no influence on frequency pattern. Also, the increase in Re increases the number of higher harmonics. The disappearance of the periodic structure altogether, is also noticed at the same Re.

The following conclusions are drawn based on the evidence presented in the last two sections:

(i) As the flow rate increases from Re of 50 (stable zone) to Re = 150 (unstable zone), the higher harmonics appear. After that the periodic structure completely vanishes.

(ii) At H/D = -0.5, this breakdown in the periodic nature occurs at Re = 150 as compared with the Re of 200 for H/D = 0.

(iii) The change in the viscosity neither influences the frequency pattern nor the breakdown of the periodic nature.

(iv) Essentially, the time series analysis, based on the LDA measurements of velocity components U and V separately, provided the same information about the underlying process. This provides the experimental evidence of the analytical conclusion drawn by Packard et al. (1980) which states that the study of one dimensional analysis is sufficient to provide information about the inherent structure of the three dimensional dynamical system.

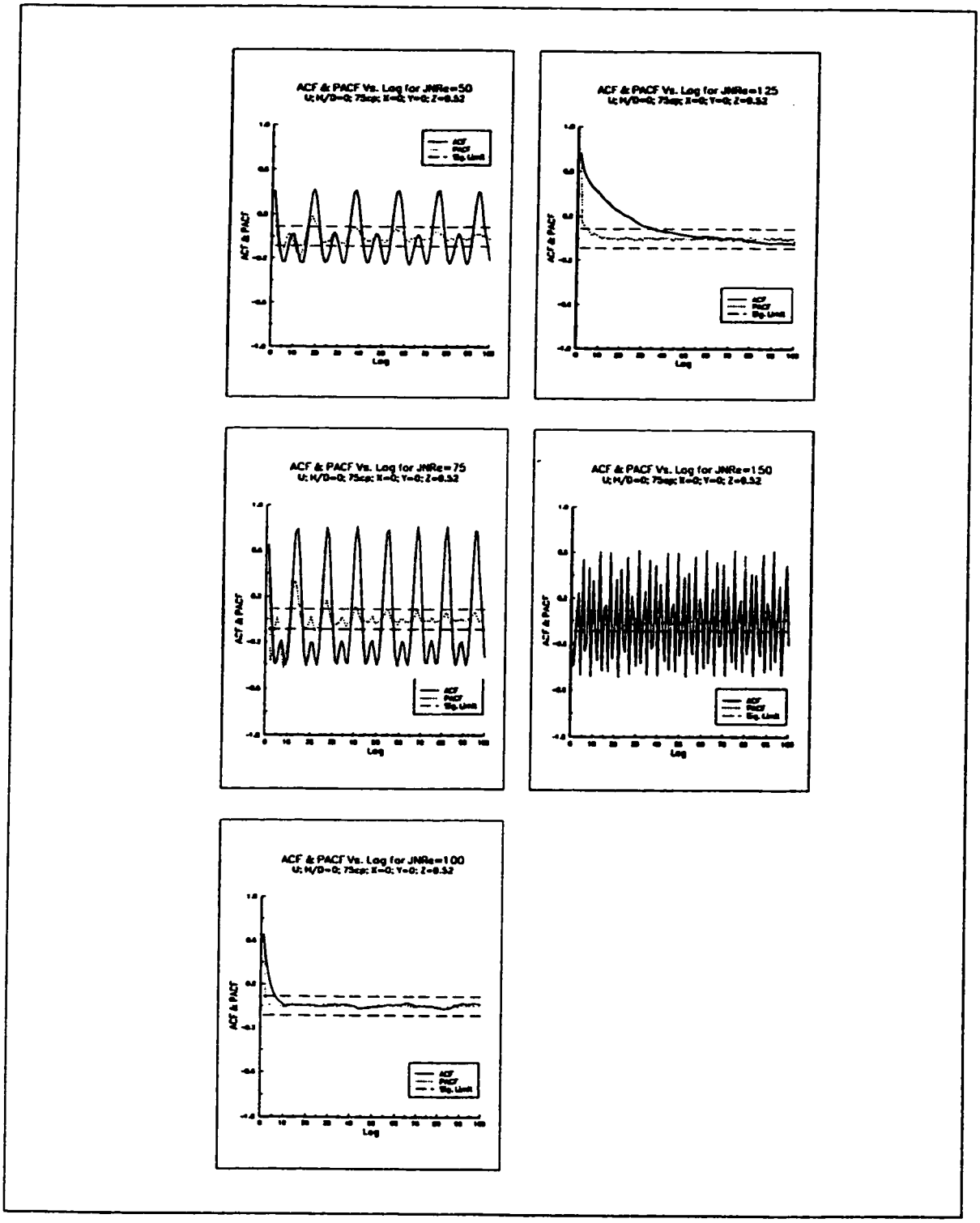

Fig. 8.2.9: ACF and PACF of radial velocity (U) at (0, 0, 9.52) for various Reynolds number with 75 cp and H/D = 0

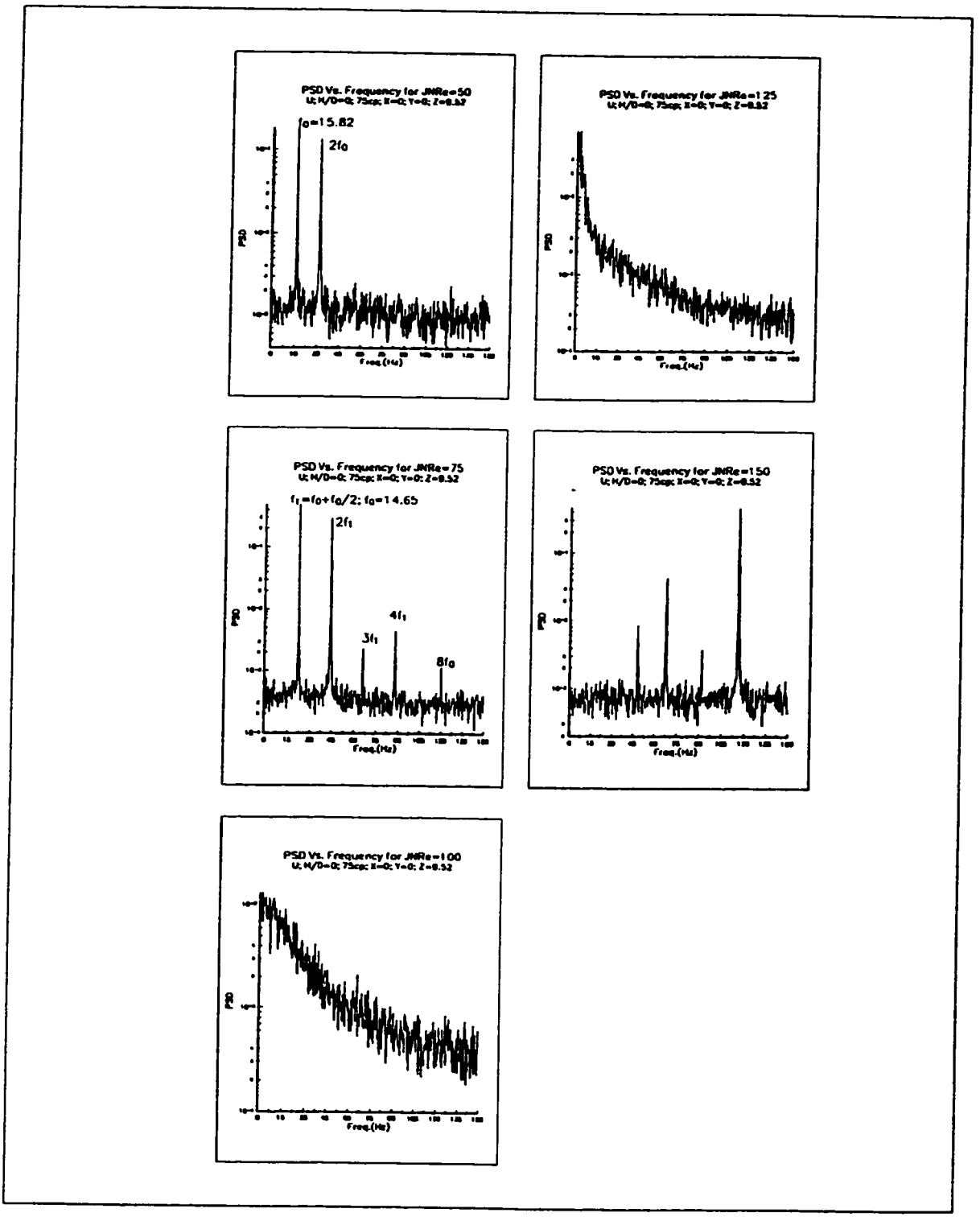

Fig. 8.2.10: PSD of radial velocity (U) at (0, 0, 9.52) for various Reynolds number with 75 cp and H/D = 0

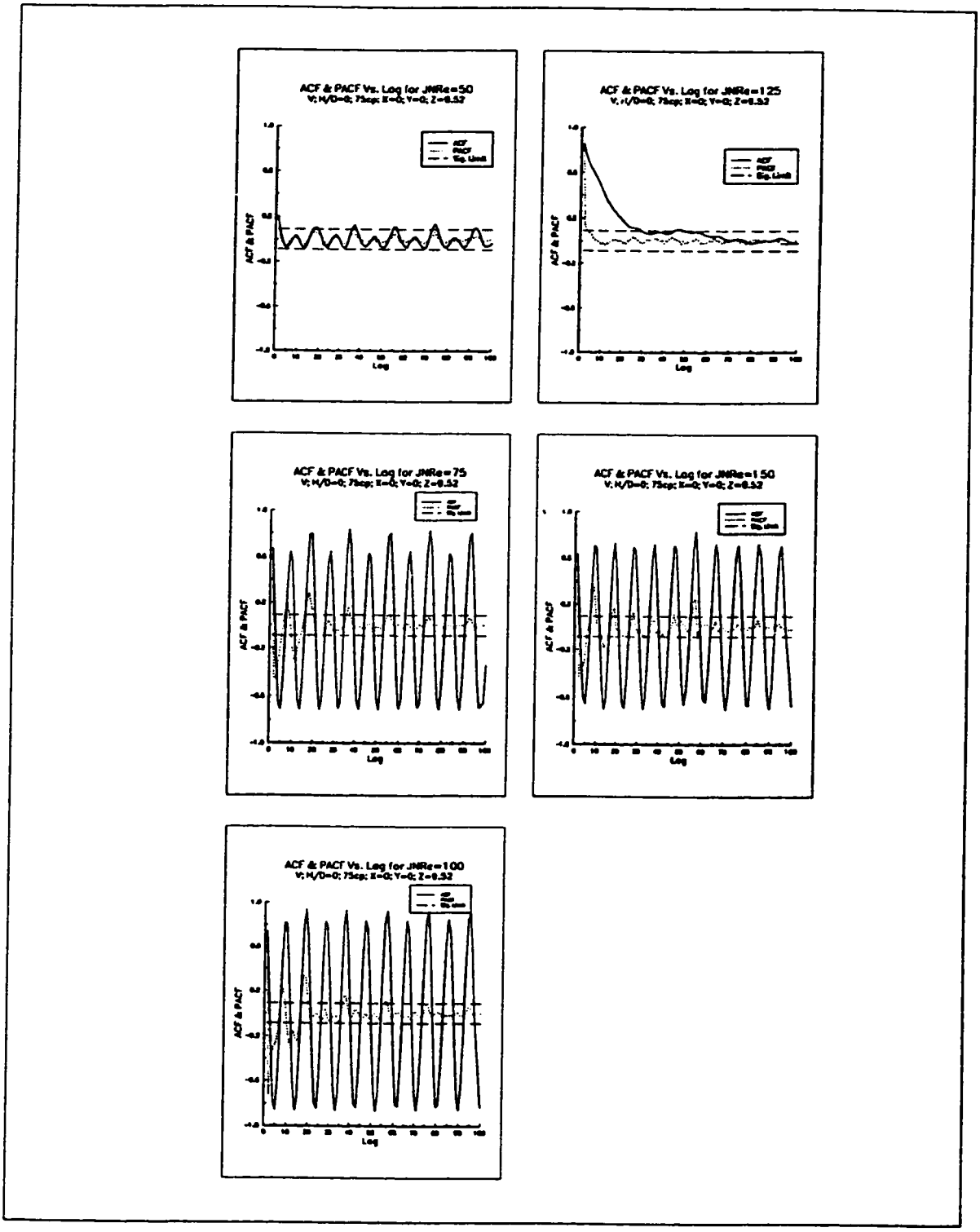

Fig. 8.2.11: ACF and PACF of axial velocity (V) at (0, 0, 9.52) for various Reynolds number with 75 cp and H/D = 0

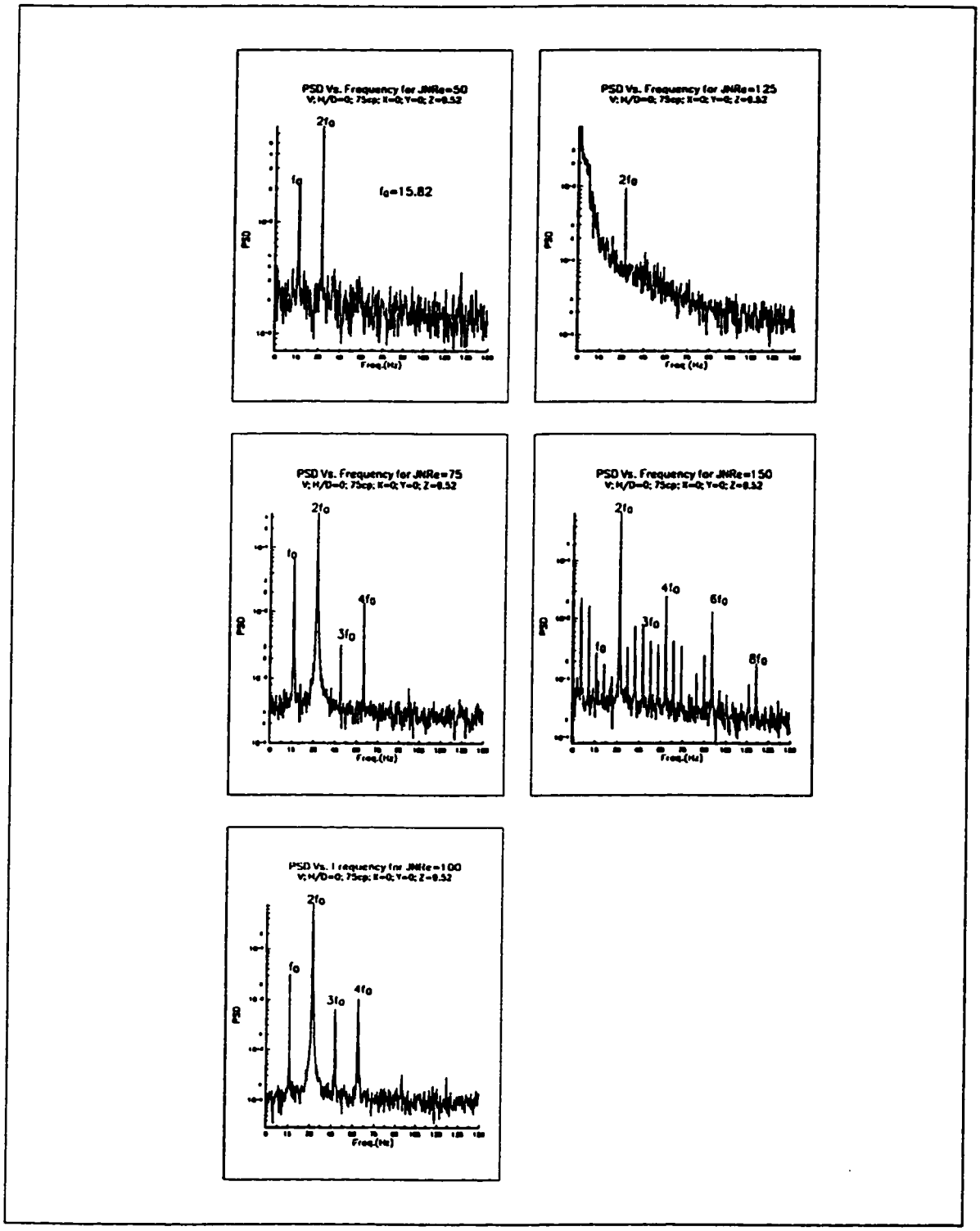

Fig. 8.2.12: PSD of axial velocity (V) at (0, 0, 9.52) for various Reynolds number with 75 cp and H/D = 0

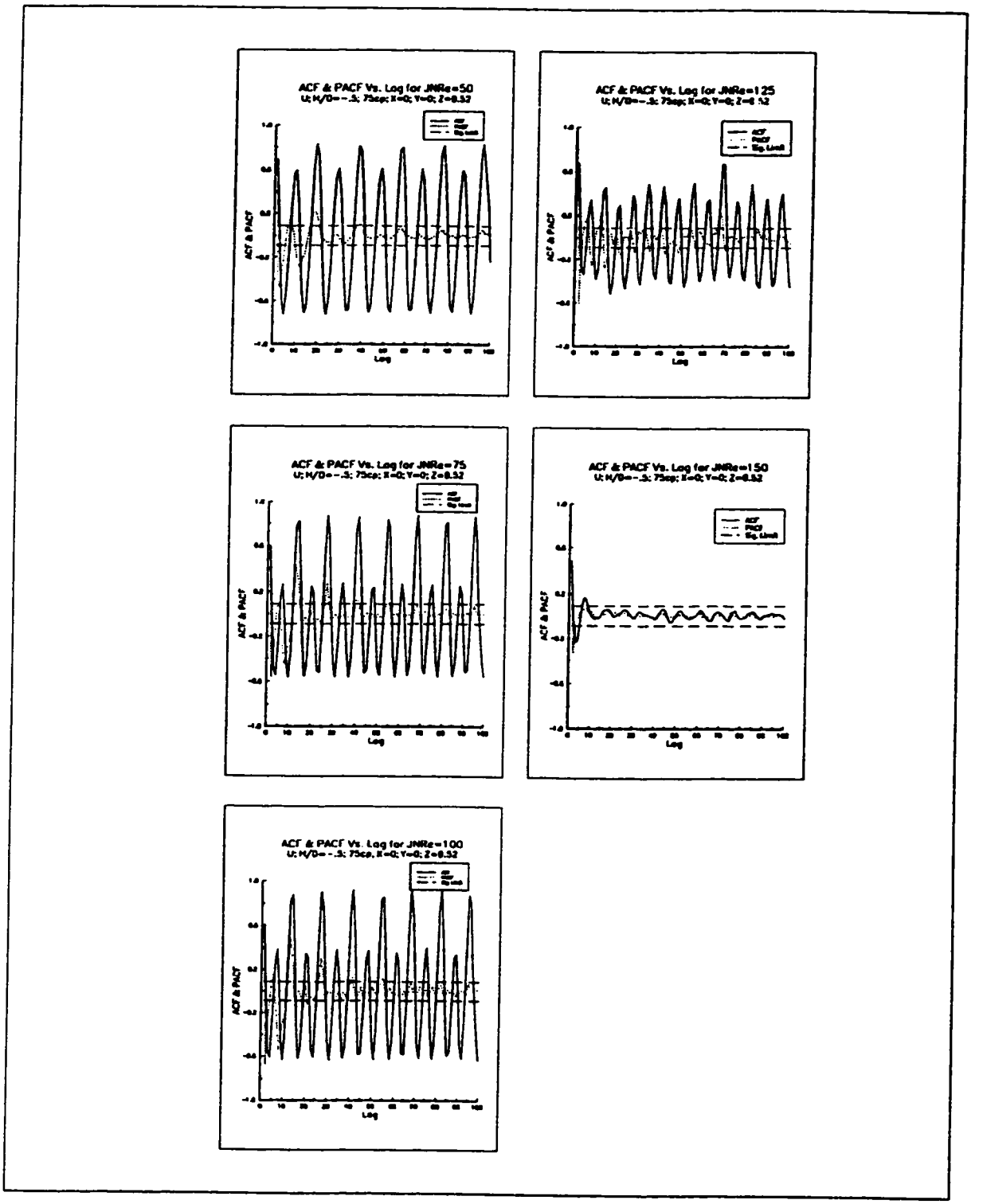

Fig. 8.2.13: ACF and PACF of radial velocity (U) at (0, 0, 9.52) for various Reynolds number with 75 cp and H/D = -0.5

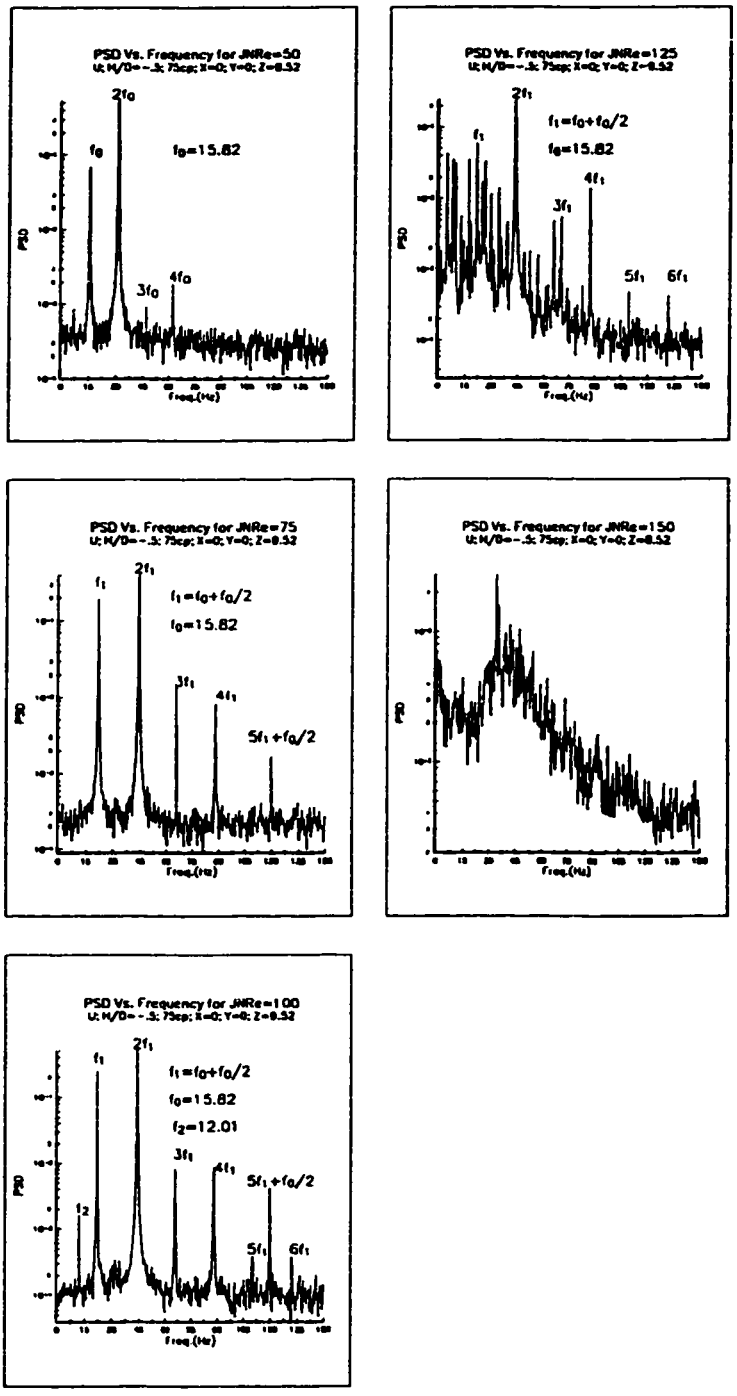

Fig. 8.2.14: PSD of radial velocity (U) at (0, 0, 9.52) for various Reynolds number with 75 cp and H/D = -0.5

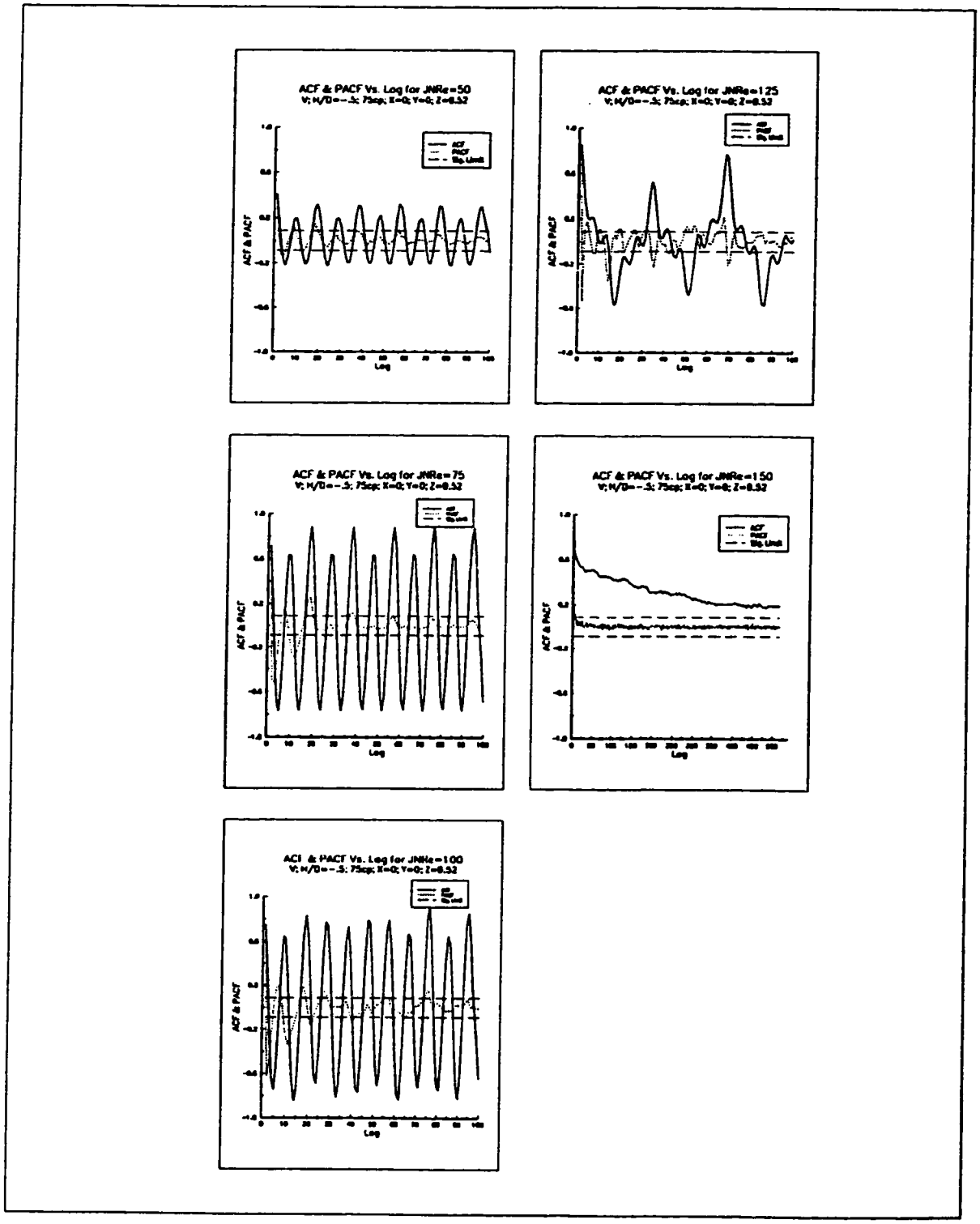

Fig. 8.2.15: ACF and PACF of axial velocity (V) at (0, 0, 9.52) for various Reynolds number with 75 cp and H/D = -0.5

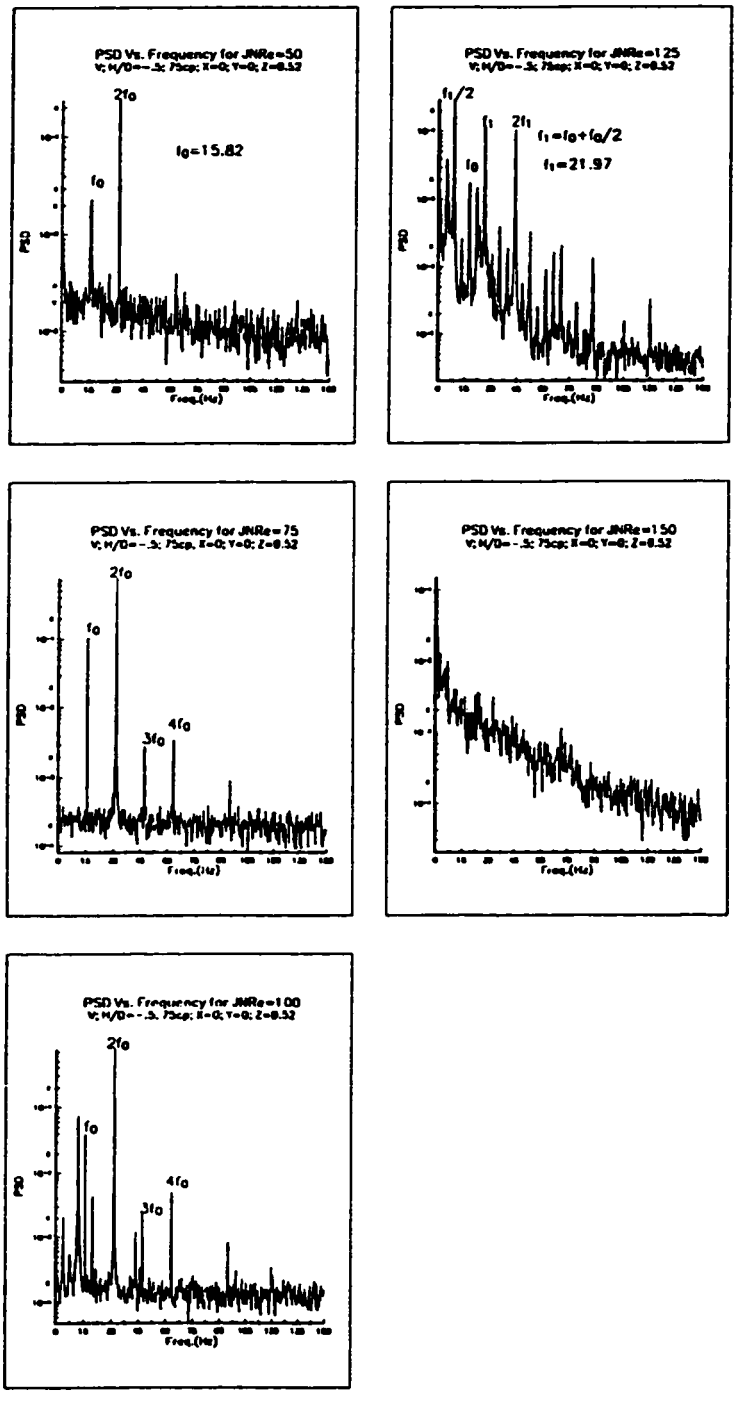

Fig. 8.2.16: PSD of axial velocity (V) at (0, 0, 9.52) for various Reynolds number with 75 cp and H/D = -0.5

8.3 Oscillation Region at each level (z) for Re = 50 and 150

The LDA data for both velocity components, U and V, have been taken on a grid (section 5.0) for two Reynolds numbers, one in the stable flow mode and the other in unstable mode. The respective values of these Reynolds numbers are 50 and 150. The data have been observed for both viscosities (39cp and 75cp) and piston positions (H/D = 0 and -0.5). In this section, the plots of amplitudes of significant frequencies are shown for each grid point at various z-planes. These significant frequencies are estimated using time series analysis on the LDA data. The planes at which no significant frequencies are obtained, have not been shown. For all the figures in this section, the coordinates of the inlet of one of the jets are (0, -12.7, 0) and the impingement plane is a vertical plane described by y = 0.

Figures 8.3.1 and 8.3.2 show the plots of amplitudes of significant frequencies for velocity components U and V, respectively for Re = 50, H/D = 0, and viscosity as 39 cp. The results indicate that the amplitude of the oscillations decreases with an increase in the value of z. For the velocity component U (Fig. 8.3.1), the amplitude of oscillation reduced to one fourth at z = 12.7 of its maximum value which was at z = 0. Similarly, for velocity component V (Fig. 8.3.2), the amplitude reduced to one tenth of its maximum value at z = 0. The largest amplitude of oscillations are found along the impingement plane at y = 0. In general, most of the significant frequencies are found on the points which lie within the area bounded by one jet diameter (2.38mm) along the jet axis or along the impingement plane. Also, this area decreases with increase in z. Finally, these are confined only along the

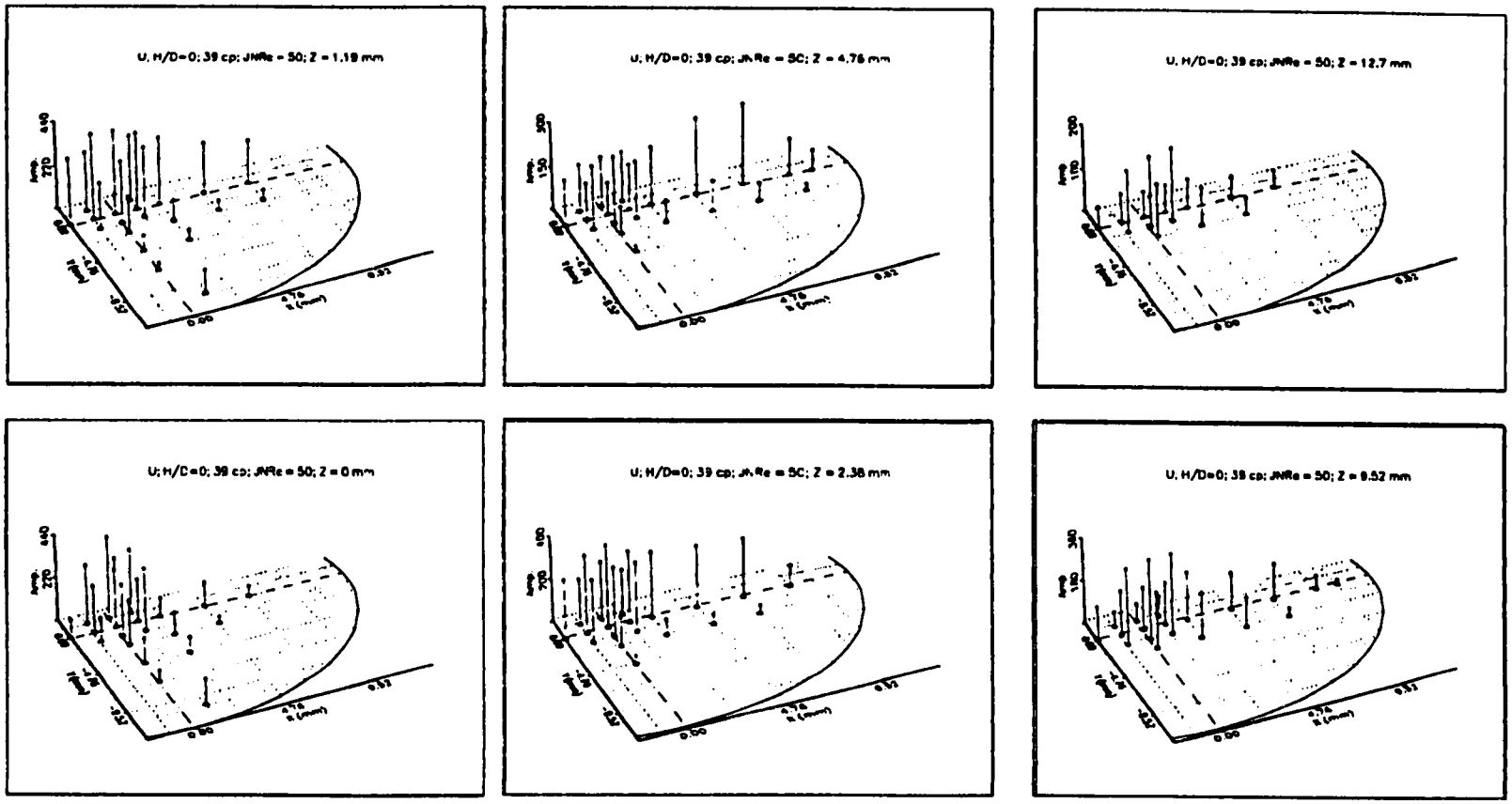

Fig. 8.3.1: Amplitude of significant frequencies of radial velocity at various Z-planes for Re = 50 with 39 cp and H/D = 0

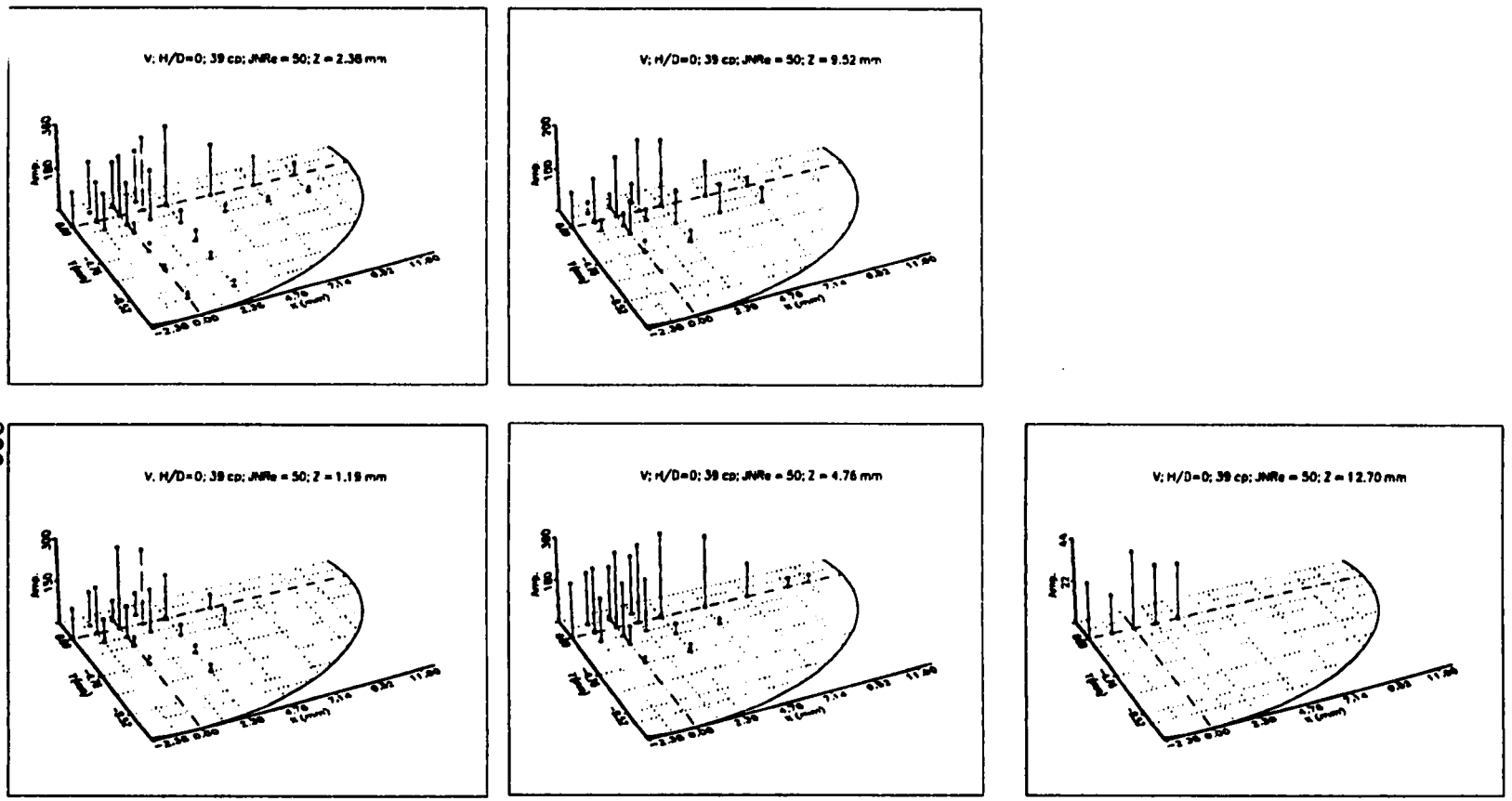

Fig. 8.3.2: Amplitude of significant frequencies of axial velocity at various Z-planes for Re = 50 with 39 cp and H/D = 0

impingement plane. This amplitude behavior and region of oscillations are not affected by the change in viscosity. It is confirmed by studying a set of data taken at viscosity of 75 cp (the figures for U and V velocities are given in appendix F).

With a change in H/D to -0.5 while keeping other parameters same (Re = 50, and viscosity of 39 cp), Figures 8.3.3 and 8.3.4 show amplitudes of significant frequencies for U and V velocity components, respectively. As earlier, the oscillation region is bounded within one jet diameter of the impingement plane except at a plane z = 0. For velocity component U, the amplitudes of these oscillations decrease as one moves away from the plane z = 0 in either direction. For velocity component V, the maximum amplitudes are found at z = 2.38 and -2.38 mm. The smallest region of oscillation is observed at z = 0 and this region has enlarged in both the directions away from z = 0 which indicates the symmetry of flow around jet axis. The behavior remains the same even at a higher viscosity of 75 cp (see appendix F).

As described in section 8.3.1, the unstable flow mode is observed at Re = 150. The significant frequencies for this mode are found only for H/D = 0 setting and not at H/D = -0.5. The amplitude of these significant frequencies in case of fluid viscosity of 39 cp, are shown in Figures 8.3.5 and 8.3.6, respectively for velocity components U and V. The oscillating region has significantly enlarged in comparison with the case of Re = 50. Almost, the entire region (all points of the grids) shows significant frequencies. Also, no reduction is observed in the amplitude of these frequencies even at planes other than z = 0. The amplitude of the oscillations near the mixhead wall is also of the same order of strength as in the central region. The oscillations do not diminish even at a plane z = 25.4. In the case of Re = 50,

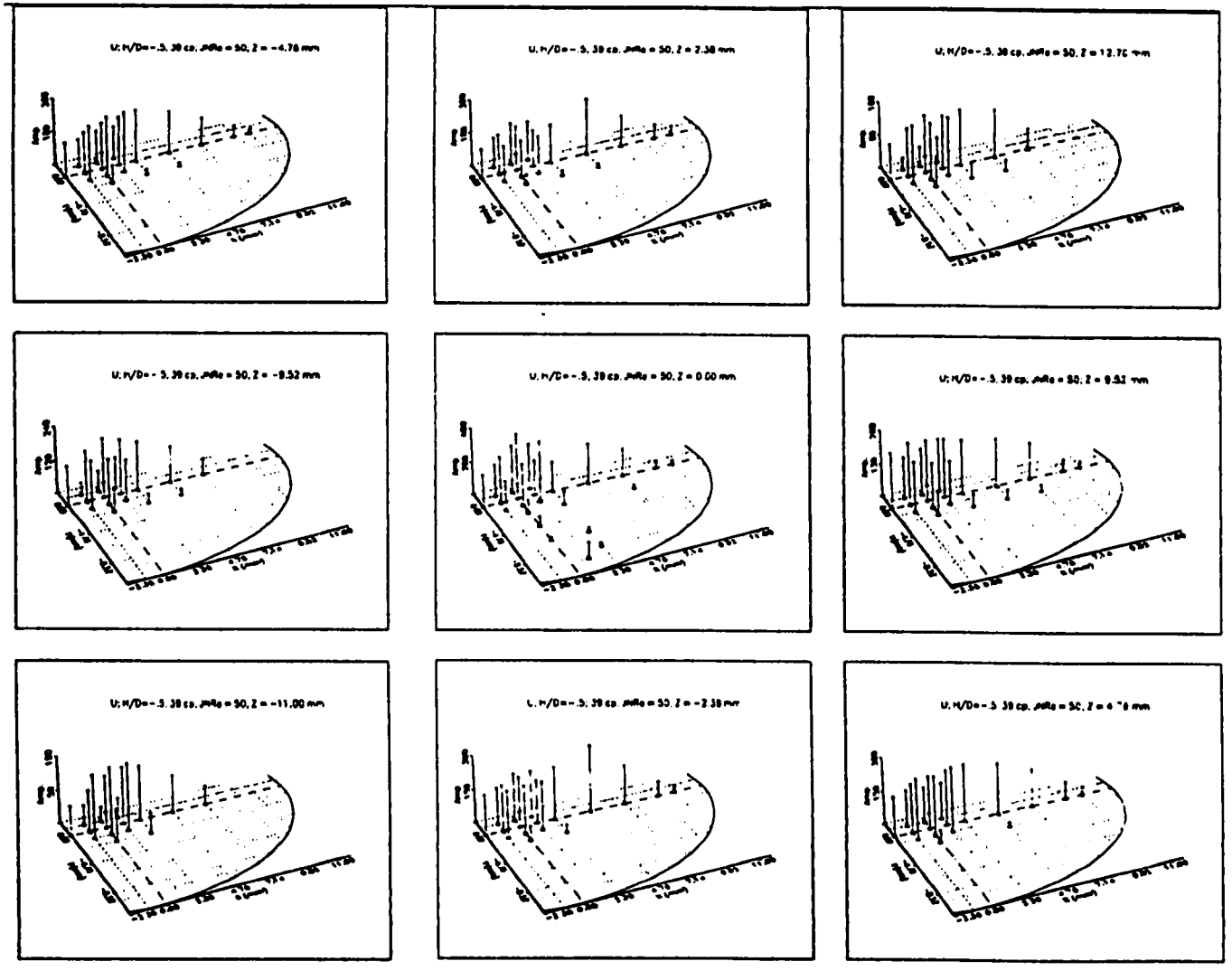

Fig. 8.3.3: Amplitude of significant frequencies of radial velocity at various Z-planes for Re = 50 with 39 cp and H/D = -0.5

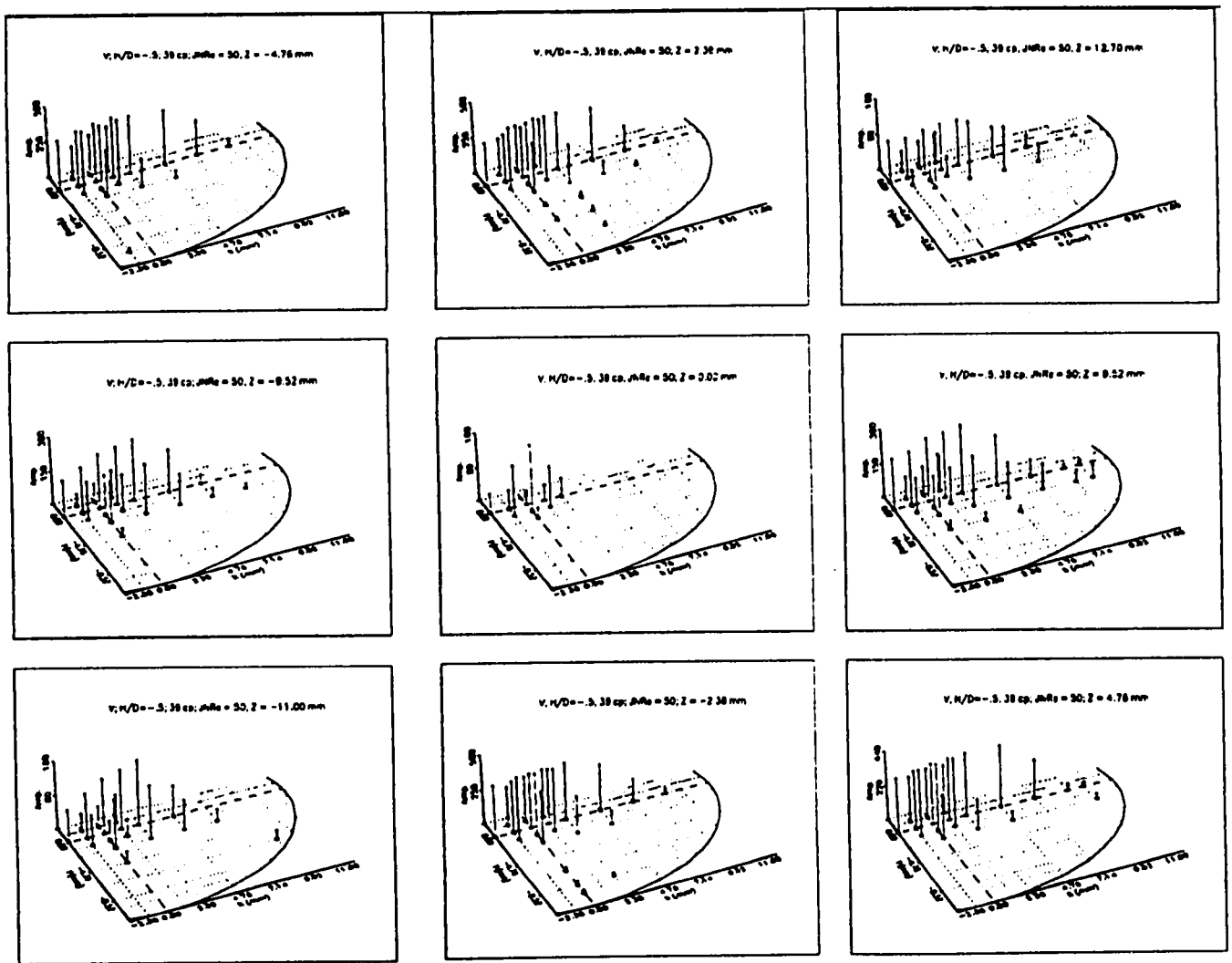

Fig. 8.3.4: Amplitude of significant frequencies of axial velocity at various Z-planes for Re = 50 with 39 cp and H/D = -0.5

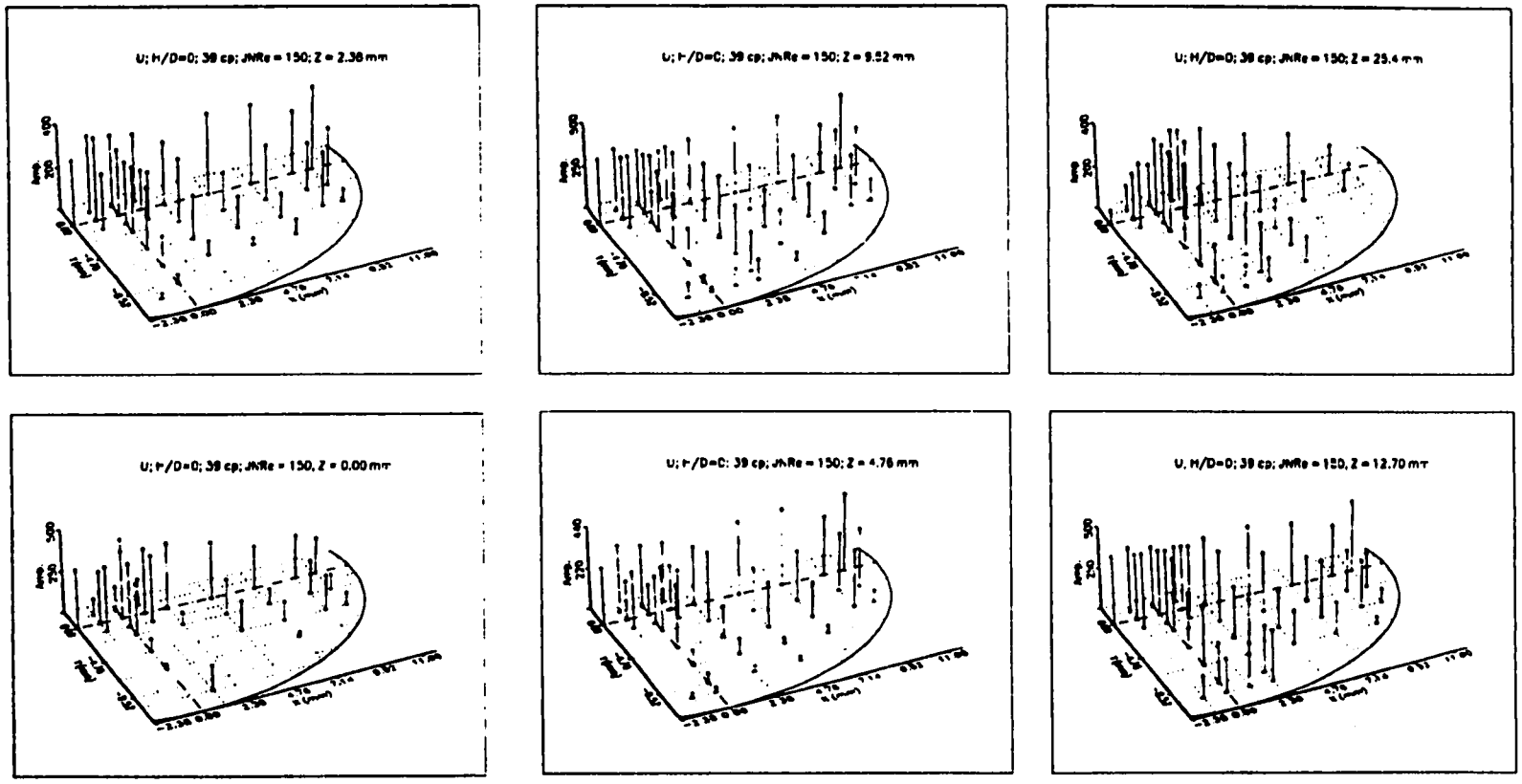

Fig. 8.3.5: Amplitude of significant frequencies of radial velocity at various Z-planes for Re = 150 with 39 cp and H/D = 0

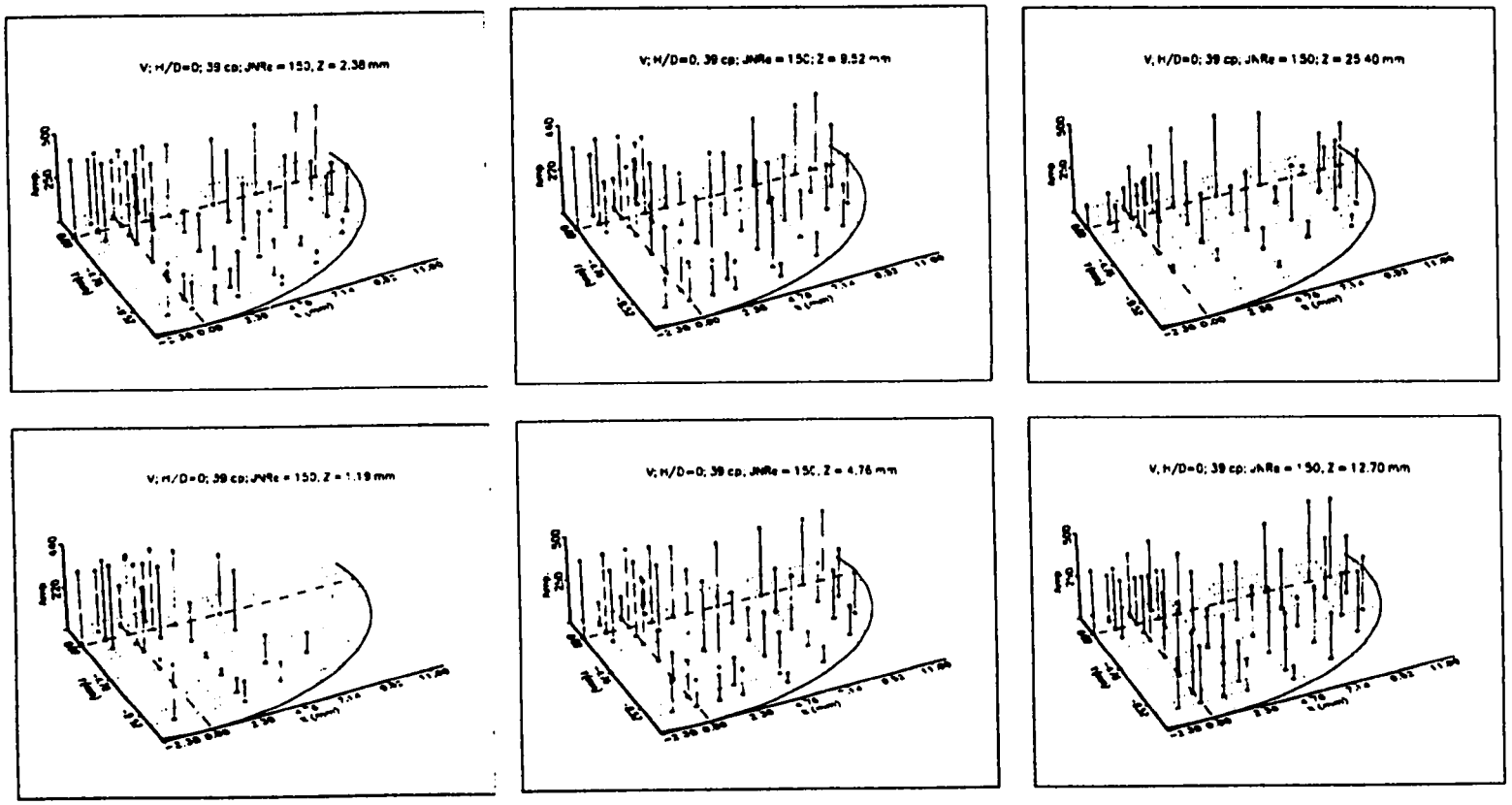

Fig. 8.3.6: Amplitude of significant frequencies of axial velocity at various Z-planes for Re = 150 with 39 cp and H/D = 0

no oscillations are found at this plane z = 25.4. Similar behavior is observed for the flow with viscosity of 75 cp. The reason for the enlargement of the oscillation region at Re = 150, lies in the fact that more energy enters in the system as flow rate is increased.

The above results indicate that the increase in Re increases the oscillation region at each z-plane. The non-existence of oscillations beyond one mixhead diameter is indirect evidence of unidirectional flow as observed earlier. Also, similar pattern of oscillations on either side of the jet axis confirm the symmetry of flow about jet axis. All these results again provide a quantitative confirmation of the previous observations based on the flow visualization.

9 Conclusions and Recommendations

An experimental investigation and analysis of the flow field produced by the impingement of two equal cylindrical laminar jets near the closed end of a confined space has been conducted in this thesis. Both the qualitative and quantitative studies have been performed for various Re, H/D, and viscosities for this configuration. For the qualitative analysis, various flow visualization methods have been used while for quantitative analysis, velocity fields (only U and V components) are obtained using LDA technique.

The viscosity has a definite impact on the observability but no significant influence on the flow patterns at given Re. At low viscosity, the flow pattern is very sensitive to any perturbation generated within the system or coming from the surroundings. It is obvious that the velocity will be lower for a fluid with low viscosity compared to a fluid with higher viscosity at a given Re. Thus, it is possible that the perturbation may be of the same order as the velocity of the fluid particles at lower viscosities. This may be one of the causes of low observability during the experiments with low viscosity fluids. In cases of fluids with high viscosity, the perturbation will be relatively low compared to the velocities of fluid particles. This enhances the observability of the flow patterns. Also, it appears that the fluids with low viscosity do not have the capacity to absorb external energy and thus fluid particles activate more even at small perturbation. This also seems to be one reason for the diminution of observability of the flow patterns at low viscosities.

The Re has a significant effect on the flow field. At low Re (<50), the flow is in a statically stable mode. At slightly higher 50<Re<100 or so, the flow pattern

changes to dynamically stable mode and the impingement plane oscillates. After Re > 100 the flow reaches an unstable mode. In fact, the vortices gradually grow with increasing Re and at a critical level they dynamically interact with each other causing the oscillation of the impingement plane. It has been found that the length of the circulating region increases in proportion to the exponent 0.4 of the Re for both static and dynamic stable zones while stability is maintained. After that, the circulating region shrinks a little bit before breaking into a totally unstable zone. Some traces of mixing (fluid transfer from one vortex to other) are also observed with increasing Re.

The piston position (H/D) plays an important role in the stability of the flow pattern. The results show that the flow pattern is always unstable at Re = 150 when the mixhead aspect ratio H/D is 0 or 0.5. However, a stable flow pattern is seen at the same Re when the H/D is increased to 0.75 and above. No stable patterns could be obtained at Re = 200 up to H/D = 1.0. It appears that the flow patterns are always unstable at very high Re ($\geq$ 150). In the stable mode, the flow looks like a mirror image about the impingement plane as suggested earlier by Powell (1960) (approximate symmetry about the jet axis).

Using a 2-D flow visualization technique (particle visualization with a laser sheet), it was concluded that the actual flow is three dimensional in the vortex region. The flow patterns seen with sectioning in the X-plane confirm that the depth of the vortices reaches up to half of the mixhead radius at Re = 50. At higher values of Re, it almost touches the wall of the mixhead. The flow study with sectioning in various Y-planes showed that there exists an irrotational flow near the mixhead axis (in the static and dynamic stable region) which, in fact, is the impingement plane.

The Z-sectioning has shown that in the neighborhood of the jet axis the flow is quadratically symmetrical with the exception of the flow directions. The study with the Z-sectioning also confirmed that no circulation existed beyond one mixhead diameter. The existence of W component of velocity in the circulating zone has also been established from the 2-D flow visualization technique. The vector and streamline plots obtained by LDA for Re = 50, and 150 also confirm the above conclusions.

The LDA data contains outliners and it is essential to remove them before calculating various statistical parameters like moments, PDF, and PSD. The time series obtained along the central line are random and strongly stationary. The PDF can be estimated using the first four moments of the time series by use of the Pearson frequency curve. These PDF curves agree very well with the PDF obtained by bin counting methods. Also, an analytical expression of the PDF is obtained using this method which is good for the mathematical analysis of the process.

Based on the LDA data along the center line (0,0,z), it is observed that symmetry exists in absolute values of radial and axial velocities in lower and upper mixing zone. The radial velocity falls to insignificants value within two jet diameters of the impingement point. On the other hand, the axial velocity attains the one-dimensional developed velocity value within 1 to 1.5 mixhead diameters downstream. Usually, the absolute axial velocity is lowest at one mixhead diameter downstream. The vigorous fluctuations are also evident up to half mixhead diameter. Thus, the whole flow field can be divided into three separate zones (i) a mixing zone up to half mixhead diameter, (ii) developed zone after one and half mixhead diameter, and (iii) developing zone between these two zones. In the developing and developed zone,

velocities are linear function of Reynolds number. An increase in viscosity, in general, has reduced the variability of the velocity measurements at all locations. This indicates an increased damping characteristic of the fluid.

The change in H/D does not influence the radial velocity along the center line except at z = 0. The differences at z = 0 are, probably, due to initial settings of the rotameters. In the mixing zone, higher axial velocities are observed for H/D = 0 than for H/D = -0.5. In the developing zone, a insignificant influence is seen while in developed zone there is no influence at all.

In the mixing zone, higher axial velocities are obtained with lower viscosity though the variance of the measurements is very large. This difference diminishes as Reynolds number is increased.

From the frequency analysis of the time series, the following conclusions can be drawn:

(i) As the flow rate increases from Re of 50 (stable zone) to 150 (unstable zone) higher harmonics exist. At Re = 200, the periodic structure completely vanishes.

(ii) The H/D has an impact upon this periodic nature. The periodic nature vanishes at Re = 150 for H/D = -0.5 which in the case of H/D = 0 occurred at Re = 200.

(iii) The change in the viscosity has no effect on the flow pattern. It neither influences the frequency pattern nor the breakdown of the periodic nature.

(iv) The time series analysis based on the LDA measurements of velocity components U and V separately, essentially, provided the same information about

the underlying process. This provides the experimental evidence of the analytical conclusions drawn by Packard et al. (1980) which states that the study of one dimensional analysis is sufficient to provide information about the inherent structure of the three dimensional dynamical system.

This study recommends that the effects of varying d/D and μ_1/μ_2 on flow patterns and flow modes should be investigated. Also, further work should be conducted to linking mixing to fluid mechanics study conducted in this thesis.

10 References

1. Adrian, R. J., "Fluid mechanics measurements", Chapter 5 Laser velocimetry, Hemisphere Publishing Co. (Distributed by Springer-Verlag), Ed. R. J. Goldstein, 1983.

2. Astrom, K. A., and Wittenmark, B., "Computer controlled systems: Theory and Design", Prentice-Hall, Inc., 1984.

3. Becker, H. A., and Booth, B. D., "Mixing in the interaction zone of two free jets", AIChE J., 21(5), 949, 1975.

4. Beltaos, S., and Rajaratnam, N., " Plane turbulent impinging jets", J. of Hydraulic Research, 11(1), 29, 1973.

5. Bogdanov, S. S., Markov, Yu. B., Moiseenko, G. S., Onufriev, A. T., and Safarov, "Spontaneous oscillations of oppositely directed jets of different density near a mountainous obstacle", Sov. Tech. Phys. Lett, 9(9), 474, 1983.

6. Buchhave, P., "Particle image velocimetry: Status and trends", Experimental Thermal and Fluid Science, 5, 586, 1992.

7. Chaghaghi, F. S, "Time series package (TSPACK)",Springer-Verlag, 1982.

8. DANTEC, "Instruction manuals for 55X modular optics, 55N10 LDA frequency shifter, and 55l90a LDA counter processor", Published by DISA information Department, 1986.

9. Denshchikov, V. A., Kondratev, V. N., and Romashov, A. N., "Interaction between two opposed jets", Fluid Dynamics, 6, 924, 1978.

10. Denshchikov, V. A., Kondratev, V. N., Romashov, A. N., and Chubarov, V. M., "Auto-oscillations of planar colliding jets", Fluid Dynamics, 3, 460, 1983.

11. Deshpande, M. D., and Vaishnay, R. N., "Submerged laminar jet impingement on a plane", J. Fluid Mech., 114, 213, 1982.

12. Drain, L. E., "The laser Doppler technique", John Wiley & Sons, 1980.

13. Durbin, J., "The fitting of time series models", Review of the institute of International Statistics, 28, 233-244, 1960.

14. Elderton, W. P., and Johnson, N. L., "Systems of frequency curves", Cambridge University Press, 1969.

15. Fisher, R. A., "Test of significance in harmonic analysis", Proc. Roy. Soc., Ser. A. 125. 54-59, 1929.

16. George, W. K., "Quantitative measurement with the burst-mode laser Doppler anemometer", Experimental Thermal and Fluid Science, 1, 29-40, 1988.

17. Goldstein, R. J. (Ed.), "Fluid mechanics measurements", Hemisphere Publishing Co. (Distributed by Springer-Verlag), 1983.

18. Gutmark, E., Wolfshtein, M. and Wygnanski, I., " The plane turbulent impinging jet", J. Fluid Mech., 88, part 4, 737,1978.

19. Hanson, S., "Visualization of alignment errors and heterodyning constraints in laser Doppler velocimeters", Proceedings of the LDA-Symposium, Copenhagen, 1975.

20. Jie, Y., Min-quan, W., Gan-ce, D., and Li, Z., "An investigation into impingement jets in cylindrical chamber", Journal of Hydrodynamics, Ser. B, 1, 90, 1991.

21. Kennedy, J. B., and Neville, A. M., "Basic statistical methods for engineers and scientists", Harper & Row, Publishers, 1976.

22. Kirillov, V. A., and Khudenko, B. G., "Calculation of the direction of the axis of a stream resulting from the mixing of turbulent jets", J. Eng. Phys., 9(5), 414, 1965.

23. Kolodziej, P., Macosko, C. W., and Ranz, W. E., "The influence of impingement mixing on striation thickness distribution and properties in fast Polyurethane polymerization", Ploy. Eng. Sci., 22(6), 388, April 1982.

24. Law, H. S., and Masliyah, J. H., " Mass transfer due to a confined laminar impinging two-dimensional jet", Int. J. Heat Mass Transfer, 27(4), 529, 1984.

25. Law, H. S., and Masliyah, J. H., " Mass transfer due to a confined laminar impinging axisymmetric jet", Ind. Eng. Chem., Fundam., 23(4), 446, 1984.

26. Lee, L. J. "Polyurethane reaction injection molding: process, materials and properties", Rubber Chem. Tech.,53,542,1980.

27. Lee, L. J., Ottino, J. M., Ranz, W. E., and Macosko, C. W., "Impingement mixing in reaction injection molding", Poly. Eng. Sci., 20(13), 859, Mid-Sept., 1980.

28. Liou, T. M., Wu, S. M., and Hwang, Y. H., "Experimental and theoretical investigations of turbulent flow in a side-inlet rectangular combustor", J. Propulsion, 6(2), 131, 1990.

29. Macosko, C. W., "RIM Fundamentals", Hanser Publishers, Distributed in Canada by Oxford University Press, Canada, 1989.

30. Makarov, I. S., and Khudenko, B. G., "Mixing of the intersecting turbulent jets", J. Eng. Phys, 8(4), 304, 1965.

31. Malguarnera, S. C., and Suh, N. P., "Liquid injection molding I. An investigation of impingement mixing", Polym. Eng. Sci., 17(2), 111, 1977.

32. Malguarnera, S. C., and Suh, N. P., "Liquid injection molding II. mechanical design and characterization of a RIM machine", Polym. Eng. Sci., 17(2), 116, 1977.

33. Marple, V. A., Liu, B. Y. H., and Whitby, K. T.," On the flow fields of inertial impactors", J. of Fluids Engg. (ASME), 394, Dec. 1974.

34. McNaughton, K. J., and Sinclair, C. G., "Submerged jets in short cylindrical flow vessels", J. Fluid Mech., 25(2), 367, 1966.

35. Merzkirch, W., "Flow visualization", Academic Press, 1974.

36. Miau, J. J., and Sun, D. J., "Streamwise vortices generated by impinging flows in a confined duct", Experiments in fluids, 7, 497, 1989.

37. Nosseir, N. S., and Behar, S., "Characteristics of jet impingement in a side-dump combustor", AIAA J., 24(11), 1752, Nov. 1986.

38. Ogawa, N., Maki, H., and Hijikata, K., "Studies on opposed turbulent jets (Impact position and turbulent component in jet center)", JSME international Journal, series II, 35(2), 205, 1992.

39. Otnes, R. K., and Enochson, L., "Digital time series analysis", John Wiley & Sons, 1972.

40. Packard, N. H., Crutchfield, J. P., Farmer, J. D., and Shaw, R. S., "Geometry from a Time Series", Phys. Rev. Letters, 45, 712, 1980.

41. Powell, A., "Aerodynamic Noise and the Plane Boundary", J. of the Acoustical Soc. of America, 32,982, 1960.

42. Prenel, J. P., Porcar, R., and Diemunsch, G.,"3D flow visualization by means of laser beam sweeps", Flow Visualization IV, Proceedings of the fourth International Symposium on Flow visualization, Aug. 26-29, 1986, Ecole National superieure de Techniques Avancees, Paris, France, Edited by Claude Veret.

43. Press, W. H., Flannery, B. P., Teukolsky, S. A., and Vetterling, W. T., "Numerical Recipes: The art of scientific computing", Cambridge University Press, 1986.

44. Quraishi, M. S., and Fahidy, T. Z., "Techniques for flow pattern studies", Chapter 28 of " Encyclopedia of fluid mechanics vol. 3, p811, ed. by N. P. Cheremisinoff ", 1985.

45. Richards, J. R., and Scheele, G. F., "Measurement of laminar jet velocity distributions in liquid-liquid systems using flash photolysis", Chem. Eng. Commun., 36, 73, 1985.

46. Saad, N. R., Douglas, W. J. M., and Mujumdar, A. S.," Prediction of heat transfer under an axisymmetric laminar impinging jet", Ind. Eng. Chem., Fundam., 16(1), 148, 1977.

47. Sandell, D. J., Macosko, C. W., and Ranz, W. E., "Visualization technique for studying impingement mixing at representative Reynolds number", Ploy. Proc. Engg., 3(1&2), 57, 1985.

48. Saripalli, K. R., "Visualization studies of jet impingement flows at McDonnell Douglas research laboratories", Flow Visualization III: Proc. of the third Int. Sym. on Flow Visualization, Sept. 6-9, University Of Michigan, 503, 1983.

49. Savas, O., "On flow visualization using reflective flakes", J. Fluid Mech., 152, 235, 1985.

50. Spalding, D. B., "Theory of mixing and chemical reaction in the opposed-jet diffusion flame", ARS Journal, 763, June, 1961.

51. Tadmor, Z., and Gogos, C. G., "Principles of polymer processing", Wiley, New York, 1979.

52. Tecplot version 6 (Interactive Data visualization for Scientists & Engineers) , Amtec Engineering, Inc., 1993.

53. Tucker, C. L., PhD Thesis, MIT, 1978.

54. Tucker III, C. L., and Suh, N. P., "Mixing for reaction injection molding. I. Impingement mixing of liquids", Poly. Eng. Sci., 20(13), 875, Mid-Sept. 1980.

55. Tucker III, C. L., and Suh, N. P., "Mixing for reaction injection molding. II. Impingement mixing of fiber suspensions", Poly. Eng. Sci., 20(13), 887, Mid-Sept. 1980.

56. Van Heiningen, A. R. P., Mujumdar, A. S., and Douglas, W. J. M., "Numerical prediction of the flow field and impingement heat transfer caused by a laminar slot jet", J. of heat Transfer (ASME), 655, Nov. 1976.

57. Van Meel, D. A., and Vermij, H., "A method for flow visualization and measurement of velocity vectors in three-dimensional flow patterns in water models by using color photography", Appl. Sci. Res., A10, 109-117, 1961.

58. Wei, W. W. S., "Time series analysis: Univariate and multivariate methods", Addison-Wesley Publishing Co. Inc., 1989.

59. Whittle, P., "The simultaneous estimation of a time series' harmonics covariance structure", Trabajos. Estadist., 3, 43-57, 1952.

60. Wolfshtein, M.," Some solutions of the plane turbulent impinging jet", J. of Basic Engg. (ASME), 915, Dec. 1970.

61. Woo, Y. R., Williams, F. P., Faughan, P. D., and Yoganathan, A. P., "Pulsatile flow visualization studies with aortic and mitral mechanical valve prostheses", Chem. Eng. Commun., 47, 23, 1986.

62. Wood, P., Hrymak, A., Yeo, R., Johnson, D., and Tyagi, A., "Experimental and computational studies of the fluid mechanics in an opposed jet mixing head", Phys. Fluids A 3(5), 1362, 1991.

Appendix A: Calculation of Jet Reynolds Number

Let V (cc) of the working fluid is collected in t (sec) from the outlet of the mixhead. The density and viscosity of the fluid are ρ (g/cc) and μ (cp). Let the rotameter for each jets are set such that ratio of total volumetric flow rate from each jet are r_1 and r_2 respectively. Thus the volumetric flow rate from mixhead (Q) is

$$Q = V/t \tag{A.1}$$

and we also have,

$$r_1 + r_2 = 1 \tag{A.2}$$

so the volumetric flow rate from one jet

$$q_1 = \frac{Q}{r_1} \tag{A.3}$$

The average velocity form this jet (of diameter d cm) is

$$v_1 = \frac{q_1}{\pi \frac{d^2}{4}} \tag{A.4}$$

Thus the jet Reynolds number for this jet is

$$Re_1 = 100\, d\rho \frac{v_1}{\mu} \tag{A.5}$$

In the study, the jets are set at equal flow rate (and same fluid is used in both jets) so

$$r_1 = r_2 = 0.5 \tag{A.6}$$

Thus substituting the value of r_1 from eq. *A*.6 into equation *A*.5, so the jet Reynolds number is,

$$Re = 100\frac{Q}{2}\frac{4}{\pi}d\frac{\rho}{\mu} \qquad (A.7)$$

In those cases when the jets are not set at equal flow rate the rotameter calibration is used to estimate the individual volumetric flow rate of each jet. Then equation *A*.4 and *A*.5 can be used to estimate the average jet velocity and average jet Reynolds number.

For the model of this study, in case of equal flow rate from each jet and same fluid from each jets, ratio of average jet velocity and mixhead (of diameter D) average velocity is

$$\frac{v_{jet}}{v_{mixhead}} = \frac{D^2}{2d^2} = 56.95 \qquad (A.8)$$

and similarly the ratio of the jet Reynolds number to the mixhead Reynolds number is

$$\frac{Re_{jet}}{Re_{mixhead}} = \frac{D}{2d} = 5.34 \qquad (A.9)$$

Appendix B: Location of the intersection point of laser beams inside the mix-head

LDA measurements are made for the probe volume where two converging beams from the front lens of LDA optics intersect each other inside the model. If the measurements are made in air and in open space then the probe volume is located at the optical axis f_1 (focal length of the front lens) distance away from the front lens. In the present system, laser beams travel through air, plexiglass (model material), and mineral oil (working fluid). The interfaces are plane and curved surfaces. For the axial velocity measurements the interfaces are only planer while for radial velocity the interfaces are planer and curved. The location of the intersection point of the beams in the model is estimated using geometrical optics. The method for calculating the location of the probe volume during radial velocity measurements is described below.

(A) Location estimation in case of radial velocity (U) measurements:

Presuming there is no model, the two laser beams b_1 and b_2 travelling through the convex front lens will intersect at point M as shown in fig. B.1. In the presence of a model made up of plexiglass (a denser medium than air) these beams refract at plane surface BF and will intersect at point N. In the model, the beams are again refracted at curved surface CG with center at point O. At this interface, the beams are entering from a denser medium (plexiglass) to a lighter medium (mineral oil). Thus, the beams move away from the normal (N2). These refracted beams finally intersect at point P in the model. At certain locations of the model, the beams will be totally reflected and there will be no intersection inside the mixhead.

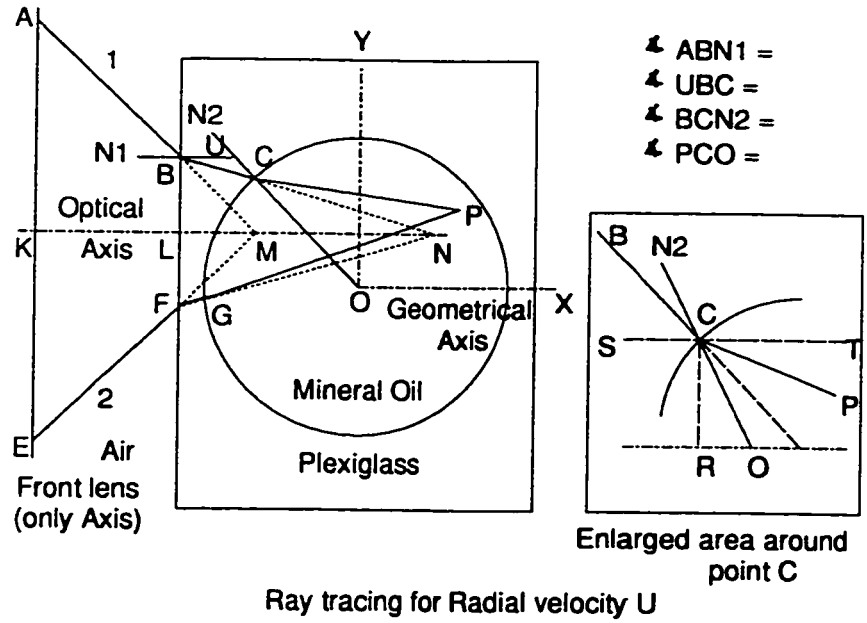

Fig. B.1: Location of the intersection point of laser beams inside the mixhead in case of axial velocity (U) measurements

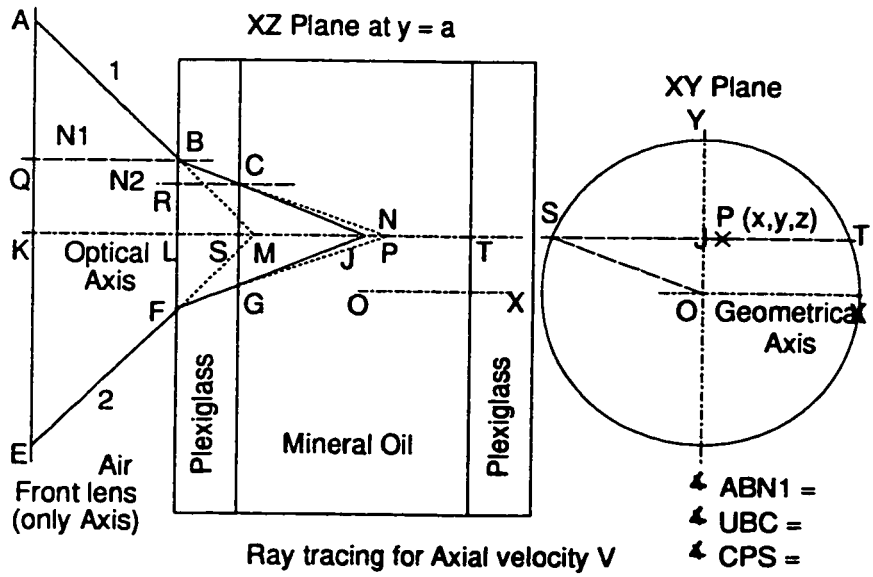

Fig. B.2: Location of the intersection point of laser beams inside the mixhead in case of axial velocity (U) measurements

The path for beam b_1 is as follows:

1. Translation in air from A to B (point 1 to 2).
2. Refraction at plane surface BF (point 2 to 3).
3. Translation in plexiglass from B to C (point 3 to 4).
4. Refraction at curved surface CG (point 4 to 5).
5. Translation in mineral oil from C to P (point 5 to 6).

The path of beam b_2 is EFGP which is similar to that of beam b_1. After the intersection of beams b1 and b2 at point P, the beams travel out of the model which is not shown in the fig. 3.1.1. The optical axis of LDA is indicated by KLMN and the geometrical axis of the model by OX. Point O the center of the model, is the origin for all the measurements. If the coordinates of b_1 (point A) and b_2 (point E) are known, the coordinates of point P can be calculated. This procedure is referred as forward mode of calculation. In the backward mode, the coordinates of point P are known and coordinates of b_1 (point A) and b_2 (point E) are calculated. For these calculations, other required parameters are as follows:

1. The refractive indices of air, plexiglass and mineral oil n_1, n_2, n_3, respectively,
2. f_1 focal length of the front lens,
3. d distance KL of model from the front lens,
4. Beam separation (b_s) AE from LDA settings,
5. Angle $\alpha = \tan^{-1}\left(\frac{b_s}{2f_1}\right)$, and
6. Radius of the circle (a).

Forward Mode :

1. Translation in air from A to B

Equation of straight line AB

$$y = mx + c \tag{B.1}$$

where,

$$m = \tan(\alpha)$$

$$c = y_A - m x_A$$

Thus the coordinates of point B are the intersection of line AB and line BF.

Eq. of line BF

$$x = d \tag{B.2}$$

Solving eqs. (B.1) and (B.2) for coordinates of point B, we have

$$x_B = x_A + d \tag{B.3}$$

$$y_B = m(x_B - x_A) + y_A \tag{B.4}$$

Similarly, the coordinates of point F are calculated using the equations of straight lines EF and BF.

2. Refraction at plane surface BF

Using Snell's law, we have

$$\sin(\beta) = \frac{n_1 \sin(\alpha)}{n_2} \tag{B.5}$$

3. Translation in plexiglass up to the circle

Equation of line BC which is obtained by solving general eq. (B.1) of straight line passing through a known point B (x_B, y_B) is

$$y = m(x - x_B) + y_B \qquad (B.6)$$

where

$$m = \tan(\beta)$$

Equation of circle with radius a and center at point O is

$$x^2 + y^2 = a^2 \qquad (B.7)$$

Point C is the intersection of the circle (eq. B.7) and straight line (eq. B.6). Substituting equation (B.1) into (B.7)

$$px^2 + qx + r = 0 \qquad (B.8)$$

where

$$p = (1 + m^2)$$

$$q = 2mc$$

$$r = c^2 - a^2$$

The values of m and c are given by equation (B.6). Solving the quadratic equation (B.8) for x yields the following two roots

$$x_{1,2} = \frac{-q \pm \sqrt{(q^2 - 4pr)}}{2p} \qquad (B.9)$$

Only one of the two roots represents the coordinates of point C and is decided by the following criteria.

(i) If the roots are complex, there is no intersection of line BC and circle i.e. the laser beam has missed the cylindrical portion of the model.

(ii) If the roots are real and equal the point C is tangent to the circle.

(iii) If the roots are real and unequal the smallest root is point C since light is coming from left side of the origin.

Once x_C is known, y_C is calculated by substituting the value of x_C in eq. (B.6)

$$y_C = m(x_C - x_B) + y_B \qquad (B.10)$$

where

$$m = \tan(\beta)$$

Similar calculations are performed on beam b_2 and the coordinates of point G are calculated.

4. Refraction at curved surface

Enlarged portion of refraction at point C is given in fig. (B.1). To find the slope of line CP tan(θ), the angle θ is calculated as follows:

From Snell's law we have,

$$n_2 \sin(\delta_1) = n_3 \sin(\delta_2) \qquad (B.11)$$

since line ST is parallel to line RO, we have

$$\theta = \beta + \delta_1 - \delta_2 \qquad (B.12)$$

$$\delta_2 = \sin^{-1}\left(\frac{n_2 \sin(\delta_1)}{n_3}\right) \qquad (B.13)$$

From triangle CRO

$$\sin(\beta+\delta_1)=\frac{CR}{CO}=\frac{y_c}{a} \qquad (B.14)$$

Substituting equations (B.13) and (B.14) into (B.12)

$$\theta=\sin^{-1}\left(\frac{y_C}{a}\right)-\sin^{-1}\left[\frac{n_2}{n_3}\sin\left(\sin^{-1}\left(\frac{y_C}{a}\right)-\beta\right)\right] \qquad (B.15)$$

For small angle $\sin(\theta)=\theta$,

$$\theta=\left(1-\frac{n_2}{n_3}\right)\frac{y_C}{a}+\left(\frac{\mu_2}{\mu_3}\right)\beta \qquad (B.16)$$

Repeating the same procedure for beam b_2 will yield the slope of the line GP.

5. Translation in mineral oil from point C to P

The point P is the intersection of lines CP and GP. The equations of lines CP and GP are

$$y=m_1x+c_1 \qquad (B.17)$$

$$y=m_2x+c_2 \qquad (B.18)$$

where

$$m_1=\tan(\theta)$$

$$m_2=\tan(\theta')$$

$$c_1=y_C-m_1x_C$$

$$c_2=y_G-m_2x_G$$

Solving equations (B.17) and (B.18) for x_P, y_P

$$x_P = \frac{c_2 - c_1}{m_1 - m_2} \qquad (B.19)$$

$$y_P = m_1 x_P + c_1 \qquad (B.20).$$

Thus, given the coordinates of points A and B, the coordinates of point P are calculated.

Backward Mode:

In this mode, the coordinates of point P are given and the coordinates of points A and E are estimated. This method is iterative in nature. The following algorithm is used:

1. Initial guesses of points A and E are made. These guesses are estimated by assuming that the model is a solid block of plexiglass or it is made of two blocks (one plexiglass and other of mineral oil).
2. Forward mode is used to calculate the new coordinates of point P.
3. New coordinates of P are compared with the given coordinates of P. If the error is within prefixed criteria, the calculations are stopped and the last guessed coordinates of A and E are the estimated coordinates. If the error is not within the prefixed criteria, procedure is followed back with new initial guess. This new guess is estimated using bisection search method.

Location estimation in case of axial velocity (V) measurements:

For the measurements of the axial velocity, the beam paths are shown in fig. B.2. The optical axis does not coincide with the geometrical axis.

The beam (b_1) translates in air from front lens to front of the model (path AB). At the interface the beam is bent towards the normal (N1). the beam again translates in the plexiglass up to point C. Following Snell's law at the interface of the plexiglass (dense medium) and mineral oil (lighter medium) this beam bends away from the normal (N2). Beam (b_1) intersects the second beam (b_2) at point P. Beam (b_2) follows the path EFGP. The point P is the location of the measuring volume. The coordinates of point P are to be estimated provided the coordinates of point A and B are known. Similar to radial velocity calculations, this mode is also referred as forward mode. Consider,

$$QB = KL = KJ - LJ = x_A - \frac{w}{2} \qquad (B.21)$$

where w is the width of the plexiglass block which is known. From right angle triangle AQB,

$$AQ = QB \tan(\alpha) \qquad (B.22)$$

The distance (OJ) between the optical axis and the geometrical axis is known. Thus from XY plane figure we have,

$$SJ = \sqrt{(OS)^2 - (OJ)^2} = \sqrt{\left(\frac{D^2}{4} - y_K^2\right)} \qquad (B.23)$$

$$RC = LS = LJ - SJ \qquad (B.24)$$

Using equations (B.23) and (B.24) and the right angle triangle BRC, we have

$$BR = RC \tan(\beta) \qquad (B.25)$$

also,

$$CS = AK - AQ - BR = \frac{b_s}{2} - AQ - BR \qquad (B.26)$$

From right angle triangle CSP, we have

$$SP = \frac{CS}{\tan(\gamma)} \qquad (B.27)$$

Thus,

$$x_P = JP = SP - SJ \qquad (B.28)$$

The remaining coordinates (y_P and z_P) of point P are same as the point K. In the Backward mode case, the following algorithm is used:

1. Initial guess of x_A is estimated assuming that beams are travelling through the plexiglass only.
2. Forward mode is used to calculate the coordinates of point P.
3. New coordinates of point P are compared with the given coordinates of point P. If the error is within prefixed criteria, the calculations are stopped. If the error is outside the criteria, based on the calculated error, a new guess of x_A is computed using bisection search method and the procedure is repeated.

Appendix C: Data Acquisition and statistical processing

(i) Grid Preparation:

In the present set up, the laser beams travel through various media (air, plexiglass, and mineral oil). Hence, the location of the intersection of these beams inside the mixhead must be determined. A method is developed using geometrical optical ray tracing principles to identify this location and has been described in section 4.4.2 and appendix (B). It is implemented in program OPTICAL. This program is menu driven. It can be used in an interactive or file mode. In the interactive mode, the relevant input data are entered based on the selection of submenu and the program outputs the beams or model coordinates. In file mode, the input data are read from a ASCII file and a corresponding output ASCII file is created. This file is further used as input for LDA data acquisition programs. The procedure for the file mode is as follows.

Initially, an input file (grid) is prepared which contains x, y, z coordinates, velocity component U or V, and mode of calculation (Forward or Backward) for each point of the selected grid. The outputs generated from processing of this input file (grid) are used as input for LDA data acquisition programs. This input file (grid) is designed in such a way that the data acquisition procedure is optimized by minimizing the movement of the traverse table and the optical adjustment of the photomultiplier from one point to the next point. The following steps are used to generate this input file (grid):

(1) Only one component of velocity is used in one file. This avoids the rotation of the laser optics between the experiments to measure the other velocity component.

(2) The points in the file are arranged in z major, x major, and y major order with slight modification. The actual sequence of point coordinates looks like (x_o, y_o, z_o), (x_1, y_1, z_1), ..., (x_1, y_1, z_n), (x_2, y_1, z_n), ..., (x_2, $y_{1\ \ 1}$), ..., (x_1, y_1, z_n), (x_1, y_2, z_n), ..., (x_1, y_2, z_1), ..., (x_1, y_m, z_n), (x_o, y_o, z_o). Here (x_o, y_o, z_o) is some reference point from where the series of experiments is started. The model is traversed back to this point once the data acquisition is completed. After adjusting the photomultiplier at (x_i, y_j, z_1) no further adjustments are needed up to point (x_i, y_j, z_n) since traversing in z direction does not alter the optical path of the laser beams. The movement from (x_i, y_j, z_k) to (x_{i+1}, y_j, z_k) or (x_{i-1}, y_j, z_k) requires only slight adjustment of photomultiplier in only one direction (x). Similarly, a movement from (x_i, y_j, z_k) to (x_i, y_{j+1}, z_k) will require slight adjustment of photomultiplier only in direction y. For the measurements of U component of velocity, less photomultiplier adjustment is needed if the model is traversed in x direction as compared to moving it in y direction (due to curvature). This is the reason for preferring x major order before y major order. For the measurement of axial component of velocity (V), this order of preference has no effect.

(ii) Model traversing and LDA data acquisition:

Model traversing is performed by sending commands to the PC21 indexer (board which control the moving of traversing table (see section 4.4.3)). This command consists of the information about the direction, velocity, acceleration, and the motor step for the controller to traverse the table. The traverse table is not equipped with an incremental optical encoder. Thus, the position tracking in the feed back loop is not possible. Software which keeps track of the position movement has been developed and used for position tracking in the feed back loop.

LDA data acquisition is performed using a DOSTEK board (section 4.4.3) which receives data from the Dantec counter. The input for this board are integers coded with the information about the sample size, trigger mode, sampling frequency, and number of data per sample. The output from this board is a sequence of two byte integers. The sequence length depends upon the number of samples and data per sample. In our case, there are three integers (2 bytes long) per sample. The above three integers contain the number of fringes crossed by particles, time taken to cross these fringes and time interval between two samples. Both the data acquisition and model traversing are performed in a semi-automatic mode using a program PC21CONT.

The program is menu driven. It has three modes of operation. In mode one, only traversing of the model from one point to other is performed on the basis of relevant input provided. In mode two, only LDA data acquisition is done. The necessary information for LDA settings are fed to the computer. Mode three performs both tasks automatically until the intervention of the operator. Before using mode three, the flow loop must be at steady state, the Doppler signal of good quality, data and validation rates are satisfactory, and the model is at some reference location (x_{org}, y_{org}, z_{org}).

1. The names of input file (this file is the output of OPTICAL program), and output file are required. This output file will contain the point coordinates, velocity component, trigger mode, sampling frequency, frequency shift, and LDA data file name.

2. Point coordinates are read from the input file and the model is traversed to this location from the last location. Program execution is suspended for a preassigned time interval, the Doppler signal quality is checked, and necessary adjustments are performed manually on the photomultiplier.

3. LDA data acquisition procedure starts. On the choice of the operator default LDA settings are used. If the default settings are not satisfactory, new settings are provided by the operator.

4. This step is done only once. Program pauses for LDA data file name (this file is binary and there is one file corresponding to each LDA data acquisition), which will be referred to as the raw data file. A procedure is implemented in this program to generate the new raw file name from the previous raw data file name. First raw file name should be of 7 characters as shown in the algorithm. First 4 characters can be any DOS valid four characters (here two letters of month and two digits of date are used) for file name. Last three characters should be three digit number. This procedure generates the raw data file name by incriminating the three digit number of the previous file by one.

5. LDA data are received from the counter and are written in the raw data file. The relevant information of the experiment is written in the output file for this point.

6. Status of the escape key is checked. If it is positive, emergency procedure is evoked. This procedure gives the chance to halt the data acquisition all together or to make minor changes in settings, if required. If the operator chooses to halt the data acquisition altogether, this program will traverse the model back from the

present point to the reference point from which this sequence of experiments was started, all open files will be properly closed and data will be saved up to the last data point.

7. LDA data are again acquired at the same point or program returns to step two. New coordinates are read and the above procedure is followed. If the input file end is noticed, model is traversed to reference point (x_{org}, y_{org}, z_{org}) and program takes a normal exit and stops.

(iii) Data Processing and Management:

The data acquired for experiments (as described in the previous section) as such do not provide much information about the flow field. Hence, these data are processed to extract the various statistical parameters and functions, and also statistically tested for the time series behavior at particular locations. The flow field is better understood quantitatively with the help of this information. This data processing is done using the program LDA on a UNIX based computer (Silicon graphics 4D35). A particular set consists of several LDA raw data files (binary) for many points with a given set of flow parameters (Re, viscosity), geometrical settings (H/D), and one master file (ASCII). This master file consists of the point coordinates, velocity component, trigger mode, sampling and shift frequencies, and the corresponding raw data file name. This master file and all the raw data binary files are transferred and properly converted from PC-format to unix-format. This set is processed by LDA program.

The main program asks the name of the master file (referred to as fl.lda in flow chart). In reality, this name without file extension will have 7 characters. It opens the master file and generates and opens three files names (summary). It also opens

these files. A brief output of each experiment is written in these summary files. One of these files has point coordinates, moments of velocity component, name of velocity component with trigger mode and raw data file name. Second summary file contains the first ten significant frequencies in the time series with raw data file name. Third file contains the associated amplitudes of these ten significant frequencies with the raw data file name. One record from this master file is read. The raw file name and other informations are assigned to proper variables. From the name of the raw file other three new file's names are generated and opened. One contains the detail of the process results. In second, the PDF results are output and the third file contains ACF, PACF, and PSD calculated by three different methods for first 512 lags. All the LDA raw data are read from the raw file and individual term of the time series of the instantaneous velocity is calculated. Various statistical tests and parameters are computed. The results are written into three summary files and three detail files. The program returns to the next record in the master file and then, the next experiment is processed. This sequence is repeated for all the experiments of a set in the master file. Once, the end of master file is reached, the execution of the program stops.

LDA generates large amount of data. In our case, just the raw data are over 200 Mbytes. The storage of large data and the management of the information from such set for further analysis are tedious tasks. The data base management program (dbaseIII) has been used for managing the process results. The three summary files generated in the processing of one set, and another file containing the Re, H/D, and viscosity information of the experiment are converted to four dbase files and a data base is created. All of these files are inter-linked through a common field, the raw

file name. Several dbase programs are written which extract the information according to the need. The output from these files are standard ASCII files which are used by graphic and spreadsheet programs for reporting and further analysis.

(iv) Outlier identification and removal

It has been observed that unpredictable and uncorrectable outliers occur during data acquisition due to several reasons such as loss of signal in transmission, failure of the data collection equipment (digitizing board and computer) and LDA electronic components (counter, frequency shifter and photomultiplier) etc. These outliers seriously bias moments and secondary statistics. Two such outliers close to each other can generate a number of spurious frequencies in the PSD (Otnes and Enochson 1972). It is essential to identify, remove, and replace these outliers to extract useful and reliable information from the set.

As a part of the data analysis programs, the following algorithm has been successfully implemented to automate outlier identification, removal and replacement:

The average ($\bar{x}$) and standard deviation (s) of a time series (x_i) are estimated including all the original data. Then each data is checked and accepted if

$$\bar{x} - ks < x_i < \bar{x} + ks \qquad (C.1)$$

The parameter k is set by the user to a value suitable for the data. In this study it is set at four. The LDA data sets (instantaneous radial or axial velocity at a observed point) used in this study approach a normal distribution. For a normal distribution,

with $k = 4$, there is one chance in 10,000 that Equation (C.1) will reject a genuine data point. After identifying the outliers locations in the time series, in the next pass the outliers are removed and replaced by fourth order interpolation

$$x_{i_{new}} = \frac{-x_{i-2} + 4x_{i-1} + 4x_{i+1} - x_{i+2}}{6} \qquad (C.2)$$

Table C.1 shows a comparison between the moments estimated with original and the modified data of radial velocity measured at origin (0,0,0) using above algorithm for a given experimental settings (Re = 50, H/D = 0; 39 cp). It can be seen that a small number of outliers significantly changes the moments. In this case, there were only two outliers out of 10,000 data. Outliers editing changes the RMS by 230% without making any significant change in the mean. This modification also changes the skewness from highly negative to almost symmetrical (Skew = 0 for symmetrical distribution), and kurtosis from highly peaked to normal distribution (kurt = 0 for normal distribution). All further statistical estimations are reported after modifying the outliers.

Table C.1: Effects of outliers editing on moments of LDA data (U)

Experimental settings: Re = 50; H/D = 0.0; Viscosity = 39 cp

Location: 0,0,0 (Intersection of jet and mixhead axis)

Statistics	Old Value	New Value	% change
Mean (m/s)	-0.046	-0.046	0
RMS (m/s)	0.043	0.013	230
Skew	-61.34	0.25	24636
Kurt	1000.00	-0.33	30310

(v) Randomness, and stationarity of data

The classical methods such as auto correlation functions (ACF), partial auto correlation functions (PACF), power spectrum density (PSD), and probability density functions (PDF) require randomness and stationarity of the time series. In this work, two nonparametric procedures, specifically, the reverse and the run tests have been used to check randomness. The reverse test is more powerful for detecting monotonic trends while the run test is more suitable in detecting fluctuating trends.

For the reverse test the following algorithm is implemented. Let x_i be the ith observation of a random variable x. There are N observations in the time series. Now, count the number of times that $x_i > x_j$ for $i < j$, where $j = i+1, i+2, \ldots, N$. Each such arrangement is called a reverse arrangement. The total of all such reverse arrangements for $i = 1, 2, \ldots, N-1$, is A. The null hypothesis, that the given time series is

an independent observation of a random variable, is accepted, if

$$A_{N;1-\alpha/2} < A \leq A_{N;\alpha/2} \qquad (C.3)$$

For the run test, each observation of a time series is classified into one of two mutually exclusive categories say plus or minus, based on the criteria like $x_i \geq \bar{x}$ (+) and $x_i < \bar{x}$ (-). The total number of runs (r) are counted, where a run is a sequence of identical observations that is followed by a different observation or no observation at all. In the plus or minus scheme every sign change is one run. The null hypothesis, that the series is random, is accepted, if r lies in the accepted region

$$r_{N/2;1-\alpha/2} < r \leq r_{N/2;\alpha/2} \qquad (C.4)$$

In Equations C.3 and C.4, α is the significance level. The limiting values of Equations C.3 and C.4 are obtained from the tabulated percentage points of the reverse arrangement distribution and the percentage points of the run distribution respectively.

To test stationarity of a large record (10,000 data points) of a time series is divided into small records of 1000 points each referred as a block. For each block, the first four moments and the autocorrelation from lag 1 to lag 30 are estimated. Thus for one record we have 10 statistics (mean, RMS, . . ., R_{01}, . . ., R_{30}) which are separated by the time interval between blocks. Regression analysis is performed for all statistics with time as the independent variable. The regression coefficient and probability are estimated. The null hypothesis, that the statistic is time invariant, is accepted if the calculated probability is greater than .05 (two tailed test at 95% confidence level).

All LDA data for axial and radial velocities (time series of instantaneous velocity) were tested and found to be random and stationary. A typical result of these tests for the center line radial velocity at origin (0,0,0) is given in Table C.2 which confirm the randomness and stationarity of the time series.

Table C.2: Randomness & stationarity test of LDA data (U)

Experimental settings: Re = 50; H/D = 0.0; Viscosity = 39 cp

Location: 0,0,0 (Intersection of jet and mixhead axis)

Ind. - Independent; prob. - Probability

Reverse test	Run test	Mean prob.	RMS prob.	Skew prob.	Kurt prob.	R_{01} prob.	R_{10} prob.	R_{30} prob.
Ind.	Ind.	0.15	0.30	0.65	0.55	0.14	0.39	0.27

(vi) Probability density function (PDF)

In this study, two methods have been used to estimate the PDF. First is the general histogram method of dividing the range into bins and counting the data which fall into each bin. From this frequency histogram the PDF is estimated as follows

$$p_j = \frac{N_j k}{N(b-a)} \qquad (C.5)$$

where p_j is the derivative of the distribution function at the midpoint of each interval. The entire range of the variable x (the instantaneous velocity), where x lies between a and b, is subdivided into k subintervals of equal length. Thus the entire range of x is broken into (k + 2) intervals. N_j is number of data points in j^{th} interval out of

a total number of data (N). Values of the parameters a, b, and k must be chosen before implementing equation (C.5). An approximation is used here, as there is no specific guide line in literature. The best estimates are made by assuming the underlying distribution. This method still only gives a pictorial approximation of the distribution having a good guess of the parameters a, b, k. In the second step, one may fit some curve by a regression algorithm to obtain an algebraic function of the PDF, which itself is not a simple task since the function is nonlinear.

Here the data set is very large, and to cover the wide range of underlying distributions, a regression algorithm, to obtain an algebraic form from the histogram, was discarded due to complexities involved. To obtain the PDF in algebraic functional form, Pearson's system of the frequency curve method is implemented (Elderton and Johnson 1969). This method analytically gives the following form of the PDF based on the sample size and its first four moments,

$$y = y_o f(x) \qquad (C.6)$$

where y, y_o, and x are PDF, scaling factor, and variable (velocity) in consideration.

The major advantages of this method are: no guess work for parameters and, assumptions of underlying distribution and data size is immaterial. This method is based on the first four moments of the data, and is a systematic method of approaching frequency distributions. The procedure is suitable for large data sets and computation does not require interaction with the user.

Analysis of LDA data (radial and axial velocities) indicated that the distribution ranges from a negative skew bell shape to a positive skew bell shape. Usually the

skewness is very moderate and most of the time the curve approaches symmetrical behavior. The symmetrical curves approach the normal curve. Most of the deviation is either near physical boundaries of the mixhead or where the velocity has been reduced to an insignificant (or very low) level. At these low velocities, higher moment calculations and statistics based on these moments are very susceptible to numerical error. The assumption of approaching a normal distribution (of velocity) is substantiated with these results.

(vii) Autocorrelation function (ACF), partial autocorrelation function (PACF), and power spectrum density of time series (PSD)

The time series (instantaneous radial or axial velocity collected with time trigger mode i. e. equally spaced) is analyzed in both the time domain and the frequency domain. Both methods give the same information about the time series, but analysis in both domains enhances the general understanding of fluid mechanics. In this study analysis in both domains is performed.

Two statistics estimated in the time domain are the autocorrelation and partial autocorrelation functions. The ACF for a stationary record is a measure of time related properties in the data that are separated by a fixed time delay. It is a correlation between x_i and x_{i+k} from the same process, separated only by k time legs, thus it is a relationship between a variable and itself (auto) at an earlier time. A plot of the ACF versus time lag gives information about the process which generates this time series. For example, a periodic function will generate a periodic ACF and for wide band random noise, the ACF will become insignificant within few lags. In this study ACF of lag k ($\hat{\rho}_k$) is estimated as follows:

$$\hat{\rho}_k = \frac{\hat{\gamma}_k}{\hat{\gamma}_0} = \frac{\sum_{t=1}^{n-k}(x_t - \bar{x})(x_{t+k} - \bar{x})}{\sum_{t=1}^{n}(x_t - \bar{x})^2}, \quad k = 0, 1, 2, \ldots \qquad (C.7)$$

where $\hat{\gamma}_k, \bar{x}$ are autocovariance function at lag k and sample mean of the time series $x_1, x_2, x_3, \ldots, x_n$. These estimated $\hat{\rho}_k$ are tested for a white noise process. This test is the approximation of Bartlett's test (Kennedy and Neville, 1976) for large sample size (10,000 data). The null hypothesis that $\hat{\rho}_k$ is zero, is rejected, if

$$\hat{\rho}_k > \frac{2}{\sqrt{n}} \qquad (C.8)$$

The PACF estimates the relationship between x_t and x_{t+k} after their mutual linear dependency on the intervening variables x_{t+1}, x_{t+2}, ..., and x_{t+k-1} has been removed. Let $\hat{x}_t$ and $\hat{x}_{t+k}$ be the estimates of x_t and x_{t+k} calculated from linear relationships of these on the intervening variables. This function physically informs one about the influence of the past random shocks. If PACFs are significant for many lags then the random shocks are remembered by the process longer than a process where the PACFs become insignificant quickly. Here the PACF ($\hat{\phi}_{kk}$) is obtained by using the recursive method, which was given by Durbine (1960). This procedure is as follows:

$$\hat{\phi}_{k+1,k+1} = \frac{\hat{\rho}_{k+1} - \sum_{j=1}^{k} \hat{\phi}_{kj}\hat{\rho}_{k+1-j}}{1 - \sum_{j=1}^{k} \hat{\phi}_{kj}\hat{\rho}_j} \qquad (C.9)$$

and

$$\hat{\phi}_{k+1,j} = \hat{\phi}_{kj} - \hat{\phi}_{k+1,k+1}\hat{\phi}_{k,k+1-j}, \quad j = 1, , 2, \ldots, , k \qquad (C.10)$$

The estimated ϕ_{kk} are tested for white noise using the Bartlett test for large sample (Eq. C.8). These algorithms for the ACF and PACF are implemented in this study.

From the flow visualization study, a vibrating impingement plane is well established, and quantification of its frequency of vibration is one of the objectives of this work. For a periodic analysis, the frequency domain analysis is a well accepted method.

In the periodogram method, the discrete Fourier transform (C_k) is computed using the FFT of the time series of N data sample at equal intervals

$$C_k = \sum_{j=0}^{N-1} x_j \exp\frac{2\pi i j k}{N}, \quad k = 0, \ldots, N-1 \qquad (C.11)$$

where i is complex notation. Then the periodogram estimate of the power spectrum at different frequencies is;

$$\hat{G}(0) = \frac{1}{N^2} |C_0|^2 \qquad (C.12)$$

$$\hat{G}(f_k) = \frac{1}{N^2}(|C_k|^2 + |C_{N-k}|^2), \quad k = 1, \ldots, \left(\frac{N}{2} - 1\right) \qquad (C.13)$$

$$\hat{G}(f_{N/2}) = \frac{1}{N^2} |C_{N/2}|^2 \qquad (C.14)$$

where f_k is defined only for the zero and positive frequencies

$$f_k \equiv \frac{k}{N\Delta} = 2f_c \frac{k}{N}, \quad k = 0, 1, \ldots, \frac{N}{2} \qquad (C.15)$$

Here overlapping averaging methods with windowing of data (Press 1986) is implemented.

Once the PSD is estimated, significant frequencies (spikes) are picked from the plot of the PSD versus frequency. Screening of individual plots for significant frequencies, for small data set, is a manageable task. Here due to the very large data set, individually screening each plot (order of ten thousand plots) for significant frequencies a daunting (if not impossible) task. A statistical test, which was developed by Fisher (1929) and Whittle (1952) to identify the first and second most significant periodic components of a series, is implemented with the extension to identify components beyond two significant components. Fisher derived an exact test for the most significant intensity (or power) ($I^{(1)}(\omega_{(1)})$) at frequency $\omega_{(1)}$, based on the following statistics:

$$T = \frac{I^{(1)}(\omega_{(1)})}{\sum_{k=1}^{n/2} I(\omega_k)} \qquad (C.16)$$

Under the null hypothesis of Gaussian white noise process $N(0,\sigma^2)$ for series x_t, he showed that

$$P(T > g) = \sum_{j=1}^{m} (-1)^{(j-1)} C_j^N (1 - jg)^{(N-1)} \qquad (C.17)$$

where $N = (n/2), g > 0$, and m is largest integer less than $1/g$. Thus, for any given significance level α, the above equation is used to find the critical value g_α such that

$$P(T > g_\alpha) = \alpha \qquad (C.18)$$

If the T value calculated from the series is larger than g_α, then the null hypothesis that the series does not contain a periodic component, is rejected. This test is called Fisher's test. For most practical purposes, for large frequency sets, the critical value g_α is approximated by the first term of equation (5.4.13). This is given by

$$P(T > g) \approx N(1-g)^{N-1} = \alpha \qquad (C.19)$$

Whittle suggested extending Fisher's test for the second largest ordinate based on the following test statistics:

$$T_2 = \frac{I^{(2)}(\omega_{(2)})}{\sum_{k=1}^{n/2} I(\omega_k) - I^{(1)}(\omega_{(1)})} \qquad (C.20)$$

where the distribution in equation (5.4.13) is used but with N being replace by $(N - 1)$. This procedure can be continued using the following statistics until an insignificant result is obtained.

$$T_j = \frac{I^{(j)}(\omega_{(j)})}{\sum_{k=1}^{n/2} I(\omega_k) - \sum_{r=1}^{j-1} I^{(r)}(\omega_r)} \qquad (C.21)$$

Equations (C.19) and (C.21) were successfully implemented in this study which enabled identification of significant frequencies without manually screening each PSD. Only the first 30 significant ordinates were searched for the significance level $\alpha = .05$. The number of 30 was selected after looking many spectrums. This procedure is suitable for data sets of all sizes, especially, for large data sets. The above procedures (ACF, PACF, and PSD) of time series analysis have been implemented and the results are discussed in chapter 8.

(viii) Computer Programs

Appendix C

Computer programs listings

OPTICAL.BAS

```
**************************************************************************
'
'
' Program to prepare file for traversing table for mixhead grid
' Based on the coordinate of the grid, necessary movements for
' table are calculated and are written to a file which is used
' for LDA data collection.
'
' Developed by Ashok K. Tyagi
' 23 rd. June 1987 For old traversing machine in FORTRAN
' Modified for new traversing table on 3rd Aug., 1989
' Next Revision Dec. 1989
'
'
'
'**** optical.bas
DECLARE SUB filem ()
DECLARE SUB intera ()
    COMMON /geom/ jdia, modelw, modell, modelh1, modelh2, mdia
    COMMON /optical/ f, bs, mu1, mu2, mu3
    COMMON /angle/ alpha AS DOUBLE, beta AS DOUBLE, gamma AS DOUBLE
'
' Every dimension is in mm.
    jdia = 2.38: modelw = 52.42: modell = 101.6: modelh1 = 63.5
    modelh2 = 158.75: mdia = 25.4
'
    f = 80!: bs = 35.05: mu1 = 1!: mu2 = 1.4893: mu3 = 1.461
'
    alpha = ATN(bs * .5 / f): sinbeta = SIN(alpha) / mu2
    beta = ATN(sinbeta / SQR(1 - sinbeta * sinbeta))
    singamma = mu2 * SIN(beta) / mu3
    gamma = ATN(singamma / SQR(1 - singamma * singamma))
DO
    CLS
    PRINT " M A I N  M E N U ": PRINT
    PRINT " 1) Interactive mode "
    PRINT " 2) File mode "
    PRINT " 3) E X I T "
    PRINT : PRINT "Type your selection ( 1 to 3 ): "
    INPUT ch$
    SELECT CASE ch$
        CASE "1"
            CALL intera
        CASE "2"
            CALL filem
        CASE "3"
            EXIT DO
        CASE ELSE
            BEEP
```

```
    END SELECT
LOOP
END

-----------------------------------------------------------------

DECLARE SUB bacforv (xr!, yr!, zr!, xm!, ym!, zm!, mode$)
DECLARE SUB forward (x1!, y1!, x2!, y2!, iflag!)
DECLARE SUB backward (x1!, y1!, x2!, y2!)
DECLARE SUB origin (x!, y!, z!, movex!, movey!, movez!, vel$)
COMMON SHARED /geom/ jdia, modelw, modell, modelh1, modelh2, mdia
COMMON SHARED /optical/ f, bs, mu1, mu2, mu3
COMMON SHARED /angle/ alpha AS DOUBLE, beta AS DOUBLE, gamma AS
DOUBLE
SUB intera
DO
    CLS
    PRINT " SUB M A I N  M E N U ": PRINT
    PRINT " 1) FIND ORIGIN "
    PRINT " 2) Given  Lens COORDINATES  : Find Model COORDINATES"
    PRINT " 3) Given Model Coordinates : Find  Lens COORDINATES"
    PRINT " 4) Print Results ( only after you once chosen 1 to 3)"
    PRINT " 5) SUB E X I T "
    PRINT : PRINT "Type your selection ( 1 to 5 ): "
    INPUT ch$
    SELECT CASE ch$
        CASE "1"
            CLS
            PRINT "Enter the coordinates of beam  intersection"
            PRINT "at the outer surface of model (towards  the"
            PRINT "focusing lens) with respect to model origin"
            PRINT : PRINT
            INPUT "X coordinate ( mm ) ", x
            INPUT "Y coordinate ( mm ) ", y
            INPUT "Z coordinate ( mm ) ", z
            INPUT "Velocity Component [U/V] ", vel$
            CALL origin(x, y, z, nx, ny, nz, vel$)
        CASE "2"
            INPUT " Lens coordinates (x,y,z in mm) ", x, y, z
            INPUT " Velocity Component [U/V] ", vel$
            IF vel$ = "U" OR vel$ = "u" THEN
                CALL forward(x, y, nx, ny, flag)
                nz = z
            END IF
            IF vel$ = "V" OR vel$ = "v" THEN
                mode$ = "F"
                CALL bacforv(x, y, z, nx, ny, nz, mode$)
            END IF
        CASE "3"
            INPUT " Model coordinates (x,y,z, in mm)", x, y, z
            INPUT "velocity Component [U/V]", vel$
            IF vel$ = "U" OR vel$ = "u" THEN
                CALL backward(x, y, nx, ny)
            END IF
            IF vel$ = "V" OR vel$ = "v" THEN
```

```
                mode$ = "B"
                CALL bacforv(nx, ny, nz, x, y, z, mode$)
            END IF
        CASE "4"
            WRITE x, y, z, nx, ny, nz, vel$
            PRINT : PRINT
            PRINT "Press y to proceed"
            DO
            LOOP UNTIL INKEY$ = "y"
        CASE "5"
            EXIT DO
        CASE ELSE
            BEEP
    END SELECT
LOOP
END SUB
```

```
DECLARE SUB bacforv (xr!, yr!, zr!, xm!, ym!, zm!, mode$)
DECLARE SUB forward (x1!, y1!, x2!, y2!, iflag!)
DECLARE SUB backward (x1!, y1!, x2!, y2!)
COMMON SHARED /geom/ jdia, modelw, modell, modelh1, modelh2, mdia
COMMON SHARED /optical/ f, bs, mu1, mu2, mu3
COMMON SHARED /angle/ alpha AS DOUBLE, beta AS DOUBLE, gamma AS
DOUBLE
SUB filem
    INPUT "Enter INPUT  file name ", fileninp$
    INPUT "Enter OUTPUT file name ", filenout$
    OPEN fileninp$ FOR INPUT AS #1
    OPEN filenout$ FOR OUTPUT AS #2
'    WRITE #2, "Lens coordinates ", " Model coordinates"
    DO UNTIL EOF(1)
        INPUT #1, x, y, z, vel$, mode$
        IF vel$ = "U" OR vel$ = "u" THEN
            IF mode$ = "B" OR mode$ = "b" THEN
                CALL backward(nx, ny, x, y)
            END IF
            IF mode$ = "F" OR mode$ = "f" THEN
                CALL forward(x, y, nx, ny, flag)
            END IF
            nz = z
        END IF
        IF vel$ = "V" OR vel$ = "v" THEN
            CALL bacforv(nx, ny, nz, x, y, z, mode$)
            tx = nx: ty = ny: tz = nz
            nx = x: ny = y: nz = z
            x = tx: y = ty: z = tz
        END IF
        WRITE #2, x, y, z, nx, ny, nz, vel$, mode$
    IF nx > mdia / 2 THEN
    WRITE #2, "Intersection of beams is outside mixhead"
    WRITE #2, nx, ny
```

```
    END IF
    LOOP
END SUB

-----------------------------------------------------------------------

COMMON SHARED /geom/ jdia, modelw, modell, modelh1, modelh2, mdia
COMMON SHARED /optical/ f, bs, mu1, mu2, mu3
COMMON SHARED /angle/ alpha AS DOUBLE, beta AS DOUBLE, gamma AS
DOUBLE
'test
SUB bacforv (xr, yr, zr, xm, ym, zm, mode$)
'
    IF mode$ = "B" OR mode$ = "b" THEN
        xmi = xm
        ti = -modelw / 2 - xm
        hi = ti * TAN(-beta)
        fa = -f + ti - hi / TAN(-alpha)
        xr = fa - xm
        yr = ym: zr = zm
    END IF
'
' NOTE ** variables ending in notation # are double precision
'
    chordhalf = SQR(mdia * mdia / 4 - yr * yr)
    t# = -(modelw / 2 - chordhalf)
    h2# = t# * TAN(-beta)
'
    DO
        x# = xr + modelw / 2          ' xr is always -ve
        h3# = x# * TAN(-alpha)
        h1# = bs / 2 - h3# - h2#
        l# = h1# / TAN(-gamma)
        xm = xr - x# - t# - l#: ym = yr: zm = zr
        IF mode$ = "F" OR mode$ = "f" THEN
            EXIT DO
        END IF
        xdiff = xmi - xm
        IF ABS(xdiff) > .001 THEN
            xr = xr + .5 * xdiff      ' Iteration for backward
        ELSE
            EXIT DO
        END IF
    LOOP
END SUB

-----------------------------------------------------------------------

DECLARE SUB forward (x1!, y1!, x2!, y2!, flag)
COMMON SHARED /geom/ jdia, modelw, modell, modelh1, modelh2, mdia
COMMON SHARED /optical/ f, bs, mu1, mu2, mu3
COMMON SHARED /angle/ alpha AS DOUBLE, beta AS DOUBLE, gamma AS
DOUBLE
SUB backward (x2, y2, x1, y1)
    xinitial = x1
    yinitial = y1
```

```
'                                   Intial guess
      t = -modelw / 2! - x1
      h = t * TAN(-beta)
      fa = -f + t - h / TAN(-alpha)
      x1 = fa - x1: x2 = x1
'     PRINT x1, y1, x2, y2
      CALL forward(x1, y1, x2, y2, flag)
'                                   Iteration
      DO
          xlast = x1: ylast = y1
          xdiff = xinitial - x2: ydiff = yinitial - y2
          IF ABS(xdiff) < .00001 AND ABS(ydiff) < .00001 THEN
              EXIT DO
          ELSE
              IF ABS(xdiff) > .00001 THEN
                  xnew = xlast + .5 * xdiff
              ELSE
                  xnew = xlast
              END IF
              IF ABS(ydiff) > .00001 THEN
                  ynew = ylast + .5 * ydiff
              ELSE
                  ynew = ylast
              END IF
              xlast = xnew: ylast = ynew
              ynew = ynew - bs / 2
              'PRINT "xdiff,ydiff", xdiff, ydiff
              'PRINT "xnew,ynew", xnew, ynew
              CALL forward(xnew, ynew, x2, y2, flag)
             IF flag = 2 THEN
              flag = 1
              EXIT DO
             END IF
          END IF
          x1 = xlast: y1 = ylast
      LOOP
END SUB

-------------------------------------------------------------------

DECLARE SUB trans (x1!, y1!, ang1!, x2!, y2!, ang2!, dis!)
DECLARE SUB refracp (x1!, y1!, ang1!, x2!, y2!, ang2!)
DECLARE SUB refracc (x1!, y1!, ang1!, x2!, y2!, ang2!)
DECLARE SUB rootsqe (a!, b!, c!, r1!, r2!, flag!)
DECLARE SUB stcuin (x1!, y1!, ang1!, x2!, y2!, ang2!, r1!, r2!)
COMMON SHARED /geom/ jdia, modelw, modell, modelh1, modelh2, mdia
COMMON SHARED /optical/ f, bs, mu1, mu2, mu3
COMMON SHARED /angle/ alpha AS DOUBLE, beta AS DOUBLE, gamma  AS
DOUBLE
SUB forward (x1, y1, x2, y2, iflag)
     DIM x(2, 6), y(2, 6), ang(2, 6), flag(2)
  x(1, 1) = x1: x(2, 1) = x1: y(1, 1) = y1 + bs / 2: y(2, 1) = y1 - bs / 2
  FOR i = 1 TO 2                ' i - identifier for beam number
    dis = ABS(x(i, 1) + modelw * .5): ang(i, 1) = alpha
    IF i = 1 THEN ang(i, 1) = -alpha
```

```
' translation in air
    CALL trans(x(i, 1), y(i, 1), ang(i, 1), x(i, 2), y(i, 2), ang(i, 2), dis)
' refraction at plane surface
    CALL refracp(x(i, 2), y(i, 2), ang(i, 2), x(i, 3), y(i, 3), ang(i, 3))
' translation up to curved surface
    slope = TAN(ang(i, 3)): intercept = y(i, 3) - slope * x(i, 3)
    a = slope * slope + 1: b = 2! * slope * intercept
    c = intercept * intercept - mdia * mdia * .25: flag(i) = 1
    CALL rootsqe(a, b, c, r1, r2, flag(i))
'     PRINT i, r1, r2
  NEXT i
  IF flag(1) = 2 OR flag(2) = 2 THEN iflag = 2
  IF flag(1) = 1 AND flag(2) = 1 THEN
   FOR i = 1 TO 2
    CALL stcuin(x(i, 3), y(i, 3), ang(i, 3), x(i, 4), y(i, 4), ang(i, 4), r1, r2)
' refraction at curved surface
    CALL refracc(x(i, 4), y(i, 4), ang(i, 4), x(i, 5), y(i, 5), ang(i, 5))
   NEXT i
'
' translation in liquid : intersection of two st. line (beam#1 & beam#2)
   m1 = TAN(ang(1, 5)): c1 = y(1, 5) - m1 * x(1, 5)
   m2 = TAN(ang(2, 5)): c2 = y(2, 5) - m2 * x(2, 5)
   x(1, 6) = (c2 - c1) / (m1 - m2): y(1, 6) = m1 * x(1, 6) + c1
   x(2, 6) = x(1, 6): y(2, 6) = y(1, 6): ang(1, 6) = ang(1, 5)
   ang(2, 6) = ang(2, 5)
'IF x(1, 6) > mdia / 2 THEN
'PRINT "At this point intersection is outside mixhead"
'PRINT x1, y1
'WRITE #2, "intersection outside mixhead", x1, y1
'PRINT "press space"
'DO
'LOOP UNTIL INKEY$ = " "
'END IF
 END IF
 x1 = x(1, 1): y1 = y(1, 1)                    ' Beam coordinates
 x2 = x(1, 6): y2 = y(1, 6)                    ' Model coordinates
'FOR i = 1 TO 2
'FOR j = 1 TO 6
'PRINT x(i, j), y(i, j),ang(i,j)
'NEXT j
'NEXT i
END SUB

------------------------------------------------------------------------

COMMON SHARED /geom/ jdia, modelw, modell, modelh1, modelh2, mdia
COMMON SHARED /optical/ f, bs, mu1, mu2, mu3
COMMON SHARED /angle/ alpha AS DOUBLE, beta AS DOUBLE, gamma AS
DOUBLE
SUB origin (x, y, z, movex, movey, movez, vel$)
    movez = 0! - z
    movey = 0! - y
'
    IF vel$ = "U" OR vel$ = "u" THEN
        movex = (bs - modelw * TAN(beta)) * .5 / TAN(alpha)
```

```
        movex = movex - f
    ELSE
        movex = (bs - (modelw - mdia) * TAN(beta) - mdia * TAN(gamma))
        movex = movex * .5 / TAN(alpha) - f
    END IF
END SUB

-----------------------------------------------------------------

' Geometrical Optics
COMMON SHARED /geom/ jdia, modelw, modell, modelh1, modelh2, mdia
COMMON SHARED /optical/ f, bs, mu1, mu2, mu3
COMMON SHARED /angle/ alpha AS DOUBLE, beta AS DOUBLE, gamma AS
DOUBLE
SUB refracc (x1, y1, ang1, x2, y2, ang2)
    '
    ' Refraction at curved surface : only slope will change
    ' radius = radius is the radius of the curved surface
    '
    x2 = x1
    y2 = y1
    ang2 = ((mu3 - mu2) / (mu3 * .5 * mdia)) * y1 + ang1 * mu2 / mu3
END SUB

SUB refracp (x1, y1, ang1, x2, y2, ang2)
    '
    ' Refraction at plane surface : only slope of the beam will
    ' change. According Snell's Law mu1 * sin(ang1) = mu2 * sin(ang2)
    '
    x2 = x1
    y2 = y1

    sinang2 = mu1 * SIN(ang1) / mu2
    ang2 = ATN(sinang2 / SQR(1 - sinang2 * sinang2))
    'PRINT "mu1,mu2,ang1,ang2", mu1, mu2, ang1, ang2
END SUB

SUB rootsqe (a, b, c, r1, r2, flag)
    ' Roots of a quadratic Equation a*x*x + b*x + c = 0
    a1 = b * b
    a2 = 4! * a * c
    a3 = a1 - a2
    IF a3 < 0! THEN
        PRINT " Imaginary roots : no intersection of beam inside "
        PRINT "                   the curved surface"
        PRINT
        PRINT "Press y to continue"
        DO
        LOOP UNTIL INKEY$ = "y" OR INKEY$ = "Y"
        flag = 2
    ELSE
        a3 = SQR(a3)
        r1 = (-b - a3) / (2! * a)
        r2 = (-b + a3) / (2! * a)
    END IF
END SUB
```

```
SUB stcuin (x1, y1, ang1, x2, y2, ang2, r1, r2)
      ' Intersection of st. line and curved surface.
      ' x2 will always be -ve in our case since we have concave surface
      '
      IF r1 < r2 THEN
            x2 = r1
      ELSE
            x2 = r2
      END IF
      slope = TAN(ang1)
      intercept = y1 - slope * x1
      y2 = slope * x2 + intercept
      ang2 = ang1
END SUB

SUB trans (x1, y1, ang1, x2, y2, ang2, dis)
      '
      ' Translation of optical beam in same medium upto given (dis)tance
      ' using Y = mX + C  Given: x1,y1, ang1 ( angle with X-axis)
      '
      ang2 = ang1
      slope = TAN(ang1)                ' m
      intercept = y1 - slope * x1      ' C
      x2 = x1 + dis
      y2 = slope * x2 + intercept
END SUB
*****************************************************************************
```

```
'*************************************************************************
'
'          PROGRAM  PC21CONT.BAS
'
'Developed by Ashok K. Tyagi 7th July 1989
'
'
' This program is used to traverse the table and LDA data acquisition
' These tasks can be done together or alone.
' Program acquire the sets of LDA data in semi-automatic mode.

DECLARE SUB Emergency (big$, short1$, short2$)
DECLARE SUB TimeWait ()
'  **** file pc21cont.bas ****
' Program to run pc21 computer controller
'
DECLARE SUB premov21 (ax!, xlast!, ay!, ylast!, az!, zlast!)
DECLARE SUB ldaaq21 (nn%, trig$, tfreq, sfreq, filen$, short1$, short2$)
DECLARE SUB move21 (add%, v$, a$, h$, dis!)
DECLARE SUB inter21 (xadd%, yadd%, zadd%, v$, a$, h$)
OPTION BASE 1
     xaddress% = 772          ' In hard ware this is Y -axis
     yaddress% = 768          ' in Hardware this is X axis
     zaddress% = 776
     motorstep% = 10000          ' 10000 step per revolution
     reald = 1!               ' 1 rev = 1 mm
     v$ = "1"                 ' velocity
     a$ = "1"                 ' accelaration
     h$ = "+"                 ' clockwise direction
'
DO                       ' start menu loop
     CLS
     PRINT " Main Menu": PRINT
     PRINT " 1) Interactive mode"
     PRINT " 2) File mode"
     PRINT " 3) LDA data collection "
     PRINT " 4) EXIT"
     PRINT : PRINT "Type your selection ( 1 to 4): "
     INPUT ch$
     SELECT CASE ch$
          CASE "1"
           CALL inter21(xaddress%, yaddress%, zaddress%, v$, a$, h$)
          CASE "2"
           nn% = 1: big$ = "N": short1$ = "N": short2$ = "N"
           INPUT "Enter input file name ( coordinate) ", fileninp$
           INPUT "Enter  output  file  name ", filenout$
           INPUT "Enter OPERATOR MODE [Y/N] ", short2$
           OPEN fileninp$ FOR INPUT AS #5
           OPEN filenout$ FOR OUTPUT AS #6
           xlast = -88.50777: ylast = 17.525: zlast = 0!
           xorig = xlast: yorig = ylast: zorig = zlast
           DO UNTIL EOF(5)
```

```
            CLS
            PRINT "Old (x,y,z) = "; x; y; z
            INPUT #5, ax, ay, az, x, y, z, vel$, mode$
            PRINT "New (x,y,z) = "; x; y; z
            PRINT "Entering in Sub. premove21 (xyz Table)"
            CALL premov21(ax, xlast, ay, ylast, az, zlast)
            xlast = ax: ylast = ay: zlast = az
            PRINT "Entering in Sub. TimeWait"
            CALL TimeWait
            DO
                PRINT "Entering in Sub. ldaaq21 (LDA DATA)"
                CALL ldaaq21(nn%, trig$, tfreq, sfreq, filen$, short1$, short2$)
        WRITE #6, x, y, z, ax, ay, az, vel$, trig$, tfreq, sfreq, filen$
                BEEP: BEEP: BEEP
                IF INKEY$ = CHR$(27) THEN
                    CALL Emergency(big$, short1$, short2$)
                END IF
                IF short2$ = "Y" OR short2$ = "y" THEN
                    INPUT "Do you want to go to next POINT [Y/N] ", ans$
                    IF ans$ = "Y" OR ans$ = "y" THEN
                        EXIT DO
                    END IF
                ELSE
                    EXIT DO
                END IF
            LOOP
            IF INKEY$ = CHR$(27) THEN
                CALL Emergency(big$, short1$, short2$)
            END IF
            nn% = nn% + 1
            BEEP: BEEP
            IF short2$ = "Y" THEN
                INPUT "Do you want to STOP DATA Collection? [Y/N] ", ans$
                IF ans$ = "Y" OR ans$ = "y" THEN
                    CALL premov21(xorig, ax, yorig, ay, zorig, az)
                    EXIT DO
                END IF
            END IF
            IF big$ = "Y" THEN
                CALL premov21(xorig, ax, yorig, ay, zorig, az)
                EXIT DO
            END IF
        LOOP
        CLOSE (5)
        CLOSE (6)
        CASE "3"
         short2$ = "Y"
      CALL ldaaq21(nn%, trig$, tfreq, sfreq, filen$, short1$, short2$)
        CASE "4"
            EXIT DO
        CASE ELSE
            BEEP
    END SELECT
LOOP
```

```
CLOSE (5)
CLOSE (6)
END
-------------------------------------------------------------------

SUB Emergency (big$, short1$, short2$)
     big$ = "N": short1$ = "N": short2$ = "N"
DO
     CLS
     PRINT : PRINT
     LOCATE 10, 50: PRINT "E M E R G E N C Y  P R O C E D U R E S"
     PRINT " Since ESC key was pressed This procedure is started"
     PRINT " Please answer carefully "
     PRINT " 1) You want to stop the program - Table will move to (0,0,0)"
     PRINT "    Data files will be closed and saved upto this point"
     PRINT "    Program will take a normal exit"
     PRINT
     PRINT " 2) You want to update LDA parameters & then run IN"
     PRINT "    AUTOMATIC MODE (note this mode is not operative)"
     PRINT
     PRINT " 3) You want to run program in  OPERATOR  MODE"
     PRINT "    i. e. At each point you have to give LDA parameters"
     PRINT : PRINT : BEEP: BEEP
     INPUT "YOUR CHOICE [ PRESS 1 OR  3] ", ch$
     SELECT CASE ch$
          CASE "1"
               big$ = "Y": EXIT DO
          ' CASE "2"
          '      short1$ = "Y": EXIT DO
          CASE "3"
               short2$ = "Y": EXIT DO
          CASE ELSE
               BEEP: BEEP
     END SELECT
LOOP
END SUB
-------------------------------------------------------------------
SUB TimeWait
     i = 1
     DO
          hour$ = MID$(TIME$, 1, 2)
          minute$ = MID$(TIME$, 4, 2)
          sec$ = MID$(TIME$, 7, 2)
     WaitSec = ABS(VAL(hour$) * 3600 + VAL(minute$) * 60 + VAL(sec$))
          IF i = 1 THEN start = WaitSec
          IF i > 1 THEN
               IF (WaitSec - start) > 30 THEN
                    EXIT DO
               END IF
          END IF
          i = 2
     LOOP
END SUB
```

```
' **** 21bsend.bas ****
DECLARE SUB send21 (address%, x$)

SUB bsend21 (address%, cmd$)
    cmd$ = cmd$ + CHR$(13)
    FOR k = 1 TO LEN(cmd$)
        x$ = MID$(cmd$, k, 1)
        CALL send21(address%, x$)      ' sending to the board
    NEXT k
    FOR mm = 1 TO 10000: NEXT mm     ' a pure delay
END SUB
```

```
SUB datain21 (d$, cmd$)
    PRINT TAB(5); "Please choose one of the following"
    PRINT
    'PRINT TAB(5); "CONTINUOUS MOVE ..... Press 1"
    PRINT TAB(5); "PRESET    MOVE ..... Press 2"
    BEEP
    DO
        zz$ = INKEY$
        IF zz$ = "" THEN
            i = 1
        ELSE
            x = VAL(zz$)
            IF (x = 2) THEN
                EXIT DO
            ELSE
                BEEP
            END IF
        END IF
    LOOP
    DO
        INPUT "Enter speed .....(0-20 rev/s)", v$
        INPUT "Enter acceleration .....(1-99 rev/s/s)", a$
        INPUT "Enter direction .... (+ = cw, - = ccw)", h$
        'IF x = 2 THEN
         'INPUT "Enter distance ....(motor steps = 10000/rev)", d$
        'END IF
        'CALL datacheck(v$, a$, h$, d$, ch)
        ch = 1
        IF ch = 1 THEN
            EXIT DO
        END IF
    LOOP
    d$ = LTRIM$(d$)
  IF x = 1 THEN cmd$ = " E MC A" + a$ + " V" + v$ + " H" + h$ + " G"
  IF x = 2 THEN cmd$ = " E MN A" + a$ + " V" + v$ + " D" + h$ + d$ + " G"
END SUB
```

```
SUB dis21 (x2, x1, d$, h$)
    dis = x2 - x1
    IF dis < 0! THEN h$ = "-" ELSE h$ = "+"
    d$ = STR$(ABS(dis * 10000)) ' 1 rev = 10000 steps (1 rev = 1mm)
```

```
END SUB
-------------------------------------------------------------------------
SUB filem21 (xadd%, yadd%, zadd%, v$, a$, h$)
END SUB
-------------------------------------------------------------------------
'**** 21inter.bas ****
DECLARE SUB move21 (add%, v$, a$, h$, dis!)
DECLARE SUB reset21 (address%)
DECLARE SUB preset21 (v$, a$, h$, d$, cmd$)
DECLARE SUB bsend21 (address%, cmd$)

SUB inter21 (xadd%, yadd%, zadd%, v$, a$, h$)
     CALL reset21(xadd%)
     CALL reset21(yadd%)
     CALL reset21(zadd%)
     INPUT "X-axis distance in mm ", dis
     IF dis <> 0 THEN
          INPUT "X-axis direction (F/B) ", xd$
          IF xd$ = "F" OR xd$ = "f" THEN dis = dis
          IF xd$ = "B" OR xd$ = "b" THEN dis = -dis
          CALL move21(xadd%, v$, a$, h$, dis)
     END IF
     INPUT "Y-axis distance in mm ", dis
     IF dis <> 0 THEN
          INPUT "Y-axis direction (L/R) ", yd$
          IF yd$ = "R" OR yd$ = "r" THEN dis = -dis
          IF yd$ = "L" OR yd$ = "l" THEN dis = dis
          CALL move21(yadd%, v$, a$, h$, dis)
     END IF
     INPUT "Z-axis distance in mm ", dis
     IF dis <> 0 THEN
          INPUT "Z-axis direction (U/D) ", zd$
          IF zd$ = "D" OR zd$ = "d" THEN dis = dis
          IF zd$ = "U" OR zd$ = "u" THEN dis = -dis
          CALL move21(zadd%, v$, a$, h$, dis)
     END IF
END SUB
-------------------------------------------------------------------------
' **** 21move.bas ****
DECLARE SUB bsend21 (address%, cmd$)
DECLARE SUB preset21 (v$, a$, h$, d$, cmd$)

SUB move21 (add%, v$, a$, h$, dis)
'    v$ = "1"                          ' for x & y axis
     IF add% = 772 THEN                ' for X -axis
          IF dis < 0 THEN h$ = "+"     ' Model moves backward
          IF dis > 0 THEN h$ = "-"     ' Model moves forward
          xx = INT(ABS(dis * 10000))
          d$ = STR$(xx)
     END IF
     IF add% = 768 THEN                ' for Y -axis
          IF dis < 0 THEN h$ = "-"     ' Model moves right
          IF dis > 0 THEN h$ = "+"     ' Model moves left
          xx = INT(ABS(dis * 10000))
          d$ = STR$(xx)
```

```
    END IF
    IF add% = 776 THEN                  ' for Z -axis
        PRINT "dis = ", dis
        IF dis < 0 THEN h$ = "-"        ' Model moves up
        IF dis > 0 THEN h$ = "+"        ' Model moves down
        xx = INT(ABS(dis * 2000))
        d$ = STR$(xx)
        v$ = ".2"
    END IF
'
    CALL preset21(v$, a$, h$, d$, cmd$)
    CALL bsend21(add%, cmd$)
END SUB
-------------------------------------------------------------------
DECLARE SUB move21 (add%, v$, a$, h$, dis!)

SUB premov21 (ax, xlast, ay, ylast, az, zlast)
'
    xaddress% = 772         ' In hard ware this is Y -axis
    yaddress% = 768         ' in Hardware this is X axis
    zaddress% = 776
    motorstep% = 10000      ' 10000 step per revolution (for x and y)
    reald = 1!              ' 1 rev = 1 mm
    v$ = "1"                ' velocity
    a$ = "1"                ' accelaration
    h$ = "+"                ' clockwise direction
'
    movex = ax - xlast
    movey = ay - ylast
    movez = az - zlast
'
    IF movex <> 0 THEN
        CALL move21(xaddress%, v$, a$, h$, movex)
    END IF
    IF movey <> 0 THEN
        CALL move21(yaddress%, v$, a$, h$, movey)
    END IF
    IF movez <> 0 THEN
        PRINT "entering move21"
        CALL move21(zaddress%, v$, a$, h$, movez)
        PRINT "movez = ", movez
    END IF
END SUB
-------------------------------------------------------------------
' **** 21preset.bas ****

SUB preset21 (v$, a$, h$, d$, cmd$)
    v$ = LTRIM$(RTRIM$(v$))
    a$ = LTRIM$(RTRIM$(a$))
    h$ = LTRIM$(RTRIM$(h$))
    d$ = LTRIM$(RTRIM$(d$))
    cmd$ = " E MN A" + a$ + " V" + v$ + " D" + h$ + d$ + " G"
    'PRINT "cmd$ = : "; cmd$
```

```
END SUB
-------------------------------------------------------------------
' **** 21reset.bas ****

SUB reset21 (address%)
   tempadd% = address% + 1
   OUT tempadd%, &H64
   OUT tempadd%, &H60
   FOR i = 1 TO 500
   NEXT i
   OUT tempadd%, &H40
   OUT tempadd%, &H60
   FOR i = 1 TO 2500
   NEXT i
END SUB
-------------------------------------------------------------------
' **** 21send.bas ****
SUB send21 (address%, x$)
     tempadd% = address% + 1
     DO
          b = INP(tempadd%)
          IF b AND &H10 THEN EXIT DO ELSE i = 1
     LOOP
     OUT address%, ASC(x$)
     OUT tempadd%, &H70
     DO
          b = INP(tempadd%)
          IF b AND &H10 THEN i = 1 ELSE EXIT DO
     LOOP
     OUT tempadd%, &H60
END SUB
-------------------------------------------------------------------
' **** 21ldaaq.bas ****
DECLARE SUB ldainp (SEG idata%, SEG nsamp&, SEG istat%, SEG ictrl&, SEG
intvl&)
DECLARE SUB ldaset (icntr%, ictrl&, intvl&, filen$, ssize%, nsamp&, trig$, tfreq,
sfreq, short1$, short2$)
SUB ldaaq21 (nn%, trig$, tfreq, sfreq, filen$, short1$, short2$)
'

     CONST nmax = 32000          ' max size for idata array
     DIM idata(nmax + 4) AS INTEGER
'
     idata(1) = 1
     idata(2) = 2
'
     IF nn% = 1 THEN             'Initialize and test the 1400 board
          ictrl& = 3          'DANTEC BOARD
          invtl& = 0
          PRINT "     Entering in Sub. ldainp (Board Init.) "
          CALL ldainp(idata%(1), 0, istat%, ictrl&, intvl&)
     END IF
```

```
    IF istat% = 0 THEN
    PRINT "     Entering in Sub. ldaset (LDA parameters) "
CALL ldaset(icntr%, ictrl&, intvl&, filen$, ssize%, nsamp&, trig$, tfreq, sfreq, short1$,
short2$)
        PRINT "     Entering in Sub. ldainp (Acquiring data) "
        CALL ldainp(idata%(1), nsamp&, istat%, ictrl&, intvl&)
        PRINT "Writing data in "; filen$
        FOR i = 1 TO nsamp&
            index = 1 + ssize% * (i - 1)
            FOR j = index TO index + ssize% - 1
                PUT #4, , idata%(j)
            NEXT j
        NEXT i
        CLOSE (4)
    ELSE
        PRINT istat%, "Board is not present or error"
    END IF
END SUB
-------------------------------------------------------------------------
' **** ldaset.bas ****

SUB ldaset (icntr%, ictrl&, intvl&, filen$, ssize%, nsamp&, trig$, tfreq, sfreq, short1$,
short2$)
    oldfn$ = filen$
    OLDFILEN$ = filen$
    lda% = 1: icnt% = 2: iadc% = 0: ssize% = 3
    IF short2$ = "Y" OR short$ = "y" THEN
        PRINT " Default LDA settings : 1) LDA DATA yes"
        PRINT "                        2) COUNTER  yes"
        PRINT "                        3) ANALOG   NO": PRINT
        INPUT " DO YOU WANT TO USE DEFAULT SETTINGS [Y/N] ", ch1$
    ELSE
        ch1$ = "Y"
    END IF
    IF ch1$ = "N" OR ch1$ = "n" THEN
        INPUT "Enable LDA data [Y/N] ", ch1$
        IF ch1$ = "n" OR ch1$ = "N" THEN
            lda% = 0
        ELSE
            lda% = 1            ' Default value lda data yes
        END IF
'
        INPUT "Enable on board counter [Y/N] ", ch1$
        IF ch1$ = "n" OR ch1$ = "N" THEN
            icnt% = 0
        ELSE
            icnt% = 2           ' Default value counter yes
        END IF
'
        INPUT "Enable analog data [Y/N] ", ch1$
        IF ch1$ = "n" OR ch1$ = "N" THEN
            iadc% = 0           ' Default no analog data
        ELSE
            iadc% = 4
```

```
        END IF
    END IF
    IF short2$ = "Y" OR short2$ = "y" THEN
        INPUT "Enable sample trigger LDA or TIMER [L/T] ", ch1$
        INPUT "Enter frequency shift ( in kHz ) ", sfreq
        INPUT "Enter no. of blocks (1000 data per block) ", num%
        DO
            PRINT : BEEP
            INPUT "Enter desired sample freq. (kHz) > 0.0 ", tfreq
        LOOP UNTIL tfreq > 0!
    ELSE
        sfreq = 4000            'Default frequency shift 1000KHz
        num% = 10               '     Number of Block = 1
        ch1$ = "T"              '    Trigger Mode "Timer"
        tfreq = .3              '    Sampling Freq. 300Hz
    END IF
    IF ch1$ = "T" OR ch1$ = "t" THEN
        issc% = 16
        istc% = 32
        intvl& = INT(312500! / (tfreq * 1000!))
        trig$ = "T"
    ELSE
        issc = 0                ' LDA trigger
        trig$ = "L"
        tfreq = 0
    END IF

'
    ictrl& = lda% + icnt% + iadc% + issc% + istc% + icntr% * 256
    ssize% = lda% * 2 + icnt% / 2 + iadc% / 4
'
    filen$ = " ": ch1$ = " "
    DO
        IF LEN(OLDFILEN$) > 3 THEN
            exnum$ = MID$(OLDFILEN$, 5, 3)
            exno = VAL(exnum$)
            exno = exno + 1
            exnum$ = STR$(exno): exnum$ = LTRIM$(RTRIM$(exnum$))
            i = LEN(exnum$)
            IF i = 1 THEN exnum$ = "00" + exnum$
            IF i = 2 THEN exnum$ = "0" + exnum$
            MID$(OLDFILEN$, 5, 3) = exnum$
            filen$ = OLDFILEN$
            PRINT " New Raw Data File name = ", filen$
        END IF
        IF filen$ = " " THEN
            DO
                INPUT "Enter RAW DATA File name ", filen$
            LOOP UNTIL filen$ > ch1$
        END IF
        IF filen$ = oldfn$ THEN
            BEEP: BEEP: BEEP
            PRINT filen$; " already exist"
        END IF
```

```
    LOOP UNTIL filen$ <> oldfn$
    nsamp& = 1000 * num%
    PRINT "LDA parameters : ", ictrl&, intvl&, nsamp&
    OPEN filen$ FOR BINARY AS #4
END SUB
```

PEARSON.BAS

```
'
OPTION BASE 1
CLS
' Pearson curve type (PDF) estimation using first four moments of DATA
INPUT "Enter InPut  File Name : ", filein$
INPUT "Enter OutPut File Name : ", fileout$
OPEN filein$ FOR INPUT AS #5
OPEN fileout$ FOR OUTPUT AS #6
PRINT #6, "** **** ** File: "; filein$; "   Pearson Curve Analysis"
PRINT #6,
PRINT #6, "   Z(mm)"; "  Beta_1"; "  Beta_2"; "   keppa"; " Type"; " J_Re";
PRINT #6, "   r"; "     m1"; "     m2"; "    a1"; "    a2"
PRINT #6,
DO UNTIL EOF(5)
     r = 0: m1 = 0: m2 = 0: a1 = 0: a2 = 0
     INPUT #5, X, y, z, v, rms, skew, curt, vid$, JNRe, meu, ph
'
     beta1 = skew * skew
     beta2 = curt + 3
     keppa = beta1 * (beta2 + 3) * (beta2 + 3) / (4 * (4 * beta2 - 3 * beta1) * (2 * beta2 -
3 * beta1 - 6))
     IF beta1 < .005 THEN
          beta1 = 0
          keppa = 0
     END IF
'
' select type of curve
'
     curve = 100
     IF keppa < 0 THEN curve = 1
     IF keppa = 0 THEN
       IF beta2 = 3 THEN curve = 0
       IF beta2 < 3 THEN curve = 2
       IF beta2 > 3 THEN curve = 7
     END IF
     IF keppa > 0 AND keppa < 1 THEN curve = 4
     IF keppa = 1 THEN curve = 5
     IF keppa > 1 THEN curve = 6
     IF ABS(keppa) > 1000 THEN curve = 3
'
' curve parameter calculations
'
    IF curve = 1 THEN
         r = 6 * (beta2 - beta1 - 1) / (6 + 3 * beta1 - 2 * beta2)
         m12 = beta1 / (beta1 * (r + 2) * (r + 2) + 16 * (r + 1))
         xx = beta1 / m12
         m12 = r * (r + 2) * SQR(m12)
         r1 = ((r - 2) + m12) / 2
         r2 = ((r - 2) - m12) / 2
         IF skew >= 0 THEN
              m2 = r1
              m1 = r2
```

```
            ELSE
                m1 = r1
                m2 = r2
            END IF
            xx = rms * SQR(xx) / 2
            a1 = xx * m1 / (m1 + m2)
            a2 = xx * m2 / (m1 + m2)
        END IF
        IF curve = 2 OR curve = 7 THEN
            m1 = (5 * beta2 - 9) / (2 * (3 - beta2))
            a1 = (2 * rms * rms * beta2 / (3 - beta2))
            IF curve = 7 THEN m1 = -m1
        END IF
        IF curve = 3 THEN
            m1 = 2 / (rms * skew)
            a1 = (2 * rms / skew) - 1 / m1
        END IF
        IF curve = 4 THEN
            r = 6 * (beta2 - beta1 - 1)
            r = r / (2 * beta2 - 3 * beta1 - 6)
            m1 = .5 * (r + 2)
            xx = 16 * (r - 1) - beta1 * (r - 2) * (r - 2)
            xx = SQR(xx)
            m2 = -r * (r - 2) * SQR(beta1) / xx
            a1 = rms * xx / 4
        END IF
        PRINT #6, USING "####.##"; SPC(2); z;
        PRINT #6, USING "####.####"; beta1; beta2; keppa;
        PRINT #6, USING "##"; SPC(2); curve;
        PRINT #6, USING "###"; SPC(1); JNRe;
        PRINT #6, USING "###.###"; r; m1; m2; a1; a2
LOOP
PRINT #6,
PRINT #6, SPC(10); "Type = 1  Y = Y0 * ( 1 + X/a1)^m1 * (1 - x/a2)^m2 "
PRINT #6, SPC(10); "      2  Y = Y0 * ( 1 - X*X/a1)^m1 "
PRINT #6, SPC(10); "      7  Y = Y0 * ( 1 + X*X/a1)^-m1 "
PRINT #6, SPC(10); "      3  Y = Y0 * ( 1 + X/a1 )^(m1*a1) * EXP(-m1*X)"
PRINT #6, SPC(10); "      4  Y = Y0 * ( 1 + X*X/(a1*a1))^-m1 * "
PRINT #6, SPC(10); "             EXP(-m2*INV. of TAN(X/a1)) "
PRINT #6, SPC(10); "Normal 0  Y = Y0 * EXP(-X*X/(2*rms*rms)) "
END
```

LDA.F

All the necessary subroutines needed for this program are not listed here. Only those subroutines which are developed and implemented by Ashok K. Tyagi, are listed here. Remain subroutines are either in public domain or licenced property of a company. These subroutines were modified (I/O) and used. Following is the list of these subroutines and their source of listings.

(A) BETAACF, BETAI, GAMMLN, MDIAN2, MOMENT, PEARSN, SPCT, and SORT2 from "Numerical recipes: The art of scientific computing" by Press et al. (1986)

(B) TSACCF, TSASPC, TSPACF, and WINDOW from "Time series package (TSPACK)" by F. S. Chaghaghi (1982)

(C) PLOT from "FORTRAN 77: An introduction to structured problem solving" by Dyck et al. (1984).

(D) CVEL, WPDF, and TLDS from DOSTEK (supplier of the data acquisition board)

```
c
      program lda
c
c     ------------------------
c     | parameter definition |
c     ------------------------
c     explanation of data arrays
c     idata - raw data input       rdata - converted input data
c     distr - pdf of single blk.   cpdf  - cumulative pdf
c     vel   - pdf interval values  time  - abs. arrival timec
c     mon = 0 for IBM color card, mon = 1 for Hercules card
c     kodec = 0 for TSI 1990, =1 for TSI 1980, =2 for DANTEC 55L90a
      parameter (nint = 50,nimax=30000,nrmax=10000,nmax=2000,mon=0,
     u          kodec = 2, nr = 514)
      integer*2 idata(nimax)
      integer isize(500), wildidx(100)
      real rdata(nrmax), old(100)
      real distr(nint), cpdf(nint), vel(nint)
      real cxx(nr), rxx(nr), phi(nr), sxx1(nr), sxx2(nr), freq(nr)
      real wrk(nr*(nr+1)/2), rxxt(30,20), sxx3(nr), ameu(20)
      real lamda, momnt(5,10), meu(20), ti(514), buff(1000)
      logical ex
      character fname(500)*11, filelda*40, fileprs*11, filefrq*11
      character rxxs(nr)*1, phis(nr)*1, c*1, veln*1, trign*1
      character filen*11, filepdf*40,filepro*40, filespc*40, flen*7
      character fileamp*11
c     ----------------------------
c     | parameter initialization |
c     ----------------------------
c     default value initialization
c     profile storage turned off
      ifile = 0
      pi = 3.14159265
c     averaging mode is initialized to ensemble
      kode = 0
c     wavelength given in um compensating for frequency in MHz
      lamda =.6328
c     angle is the full intersection angle as read from the
```

```
c     Dantec (80mm focal length and 34mm beam separation) front lens
      angle = 24.7132
c     frequency shift is given in MHz and initialized here
      shift = 4.0
c
c     timer frequency to measure time between events(kHz)
c     it is assumed that jumper CJ6 is set to B-C (programmable timer
c     at 2500 kHz, earlier versions were set to 2385. kHz),
c     and CJ11 is set (24 bit counter word), and that SYNC (pin 5)
c     is jumped to INDEX/RESET (pin 2) on connector J103 (i.e.
c     on-board counter measures time between events)
      tfreq = 1250.0
c
c     now set default sampling frequency for the case of
c     event triggering with programmable timer (kHz)
      sfreq = 0.3
      nwords = 3000
c
c     choose TSI(1) or Dantec(0) counter
      icntr = 0
      if(kodec.lt.2) icntr = 1
c
c to read a *.lda file
c
      write(6,600)
  600 format(2x,'Enter input (*.lda file) name : ')
      read(5,'(a)') filelda
      write(6,610)
  610 format(2x,'Enter number of files in t3 : ')
      read(5,500) norec
      write(6,620)
  620 format(2x,'Enter number of lag for rxx : ')
      read(5,500) lag
  500 format(i3)
      open(8, file=filelda, status='old')
      open(9, file='t3', status='old')
      do 10 i = 1 ,norec
        read(9,900) fname(i), isize(i)
   10 continue
  900 format(a11,1x,i5)
c
c ** Open summary file for ONE *.lda file
c
      flen(1:7) = filelda
      fileprs = flen//'.prs'
      filefrq = flen//'.frq'
      fileamp = flen//'.amp'
      open(10, file = fileprs, status = 'new')
      open(11, file = filefrq, status = 'new')
      open(12, file = fileamp, status = 'new')
      write(10,1000)
      write(11,1100)
      write(12,1200)
```

```
c
 3000 read(8,*,end=4000)xp,yp,zp,ax,ay,az,veln,trign,sfreq,shift,filen
c
      shift = shift/1000.
      do 20 i = 1, norec
        if (fname(i) .eq. filen)  index = i
   20 continue
      ifsiz = isize(index) / 2
c
c ** Opening of 3 files for each RAW_DATA file {*.pro For Process
c ** data,  *.pdf for Probability density function and  *.spc
c **                for Spectrum, Auto and Partial Corealtion}
      flen(1:7) = filen
      filepro = flen//'.pro'
      filepdf = flen//'.pdf'
      filespc = flen//'.spc'
      open(86, file = '/home/scratch/tyagi/'//filepro, status = 'new')
      open(87, file = '/home/scratch/tyagi/'//filepdf, status = 'new')
      if (trign.eq.'T') then
      open(88, file = '/home/scratch/tyagi/'//filespc, status = 'new')
      endif
c
c  conversion factor (m/s)/MHz computed here
      conv = lamda/(2.*sin(angle*pi/(180.*2.)))
      if (trign.eq.'T') then
        intvl = int(312500./(sfreq*1000.))
      endif
c
c       write(lu,'(a)') ' Enter source filename : '
c       read(lu,102) filen
c102    format(a)
c
c ** Openinf RAW_DATA file and READING the data
c
      open(85,file=filen,status='old',access='direct',
     1  recl=isize(index))
      read(85,end=2000,rec=1) (idata(i),i=1,ifsiz)
c
c       ---------------------
c       | data processing |
c       ---------------------
c
      istart=1
      inc=1
      if (mod(ifsiz,1000).eq.0.) then
        ifsiz = ifsiz/3
        inc = 3
      endif
      write(6,*) inc,ifsiz
      incr=1
      kode = 0
c Raw data processing
      call cvel(idata(istart),inc,rdata,incr,ifsiz,shift,conv,kodec)
c Moment calculation
```

```
      call moment(rdata,ifsiz,ave,adev,sdev,var,skew,curt)
      write (86, 8600)  xp, yp, zp, veln, trign, flen
      write (87, 8600)  xp, yp, zp, veln, trign, flen
      if (trign.eq.'T') then
        write (88, 8600)  xp, yp, zp, veln, trign, flen
      endif
      write (86, 8605)
      write (86, 8610) ifsiz, ave, sdev, adev, skew, curt
c Wild card editing
      do 22 i = 1, 100
        wildidx(i) = 0
        old(i) = 0.
   22 continue
      call wildedt(rdata,ifsiz,ave,sdev,iwild,wildidx,old,m)
      write (86, 8612) iwild
      if (iwild .gt. 0) then
        call moment(rdata,ifsiz,ave,adev,sdev,var,skew,curt)
        write (86, 8613)
        do 25 i = 1, iwild
          write (86, 8614) wildidx(i),old(i),rdata(i)
   25   continue
        write (86, 8615)
        write(86,8610) ifsiz, ave, sdev, adev, skew, curt
      endif
      write (87,8610) ifsiz, ave, sdev, adev, skew, curt
      if (trign.eq.'T') then
        write (88,8610) ifsiz, ave, sdev, adev, skew, curt
      endif
c Output to *.prs FILE
      write(10,1010) xp, yp, zp, veln, trign, ave, sdev, adev,
     1           skew, curt, flen
c BIG WARNING - Jumping out of loop due to strange data set
c           i.e. All data appear to equal to each other
      if(abs(var) .le. 1.e-6) then
        write(86,*) ' RDATA equal. Check lab record. Processing Stop'
        write(87,*) ' RDATA equal. Check lab record. Processing Stop'
        if (trign.eq.'T') then
          write(88,*) ' RDATA equal. Check lab record. Processing Stop'
        endif
        close(85)
        close(86)
        close(87)
        if (trign.eq.'T') then
          close(88)
        endif
        go to 3000
      endif
c PDF calculation for whole set
      vmin = ave - 4.*sdev
      vmax = ave + 4.*sdev
      pdelta = (vmax - vmin)/nint
      do 30 i = 1 , nint
        vel(i) = (i-.5)*pdelta + vmin
        cpdf(i) = 0.
```

```
        distr(i) = 0.
   30 continue
      total = 0.
      call wpdf(rdata,ifsiz,distr,nint,vmin,vmax,total,kode)
      do 40 i = 1,nint
        cpdf(i) = distr(i)/(total*pdelta)
   40 continue
      write (87,8700) veln
      do 50 i = 1 , nint
        write (87,8710) vel(i),cpdf(i)
   50 continue
c
c If trigger is LDA then there is no ACF, PACF and Spectrum
c This is a jump in the case of trign='L'
c
      if (trign.eq.'T') then
c
c SPECTRUM calculation using block averaging and fft method
c
        call tlds(rdata, sfreq, ifsiz, sxx1)
c
c Standardize the time series { mean = 0.0 & std = 1.0 }
c
        do 60 i = 1, ifsiz
          rdata(i) = (rdata(i) - ave)/sdev
c         if (i.le.1024) then
c           write(86,*) rdata(i)
c         endif
   60   continue
        ave = 0.
        var = 1.
c
c ACF, PACF and SPECTRUM  for whole set using conventional method
c
        call tsaccf(rdata,ifsiz,ave,var,cxx,rxx,rxxs,lag)
        ij = ifsiz
        nf = lag
        dlt = 1.0
        nw = 3
        call tspacf(ifsiz, rxx, phi, phis, lag, wrk)
        do 63 i = (lag+1), 2, -1
          cxx(i) = cxx(i-1)
   63   continue
        cxx(1) = 1.0
        call tsaspc(freq, cxx, sxx2, lag, nf, dlt, ij, nw)
        k = (ifsiz - lag)/(2*lag)
        ovrlap = .true.
        call spct(rdata,sxx3,lag,k,ovrlap,wrk,cxx,den)
        write(6,*) k,den
        call tablep(rxx,rxxs,phi,phis,50)
        write (88,8800)
        do 65 i = 1, (nf-1)
          x = freq(i+1)*300
          sxx1(i) = 10.**sxx1(i)
```

```
          y = sxx3(i+1)
          z = sxx2(i+1)
          write (88,8810) x, sxx1(i), y, z, rxx(i), phi(i)
   65   continue
c ********************************************************
c
c IF YOU WANT TO USE PLOTING SUBROUTINE PACKAGE TEHN
c 1. REMOVE 'c' FROM THE FOLLOWING LINES
c 2. RECOMPLIE THE PROGRAM AND INCLUDE PLOT.O FILE AT LINK
c   This SUBROUTINE PLOT has been taken from "FORTRAN 77: An
c   introduction to structured problem solving" by Dyck, LAwson,
c   and smith (1984)
c ** plotting of PDF & Spectrum **
c     c = 'p'
c     ncharx = 61
c     nchary = 41
c     icode = 1
c     call plot(ncharx,nchary,c,icode,nint,vel,cpdf)
c     c = 's'
c     nf = lag - 1
c     call plot(ncharx,nchary,c,icode,nf,freq,sxx1)
c     call plot(ncharx,nchary,c,icode,nf,freq,sxx2)
c
c ********************************************************
c
c ** F&W test for significant frequency
        call fiswhi(freq,sxx2,nf,flen)
        nf = lag - 1
c
c ** land here in case of trign = 'L'
      endif
c
c Run and Reverse Test for Random and Independent data block
c
     kn = 2*ifsiz/1000
     do 70 i = 1 , kn
       meu(i) = 0
       ti(i) = i
  70 continue
     do 80 i = 1 , kn
       do 90 j = 1 , 500
         k = (i-1)*500 + j
         meu(i) = rdata(k) + meu(i)
  90   continue
       meu(i) = meu(i)/500
       ameu(i) = meu(i)
  80 continue
     call mdian1(ameu,kn,xmed)
     call randomt(meu,xmed,ifsiz)
c
c Stationary Test for each block
     kn = kn/2
     nblk = 1000
     do 100 i = 1 , kn
```

```
        ti(i) = float(i)
        do 110 j = 1 , nblk
          ij = (i-1)*nblk + j
          buff(j) = rdata(ij)
  110   continue
      call moment(buff,nblk,ave,adev,sdev,var,skew,curt)
      momnt(1,i) = ave
      momnt(2,i) = sdev
      momnt(3,i) = skew
      momnt(4,i) = curt
      momnt(5,i) = adev
      ave = 0.
      var = 1.
      llag = 0
      if (trign.eq.'T') then
        llag = 30
        call tsaccf(buff,nblk,ave,var,cxx,rxx,rxxs,llag)
        do 115 k = 1 , llag
          rxxt(k,i) = rxx(k)
  115   continue
      endif
  100 continue
      write(86,8657)
      do 120 i = 1 , (llag+5)
        do 130 k = 1 , kn
          ti(k) = float(k)
          if ( i .gt. 5 ) then
            if ( i .eq. 6 .and. k .eq. 1) then
              write(86,8658)
            endif
            meu(k) = rxxt(i,k)
            in = i - 5
          else
            meu(k) = momnt(i,k)
            in = i
          endif
  130   continue
      call pearsn(ti,meu,kn,r,prob,z)
      write(86,8660) in,r,prob,z
  120 continue
c
      close (85)
 2000 continue
      close (86)
      close (87)
      if (trign.eq.'T') then
        close (88)
      endif
      go to 3000
 4000 continue
c
      close(12)
      close(11)
      close(10)
```

```
      close(9)
      close(8)
      stop
 1000 format(10x,' X(mm)',' Y(mm)',' Z(mm)',5x,'vel(m/s)',
     1     ' RMS',2x,'adev',4x,'skew',3x,'Kurt',3x,'File')
 1010 format(10x, 3(f6.2, 1x), 2(a1), 1x, 5(f6.3, 1x), a7)
 1100 format(10x,'First 10 Significant Frequency(Hz) in the',
     1      ' Order (F&W Test)',//,5x,'1',6x,'2',6x,'3',6x,'4',
     2    6x,'5',6x,'6',6x,'7',6x,'8',6x,'9',5x,'10',3x,'FileID')
 1200 format(10x,'Amplitude of 1st ten freq.(HZ) in Order',//,
     1     5x,'1',6x,'2',6x,'3',6x,'4',6x,'5',6x,'6',6x,'7',
     2     6x,'8',6x,'9',5x,'10',3x,'FileID')
 8600 format(14x,'(x,y,z) = ',2x,3(f6.2,1x),a1,2x,a1,2x,a7)
 8605 format(25x,'BEFORE WILD DATA EDITING')
 8610 format(14x,'n:',i5,'Avg(m/s):',E10.4,' RMS(m/s):',e10.4,/,
     1     14x,'ADEV(m/s):',e10.4,' SKEW:',f8.4,'KURT:',f8.4)
 8612 format(25x,'Number of Wild data = ',i3)
 8613 format(25x,'No. ',2x,'Old Value',2x,'New Value')
 8614 format(25x,i5,2x,f8.4,3x,f8.4)
 8615 format(25x,' AFTER WILD DATA EDITING')
 8657 format(2x,'Stationarity Test : y=a+bx where x is record #'
     1 /,2x,' (IND) & y is moment or Rxx for different lag(DEP)',/,
     2 2x,' [ Low value of cor. & high value of Prob. means there',/,
     3 2x,'  is no relationship between y and x ]',//,
     4 2x,'Moment',2x,'Corelation',2x,'Probability',2x,'Fisher Z')
 8658 format(2x,'Rxx(lag)')
 8660 format(2x,2x,i2,6x,f5.2,7x,f5.2,7x,f5.2)
 8700 format(27x,a1,' (m/s)',5x,' PDF')
 8710 format(27x,f8.4,2x,g10.4)
 8800 format(13x,'Freq(Hz)',2x,' PSD(LDS) ',2x,' PSD(OVR) ',
     1     2x,'PSD(via Rxx)',2x,'Rxx',5x,'Phi')
 8810 format(13x,f8.3,2x,3(e10.3,1x)
     1,f6.3,2x,f6.3)
      end

c
      SUBROUTINE wildedt(buffer,ifsiz,ave,sdev,count,wildidx,old,m)
c
c     Given average and standard deviation of array buffer
c     this program identifies the outliner
c
c     Lower limit:  ave - 4*sdev & Upper limit ave + 4*sdev
c
c     Wild card ( outliner ) lies out side the above criterion
c
      DIMENSION buffer(*), old(*)
      REAL low , high
      INTEGER count , wildidx(*)
c
      m = 0
      count = 0
      low = ave - 4.*sdev
      high = ave + 4.*sdev
      DO 10 i = 1 , ifsiz
```

```
        IF ( count .GT. 101 ) THEN
          m = 1
          GO TO 20
        ENDIF
        IF ( buffer(i) .LT. low ) THEN
          count = count + 1
          wildidx(count) = i
        ENDIF
        IF ( buffer(i) .GT. high ) THEN
          count = count + 1
          wildidx(count) = i
        ENDIF
   10 CONTINUE
   20 CONTINUE
c
c    Interpolation section : Removal of wild data
c    using that the fourth difference is zero
c
     IF ( count .GT. 0 ) THEN
       DO 30 j = 1 , count
         n = wildidx(j)
c
c Taking care for begining and end of the record
c if n<3 or n>(ifsiz-2)
c
         IF ( (n-1) .LE. 0 ) THEN
           a1 = buffer(n+1)
         ELSE
           a1 = buffer(n-1)
         ENDIF
         IF ( (n-2) .LE. 0 ) THEN
           a2 = buffer(n+2)
         ELSE
           a2 = buffer(n-2)
         ENDIF
         IF ( (n+1) .GT. ifsiz ) THEN
           b1 = buffer(n-1)
         ELSE
           b1 = buffer(n+1)
         ENDIF
         IF ( (n+2) .GT. ifsiz ) THEN
           b2 = buffer(n-2)
         ELSE
           b2 = buffer(n+2)
         ENDIF
c
c NO wild card should be used in INTERPOLATION
c check
c
```

```
          IF ( wildidx(j+1) .GT. 0 ) THEN
            IF ( (n+1) .EQ. wildidx(j+1) ) THEN
              b1 = ave
            ENDIF
            IF ( (n+2) .EQ. wildidx(j+1) ) THEN
              b2 = ave
            ENDIF
          ENDIF
          anew = ( - a2 + 4.*a1 + 4.*b1 - b2 ) / 6.0
          old(j) = buffer(n)
          buffer(n) = anew
   30   CONTINUE
      ENDIF
      RETURN
      END
c
      SUBROUTINE randomt(meu,xmed,ifsiz)
c
      REAL nruns,meu(*),a(20),rnl(6),rnh(6),anl(6),anh(6)
      CHARACTER test*7,hyp*8,obs*11
      DATA rnl / 2., 3., 3., 4.,  5.,  6./
      DATA rnh / 9.,10.,12.,13., 14., 15./
      DATA anl /11.,18.,27.,38., 50., 64./
      DATA anh /33.,47.,63.,81.,102.,125./
c REVERSE TEST
c Vector anl : alpha = .05 a(n:(1-alpha/2)) for n = 10,..,20
c      anh :           a(n:alpha/2)
c From Table A.7
c RUN TEST
c Vector rnl : alpha = .05 r(n:(1-alpha/2)) for n = 5,..,10
c Vector rnh             r(n:alpha/2)
c From Table A.6 of RANDOM DATA: Analysis & Measurement Procedures
c               by Bendat & Piersol (1985)
c
c ** Reverse TEST
c
      test = 'REVERSE'
      n = 2*ifsiz/1000
      DO 10 i = 1 , n
        a(i) = 0.0
   10 CONTINUE
      sum = 0
      k = n/2
      k = k - 4
c
      DO 20 i = 1 , (n-1)
        DO 30 j = i , n
          IF ( meu(i) .GT. meu(j) ) Then
            a(i) = a(i) + 1
          ENDIF
   30   CONTINUE
        sum = sum + a(i)
   20 CONTINUE
```

```
c
      IF ( ( sum .GT. anl(k) ) .AND. ( sum .LE. anh(k) ) ) THEN
        hyp = 'ACCEPTED'
        obs = 'INDEPENDENT'
      ELSE
        hyp = 'REJECTED'
        obs = '  DEPENDENT'
      ENDIF
      WRITE (86,600) test , hyp , obs , k , anl(k) , sum , anh(k)
c
c ** RUN TEST
c
      test = '  RUN  '
      nhalf = n/2
      nruns = 1
      IF ( meu(1) .LT. xmed ) THEN
        m1 = 0
      ELSE
        m1 = 1
      ENDIF
      DO 40 i = 2 , n
        IF ( meu(i) .LT. xmed ) THEN
          m2 = 0
        ELSE
          m2 = 1
        ENDIF
        IF ( m1 .NE. m2 ) THEN
          nruns = nruns +1
          m1 = m2
        ENDIF
   40 CONTINUE
c
      IF ( ( nruns .GT. rnl(k) ) .AND. ( nruns .LE. rnh(k) ) ) THEN
        hyp = 'ACCEPTED'
        obs = 'INDEPENDENT'
      ELSE
        hyp = 'REJECTED'
        obs = '  DEPENDENT'
      ENDIF
      WRITE (86,600) test , hyp , obs , k , rnl(k) , nruns , rnh(k)
      RETURN
  600 FORMAT (4X,'By ',A7,' TEST at 5% level of  significance',/,
     1     2X,'hypothesis is ',A8,'. ',A11,' OBSERVATIONS',//,
     2     2X,'K = ',I4,2X,'L_Limit = ',F6.2,2X,'A = ',F6.2,2X,
     3       'U_Limit = ',F6.2)
      END
C
      SUBROUTINE FISWHI(A,B,N,FILEN)
C  Input : Vector A(N)    &   Vector B(N)
C        frequency(f)       Spectrum I(f)
C  Output :  Array C(I,J)
C  [ I = 1    2        3                4        5 ]
C   Freq(f)  I(f)  Points in distribution(N)  g(alpha)     T
```

```
C    J to indicate number of significant I(f) at f.
C  TEST for a sig. I(f) { ordinate at f }: calculated T > g
C  at a given significance level ( alpha = 0.05 ).
C  significance level (alpha = 0.05).
     INTEGER FF
     PARAMETER (FF=12)
     DIMENSION A(*), B(*)
     REAL  SUM, ALPHA, C(5,30)
     CHARACTER FILEN*7
     NUM = N
C
C Sort the array B in ascending order and mix the array A
C to keep the same mapping between A and B
C
     CALL SORT2(NUM,B,A)
C
C Fisher and Whittle test for the significance of largest
C periodgram ordinate
C
     ALPHA = 0.05
     SUM = 0.0
     DO 10 I = 1 , 5
       DO 20 J = 1 , 30
         C(I,J) = 0.0
 20    CONTINUE
 10  CONTINUE
     DO 30 I = 1 , N
       SUM = SUM + B(I)
 30  CONTINUE
     DO 40 I = 1 , 30
       N = NUM - ( I - 1 )
       G = 1. - ( ALPHA / FLOAT(N) ) ** ( 1. / FLOAT(N-1) )
       T = B(N) / SUM
       IJUMP = 1
       IF ( T .GT. G) THEN
         A(N) = A(N)*300.
         C(1,I) = A(N)
         C(2,I) = B(N)
         C(3,I) = FLOAT(N)
         C(4,I) = G
         C(5,I) = T
         IJUMP = 2
         SUM = SUM - B(N)
       ENDIF
       IF ( IJUMP .EQ. 1 ) GO TO 50
 40  CONTINUE
 50  I = I - 1
     WRITE(86,8600) CHAR(FF),I
     IF ( I .GT. 0 ) WRITE(86,8610)
     DO 60 K = 1 , I
       WRITE(86,8620) K, (C(J,K),J=1,5)
 60  CONTINUE
     WRITE(11,1100) (C(1,K),K=1,10),FILEN
     WRITE(12,1200) (C(2,K),K=1,10),FILEN
```

```
   RETURN
8600 FORMAT(A1,2X,'Fisher (& Whittle) Test for Significant periodic',
   1 ' component at frequencies'//,2X,'Only ',I2,' Spectrum',
   2 ' Ordinates are Significant'//)
8610 FORMAT(3X,'#',' Frequency(Hz)',6X,'I(f)',6X,'Points ',
   1     2X,'g(alpha)',4X,'T')
8620 FORMAT(2X,I2,2X,F7.3,7X,E12.5,2X,F7.0,2X,F7.4,2X,F7.4)
1100 FORMAT(2X,10(F6.2,1X),A7)
1200 FORMAT(2X,10(f6.1,1x),A7)
   END
```

Appendix D: Table D1: Vortices growth parameters

D = Mixhead diameter; H = Piston location in mixhead; Re = Jet Reynold number
l = length of circulation zone; s = Distance between center of vortices

Re	H/D	Viscosity (cp)	s/D	l/D	Index
0	All	All	1	0.00	Theory
15	0.0	75	0.60	0.38	6.1.5.1(a)
16	0.0	75	0.72	0.48	Video #6D
25	0.0	75	0.40	0.57	6.1.5.1(b)
25	0.0	75	0.34	0.61	6.1.5.1(c)
31	0.0	75	0.45	0.62	Video #6D
50	0.0	75	0.35	0.81	6.1.5.1(d)
50	0.0	75	0.35	0.81	6.1.5.1(e)
50	0.0	75	0.31	0.82	6.1.5.1(f)
50	0.0	75	0.26	0.84	6.2.2.1(a)
50	0.0	75	0.34	0.82	Video #6D
75	0.0	75	0.34	1.06	Video #6D
75	0.0	75	0.35	0.97	6.1.5.2(a)
75	0.0	75	0.31	0.97	6.1.5.2(b)
75	0.0	75	0.31	0.98	6.1.5.2(c)
75	0.0	75	0.35	0.98	6.1.5.2(d)
75	0.0	75	0.35	0.95	6.1.5.2(e)
100	0.0	75	0.39	0.96	6.1.5.3(a)
100	0.0	75	0.35	0.90	6.1.5.3(b)
100	0.0	75	0.31	0.87	6.1.5.3(c)
100	0.0	75	0.31	1.03	Video #6D
125	0.0	75	0.31	0.96	Video #6D
16	0.50	75	0.69	0.48	Video #6D
31	0.50	75	0.45	0.65	Video #6D
50	0.50	75	0.31	0.82	Video #6D
50	0.50	75	0.41	0.95	6.1.5.5(a)

Table D1 (contd.)

Re	H/D	Viscosity (cp)	s/D	l/D	Index
50	0.50	75	0.37	0.90	6.1.5.5(b)
75	0.50	75	0.37	1.11	6.1.5.5(c)
75	0.50	75	0.31	1.08	Video #6D
75	0.50	75	0.36	1.13	6.1.5.5(d)
100	0.50	75	0.31	1.08	Video #6D
125	0.50	75	0.17	0.96	Video #6D
31	0.00	39	0.36	0.71	6.2.1.1(a)
43	0.00	39	0.28	0.77	VHS #6
49	0.00	39	0.28	0.85	6.2.1.1(b)
57	0.00	39	0.29	0.99	6.2.1.1(c)
69	0.00	39	0.27	1.05	6.2.1.1(d)
70	0.00	39	0.28	0.99	VHS #6
77	0.00	39	0.25	1.05	6.2.1.1(e)
98	0.00	39	0.28	0.99	VHS #6
43	0.50	39	0.31	0.78	VHS #6
50	0.50	39	0.32	0.89	6.2.1.1(e)
70	0.50	39	0.28	1.06	VHS #6
73	0.50	39	0.30	1.07	6.2.1.4(b)
76	0.50	39	0.29	1.08	6.2.1.4(c)
94	0.50	39	0.30	1.39	6.2.1.4(d)
98	0.50	39	0.22	1.17	VHS #6
9	0.25	90	0.81	0.34	6.2.3.1(a)
37	0.25	90	0.36	0.72	6.2.3.1(b)
60	0.25	90	NA	0.83	Lab Notes
88	0.25	90	0.29	1.01	6.2.3.1(c)
88	0.25	90	0.30	1.03	6.2.3.2(a)
95	0.25	90	0.33	0.87	6.2.3.2(b)
111	0.25	90	0.36	0.59	6.2.3.2(c)
111	0.25	90	0.34	0.56	6.2.3.2(d)

IMAGE EVALUATION TEST TARGET (QA-3)

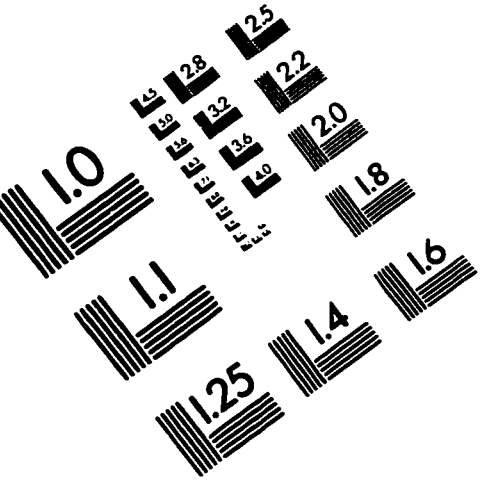

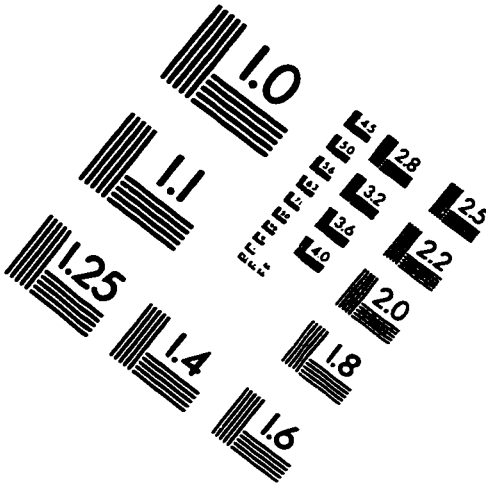

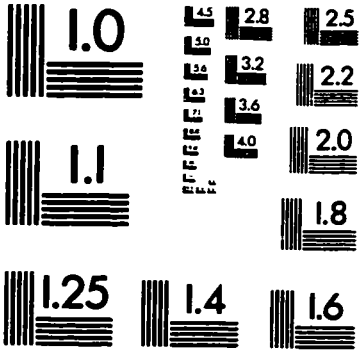

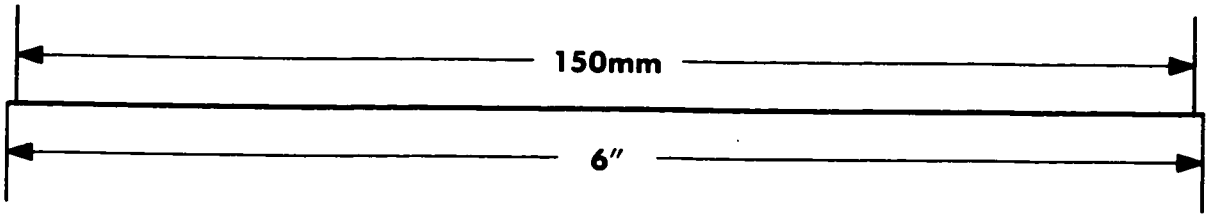

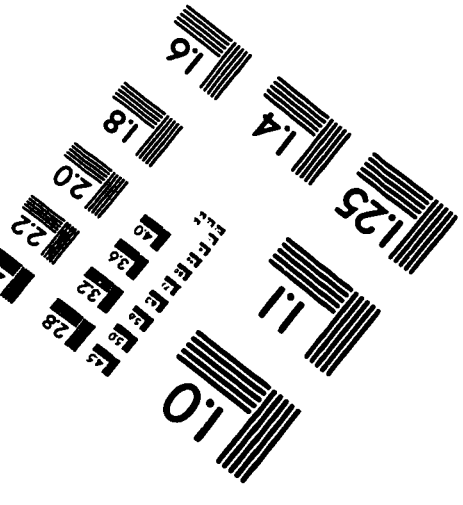

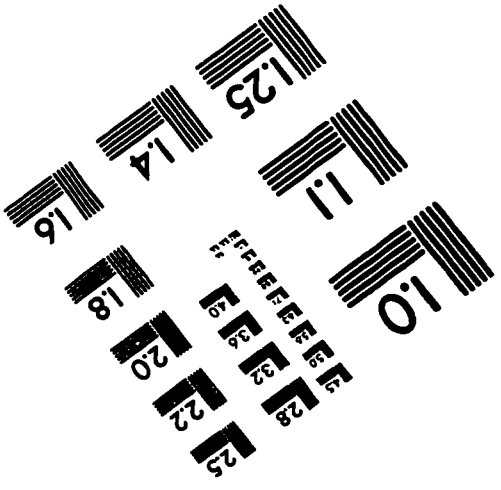

APPLIED IMAGE, Inc
1653 East Main Street
Rochester, NY 14609 USA
Phone: 716/482-0300
Fax: 716/288-5989